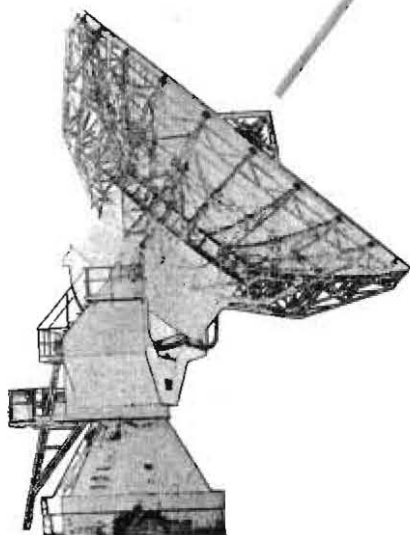


Spacecraft Operations

Final Report



IUE

Spacecraft Operations

Final Report

ESA SP-1215: Final Report IUE-Spacecraft Operations

Prepared by: Ms. Ana Pérez Calpena and Ms. Judy Pepoy

Project Manager: Dr. W. Wamsteker

Published by: ESA Publications Division, ESTEC
Noordwijk, The Netherlands

Editor: R.A.Harris

International Standard Book



Number: ISBN 92-9092-459-4




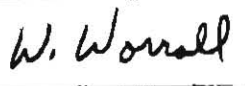

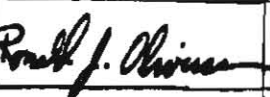

Copyright: © 1997 by European Space Agency



Price: 70 Dutch Guilders

Printed in: The Netherlands

DOCUMENT APPROVAL

Prepared by	Organisation	Signature	Date
A. Perez Calpena	INSA		01 May 1997
J. Pepoy	ATSC		30 May 1997

Approved by	Organisation	Signature	Date
F. Alcaraz	INSA/VILSPA M&O Mngr.		10 July 1997
W. Wamsteker	ESA/VILSPA/IUE project Mngr.		11 July 1997
V. Claros	ESA/VILSPA/IUE Miss. Ops. Mngr.		14 July 1997
W. Worrall	NASA/GSFC/IUE Project Mngr		24 July 1997
Y. Kondo	NASA/GSFC/ IUE Project Scientist		25 July 1997
R. Oliverson	NASA/GSFC/ IUE Deputy Project Scientist		24 July 1997
R.J. Sodano	NASA/GSFC/IUE Mission Director		22 July 1997

Authorized by	Organisation	Signature	Date
G. Delmas	ESA/ESOC/H/MOD		17 July 1997
A. Michalitsianos	NASA/GSFC/LASP Chief		24 July 1997

Abstract

The present document describes the mission operations associated with the International Ultraviolet Explorer (IUE) spacecraft, in the context of the 18.5 years of orbital operations in the IUE Project, which was a collaboration between NASA, ESA and PPARC.

In Chapter 1 the objectives of the IUE mission, the goals and capabilities of the spacecraft, the payload and the ground segment are described, as well as some examples of the scientific capabilities of the project. The characteristics of the spacecraft, the spacecraft subsystems and the ground observatory control systems are detailed in Chapter 2. Chapter 3 lists the main spacecraft events in the course of the 18 years of the duration of the orbital operations. In Chapter 4, the IUE orbit and its evolution are described. The most important problems in the spacecraft subsystems are described in Chapter 5 together with the solutions. Special emphasis is given to the different attitude control systems associated with the progressive gyro failures, culminating in the 1-Gyro control system used during the last six months of orbital operations. In Chapter 6, the spacecraft thermal design is described. The three appendices contain important dates in the area of spacecraft operations:

- ▶ Appendix A: Earth shadow seasons.
- ▶ Appendix B: Orbital corrections (Delta-V's).
- ▶ Appendix C: On-Board-Computer malfunctions.

Contents

Document approval	iii
Abstract	v
Contents	vii
List of acronyms and abbreviations	ix
1. Introduction	1
2. General spacecraft description	3
3. Operations highlight summary	13
4. Orbit	24
4.1. Orbital corrections (Delta-V)	33
5. Subsystems	34
5.1. Power subsystem	35
5.1.1. Solar array	35
5.1.1.1. Beta restrictions	40
5.1.1.2. Solar array EOL characterization	40
5.1.2. Batteries	41
5.1.2.1. Battery 1 degradation	43
5.1.2.2. Battery EOL characterization	44
5.1.3. Shadow	44
5.2. Command subsystem	51
5.2.1. Command decoder anomalies	53
5.3. Communications system	54
5.3.1. S-Band system	54
5.3.1.1. S-Band power amplifier 4 anomaly	56
5.3.2. VHF system	56
5.3.2.1. Ranging	56
5.4. Data Handling subsystem	57
5.4.1. DMU anomaly	61
5.4.2. DMU radiation monitor	65
5.5. Attitude control subsystem	72
5.5.1. Inertial Reference Assembly	73
5.5.1.1. Gyro failures	74

5.5.1.2. Gyro drift rates	76
5.5.2. Fine Sun Sensor	77
5.5.2.1. FSS anomalies	79
5.5.3. Coarse Analog Sun Sensor	80
5.5.4. Spin Mode Sun Sensor	80
5.5.5. Panoramic Attitude Sensor	80
5.5.5.1. PAS anomalies	80
5.5.6. Accelerometer	81
5.5.7. Fine Error Sensor	81
5.5.7.1. FES geometric calibration	84
5.5.7.2. FES 2 reference point shift anomaly	85
5.5.7.3. FES 2 star count variations anomaly	85
5.5.7.4. Scattered light anomaly	85
5.5.7.5. Streak light anomaly	87
5.5.8. Reaction Wheel	90
5.5.9. Hydrazine Auxiliary Propulsion System	90
5.5.9.1. HAPS heater group 1 failure	99
5.5.9.2. N ₂ H ₄ venting	99
5.5.10. Control Electronics Assembly	101
5.6. The Onboard Computer	103
5.6.1. OBC Patches	110
5.6.2. 3-Gyro System.	112
5.5.3. 2-Gyro/FSS System.	113
5.6.4. 1-Gyro System	114
5.6.5. Attitude recovery procedures	118
5.6.6. OBC anomalies	119
5.7. Scientific Instrument	122
5.7.1. Camera Operating Sequence	128
5.7.2. LWP Scan Control Logic anomaly.	129
5.7.3. LWP flux anomaly	129
5.7.4. LWR anomaly	129
5.7.5. Microphonics.	130
5.7.6. LWP Scan Control Logic Anomaly	130
5.7.7. SWR failure	130
6. Spacecraft Thermal Design	131
Appendix A. Earth shadow seasons.	143
Appendix B. Delta-Vs	145
Appendix C. OBC malfunctions	147
Source Documents	151
List of figures.	156

List of acronyms and abbreviations

A/D	analog to digital
ABG	gyro measured body angle
ABM	apogee boost motor
ac	alternating current
ACS	attitude control subsystem
AM	amplitude modulation
ANC	automatic nutation control
AS	analog sub-commutator
BLT	Greenbelt tracking station
BOL	beginning of life
CCIL	Control center Interactive Language
CEA	control electronics assembly
CEB	control electronics box
CEM	camera electronics module
CHM	camera head module
CPM	central processing module
CPU	central processing unit
CRU	command relay unit
CSIM	camera supply interface module
CSIU	camera system interface unit
CSS	coarse sun sensor
DAC	digital to analog converter
dc	direct current
DDPS	Digital Data Processing System
DEC	Digital Electronics Corporation
DET	Direct Energy Transfer
DKLP	camera deck near longwave prime temperature
DKSP	camera deck near shortwave prime temperature
DMA	direct memory access
DMU	data multiplexer unit
DS	digital sub-commutator
DWG	digital word gate
ECU	electronics control unit
EDS	experiment display system
EEA	experiment electronics assembly
EOL	end of life
ESA	European Space Agency
ESTEC	European Space and Technology Centre
EV	engine valve
EVCL	engine valve command logic
FES	fine error sensor
FM	frequency modulation
FOD	Flight Operations Directive
FOV	field of view
FPM	flux particle monitor

FSS	fine sun sensors
GSFC	Goddard Space Flight Center
HAPS	Hydrazine Auxiliary Propulsion System
HTE	high-thrust engine
HVPS	high voltage power supply
I/O	input/output
IOR	interrupt override register
IRA	inertial reference assembly
ISR	interrupt register storage
ITF	intensity transfer function
IUE	International Ultraviolet Explorer
IUEOCC	IUE Operations Control Center
LOS	loss of signal
LSB	least significant bit
LSR	lockout status register
LTE	low-thrust engine
LWP	long wavelength prime
LWR	long wavelength redundant
MAM	mission adapter module
MER	Mission Equipment Room
MOR	Mission Operations Room
MSB	most significant bit
MTBF	mean time between failure
MXR	multiplex ratio
NASA	National Aeronautics and Space Administration
NEP	North Ecliptic Pole
NSA	nutation sensor assembly
OBC	onboard computer
PAS	panoramic attitude sensor
PM	phase modulation
PROC	procedure
PSE	power supply electronics
R&RR	range and range rate
REM	remote engine module
RF	radio frequency
ROM	read-only memory
RW	reaction wheel
S/C	spacecraft
SCL	scan control logic
SDC	serial digital command
SEC	secondary electron conduction
SI	scientific instrument
SIO	special input/output
SOC	Scientific Operations Center
SRATE	data sample rate
SU	sensor unit
SWP	short wavelength prime

1. Introduction

The IUE spacecraft was launched in January 1978 from Cape Canaveral, Florida. It was the first astronomical satellite to have been placed into a geosynchronous orbit and also the first scientific satellite that allowed a large number of visiting astronomers to make real time observations of ultraviolet spectra. The planned mission lifetime was between three and five years. In the end, IUE had accumulated 104,470 spectra images during 18.5 years of in-orbit operations.

Despite the difficulties that arose during the mission, IUE accomplished all scientific goals. When its fourth gyro failed in 1985, IUE continued its operations using only two gyros. The continuation of the mission was achieved with an innovative redesign of on-board and on-ground systems.

Even when the fifth gyro failed in the last year of the IUE, the science observing program could be completed. The spacecraft was three-axis stabilized under a 1 gyro system.

The IUE operations ended on September 30, 1996, at 18:44 U.T.

The IUE Project objectives were to design, fabricate, test and place into geosynchronous orbit an ultraviolet astronomical three-axis controlled observatory intended primarily for use as an international research facility. The design lifetime of the hardware was 3 years with a goal, including the sizing of consumables and degradable hardware, of 5 years.

Astronomers used this observatory to carry out their own observing programs without going through tedious training courses in the specialized techniques of operating a telescope in Earth orbit. In low Earth orbit, such special techniques become necessary because this geometry changes so rapidly that the observer has little opportunity to evaluate and take advantage of particular observing situations as they arise. The observer must rely on preplanned automatic sequences that are often indirectly responsive to the scientific requirements of the observation.

The choice of a geosynchronous orbit is important in achieving the objective of a guest observatory where the observers can remain experts in astronomy without the need to become experts in satellite orbit operations. The geosynchronous orbit does restrict the weight and the size of the telescope that can be considered; however, with the IUE, this restriction was largely counterbalanced by the telescope instrumentation, which had been designed to carry out the scientific objectives of the mission with considerable efficiency.

The following list is a summary of the IUE scientific goals prior to launch:

- ▶ Obtain high-resolution spectra of stars of all spectral types in order to determine more precisely the physical characteristics of these stars.
- ▶ Study gas streams in and around some binary systems
- ▶ Observe faint stars, galaxies, and quasars at low resolution and interpret these spectra by reference to high-resolution spectra.

- ▶ Observe the spectra of planets and comets as these objects become accessible.
- ▶ Make repeated observations of objects which show variable spectra.
- ▶ Define more precisely the modifications of starlight caused by interstellar dust and gas.

To achieve the scientific goals previously stated, the spacecraft had to be able to point anywhere on the celestial sphere, except within 45° of the sun, with an accuracy of ± 1 arcsecond. The control system had to be able to re-point the telescope to a new target star over a fairly wide angle (up to 60°) with a rate of 4.5 degrees per minute per axis and guarantee that the desired new target star falls within the 16 arcminute diameter field of view of the fine error sensor. To perform spectroscopy on the faint stars with the desired resolution, the control system had to hold a 1 arcsecond diameter star image within a 3 arcsecond diameter spectrograph entrance aperture long enough to permit an integrated exposure of 1 hour duration by the spectrograph camera. Battery storage was required on the spacecraft to provide sufficient power to maintain attitude control and critical spacecraft subsystems during solar eclipses.

IUE was an international undertaking. The satellite and optical instrumentation were provided by the National Aeronautics and Space Administration's (NASA) Goddard Space Flight Center (GSFC), and the vidicon cameras used as detectors in the scientific instrument were provided by the United Kingdom Science Research Council. The European Space Agency (ESA) supplied the solar arrays for the satellite and also constructed the European control center Villafranca Satellite Tracking Station (VILSPA).

This international cooperation continued during control operations, which were mainly conducted in the two mentioned ground stations, GSFC and VILSPA.

- ▶ The GSFC ground system comprises three major sites: the Greenbelt tracking station (BLT), the IUE Operations Control Center (IUEOCC) which houses the operations computers and the Mission Operations Room (MOR), and the Scientific Operations Center (SOC). The MOR in the IUEOCC was used by spacecraft analysts to monitor the status of the spacecraft. The SOC was used for the telescope operators, resident astronomers and guest observers to conduct scientific operations and scientific data processing. Around October 1985, Wallops Flight Facility (WPS) replaced the Greenbelt tracking station as primary US ground station.
- ▶ The VILSPA ground system houses the MER (Main Equipment Room) and control rooms (Observatory and Control Room), which consists of elements functionally identical to the BLT and IUEOCC; however, both scientific and spacecraft operations were conducted in the IUE dedicated control rooms at VILSPA.

The following sections will describe the characteristics of the orbit, the spacecraft, the spacecraft subsystems and the thermal design, and their evolution along the mission; as well as the technical problems, constraints and problem solving techniques used during the IUE program.

2. General spacecraft description

The IUE spacecraft is shown in mission orbit configuration and in an exploded view in figures 2-1 and 2-2 respectively.

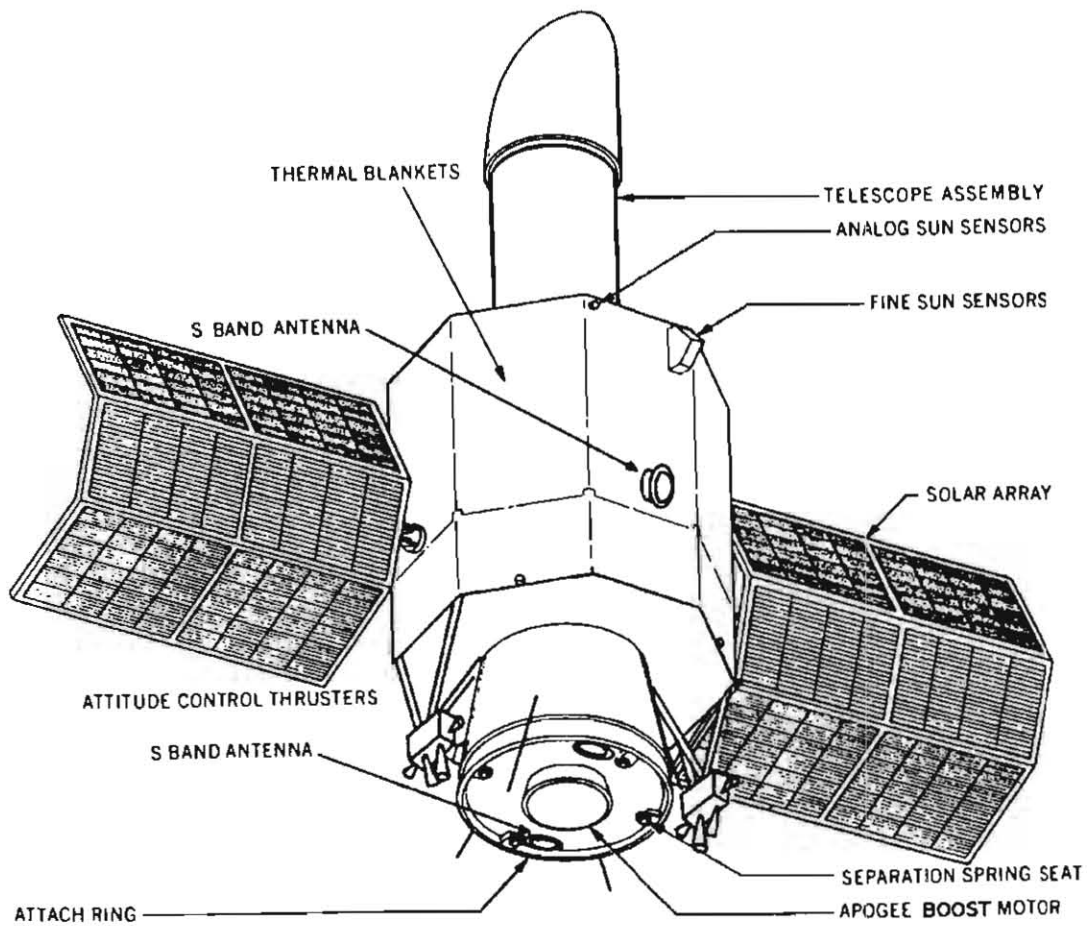


Figure 2-1. IUE Spacecraft in Mission Orbit Configuration.

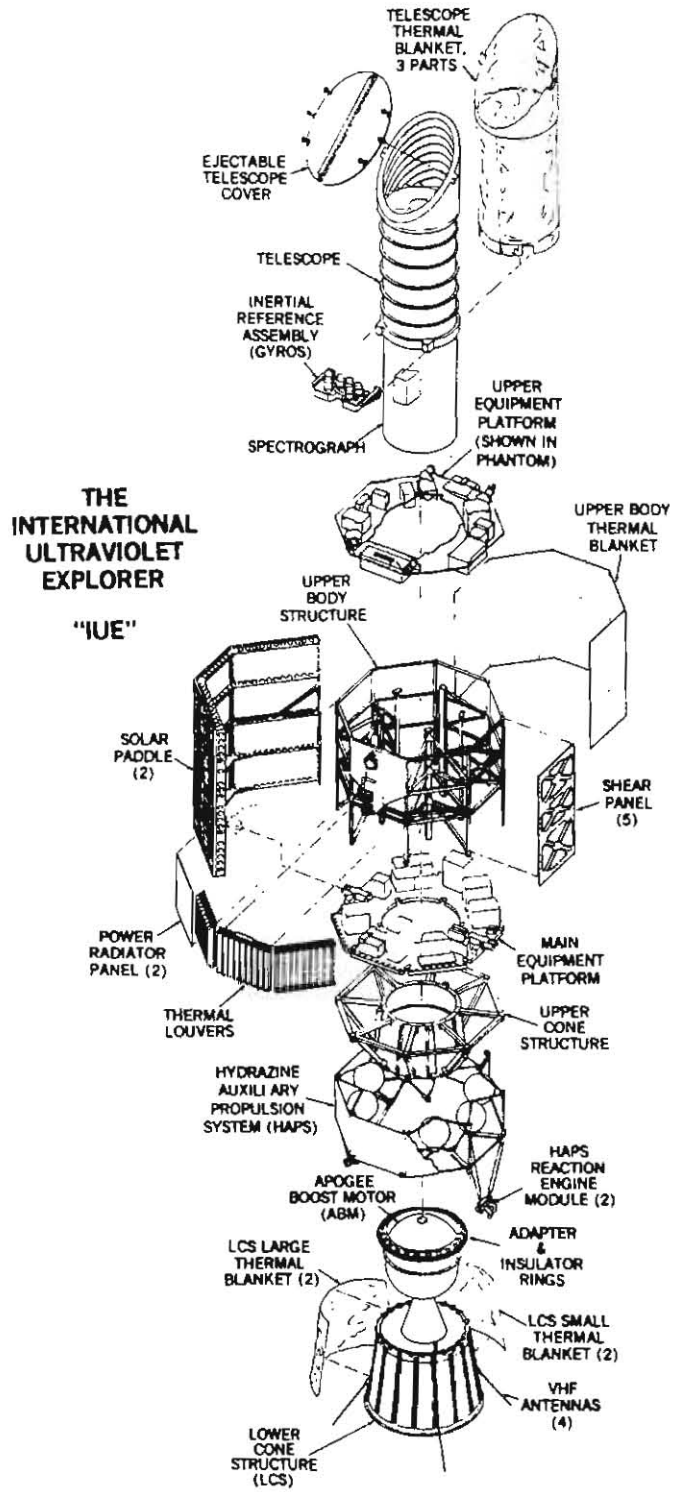


Figure 2-2. IUE Exploded View

The spacecraft's main body is octagonal in shape; and its fixed solar arrays extend outward from two opposite sides. In mission orbit, the attitude control system maintains the spacecraft orientation such that the front of the solar arrays always face toward the Sun and thermal louvers face away from the Sun. Thermal louvers, thermal blankets, heat pipes mounted to the underside of the main equipment platform, and heaters within the spacecraft main body and scientific instrument provided thermal control and maintained temperatures within acceptable ranges.

The apogee boost motor used to insert the spacecraft from transfer orbit into synchronous orbit and the hydrazine auxiliary propulsion system are both located in the lower cone assembly. The hydrazine auxiliary propulsion system was required for nutation control, precession, and despin during the transfer orbit operations and was used for Sun acquisition, reaction wheel momentum unloading, station acquisition, and east-west station keeping during the mission orbit. The hydrazine system consists of tanks, plumbing, thruster assemblies, valves, heaters, and supporting structure. The composite of this hardware forms an integrated, self contained unit.

The majority of the higher power electronics equipment is located on the main equipment platform within the main spacecraft body and adjacent to the louvers, while the experiment electronics, the attitude control reaction wheels, gyro electronics, and Sun sensor electronics are located on the spacecraft upper equipment platform.

The Scientific Instrument, consisting of the telescope and spectrograph, is mounted to the spacecraft structure by means of a strong ring. The strong ring rests on three columns which carry the load to the lower spacecraft structure and these columns are supported laterally by truss members of the main body structure.

An inertial reference assembly is mounted directly to the strong ring to simplify alignment and to minimize relative motion between the inertial reference sensor and the scientific instrument. This arrangement permitted alignment of the scientific instrument and the inertial reference assembly as an integral unit and it assures maximum precision with regard to pointing the telescope.

The inertial reference assembly was the primary rate and position sensor for the attitude control subsystem and it provided the spacecraft with position stability on the order of a fraction of an arc-second. Fine error sensors and fine Sun sensors afford the inertial reference a drift trim and highly accurate position reference capability. The fine error sensors are in fact two axis star trackers that are mounted within the spectrograph along with the vidicon cameras that were used to store the spectral images. The importance of the fine Sun sensor and the fine error sensor increased along the mission. The Two-Gyro/FSS system used the fine Sun sensor in combination with the two remaining gyros to provide three axis control. In a similar way, the One-Gyro system provided a course spacecraft stabilization using the fine Sun sensor and the last gyro, and, a fine control, adding the fine error sensor measurements.

The spacecraft characteristics are summarized in the next table.

Characteristics	Description
Spacecraft Weight	312 kg
Scientific Instrument Weight	122 kg
Apogee Motor Weight	237 kg
Launch Vehicle Adapter Weight	29 kg
Total Launch Weight	700 kg
Launch Vehicle	Delta 2914
Life	3 - 5 years
Orbit (Mission)	Elliptical Geosynchronous (28.6° inclination)
Power Required (Spacecraft & Experimentation)	210 watts average
Array Capability (Beginning of Life)	424 watts at beta equal to 67.5° 238 watts at beta equal to 0° and 135°
Batteries (2)	6 ampere-hour NiCad (17 cells each)
Telemetry Bit Rate	1.25 kbit/sec to 40 kbit/sec with fixed and reprogrammable formats
Command	PCM/FSK/AM, 800 bits/sec
Stabilization and Control	Spinning during transfer orbit, 3 axis stabilized with better than 1 arc-second control for mission orbit.

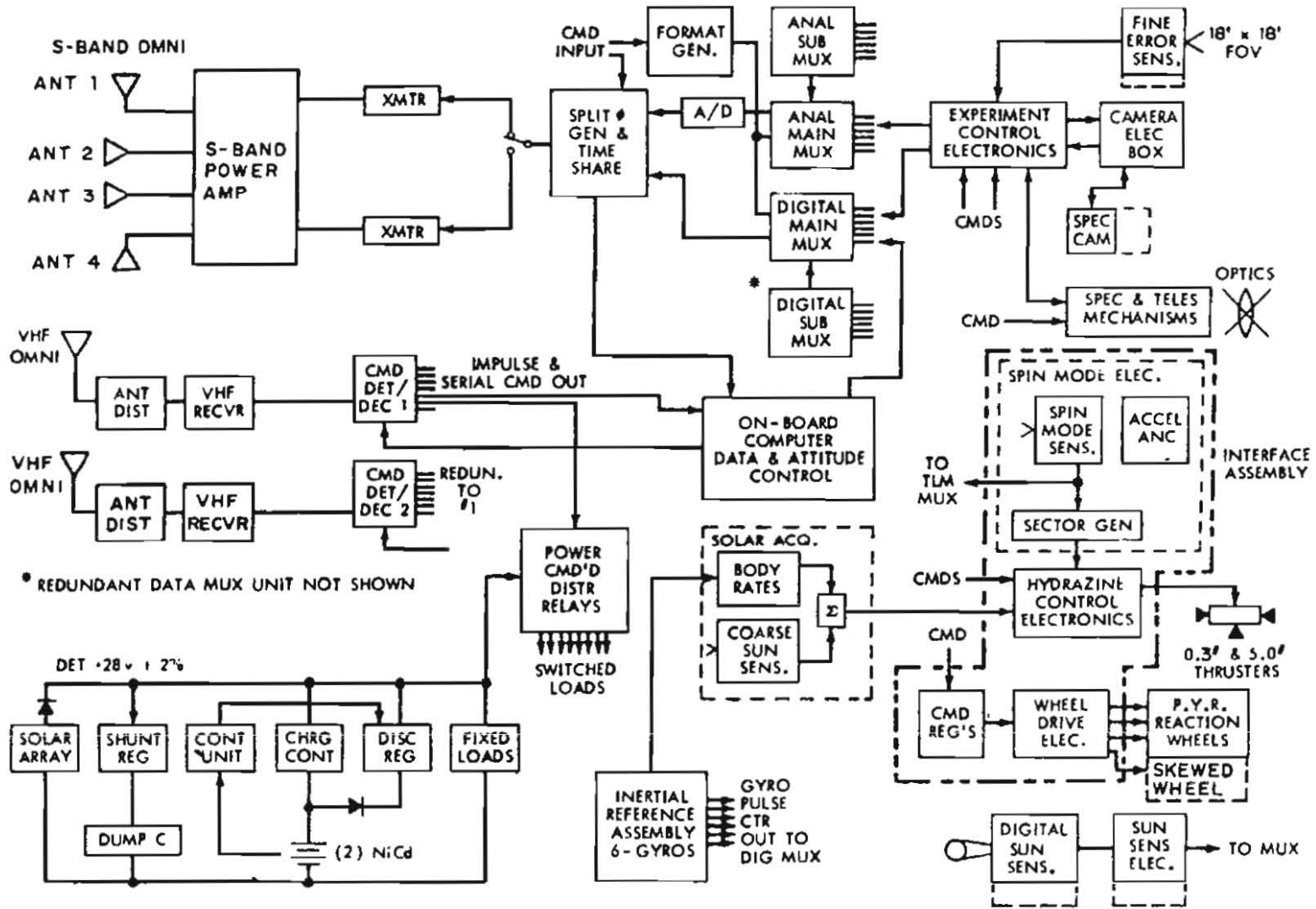
Spacecraft subsystems.

The major subsystems that are required to support the operation of the scientific instrument as well as the spacecraft itself include the power, communications, command and data handling, and stabilization and control subsystem.

The figure 2-3 is an overall system block diagram. Duplication is used extensively to ensure long term reliability.

In the discussion that follows, each of the major spacecraft subsystems is described. More details about each subsystem are given in section 5, where the technical characteristics are explained, as well as the evolution of the mission and the anomalies experienced.

Figure 2-3. IUE System Block Diagram.



Power was provided by two solar arrays and a highly efficient distribution and regulating system. During eclipse, and other periods when demand exceeds solar array output, power was provided through a boost regulator from two 6 ampere-hour nickel-cadmium batteries.

The communications subsystem consists of VHF transponders, S-band transmitters, RF amplifiers and antennas. The characteristics of the VHF and the S-band systems are summarized in the next table.

	VHF	S-band
Transmitter frequency	138.860 MHz	2249.80 MHz
Power output	6 watts.	6 watts.
Modulation	PCM/FSK/AM	PM
Telemetry rate	800 bit/sec	1.25 kbit/sec to 40 kbit/sec with fixed and reprogrammable formats
Antenna polarization	Turnstile	Circular
Antenna pattern	Omnidirectional	60° conical
Receiver frequency	148.980 MHz	-
Receiver sensitivity	-106 dBm	-

The S-band system was used only for transmission of telemetry data. The two transmitters can be connected to any of four power amplifier antenna combinations, but only one transmitter and one power amplifier may be selected at any one time and this will depend on which antenna has the most favourable view of the Earth. The VHF system consists of duplicate transponders and a four-element turnstile antenna and was used for the reception of ground generated commands, the turn-around transmission of range and range-rate signals for tracking the spacecraft, and also to provide a backup telemetry down-link.

Commands initiated by the onboard computer or received directly from the ground are all processed by the two command decoders.

The data handling system is composed of the data multiplexer and the onboard computer. The data multiplexer serves as the spacecraft telemetry encoder and as the input data interface between the onboard computer and the rest of the spacecraft. 8-bit words are transferred to a serial data stream which is alternately made available to the ground and to the onboard computer using time sharing techniques. The telemetry bit rate was selectable by ground command from 1.25 to 40 kbit/sec.

The onboard computer performed all attitude control computations and issued all reaction wheel torquing commands. It performed self-checks, monitored spacecraft performance safety functions, controlled camera exposure times and stored commands.

The stabilization and control system was used in orbital maneuvers which include station keeping, pointing, and maneuvering of the spacecraft. It has three different reference systems:

- Six gas-bearing, pulse rebalanced, inertial-grade gyroscopes providing 0.01 arcseconds integrated rate resolution over 600 arcseconds per second.
- Star trackers (the FESs) in the scientific instrument which use the telescope optics to provide an angular resolution of 0.27 arcseconds throughout a 16 arcminutes field-of-view. Comet Hyakutake as seen by IUE's FES is displayed in figure 2-4.
- A two axis digital Sun sensor (FSS) which provides angular resolution to 15 arcseconds over a field-of-view of $64^\circ \times 124^\circ$.

When a bright star is within 9 arcminutes of the target source, the guidance system used the FES for position information and the gyro system for rate damping. When a guide star was not available, precision-hold depended solely on a well-trimmed gyro reference with low frequency updates from the target or other source. The One-Gyro system always needed the FES to provide fine control.

The control system used a set of momentum exchange reaction wheels for attitude control and relied on the hydrazine thrusters for momentum dumping.

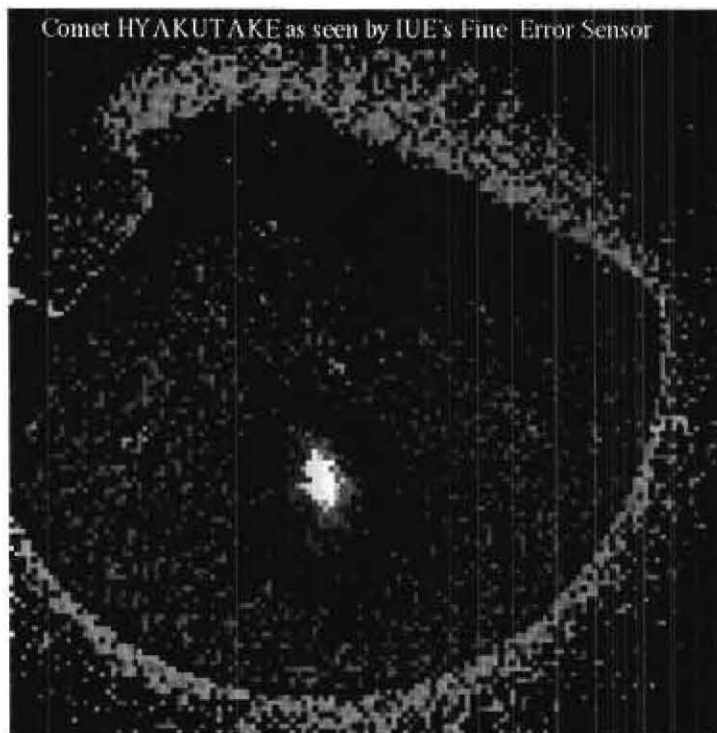


Figure 2-4. Hyakutake FES image (March 26, 1996).

The active thermal control system used louvres, insulation, heat pipes and heaters. Multi-nodal analysis of a thermal model and solar simulation tests were used to prove the design. The spacecraft may be divided into five sections, each with unique thermal requirements: the hydrazine bay, the main spacecraft compartment, the telescope, the spectrograph and the solar arrays.

Ground observatory control systems.

Unlike previous unmanned astronomy spacecraft, IUE was operated in real-time by guest observers who generally lacked detailed knowledge of the complex spacecraft and ground systems. Ground operating procedures were, therefore, designed to allow the observer's research programme to be accomplished by selection from a library of modular preprogrammed operating sequences.

IUE ground control was based on a large real-time computer software system to process telemetry and commands. Relatively complex spacecraft operations were accomplished by calling a series of operating procedures, each designed to accomplish a particular function, such as reading an image from a camera. Procedure execution was controlled by trained spacecraft controllers. A computerized image processing system was then run offline to correct the astronomical images and produce a spectrum in absolute units as a function of wavelength. The processing sequence consisted of geometric and photometric correction, wavelength identification, data extraction and system efficiency correction and used calibration tables derived from period analysis of calibration images.

The next figures shows the last IUE images taken on September 27, 1996, and their extracted spectrum.

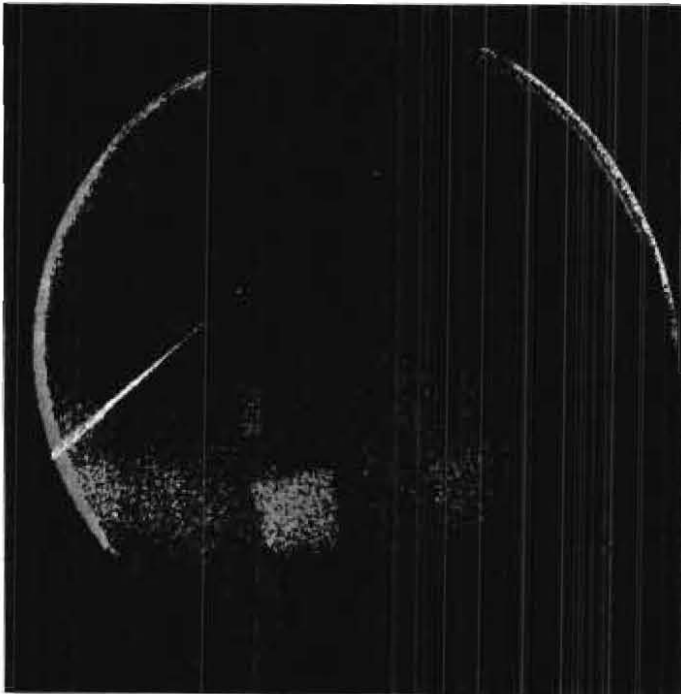


Figure 2-5. SWP 58388 raw image.

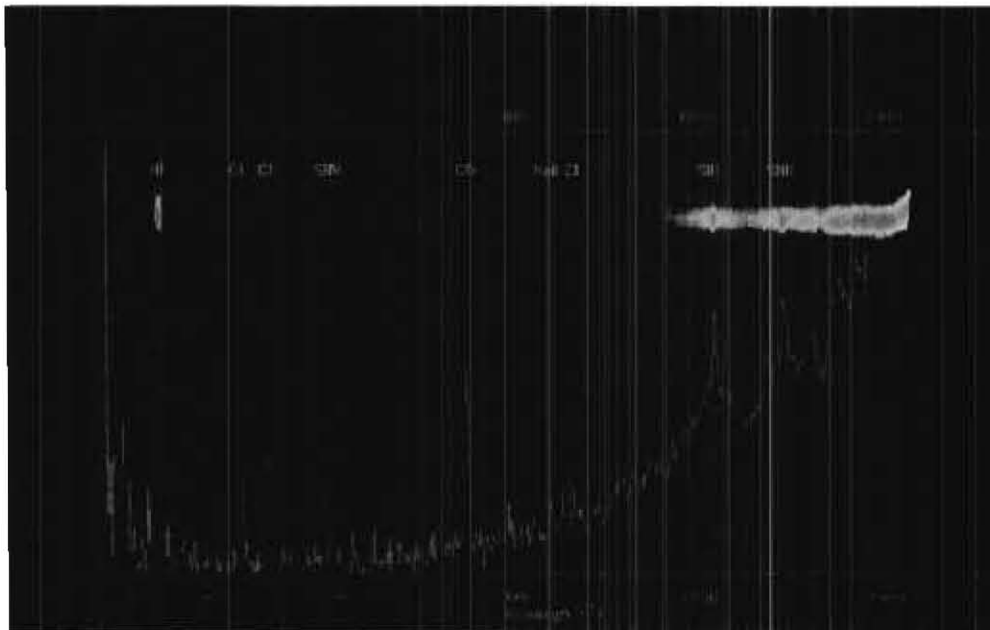


Figure 2-6. SWP 58388 extracted spectrum.

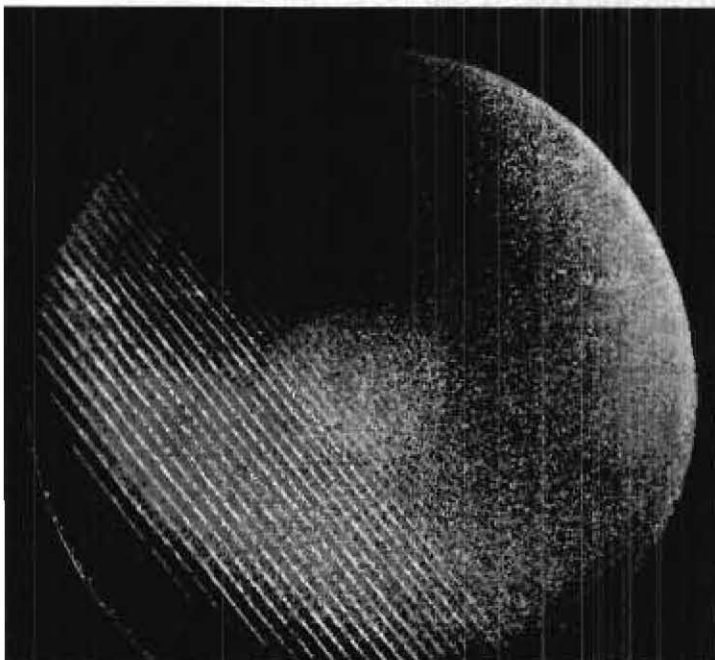


Figure 2-7. LWP 32696 raw image.

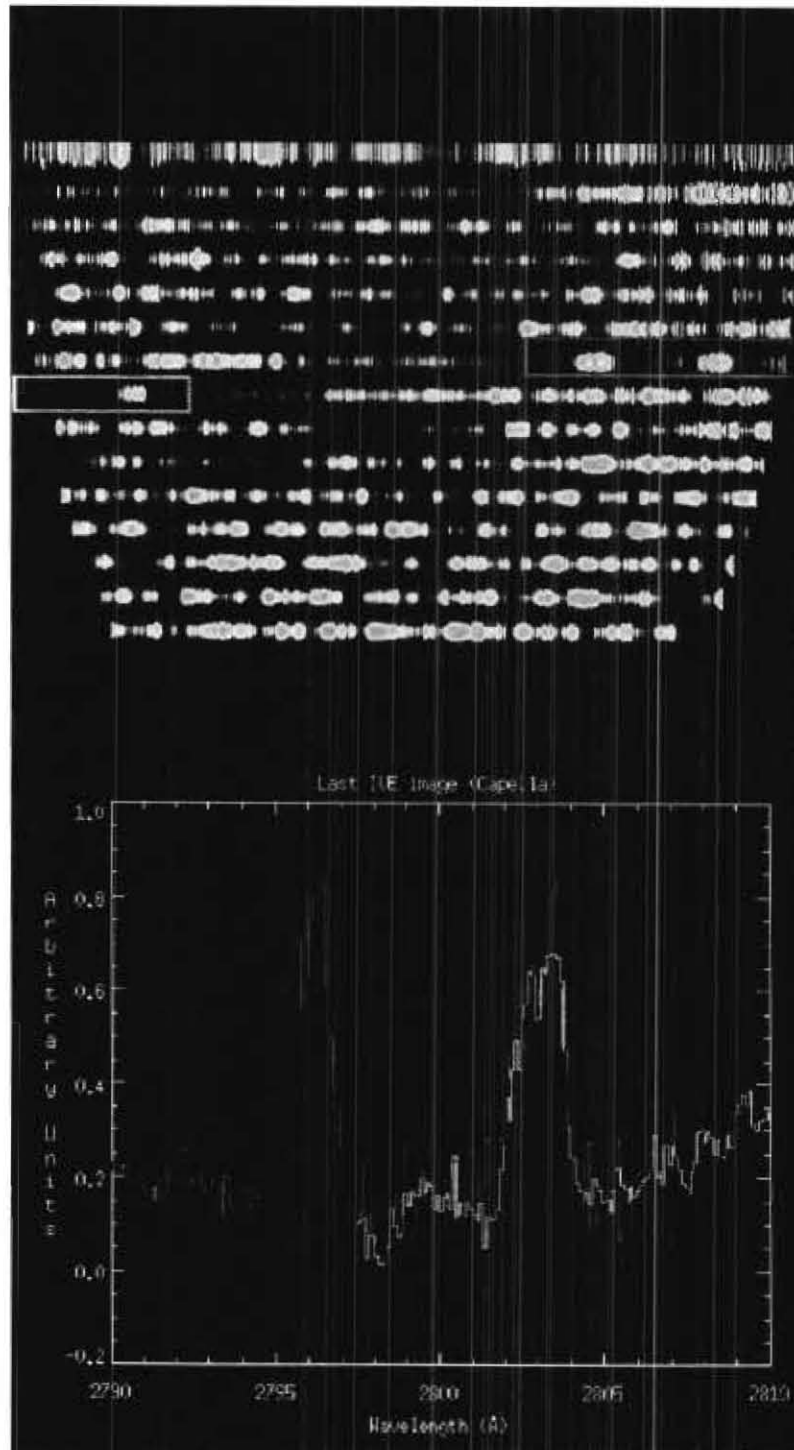


Figure 2-8. LWP 32696 extracted spectrum.

3. Operations highlight summary

1978

January 26.

The International Ultraviolet Explorer was launched, at 17:36 UT, with an initial plan of revolving around the earth three times for a transfer orbit and then boosting to geosynchronous orbit.

January 27.

Due to high temperature, the apogee boost motor firing took place at 14:54 UT and placed IUE into geosynchronous orbit after the first intermediate revolution. This early transfer phase was flawless.

January 28.

The following events were carried out successfully,

- Despin.
- Solar array deployment.
- Sun acquisition and sun hold shortly.

The launch and early orbit phase was terminated at 12:36 UT.

January 29.

The PAS#1 failed due to a shift register malfunction. The redundant PAS was put into use.

January 30.

Camera and focus mechanism were checked out. Primary and secondary mirror heaters as well as camera deck heaters were switched on at 14:30 UT.

The telescope dust cover was ejected successfully at 16:20 UT.

The OBC began to indicate problems due to a violation of an operating constraint prohibiting a 16:1 multiplex ratio (1.25 kbps rate).

January 31.

The first major slew to the north ecliptic pole was initiated at 15:43 UT and ended at 16:25 UT.

AT 19:14 UT the spacecraft lost OBC control due to an unknown reason caused by OBC Worker-0, and the s/c attitude was lost.

LWR camera was switched on at 17:59 UT and configured in standby mode.

February 1.

SWR camera was switched on at 11:30 UT and configured in standby mode.

Initial switch on of FES#1 was conducted at 15:51 UT. The first FES image collected from IUE containing 1 star of approximately 11 magnitude.

February 3.

Calibration images were collected from the LWR and SWR cameras.

February 5.

The initial switch on of the LWP camera was performed.

February 9.

The first spectrograph image was received at VILSPA, containing the LWP high resolution spectrum of target "CAPELLA".

The Scientific Instrument was tested: camera check-out, in-flight camera reoptimization, photometric calibration and intensity transfer function (ITF) calibration.

February 13.

A malfunction of the LWP camera (the scan control logic anomaly) was detected. The scan beam did not sweep as expected during read mode.

February 19.

The SWR camera experienced some voltage drops.

February 21.

The FES#2 was declared the prime FES. By design FES#1 received 30% of the impinging stellar flux and FES#2 received the 70% portion.

March 27.

Solar array temperature sensors showed erroneous indications.

April 3.

The routine observations started. LWR and SWP were declared prime cameras.

July 24.

A 3 gyro software matrix was uplinked to the OBC. This was done to determine the feasibility of running on 3 gyros during IUE's second shadow season in order to save power.

September 23.

A malfunction of the SWR camera was detected in the GRID-1 voltage, which is a part of the camera read electronics.

1979**March 14.**

Gyros 2, 4 and 6 were turned off as a part of shadow preparations. The OBC 8K memory was loaded with 1, 3 and 5 gyro matrix. It saved the spacecraft 17 watts of power, improving the power profile during shadow.

April 18.

Gyro 6 failed to start when the three gyros 2, 4 and 6 were turned on following shadow. Numerous attempts were made to restart the Gyro 6 spin motor but all were unsuccessful.

May 29.

An OBC HIT protection was entered in the 4K memory back-up. An OBC hit was a specific type of corruption to hardware stored values in the OBC, which usually resulted in an OBC crash (see section 5.6.5.)

June 20.

Another unsuccessful attempt was made to restart Gyro 6.

August 1.

The Gyro 6 heater was set to high, 5 hours prior to another attempt to turn on this gyro again. A command to turn on the gyro during a maneuver was sent when the ABG on the slewing axis was one degree. This permitted the maximum amount of oscillation and torque from the wheels during the 27 seconds that the gyro starting voltage was applied. This attempt to restart Gyro 6 was unsuccessful.

October 25.

An intermittent change of aperture locations in the FES#2 was noted, when the expected drop of light did not take place while moving targets into the small apertures. It was assumed that the FES electrical characteristics changed or a mechanical shift of the aperture faceplate took place. This problem was called the FES reference point shift anomaly (see section 5.5.7.2).

November 8.

As a result of the information obtained from the last three OBC dumps acquired after crashes in previous months, the OBC software was patched in 33 locations.

1980**January 2.**

The FES reference point shift anomaly was seen again. The problem was not found to be a mechanical shift, but was thought to be related to the FES electronics.

January 9.

The OBC was patched to collect data to study the HIT problem.

January 29.

The OBC was patched again. In this case, the NO-OP instruction in the idle task loop was changed to a HALT in order to save power and lower the OBC temperature.

March 31.

The NO-OP was reinstalled in the OBC. Evaluation of engineering data indicate no reduction in power and temperature with the new configuration. Since the NO-OP instruction greatly reduced bus noise, the decision was made to return to the previous one.

May 27.

The Command Decoder#1 was used as prime in order to investigate the cause of various command anomalies (see section 5.2.1.).

June 12.

The OBC and radiation monitor were powered down as a result of a failure in Command Decoder#1 and the spacecraft attitude was lost. Decoders were switched again putting Decoder#2 in use.

December 15.

HAPS heater group number 1 failed to warm up after it was switched on, the redundant one (HAPS heater group number 2) was used.

1981**January 21.**

The OBC was reset following an OBC crash. Upon start up the OBC automatically selected the Command Decoder#1 to receive the OBC commands (see section 5.2.).

January 23.

A restart of Gyro 6 was attempted though cycling the gyro on and off every 25 seconds. This procedure had worked for two gyros on the HEAO-3 spacecraft. The turn on was unsuccessful for IUE.

February 1.

The OBC worker 7 was switched on to provide additional information for troubleshooting in case OBC hardware errors were detected.

August 9.

The temperatures of Gyros 1 and 3 had been decreasing since July 1.

August 18.

The Gyro 6 heater was powered up to heat the area, but as Gyro 2 temperature and current rose abnormally, the Gyro 6 heater was turned off in order to return the Gyro 2 to the normal state.

September 8.

Gyros 1 and 3 temperatures dropped again and maneuver accuracy continued to decline. A new OBC matrix without Gyro 1, which was considered the primary source of error, was uplinked.

September 22.

A new set of scaling factors for Gyros 1, 2, 3, 4 and 5 was uplinked to the OBC.

November 21.

A new set of scaling factors for Gyros 2, 3, 4 and 5 was uplinked to the OBC. The large errors observed after coarse maneuver termination were improved.

1982**February 23.**

Numerous OBC crashes were caused by Interrupt 14 during the last year (see Appendix C). So, a patch was uplinked to the OBC to protect against this problem.

March 2.

A new malfunction of Gyro 1 was observed when the torque rebalance loop indicated saturation. Gyro 1 was considered as being lost.

April 26.

A gradual increment of the temperature of Gyro 5 was measured. An improved gyro scale factor had to be uplinked.

May 25.

A badly decoded and executed command placed the SWP camera in an incorrect configuration (see section 5.2.1.).

July 27.

The Gyro 2 motor current increased from a nominal 60 mA to 214 mA in 9 seconds. Turning the gyro off and on was tried but nothing happened. The Gyro 2 had stalled. Gyros 3, 4 and 5 were used in the control matrix while a new system using 2 gyros and FSS began to be developed.

December 4.

A new set of scaling factors for Gyros 3 and 4 was uplinked in order to reduce the maneuver errors.

1983**January 9.**

New scale factors for gyros 3 and 5 were uplinked.

March 30.

A re-occurring flare was seen on the LWR camera images (see section 5.7.3.).

March 31.

The 2 Gyro + FSS was successfully tested with the spacecraft.

April 13.

A test with Gyro 1 was performed because its stability appeared to have improved. The test showed the gyro to still have excessive noise in its output signal.

August 31.

The undervoltage detectors on both batteries were turned off. This action was taken as a precaution because if only one cell failed, an entire spacecraft shutdown might occur.

October 16.

The LWP camera was declared the prime long wavelength camera. This was due to the LWR anomaly.

December 11.

Gyro 1 stopped spinning leaving Gyros 3, 4 and 5 as the three remaining operational gyros.

18

1984

March 16.

New scale factors were uplinked for Gyros 3 and 5.

July 16.

The spacecraft experienced a sudden unexpected change in momentum. The attitude control system was able to control the motion, but it could not be attributed to an onboard system.

July 23.

The scan control logic of the SWP camera skipped two pixels of video data during a read.

August 31.

The telescope sun shutter unexpectedly closed (see section 5.7.).

September 24.

S-Band antenna 4 began to show large fluctuations in its output power, which were directly associated with fluctuations in the power drawn by the power amplifier.

September 26.

The telescope sun shutter unexpectedly closed again.

1985

April 15.

FES#2 demonstrated anomalous behaviour. When tracking on a star of known brightness, the magnitude count fluctuated erratically (see section 5.5.7.3.).

April 30.

Both PASs were turned off.

May 15.

New scale factors were uplinked for Gyros 3, 4 and 5 to improve the maneuvering accuracy.

June 16.

FES#2 star magnitude count variation were observed again when the fine error sensor was configured in fast track underlap mode.

July 17.

New scale factors were uplinked for Gyros 3, 4 and 5.

August 17.

Gyro 3 failed at approximately 05:00 UT. The spacecraft had to be placed in sunbath and scientific operations were suspended.

Attempts to restart gyros 3 and 6 were unsuccessful.

August 18.

The 2-Gyro FSS back-up control system was loaded into the 8K OBC and testing began.

August 28.

PAS#2 was tested and found that it no longer worked.

September 30.

The observing program was restarted.

October 4.

FES#2 counts fluctuated erratically.

October 9.

Sun shutter closed without being commanded shut.

November 26.

The sun shutter was commanded closed but remained in the 'slew' mode. It was reopened and closed successfully.

1986**January 9.**

FES#2 displayed more anomalous behaviour.

May 14.

A patch was made to the OBC in an attempt to keep the roll axis in a fine control mode as well as to reduce power consumption when the OBC uses the FSS to control that axis.

August 31.

Sun shutter closed without being commanded.

October 7.

A new control system (the 1-Gyro/FSS control system) was developed to be used in case of another gyro failure.

1987**January 20.**

Battery#1 raised suspicion on its performance. Tests were carried out and batteries proved to be operational. The Battery#1 third electrode was giving an anomalous signal so it was a bad charge indicator.

It was recommended that charge/discharge operations be done without using third electrode voltages as full charge indicators or to provide charge control.

April 28.

A bad scan was detected on the LWP camera, it was a known camera malfunction. The ground system software was prepared to detect and correct this condition automatically.

November 30.

Another bad scan was detected on the LWP camera.

1988**March 9.**

FSS gave corrupt data while the spacecraft was slewing. The attitude control was lost.

A study was made as to the viability of switching to the backup heads on each FSS system, but the collected data showed this configuration to be as bad as the prime one (see section 5.5.2.1.).

July 29.

During an attempt to promote discharge of the batteries, both PASs were commanded on, but only PAS#1 responded by drawing current. Analysis of the data suggested a relay failure.

November 28.

The spacecraft attitude control degraded into oscillations as a result of the beta 75° crossover point of the FSS. The problem corrected itself when the dangerous region was left (see section 5.6.5.).

December 1.

Worker 3 was uplinked to the spacecraft. Tests of the new code showed it to work but it was not used because cycling the cameras so rapidly could damage them.

1989**September 5.**

FSS gave corrupt data while the spacecraft was slewing. The maneuver had to be stopped by ground command.

October 2.

A new wheel unload program was used to reduce the frequency of required Delta-Vs, by selecting the most favourable momentum-wheel unload jet firings to counteract the westward drift of the spacecraft.

1990**February 22.**

The third electrode on Battery#1 was turned off.

March 10.

The Gyro 5's drift rate changed abruptly.

March 19.

The third electrode on Battery#2 was turned off (see section 5.1.2.).

May 25.

A new configuration was used in the power system due to the Battery#1 degradation and third electrode malfunction: Battery#1 Main Charger ON, Battery#2 Low Trickle Charger only and both batteries 3rd electrode OFF (see section 5.1.2.1.).

August 26.

"Top-off"s were performed on a weekly basis on Battery#1 to ensure a full charge on this battery (see section 5.1.2.).

October 17.

The engineering testing of the 1-Gyro attitude control system was completed. A spacecraft test was performed successfully.

November 1.

Sun shutter closed without being commanded shut.

December 9.

FSS gave corrupt data while the spacecraft was slewing. The maneuver had to be stopped by ground command.

December 18.

The OBC had to be restarted due to a synchronization problem with the data received from the DMU.

1991**January 27.**

Several FES images of different stellar fields showed a large background event. This problem was called the FES Scattered light anomaly (see section 5.5.7.4.).

February 5.

The current reading coming from Gyro 5 dropped to 0 amps and remained there. However Gyro 5 continued to work properly.

May 14.

The FPM began to produce erratic data.

July 24.

The flux level in a LWP camera image was about 25% below expected for unknown reasons. This problem was named the LWP flux anomaly (see section 5.7.3.).

July 30.

Appreciable scattered light in the FES camera at approximately 13 magnitude level was seen again.

1992

May 23.

The Gyro 5 drift rate increased abruptly.

September 14.

The FES level of contaminated light experienced a strong increase. The behaviour of this problem was different than the previous light in several aspects. It was called the FES Streak light anomaly (see section 5.5.7.5.).

1993

April 26.

Some special maneuvers about the roll axis were performed to evaluate the cause of the FES Streak Light problem. They did not produce any solution.

1994

October 4.

The Gyro 5's drift rate changed abruptly.

October 24.

Raw values of some telemetry points changed to a fixed value (159) during periods of high OBC temperature and while the spacecraft was in 1B format. This was called the DMU anomaly (see section 5.4.1.).

1995

January 1.

The raw values of some other telemetry points changed to 63.

January 8.

The corrupted number 159 began to appear in the spectrograph images.

August 5.

A sudden drop of -10 dBm in S-Band PA#4 down-link signal strength was observed.

1996**March 6.**

Gyro 5 was switched off by a faulty command and could not be restarted. Several attempts to restart the Gyro 6 were also unsuccessful.

The spacecraft had to be placed into Sunbath mode and the scientific operations were suspended.

March 11.

The 1-Gyro system was loaded into the OBC. The spacecraft came back under the OBC control with only one remaining gyro.

April 4.

The observing program was restarted.

May 10.

FSS corrupt data produced a brief loss of attitude control and a loss of attitude several times, due to the new control law not being able to recover from the corrupted data condition (see section 5.5.2.1.).

September 30.

All remaining hydrazine was vented. The batteries were discharged and switched off when their voltages reached 17 volts. The radio frequency transmitter was turned off at 18:44 UT.

4. ORBIT

IUE was successfully launched on January 26, 1978 at 17:36 UT on a Delta launch vehicle.

The spacecraft was placed into geosynchronous orbit through one stage of spin-stabilized flight and two stages of three axis-controlled flight. Prior to the Delta third stage burn for injection into the transfer orbit, the spacecraft and third stage assembly were spun-up to 60 rpm by the Delta spin table. After injection from the parking orbit into the transfer orbit and separation from the Delta's third stage, an automatic nutation control (ANC) system on the spacecraft was initiated because the moment of inertia ratio with respect to the spin vector was unfavourable. This spin mode lasted about 21 hours. Along the transfer orbit, range and range rate (R & RR) measurements were made to accurately predict the orbit and time of apogee motor firing. Additionally precession of the spin vector was determined to align the apogee motor in the proper direction for boost into the synchronous orbit. At apogee, the motor was commanded to ignite by ground command.

When the desired station was obtained, the spacecraft was despun in two phases to gain three-axis gyro rate control. In the first phase, the IUE was spun up to 2 to 5 degrees per second, and the solar arrays were deployed. In the second phase, the IUE was rate damped to 0.25 degrees per second. The early orbit phase was concluded after the spacecraft was aligned with the sunline normal to the primary plane of the solar arrays.

The orbital elements measured on January 27, after the geosynchronous orbit was reached, were exceptionally good.

	Predicted	Actual
Semi-Major axis (a):	42164 km	42156 km
Eccentricity (e):	0.250	0.239
Inclination (I):	28.7 degr.	28.63 degr.
Argument of perigee (ω):	257 degr.	257.04 degr.
Period (P):	23.93 hrs	23.927 hrs
Perigee height (Pe):	25230 km	25669 km
Apogee height (Ap):	46340 km	45887 km

The mission requirements specified GSFC visibility time had to be 24 hours per day and VILSPA visibility time had to be at least 10 hours per day, these were satisfied with these orbital elements. To maintain these requisites, station keeping maneuvers (Delta-V) had to be performed periodically throughout the mission. In this way, the science operations were conducted 16 hours per day from GSFC and 8 hours per day from VILSPA until September 30, 1995. On this date, the spacecraft operation changed, VILSPA conducted science operations 16 hours per day and GSFC maintained the spacecraft health and safety the remaining 8 hours. This new distribution, which was called Hybrid Operations, needed different visibility conditions which were achieved with extra Delta-Vs.

Like all other satellites, the IUE orbit is described by Kepler's law. To describe the motion of an object in a Keplerian orbit, a standard set of 6 orbital elements is used. Five elements are needed to describe the shape, size and orientation of the orbit, and one is needed to pinpoint the satellite along its orbital path. In addition to these laws, there are certain physical forces acting on an

orbiting object that will cause changes in all orbital parameters. These perturbations may be generated by several sources, including gravitational effects (from the Earth, Moon or Sun), atmospheric drag, or solar pressure.

Following is a list of the 6 major orbital elements along with a brief explanation of each term. Also shown for each element is a graph illustrating how it evolved over the life of the spacecraft.

- **Semi-Major Axis (a).** The semi-major axis is defined as the average of the apogee and perigee radii of an orbit. It is measured in km and specifies the size of an orbit (figure 4-1).

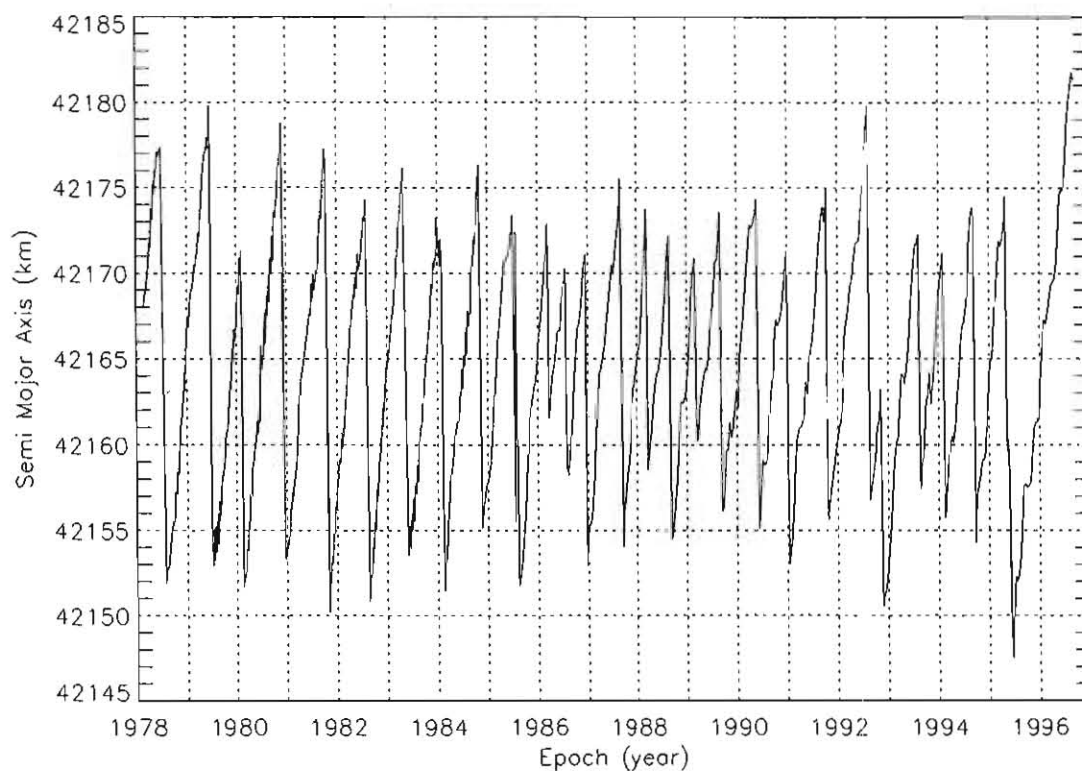


Figure 4-1. History of semi-major axis.

- **Eccentricity (e).** The eccentricity is defined as the difference between the apogee and perigee radii divided by their sum. This parameter specifies the shape of the orbital ellipse and is dimensionless (figure 4-2).

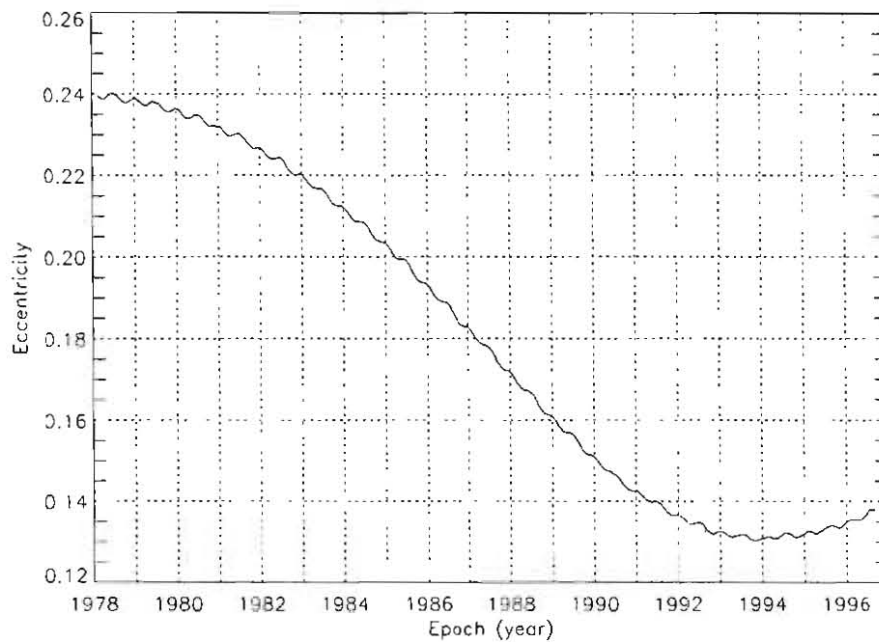


Figure 4-2. History of eccentricity.

- Inclination (I).** The inclination of an orbit is the angle between its angular momentum vector and the Earth's North pole. It is also known as the angle between the orbital plane and the Earth's equatorial plane. This magnitude is measured in degrees (figure 4-3).

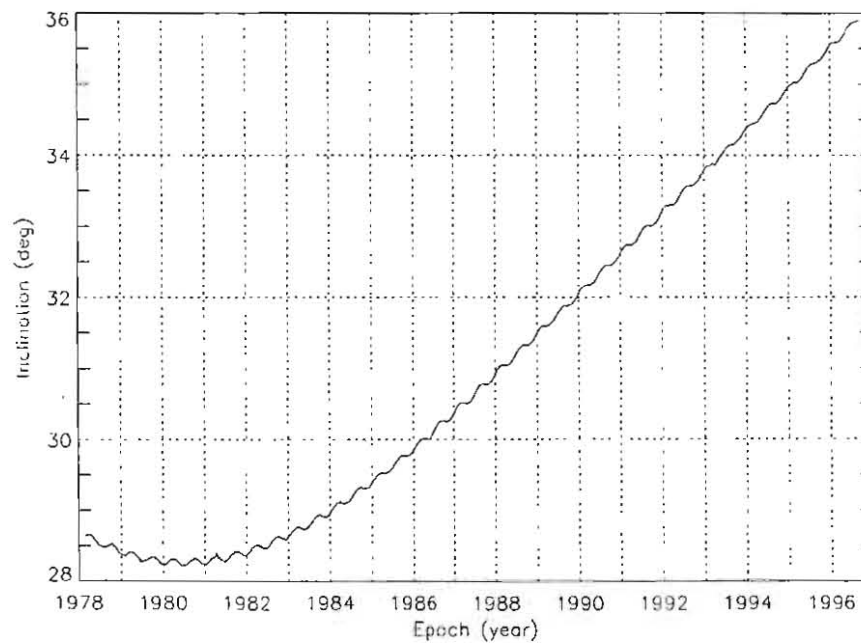


Figure 4-3. History of inclination.

- Right Ascension of the Ascending Node (Ω).** The RA of the Ascending node is a measurement (in degrees) from the Vernal Equinox (Right Ascension = 0°) to where the orbital plane and the Earth's equatorial plane intersect. The measurement is made counterclockwise from RA= 0° to where the orbital plane makes its south to north crossing of the equatorial plane (figure 4-4).

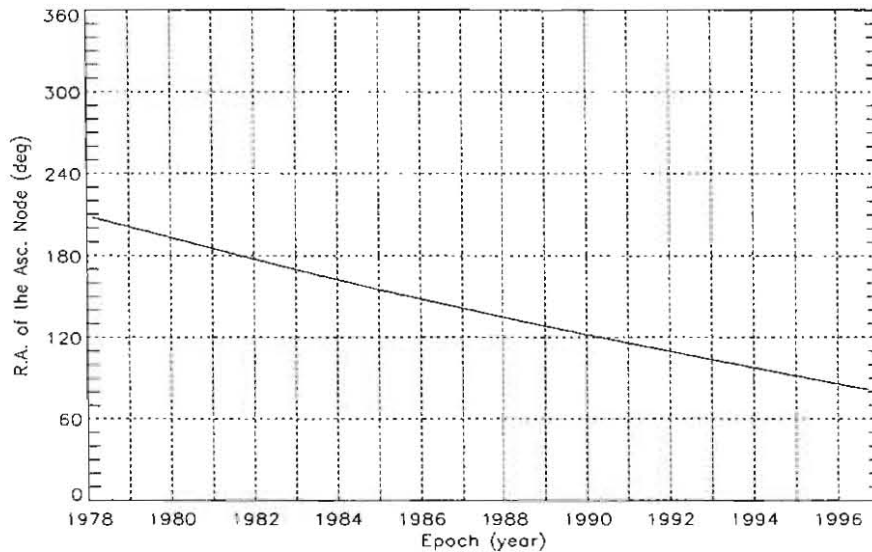


Figure 4-4. History of right ascension of the ascending node.

- Argument of Perigee (ω).** The argument of perigee is the angle between the Ascending node of the orbit and orbit perigee. It is measured in the direction of travel of the spacecraft and in the plane of the orbit in degrees (figure 4-5).

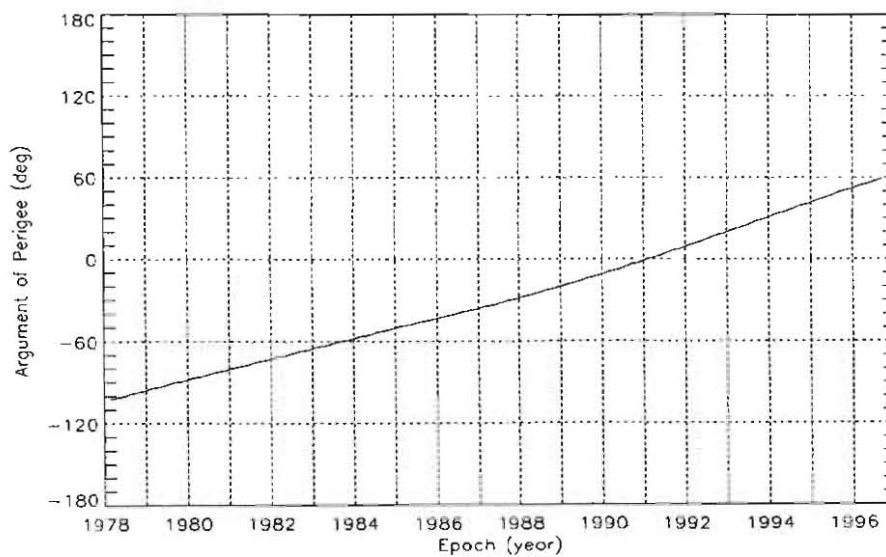


Figure 4-5. History of argument of perigee.

- **Mean Anomaly (M).** The mean anomaly represents the position of the spacecraft relative to its ascending node at a given time. It is measured, like the Argument of Perigee, in the direction of travel of the s/c and in the plane of the orbit in degrees (figure 4-6).

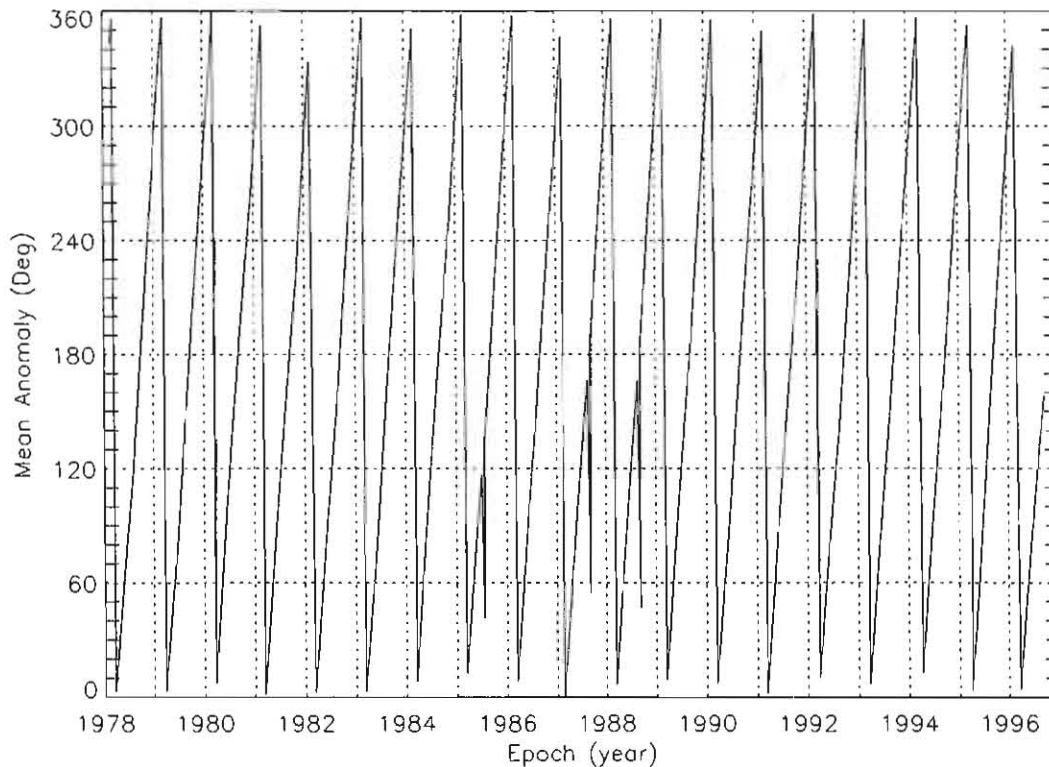


Figure 4-6. History of mean anomaly.

Orbit Perturbations.

Below is a brief explanation of some of the forces acting on an orbiting object and their impact on IUE.

- ▶ **Atmospheric Drag.** For IUE the Earth's atmosphere is not a factor as its perigee is approximately 30,200 km. The atmospheric drag has a significant effect for satellites below 1000 km.
- ▶ **Earth Gravitational Forces.** The deviation of the Earth from a perfect sphere is mainly responsible for the changes seen in the Right Ascension of the Ascension Node, Argument of Perigee, Mean Anomaly, and for the westward drift of IUE's ground trace. This perturbation produces the changes in visibility which are corrected with Delta-Vs.

- ▶ **Lunisolar Gravitational Forces.** The lunisolar gravitational forces takes into account the effects on an orbit produced by the gravitational pull of the Moon and Sun. These forces contribute to the long-term changes in the Right Ascension of the Ascending Node and the Argument of Perigee, and also produce long-term changes in inclination and eccentricity. The figures 4-7 and 4-8 show the predicted changes and the measured ones.

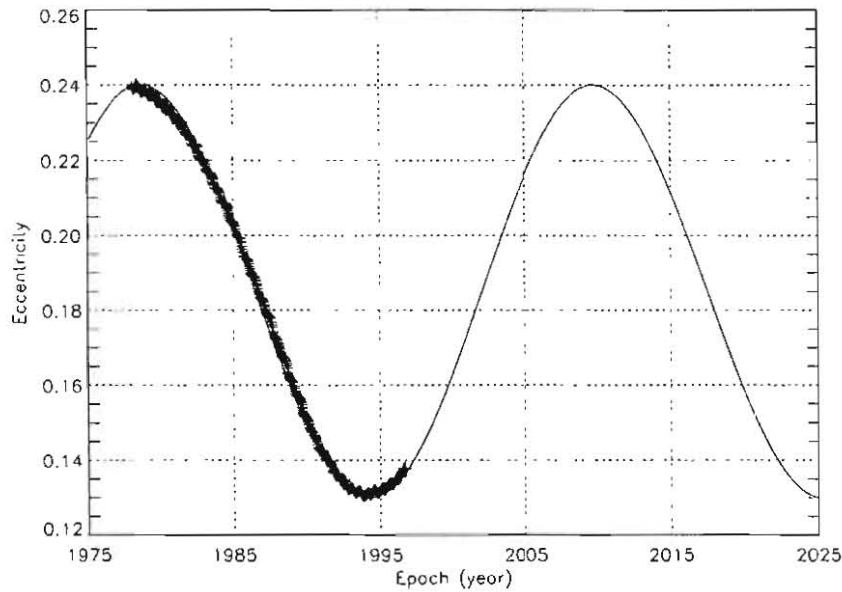


Figure 4-7. Predicted Long-Term Changes in IUE Orbital Eccentricity.

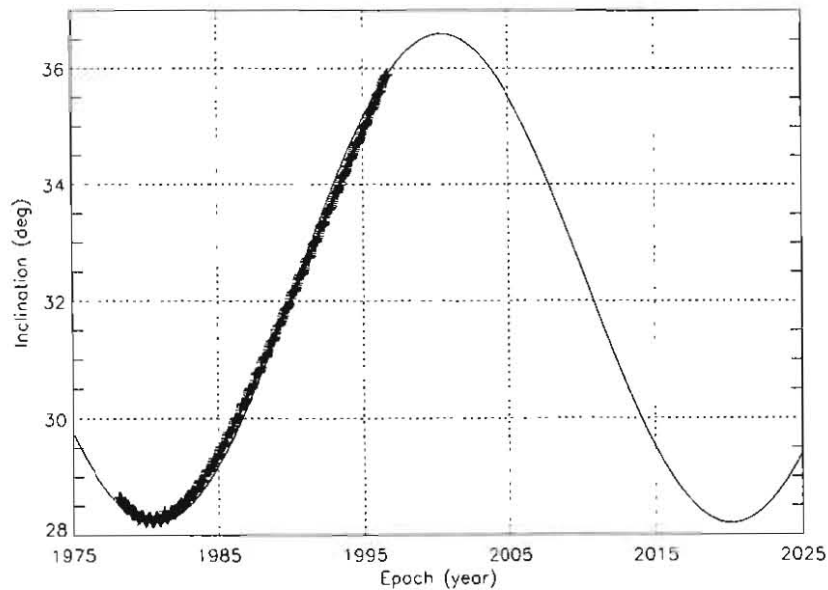


Figure 4-8. Predicted Long-Term Changes in IUE Orbital Inclination.

- ▶ **Solar Radiation Pressure.** The sun is constantly emitting radiation, which induces perturbations on the orbit. The radiation pressure from the Sun imparts a continual force on the spacecraft which has the effect of performing a small Delta-V. Six months later the change in the Sun and the IUE geometry will produce similar forces in the opposite direction. The eccentricity and inclination undergo periodical changes during the year as shown in the figures 4-9 and 4-10.

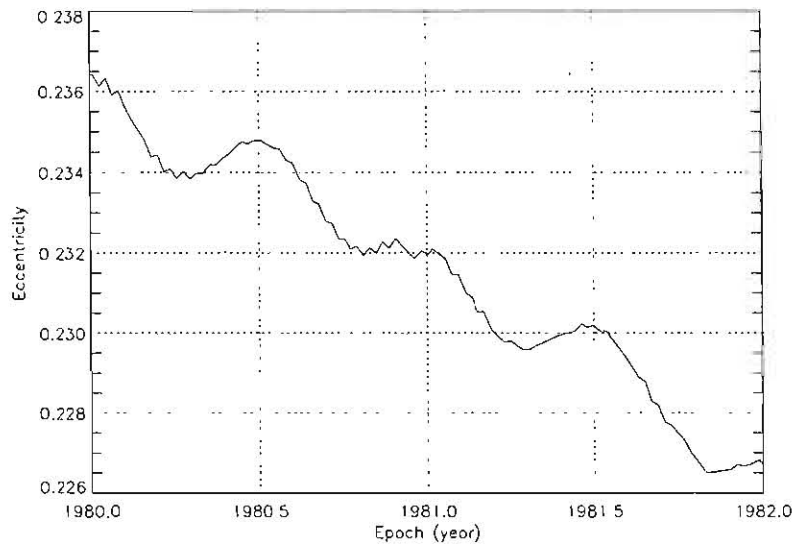


Figure 4-9. Periodical changes in eccentricity.

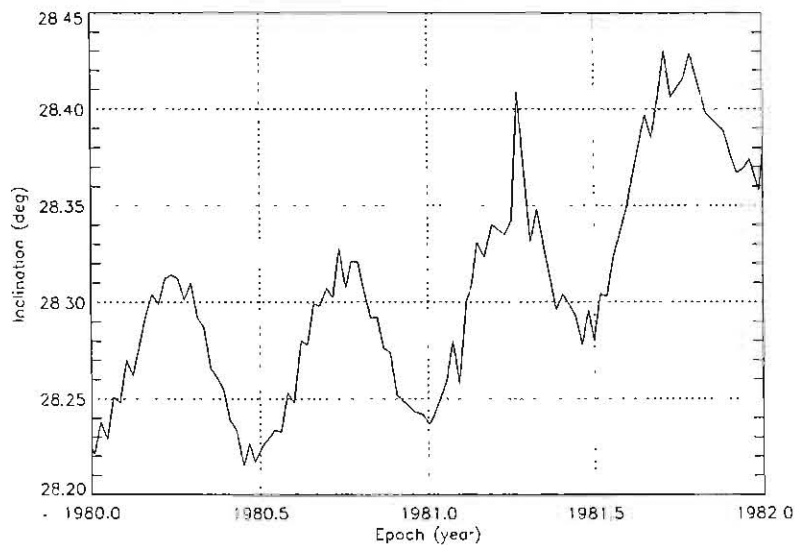


Figure 4-10. Periodical changes in inclination.

The ground trace continually changed from launch until the end of the IUE program. The next figures are examples of the IUE ground trace on twelve different dates. In the figures, there is also a line which represented the VILSPA visibility region for a 3° antenna elevation.

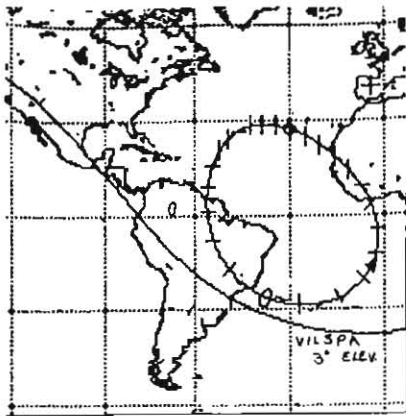


Figure 4-11. Ground trace at 01/30/1978.

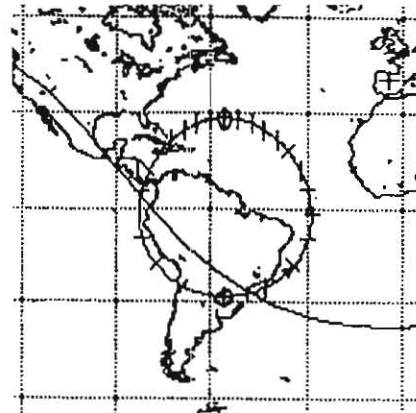


Figure 4-12. Ground trace at 01/01/1980.

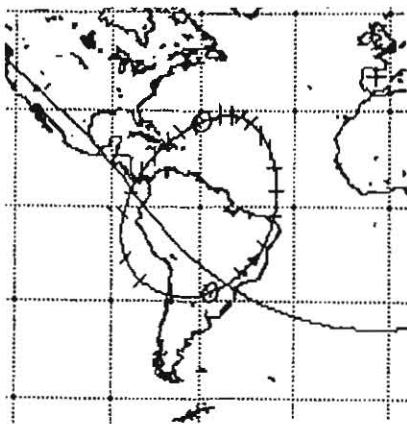


Figure 4-13. Ground trace at 01/01/1982.

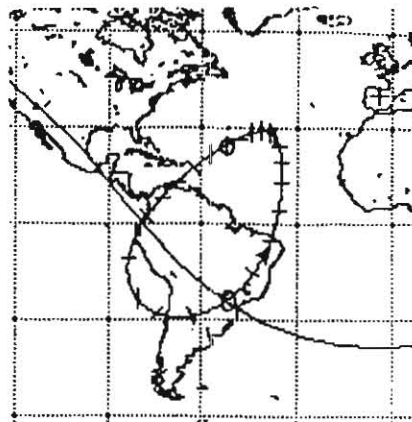


Figure 4-14. Ground trace at 01/01/1984.

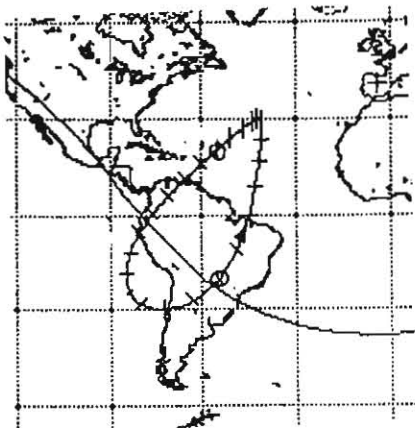


Figure 4-15. Ground trace at 01/01/1986.

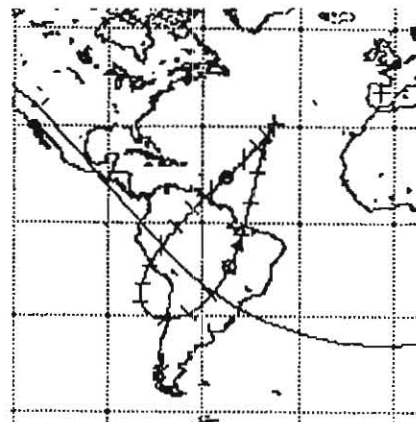


Figure 4-16. Ground trace at 01/01/1988.

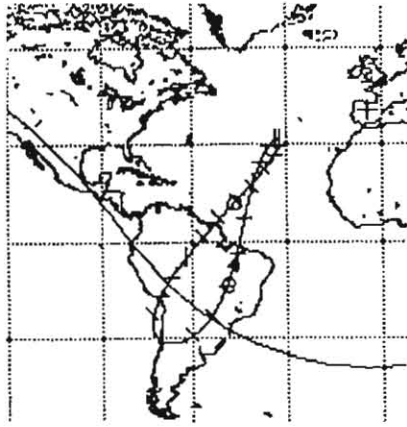


Figure 4-17. Ground trace at 01/08/89.

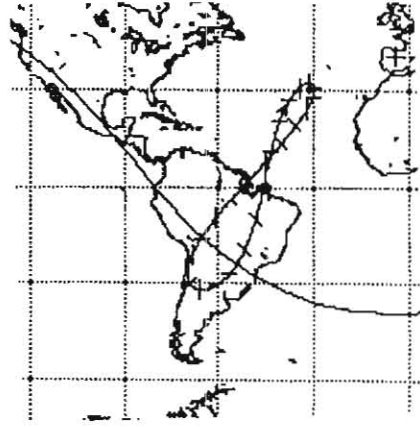


Figure 4-18. Ground trace at 01/09/1990.

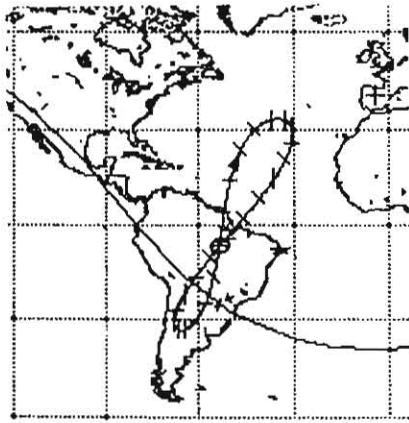


Figure 4-19. Ground trace at 01/08/1992.



Figure 4-20. Ground trace at 01/08/1994.

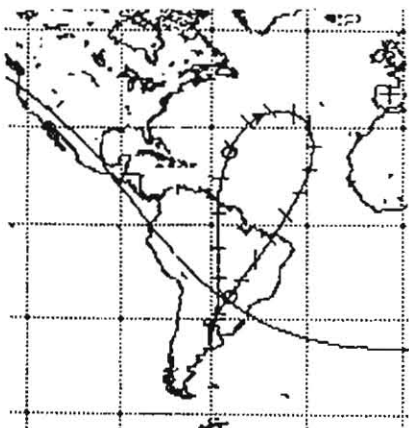


Figure 4-21. Ground trace at 01/10/1995.

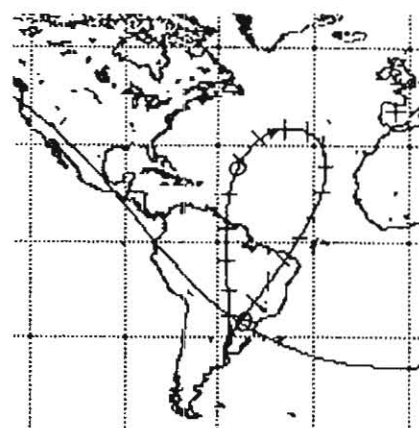


Figure 4-22. Ground trace at 07/09/1995.

4.1. Orbital corrections (*Delta-V*)

The major in-plane perturbation is caused by the ellipticity of the Earth, which causes large in-plane angle oscillations of the spacecraft around the closest minor axis of the equatorial section. The Earth's minor axis (which contains a stable point at either end) is located at 255.3 degrees east longitude and 75.3 degrees east longitude. As the IUE was located around 300 degrees east longitude, the spacecraft was drawn to 255.3 degrees east longitude, which is to the west of its position. This constant westward drift had to be countered periodically to maintain the station operations by performing Delta-V maneuvers. In this way, the ground trace of IUE could be normally kept between longitudes of 270 and 330 degrees west until September 30, 1995, as shown the figure 4-23. After that, the longitude position was further altered, to around 340 degrees, to increase the VILSPA visibility as the hybrid operations mode required.

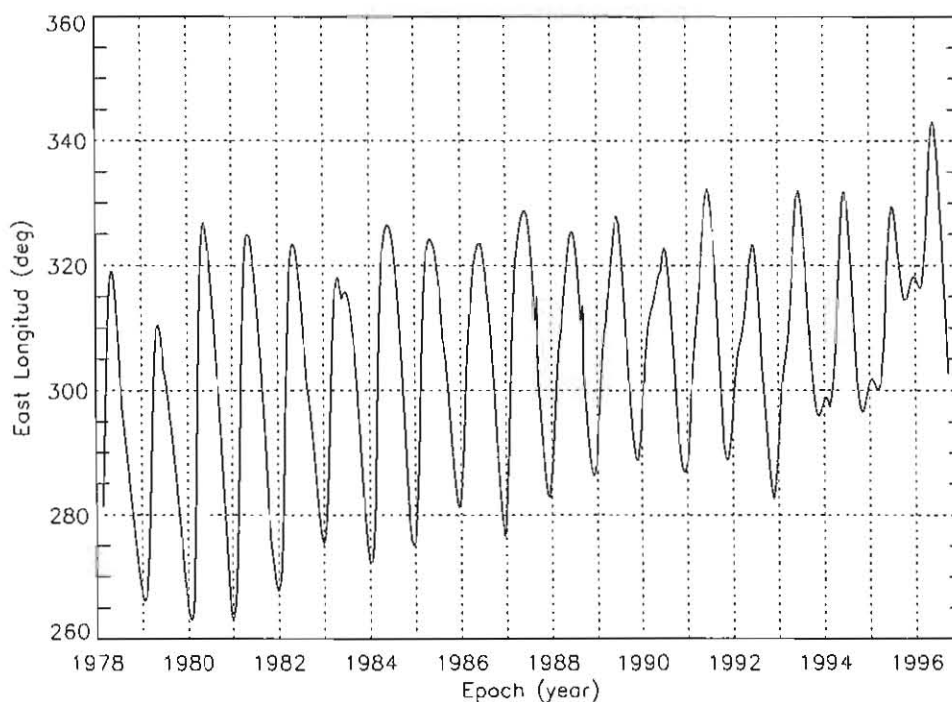


Figure 4-23. History of east longitude.

Along the spacecraft life, thirty Delta-V maneuvers were successfully performed (see Appendix B) and only two had to be aborted during their execution due to an OBC software malfunction.

A normal Delta-V was carried out by firing two 5 pounds thrusters, jets 2 and 8 (see section 5.5.9. and section 5.6.), during a time less than 15 seconds, to minimize the stress of the thrusters. An OBC program (Worker 19) performed both the burn and the attitude control. This program also used the low thrust jets to maintain the attitude control during the burn.

5. SUBSYSTEMS

The International Ultraviolet Explorer can be divided into five subsystems which are required to support the operation of the scientific instrument as well as the spacecraft itself.

Complete details of these subsystems and the behaviour of their components along the spacecraft life are presented in succeeding sections; however, the five subsystem with brief summaries, are as follows:

- **Power subsystem.**

The power subsystem provides all the necessary electric power to the IUE and can be divided into two areas: batteries and solar panels.

- **Command subsystem.**

IUE deals with two redundant command decoders which process all commands received from ground (via radio frequency subsystem) and the OBC.

- **Communications subsystem.**

The radio frequency subsystem provides for all communications to and from the IUE and the ground stations. This subsystem consists of both S-Band and VHF transmitters and a VHF receiver.

- **Data handling subsystem.**

The data handling subsystem consists of data multiplexers, and the **onboard computer**. This subsystem encodes both spacecraft and scientific instrument telemetry. The OBC performs the attitude control system computations and issues control commands.

- **Attitude control subsystem.**

This subsystem provides IUE attitude control. The ACS can be divided into eight areas: reaction wheels, gyros, fine error sensors, coarse sun sensors, fine sun sensors, **onboard computer**, control electronics assembly and hydrazine auxiliary propulsion system.

All these subsystems were needed to provide a real-time observatory that was capable of obtaining both high and low resolution spectra.

The **Scientific Instrument** consists of the 45-cm Ritchey Chretien telescope, the fine error sensor, the echelle spectrographs and the cameras: two redundant long-wavelength and two redundant short-wavelength cameras. The SI is required to perform high resolution ($\approx 0.1 \text{ \AA}$) and low resolution spectroscopy ($\approx 6 \text{ \AA}$) in the spectral region between 1150 \AA and 3200 \AA .

5.1. Power Subsystem

The power subsystem on the IUE spacecraft is a direct energy transfer (DET) system. The primary source of power is the spacecraft solar array which consists of two deployable paddles mounted to the spacecraft structure. Power from the solar paddles is transferred directly to the spacecraft bus which is regulated at +28.0 volts $\pm 2\%$. The lack of any series elements between the solar array and the spacecraft loads provides for a transfer of array power to the loads at nearly 100 percent efficiency. Power during solar eclipses and other periods when demand exceeds solar array output is provided by two 6 ampere-hour nickel-cadmium batteries through a boost regulator. The power supply electronics (PSE) is of modular design and consists of two power modules operating in unison through a mission adapter module (MAM). The PSE conditions the outputs from the two power sources, the solar array and the batteries, at +28.0 volts $\pm 2\%$.

Three modes of operation had been defined, depending on the available solar array power and the spacecraft load requirements, which are referred to as power positive, power negative and power neutral.

- ▶ Power positive. The solar array power is greater than the spacecraft load. In this case, the PSE will first provide battery charge current and then dump the excess array power through the use of dump resistors attached to shear panels that are located on the antisun side of the spacecraft.
- ▶ Power negative. The spacecraft load exceeds the solar array output, so the difference in power will be supplied by discharging the batteries through the boost regulator.
- ▶ Power neutral. The spacecraft load is equal to the solar array power. In this case, the PSE will be in a non desirable mode called dead-band.

The IUE power subsystem was designed to support transfer and mission orbit operations during three years with a five year design goal. In order to assure this objective, the design was influenced by the following basic requirements: use of conventional solar conversion/energy storage system with proven design techniques, use of redundant units where necessary to assure maximum confidence in achieving design goal, standardization of basic subsystem functions for maximum commonality with other spacecraft design were required and inhibition of automatic switch over to redundant units because of reliability considerations.

5.1.1. Solar array

The solar array was supplied by ESA with the design and development under the control of the European Space and Technology Centre (ESTEC). It is comprised of two rigid solar cell paddles with three panels on each (one central panel, 70.5 cm X 54.8 cm, and two lateral panels, each 70.5 cm X 67.8 cm). The lateral panels are attached to opposite sides of the central panel with each lateral panel plane making a 45° angle with the central panel plane. In the launch configuration, the solar paddles were stowed wrapped around the spacecraft body. After IUE was transferred into geosynchronous orbit, they were deployed along the pitch (Y) axis, rotated, and locked at a 22.5° angle with respect to the spacecraft roll (X) axis. The plane of each array is perpendicular to the XZ plane of the spacecraft. The orientation of the spacecraft is controlled

such that the sun is always in the XZ plane.

Each array panel has a honeycomb-type construction. There are 4980 2 cm x 2 cm silicon solar cells bonded to the array structure with silicon adhesive. The cells are 0.02 cm thick and have a resistivity of 1 ohm per centimetre. The cover glasses are 0.01 cm thick cerium-doped microsheet and provided protection for the cells against immediate catastrophic radiation damage. To improve wiring reliability and reduce the risk of a short circuit on the 28-volt main bus, it was found preferable to mount blocking diodes in the spacecraft. Multiple wires link the diode board to all subpanels, ensuring current equalization in the pins of the connectors. One single connector is used per paddle. Each paddle is also equipped with temperature sensors, although four of them failed soon after launch. This had no effect on spacecraft operations.

The current generated by the solar cells is affected on a temporary basis by solar illumination and temperature and, in a permanent way, by radiation damage.

- **Solar Illumination.**

The illumination of the solar array is most directly influenced by the angle beta (angle between the sunline and the roll axis). So, the maximum output is at beta equal to 67.5° where the sunline is normal to the surface of the central panels.

Also influencing the solar illumination of the array is the solar intensity, which follows a $1/r^2$ law based on the distance between the earth and the sun. The solar intensity is greatest in January when the earth is closest to the sun and least in July when the earth is farthest from the sun, as shown the figure 5-1.

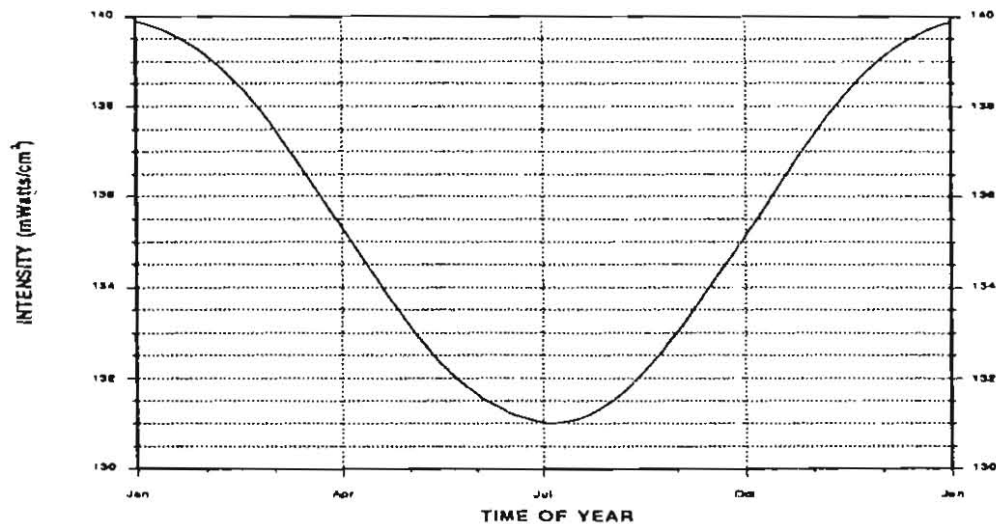


Figure 5-1. Solar Intensity vs. Time of Year.

- **Temperature.**

The current and voltage characteristics of the solar array are influenced by temperature. An increase in temperature causes a slight increase in cell current but a significant decrease in the voltage.

The figure 5-2 shows the data gathered while the temperature sensors were operational.

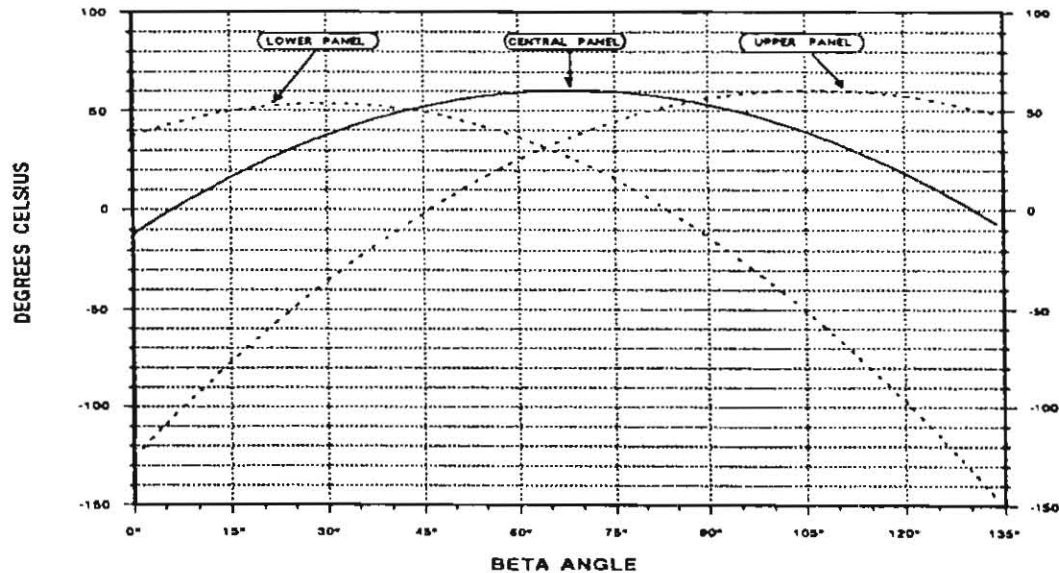


Figure 5-2. Solar Panel Temperatures.

Radiation Damage

Solar radiation varies from year to year and has a great influence on the level of solar array degradation. For example, the solar cycle maximum around 1989 produced a 9.74% reduction in power output capability, measured from February 1989 to February 1990, while the average degradation produced between consecutive years until this date had been 2.8%.

The figure 5-3 shows a history of the solar array output from launch to the end of life. Raw data were collected in the allowable beta range for each year. An equation designed to take the geometrical design of the solar array into account was used to produce best fit values from the collected data, as the raw telemetry values had been proven to be inaccurate.

$$I_{SA} = I_1 + s + v + 0.0086 (I_s + s + v)$$

Where,

I_{SA} is the actual solar array output

I_1 is the solar array current as read from telemetry

I_s is the spacecraft current as read from telemetry

s is 0, 0.014 or 0.028 amps depending on whether 0, 1, or 2 s-band transmitters are on

v is 0, 0.023 or 0.046 amps depending on whether 0, 1, or 2 transmitters are on

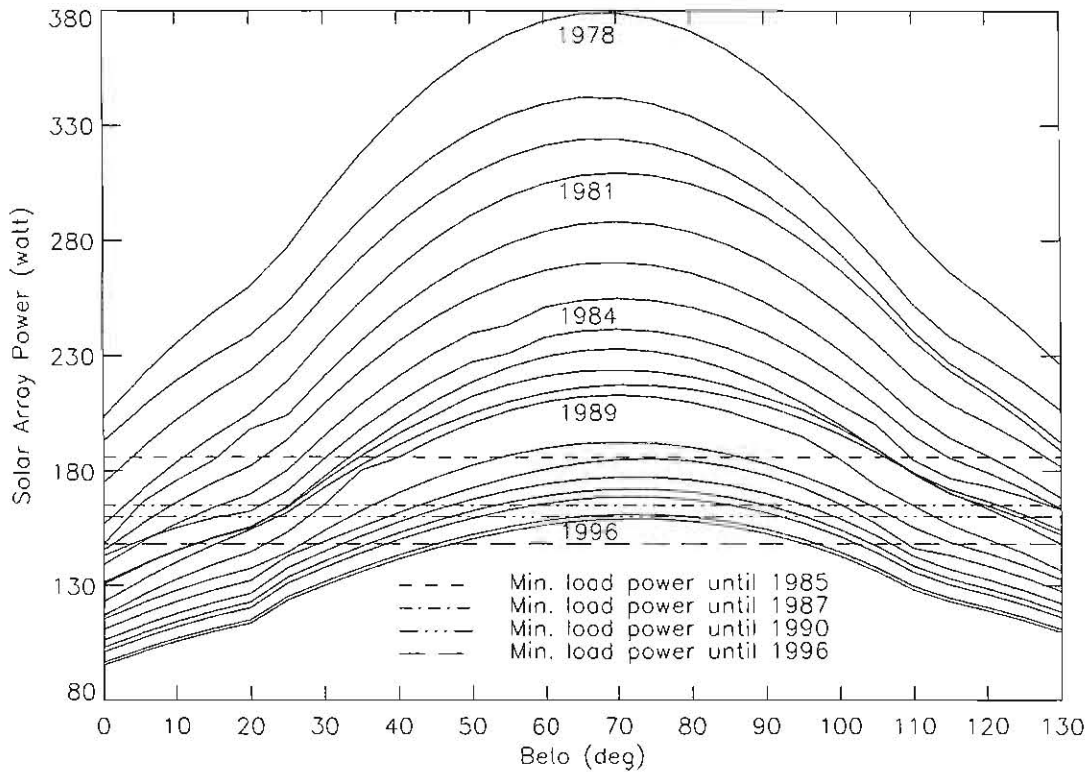


Figure 5-3. History of average solar array output.

The annual degradation computed at beta 67° is shown in the figure 5-4. The degradation has always been under the pre-launch expected value of 10% per year.

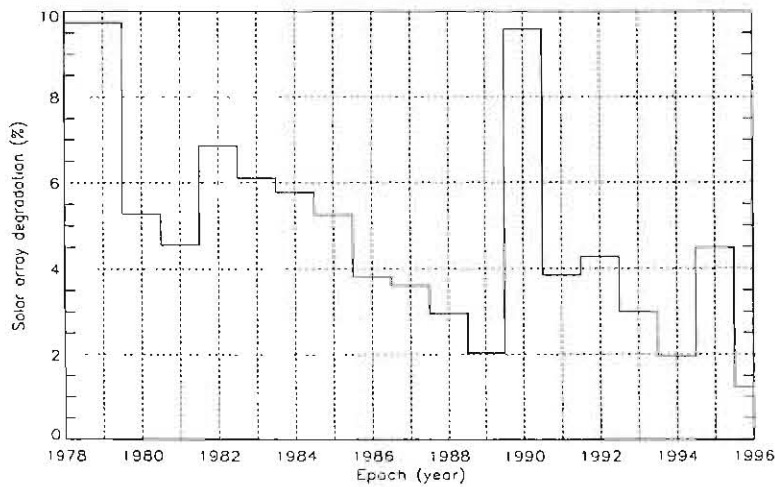


Figure 5-4. History of solar array degradation.

Solar array #1 has been producing slightly more than solar array #2 since launch, as shown in the figures 5-5 and 5-6 (this data was measured on September 29, 1996).

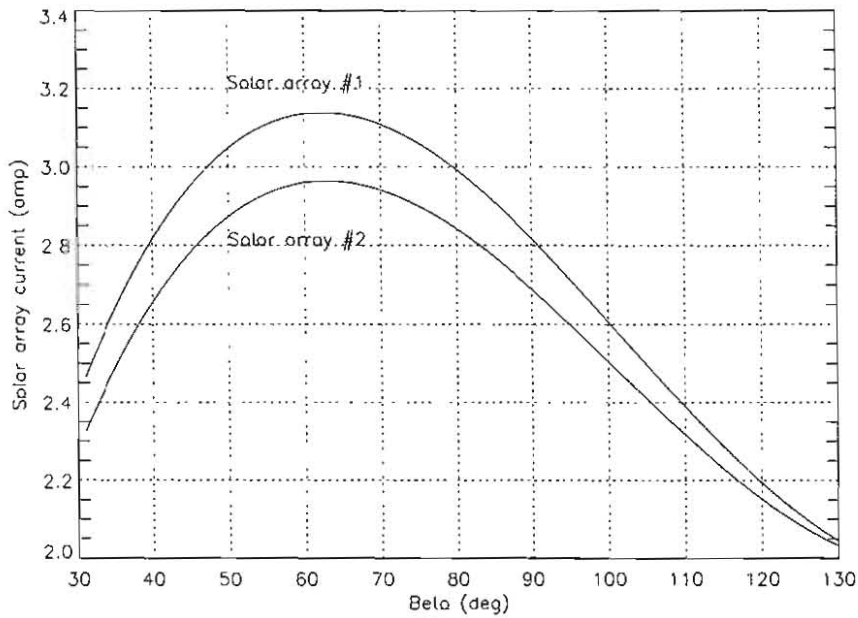


Figure 5-5. Solar array 1 and 2 output on September 29, 1996.

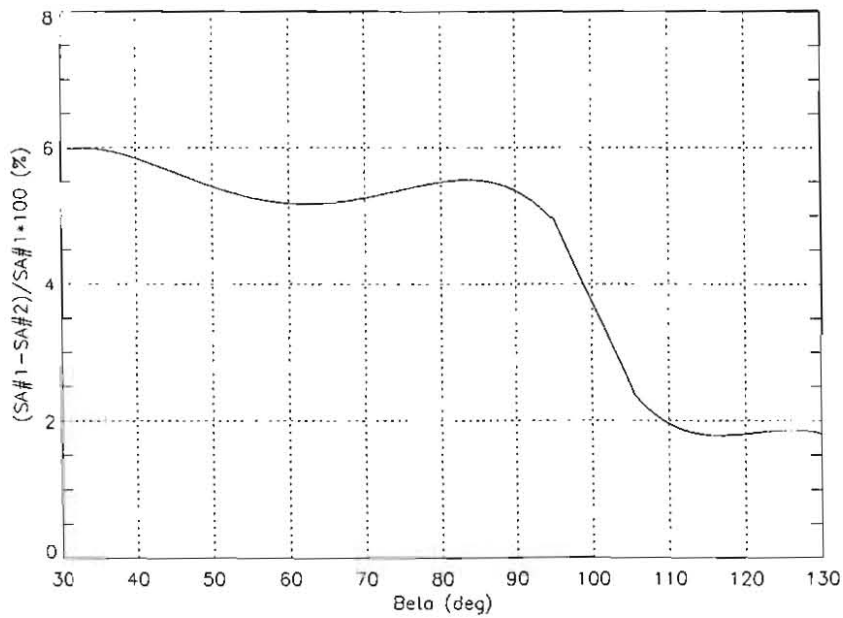


Figure 5-6. Comparison between solar array 1 and 2 vs. Beta.

5.1.1.1. Beta restrictions

The operational beta range continually decreased from the beginning to the end of the spacecraft life due to power and thermal restrictions. The power positive beta range is defined as the beta range where the solar array current is greater than the spacecraft load. Along the IUE life, the spacecraft load was decreasing due to several changes in the control mode and the failure or degradation of several devices. The power positive beta ranges for each February and the average spacecraft load in the correspondent year are shown in the table below.

Year	Beta Range	S/C load (watt)
1978-1984	24° - 120°	186
1985	25° - 115°	186
1986	25° - 121°	165
1987	25° - 120°	165
1988	24° - 120°	160
1989	28° - 112°	160
1990	30° - 112°	160
1991	31° - 113°	148
1992	31° - 112°	148
1993	30° - 109°	148
1994	35° - 103°	148
1995	41° - 102°	148
1996	41° - 102°	148

5.1.1.2. Solar array EOL characterization

The Solar Array Characterization was performed on the 29th of September in 1996, it was a part of the plan for the IUE End Of Life operations. The test consisted of collecting solar array current measurement while maneuvering the spacecraft from 31° to 130° beta angle. Throughout the life of IUE the solar array data has been collected only at the beta angles permitted during planned science operations, which has provided data points within a limited region (roughly 40° - 100°) centered on the power positive range of sun angles. In this EOL test the spacecraft supplied a more complete set of data which added the last values on the total radiation dosage experienced by the IUE. These data (shown in figure 5-7) provided a unique set for possible comparison to the current models of the radiation environment. The discontinuities at approximately beta 58° and 90° are caused by thermal variations experienced by the solar arrays resulting from the manner in which the spacecraft was maneuvered in collecting these data.

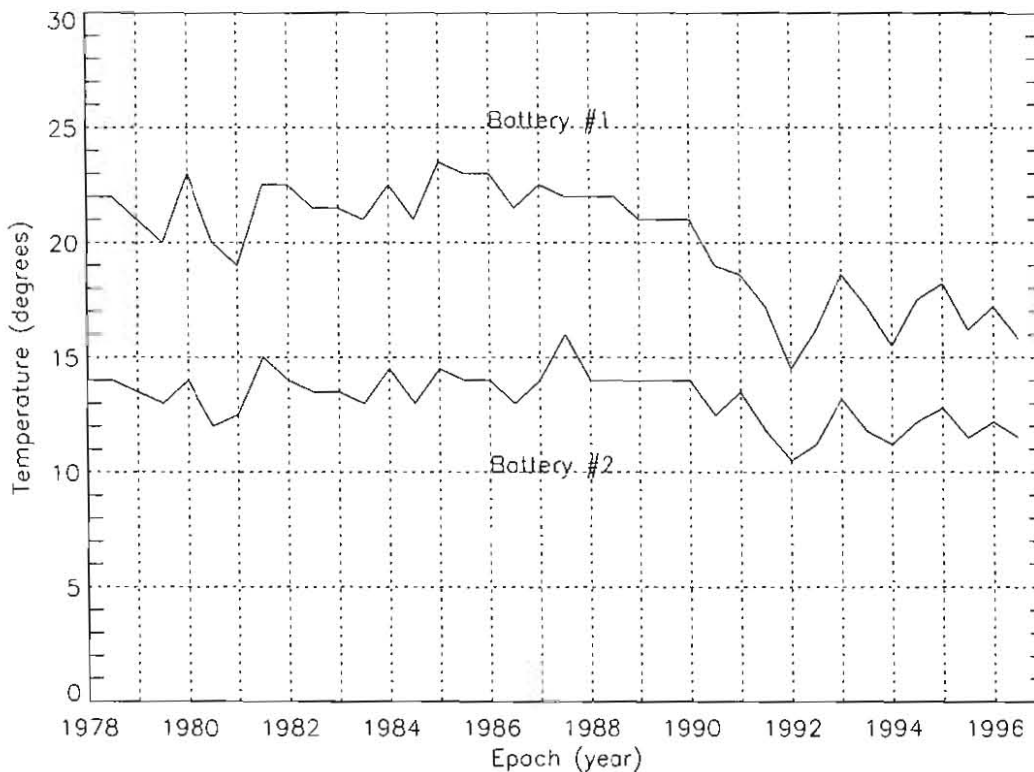


Figure 5-7. Solar array EOL characterization.

5.1.2. Batteries

The IUE power subsystem uses two nickel-cadmium batteries interfaced through the mission adapter module in a parallel discharge/independent charge configuration. The batteries have 6 ampere-hour capacity and are used to power the essential loads during shadow periods, which occur during the equinox solar eclipse periods. The selection of nickel-cadmium batteries was based on the 3-year design life requirement (5-year design goal) and the demonstrated cycle capability under repetitive deep discharges. Each battery contains 17 series-connected cells and weighs 13.6 pounds. Each cell has both the positive and negative terminal insulated from the cell case to ensure maximum reliability. Each battery also contains one cell which incorporates a third electrode for overcharge control.

Temperature

The IUE battery size was predicated on an average battery life temperature of 10° Celsius with variations during the 3 year life of $\pm 10^\circ$ Celsius. As shown in the figure 5-8, a temperature difference appeared between the two batteries and remained that way during the entire spacecraft life. Battery #1 was about 6° warmer than Battery #2, which is less exposed to solar radiation than the first one.

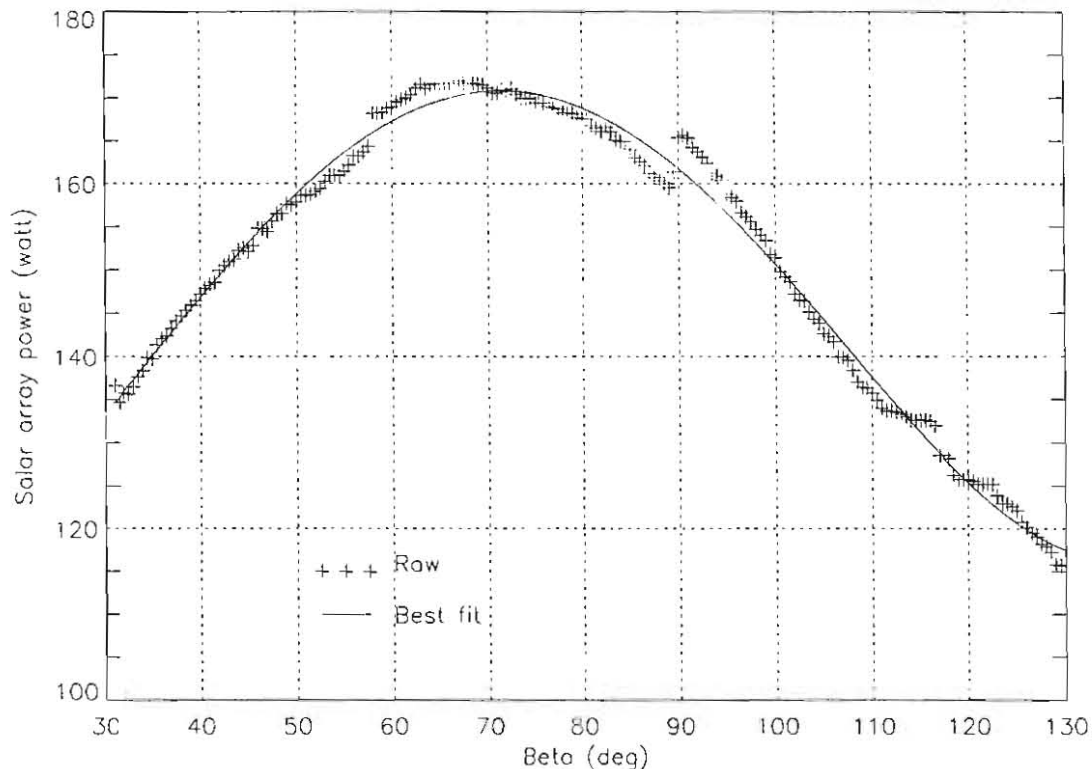


Figure 5-8. History of average temperature of the batteries.

Heat dissipation occurs from battery discharging and battery overcharging. For an average spacecraft load of 185 watts and a boost regulator efficiency of 90%, the dissipation will be approximately 18 watts per battery during discharge and about 3 watts per battery during overcharge.

Charge control

Each battery is charged from the 28 volt bus through a series type charger. Charging is accomplished using a maximum current / maximum voltage limit concept. With a charge rate of 0.6 amperes, the battery recharge time following a 72 minutes eclipse would be approximately 11 hours. When not in shadow season, the batteries are charged at a much lower rate. This feature is accomplished by charging the battery from the 28 volts bus through one of two resistors, which can be selected by a command relay. These are the trickle-high or trickle-low modes.

At the beginning of the IUE life, battery charging at 0.6 amperes was maintained until the third electrode signalled the battery charger to begin reducing the rate of charge. Thereafter, charge rate was a function of third electrode voltage. In that way, the primary advantage gained was the reduction of battery thermal dissipation during the long periods when the spacecraft was power positive. During the shadow season 19 (January, 1987), the third electrode behaviour became erroneous and it was necessary to perform recharge independent of the third electrode. On February 22, 1990 the third electrode on Battery #1 was turned off, and on March 19, 1990 the

third electrode on Battery #2 was also turned off.

Undervoltage and overcurrent protection.

Undervoltage protection is provided by two voltage detectors on each battery. One detector is connected to eight cells, the other is connected to nine cells. With the undervoltage detectors turned on, detection of an undervoltage condition (17 volts) on either battery would result in the automatic removal of all nonessential loads (everything but VHF receivers and command decoders).

The undervoltage detectors on both batteries were turned off on August 31, 1983. As the batteries aged, there was an increasing probability that the capacity of one or more cells in the batteries would become depleted with the batteries in use under heavy load conditions.

There are also undervoltage (26.5 volts) and overcurrent (12 amperes) detectors on the main bus. At the end of the mission, only the overcurrent detector was on.

5.1.2.1. Battery #1 degradation

The health of Battery #1 came into question since the end of shadow season 26 in August, 1990. On May 25th, 1990, Battery #1 had been already configured with the main charger on permanently, with the usual trickle-low mode reserved for over-voltage, over-temperature or under-charge conditions.

On August 26, the charge current dropped to 0.0 amperes and remained there, with the battery voltage at 24.72 volts, the charge current had been gradually decreasing for several months. The trickle-low charger was commanded on in an attempt to force some charge current into Battery #1. Within ten minutes the battery voltage had exceeded its redline limit of 25.84 volts and the main charger was commanded back on, discontinuing any charge current. The battery voltage returned to 24.72 volts, the maximum allowed by the main chargers. The rapid rise in battery voltage in response to the forced charge current indicated that the battery was fully charged and the main charger was operating correctly. The concern was that a lack of charge current can cause crystallization of the battery plates, impairing their performance. There was also the problem of forced charging producing hydrogen gas, possibly with enough pressure to rupture the battery case. To avoid any of these undesirable situations, a weekly charging routine was used to get some charge current into Battery #1 without overcharging it. This operation was called top-off.

Top-off

“Top-off” was called a procedure to ensure that full-charge on the batteries was maintained in the absence of the third electrode control. Top-off’s were performed weekly on battery 1.

The charge sequence consists of turning off the main charger, so the battery receives a low trickle charge. This charge, however, raises the battery voltage and must be removed before the voltage becomes too high (25.84 volts). Each charging sequence lasted on the order of minutes before this high battery voltage dictates that the charger be turned back on.

5.1.2.2. Battery EOL characterization

A characterization of the batteries was desirable for comparison to pre-launch data on the batteries. This test was intended to determine the degradation of Battery #1, determine the EOL capacity on Battery #2, determine the charge efficiency of the batteries under various IUE charge control modes, determine the state of the third electrode and implement the lessons learned on the battery management of on-board UARS, EUVE, ERBS and TOPEX batteries.

The operations necessary to collect the desired battery data consisted basically of discharging the batteries each on an individual basis as well as together. The minimum voltages and depths of discharge reached are shown in the table below.

Day	Configuration	Duration (minutes)	Min. voltage (volt)		D.O.D (%)	
			Bat#1	Bat#2	Bat#1	Bat#2
26	Only Battery#2 ON	168 m	-----	18.0 v	-----	73.9 %
27	Only Battery#1 ON	180 m	18.0 v	-----	69.0 %	-----
28	Both Batteries ON	74 m	21.2 v	21.2 v	16.8 %	15.1 %
29	Both Batteries ON	114 m	20.6 v	20.6 v	26.7 %	26.1 %

5.1.3. Shadow

Twice a year the IUE experienced a shadow season when the Earth moves between the spacecraft and the Sun. This "Shadow Season" lasted between 24 and 30 days, with the duration of the daily shadow varying from a few minutes up to a maximum of 82 minutes. The daily shadow consisted of two parts, penumbra and umbra. During penumbra or light shadow, the spacecraft was partially shielded from the Sun. During umbra or deep shadow, the spacecraft was completely shielded from the Sun by the Earth. Special consideration was given to spacecraft configuration and operations concerning temperatures and power loads during shadow periods. While in the umbra portion of shadow, the spacecraft was entirely dependent on its two 6 ampere-hour batteries for its power requirements.

The minimum load configuration during shadow seasons changed along the spacecraft life. Excessive use of the batteries accelerated the aging of the batteries considerably during the first eclipse seasons. Although, the battery design parameter indicated a maximum limit of 80% for the depth of discharge, it was evident, during the second shadow season, that the amount of power required from the batteries was excessive if the batteries were to survive more than five years. Therefore, it was decided to limit the depth of discharge to about 50 %. In order not to exceed this value, the load configuration during the eclipse periods was modified as is explained below.

- ▶ S-Band system off.

- ▶ PASs off.
- ▶ Science instrument heaters off.
- ▶ Until shadow season 4 the Gyros 2, 4 and 6 were turned off for the duration of the eclipse season. After the third eclipse all attempts to restart Gyro 6 failed, so, the decision was made not to turn the gyros off for eclipse seasons.
 - After shadow season 4, Gyro 6 and its heater off; all gyro heaters low.
 - After shadow season 10, Gyro 2 and 6 off and their associated heaters off.
 - After shadow season 13, Gyro 1, 2 and 6 off.
 - After shadow season 26, Gyro heaters 4 and 5 on high, all other gyro heaters off.
 - At shadow season 38, Gyro 4 on, Gyro heaters 4 and 5 on high, heater 6 on low, all other gyro heaters off.
- ▶ After the shadow season 29 the FPM was turned off due to a failure. The SMSS, which was useful only during the launch phase of IUE, received power from the same relay as the FPM, thus it was also powered off.
- ▶ VHF on. After shadow season 5, the VHF was cycled on for 1 minute then off for 4 minutes when ever the depth of discharge was predicted to be greater than 50 %.
- ▶ SWP camera in standby mode.
- ▶ After shadow season 5, the long wavelength camera indicated as prime (LWP or LWR) was turned off, when the depth of discharge predicted exceeded 50 % except in shadow seasons 31, 33, 35 and 37.
- ▶ The OBC computer NO-OP instruction changed to HALT instruction from shadow season 5 to 29.
 - After shadow season 18, two different modes of attitude control were used: FES Only mode, which consist of the FES tracking a guide star for pitch and yaw control and gyros for roll control, and a new mode called Shadtrack. This mode is a combination of two attitude control workers: worker 10 (hold on wheels) and worker 0 (hold/slew), the first one maintains the attitude control while worker 0 monitors the spacecraft drift in the pitch and yaw axes using the gyros. After shadow, control of the spacecraft attitude is returned to worker 0 which slews the spacecraft back to the original position by zeroing out the accumulated angular errors. When the predicted depth of discharge was to exceed 50 %, Shadtrack was used.
 - After shadow season 28, a patch referred to as Automatic Worker 10 (AUTOW10) was uplinked to prevent a complete loss of attitude control in the event that track was unexpectedly broken during the daily shadow period. If a loss of star presence causes track to be broken, with the AUTOW10 code in line and activated, control is immediately and automatically transferred to the Shadtrack mode.
 - After shadow season 29, the control with FES Only mode was improved by reducing the roll gain. This mode was used during the whole shadow.

The battery recharge policy was also redefined along the mission life. At the conclusion of eclipse season 18, Battery #1's third electrode voltage reading began to steadily decline. Because of the erroneous readings the third electrode was no longer used to determine the charge state of

the batteries. For the shadow season 19, the batteries were recharged to 115-120 % of the measured discharge. For the next shadow season (20), a manual recharge procedure was implemented. To ensure that the batteries were fully charged for the daily shadows, the amount of charge returned to the batteries was 130 % of the measured discharge. This method was followed in the next shadow seasons until shadow season 26. On May 25, 1990, the main charger on Battery #1 was turned on and remained on permanently. Battery#2 was declared to be fully charged by achieving a predefined increase in the battery's temperature which was correlated to an approximate amount of recharge.

After shadow season 12, reconditioning of both batteries was observed. Battery reconditioning occurs when a battery is drained close its minimum capacity and then slowly recharged back to full capacity. The battery cells are rejuvenated during this process, thus, resulting in greater battery capacitance.

The next figures display several shadow parameters over the life of the IUE, such as the battery power sharing, the booster efficiency at minimum voltage, the maximum length of umbra, the temporal occurrence (the shadow season dates are also displayed in Appendix A), the spacecraft bus power during shadow minimum load configuration, the maximum depth of discharge and the battery voltage compared to the depth of discharge.

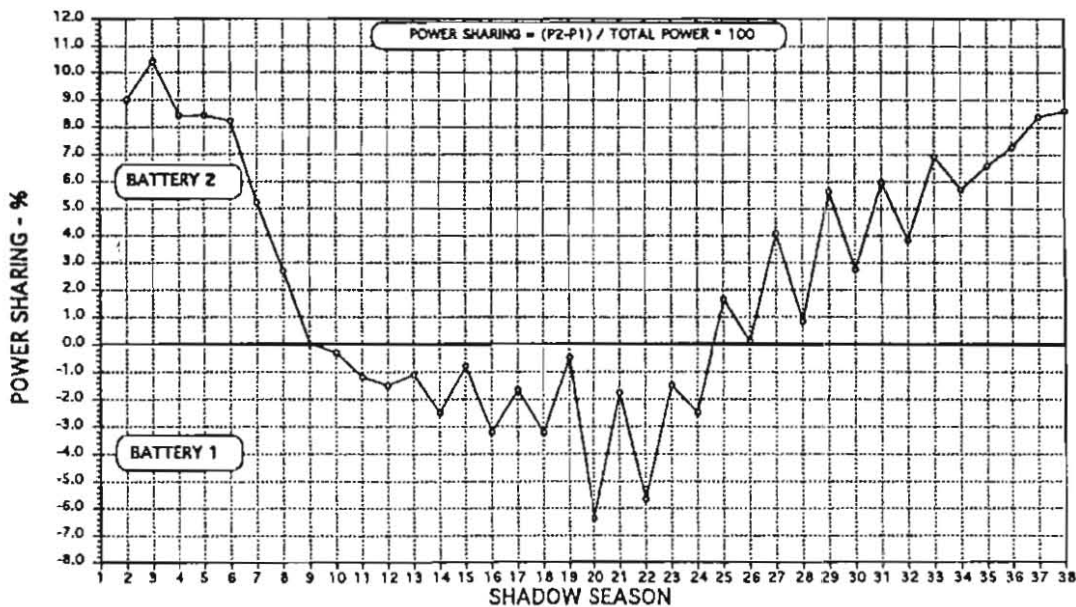


Figure 5-9. Average Battery Power Sharing vs. Shadow Season.

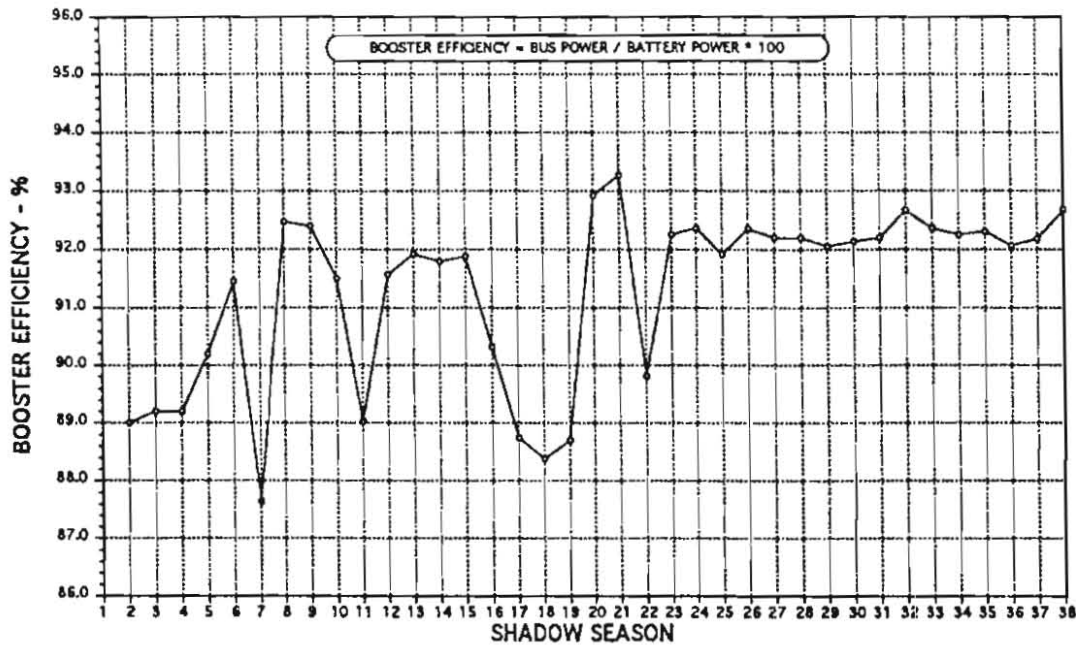


Figure 5-10. Average Booster Efficiency vs. Shadow Season.

Due to the variations in battery discharge current and spacecraft load current during the time of minimum voltage, an accurate calculation of booster was difficult. Beginning with shadow season 23 a new method that involves averaging these values during the duration of minimum voltage has been used.

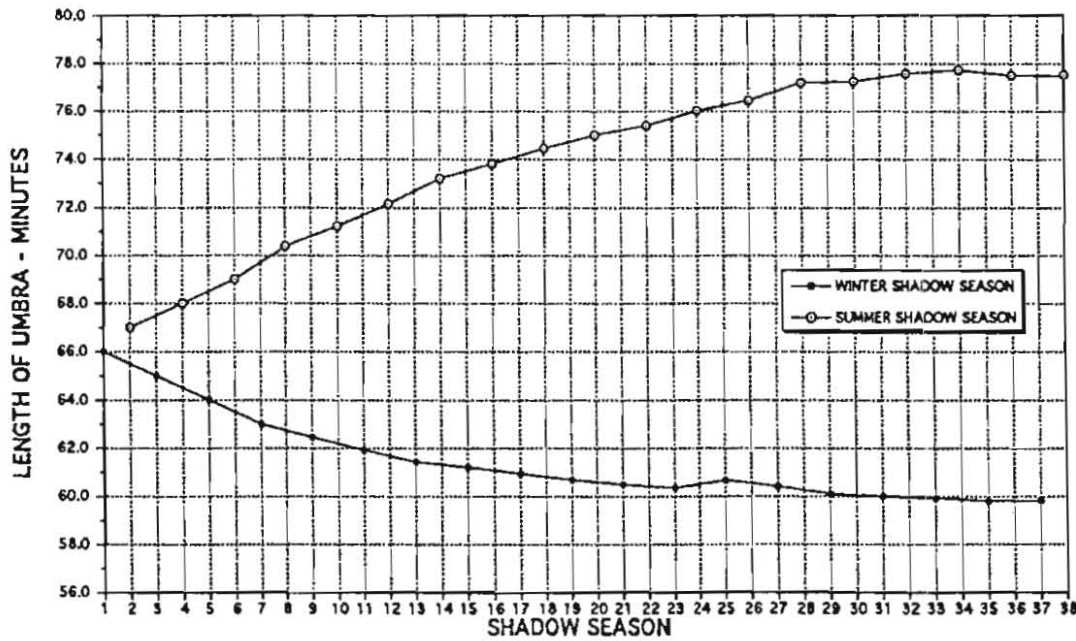


Figure 5-11. Maximum Umbra Length vs. Shadow Season.

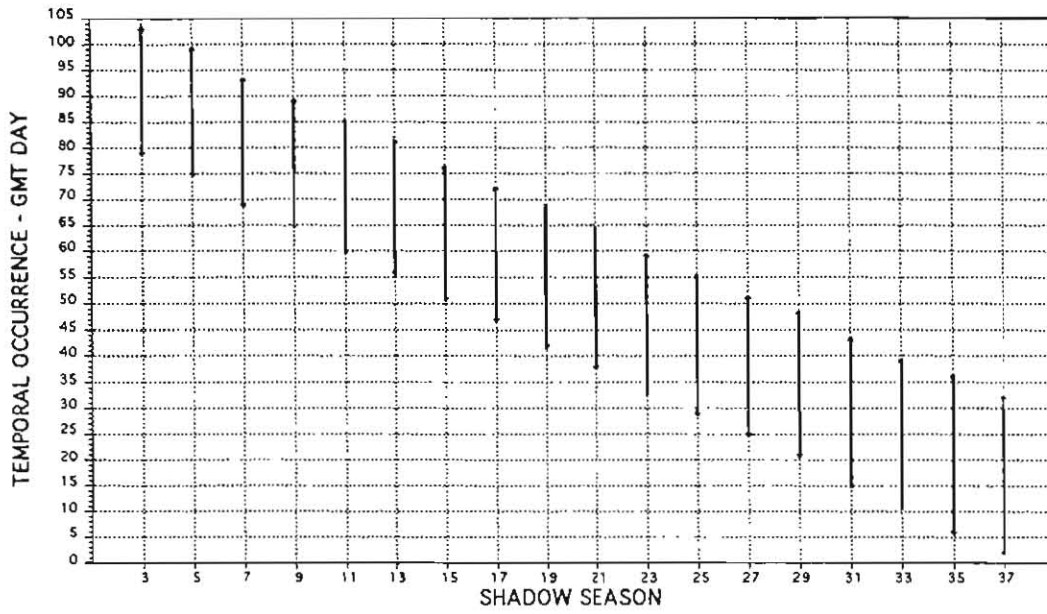


Figure 5-12. Winter Shadow Season Temporal Occurrence.

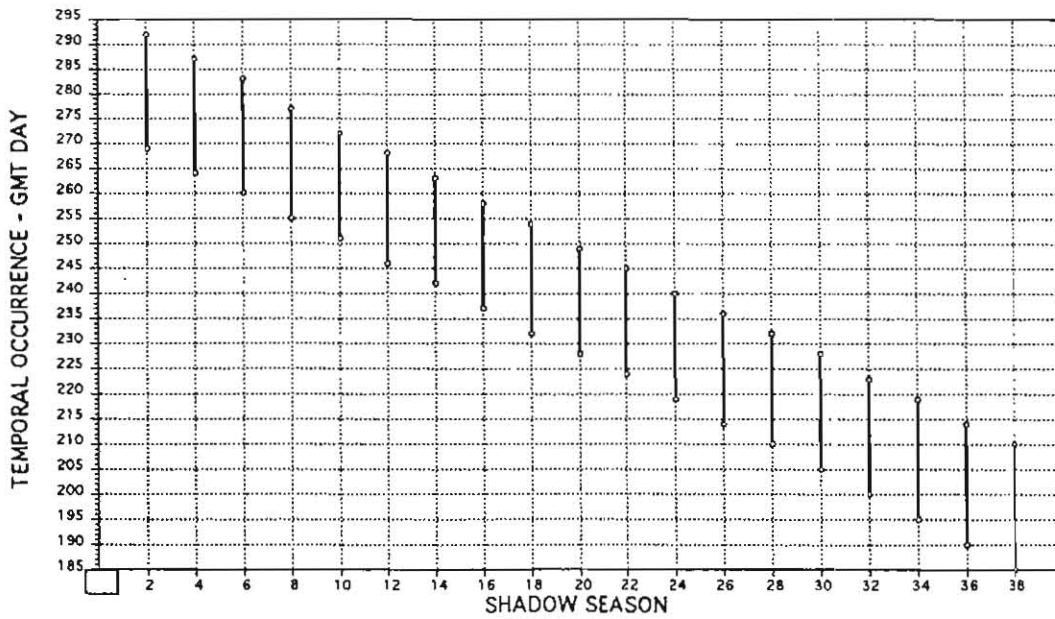


Figure 5-13. Summer Shadow Season Temporal Occurrence.

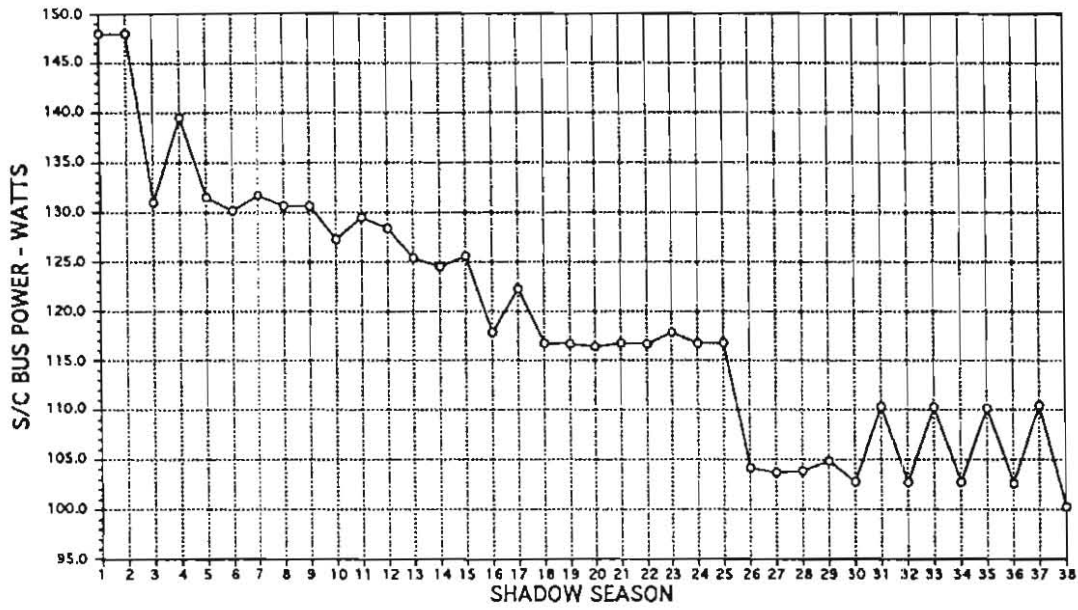


Figure 5-14. S/C Bus Power During Minimum Load vs. Shadow Season.

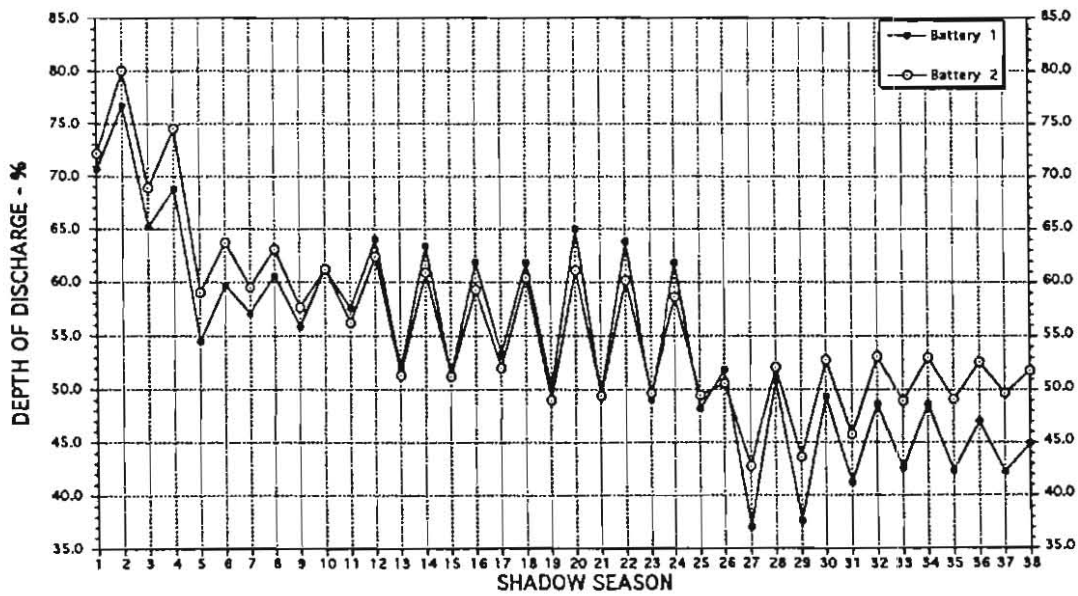


Figure 5-15. Maximum DOD vs. Shadow Season.

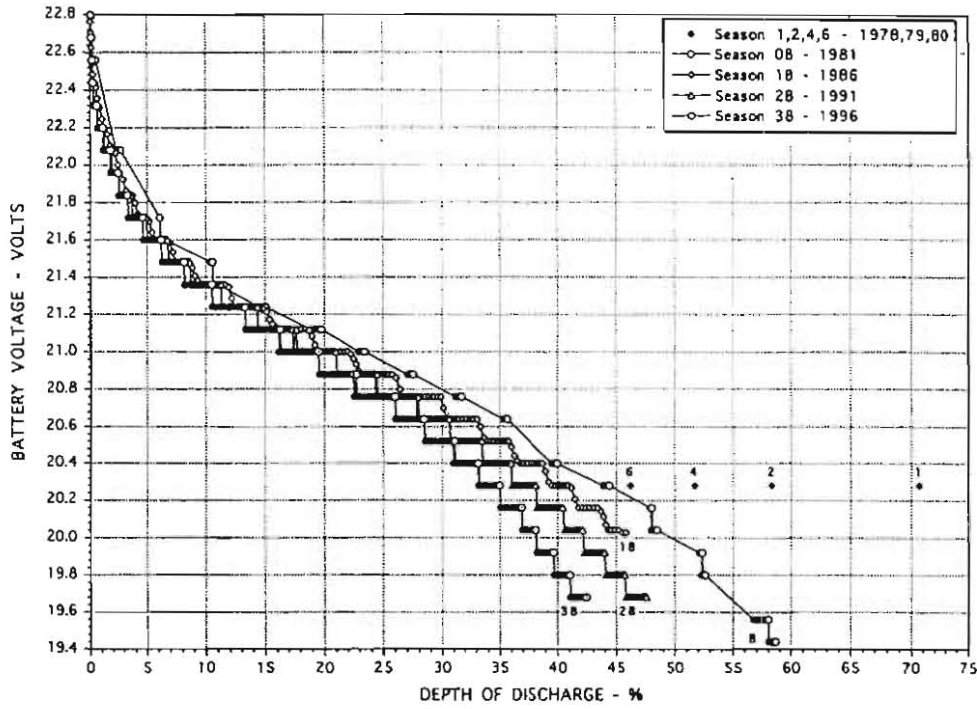


Figure 5-16. Battery 1 Voltage vs. DOD during Season 1-38.

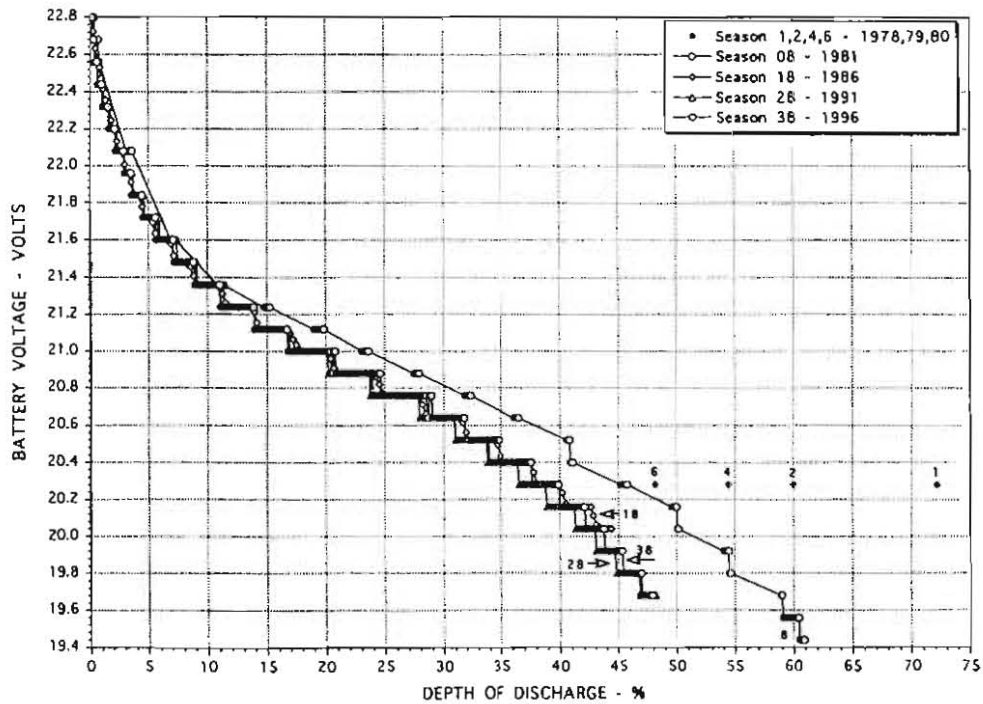


Figure 5-17. Battery 2 Voltage vs. DOD during Season 1-38.

Although the data sets for shadow seasons 1, 2, 4 and 6 were limited, the single points are included in the figures to provide a complete image of the batteries' performance.

5.2. Command Subsystem

The IUE command subsystem consists of redundant command decoders and a command relay unit (CRU), as is shown in the figure 5-18. The CRU contains circuit redundancy up to the individual relay and relay driver stage. Three types of commands are available; impulse and serial commands are distributed by decoders 1 and 2, and relay closures are provided by the CRU.

- ▶ The impulse command is a positive 10 volts pulse with a 15 millisecond duration. There are 128 impulse commands available from the command decoder.
- ▶ The serial command is a positive 10 volts logic signals, and the clock transfer rate is 4.27 kHz. Each serial command will provide 37 bits of programmable information. There are 48 individually buffered serial commands available from each command decoder.
- ▶ The relay closure commands are executed using a serial command to the CRU. Sixty-four latching relay closures are provided. Most of the CRU's are used to switch primary +28 volts power to spacecraft subsystems. The pyrotechnic circuitry also used the CRU. This circuitry controls by serial and discrete commands the apogee boost motor ignition, the solar array deployment and the telescope cover release. This pyrotechnic circuitry is completely redundant.

Each command decoder can process command messages from two sources: a VHF receiver analog signal and digital information from the OBC.

Command detector and decoder characteristics	
Input signal	Modulation PCM/FSK - AM Subcarrier 8 kHz / 12 kHz Bit rate 800 Hz
Command rate	Ground station originated 13 per second Computer or stored command 33 per second
Command capacity	Discrete: 128 outputs/10 V, <1k Ω source impedance, 15 msec positive duration. Serial: 48 individually addressed and buffered 37 bits each with NRZ data, 4.27 kHz clock, 37 bit positive envelope, all 10 V logic, <1k Ω source impedance, rise fall times < 5 μ s.

The command decoder contains three distinct circuit groups: analog circuits, digital logic circuits and dc/dc converter. The analog circuits demodulate the input signal and convert the information contained to three digital output signals which are data, voltage-controlled oscillator (VCO) clock and a data present signal. The first two signals transfer the uplink command information to the digital logic circuits for processing, while the last one allows the digital logic to proceed with command processing only when adequate bit error rate probability exists. The digital logic circuits

process this command information from the analog circuits and OBC command data which are assumed to be transferred by an error free channel and are executed as received. Sixty bits of data are processed for each uplink command executed, and 44 bits are processed for OBC issued commands; the only difference between them is the OBC commands do not contain the parity code or the decoder address. The OBC commands were directed to a single decoder by the selection of the corresponding output channel.

The decoders use time share command execution (15 millisecond intervals) to avoid priority conflict. OBC command data are transferred to a decoder during the time interval when uplink spacecraft commands are being executed. The time-share intervals of command decoder 1 and command decoder 2 are not synchronized. For this reason, it was thought that both the uplink and OBC commands should be addressed to the same decoder.

After the launch of the IUE, command decoder 1 was used by both the ground command and the OBC until June 1980. On June 12, 1980 a spacecraft anomaly occurred in which decoder 1 apparently malfunctioned and incorrectly interpreted a command uplinked from the ground. Although this anomaly was proved not to be related with the decoder, the command decoder function for both the ground system and the OBC was transferred to decoder 2. On January 21, 1981 the OBC was reset following an OBC crash. The command decoder 1 was automatically selected by the OBC although the related telemetry point indicated it was still using decoder 2. So, the ground commands were sent to decoder 2 while OBC commands were sent to decoder 1. This situation was not discovered until September, 1992. Since any apparent conflicts appeared during the eleven years while in this configuration, this configuration was maintained until the end of the mission. It should be noted that a conflict in commanding between the OBC and ground command would only occur if both systems were to attempt to command the same device at the same time. By 1981 ground operations had been refined to the point that it was very unlikely that the ground would issue commands to the same device the OBC may be commanding.

Command verification

When the command decoder accepts a ground generated command, it increments a command execution counter. The command encoder on the ground computer compares the number of commands it sent out to the number of commands accepted by the decoder indicated by this counter. If the two numbers agree, the command is verified. If they do not agree, the ground computer tries to send the command up to two more times before displaying a verification failure message to the initiating console and halting the executing procedure until the controller retransmits, clears or skips the command.

Critical commands and data blocks are not automatically retransmitted in the event of a verification failure on the first attempt. A command is designated as critical because accidental transmission is potentially dangerous to the spacecraft. It must be approved by the shift leader console before transmission.

Procedures

To minimize the chance of error when sending commands to the spacecraft, most commanding is done using pre-programmed procedures (PROCs). PROCs are programs which are stored in

the ground computer and then called up, by keyboard entry, by the spacecraft controllers. A PROC executes all commands needed for equipment reconfiguration and the actual operation. Each step of a PROC is also accompanied by an explanation of what is being done. There are PROCs for most spacecraft operations as well as for ground system operations such as setting up the system after initialization and science operations.

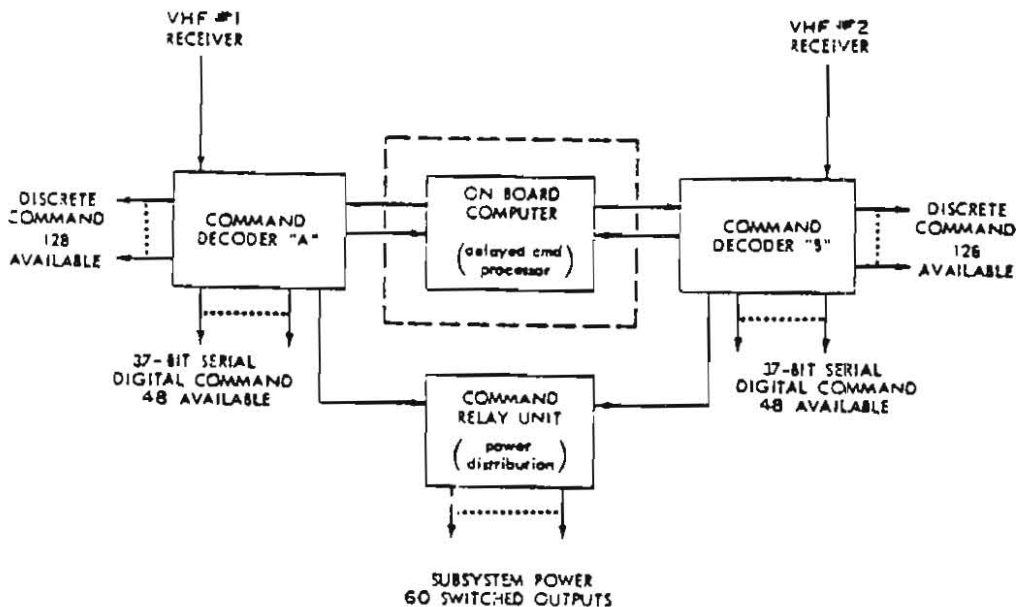


Figure 5-18. IUE Command Subsystem Block Diagram.

5.2.1. Command decoder anomalies

During the spacecraft life, two problems associated with the command decoders occurred.

On the 27th of May in 1980, decoder 1 was used for a few days to check out a problem with camera commanding, which did not turn out to be a decoder problem. A few days later, June 12, the OBC and radiation monitor were powered down and the spacecraft attitude was lost. A sun acquisition on jets was performed, and as the spacecraft was evaluated, both were turned on again. The crash was a result of a failure in command decoder 1. It occurred immediately following a command to the DMU. The penultimate command had been to the CRU. Serial data from the DMU command was tagged with the previous CRU address, causing several relays to be commanded. Pyrotechnic circuitry had been armed, and was immediately disarmed. As a consequence of this event, the decoders were switched again putting command decoder 2 into use.

On the 25th of May in 1982, the SWP camera was commanded to an abnormal configuration when command decoder 2 took the address of a previous command with the data portion of the intended command.

5.3. Communications Subsystem

The communications system consists of two redundant VHF transponder systems, two redundant S-band transmitters with four S-band power amplifiers, and associated antenna systems. The communications system interfaces with the power supply subsystem, telemetry encoder output, and command decoder input. Functionally, this system provides the means for transmission of telemetry data, reception of ground generated commands, and a way of tracking the spacecraft using the Goddard Range & Range Rate (R&RR) system.

5.3.1. S-band system.

Characteristics of the S-band system include the following,

- ▶ Transmitter frequency 2249.80 MHz
- ▶ Power output 6 W
- ▶ Output modulation Phase modulation (pm)
- ▶ Antenna polarization Circular

The S-band system consists of two redundant transmitters and four power amplifiers with individual antennas. The S-band system is used for transmission of telemetry data. Both of the transmitters are connected to each of the power amplifier/antenna combination. Only one transmitter and one power amplifier/antenna are activated by command at any one time. Selection of a particular power amplifier depends upon a favourable view of the Earth tracking station by its associated antenna.

The IUE S-band antenna sensitivity plot for the four power amplifiers is show in the figure 5-19.

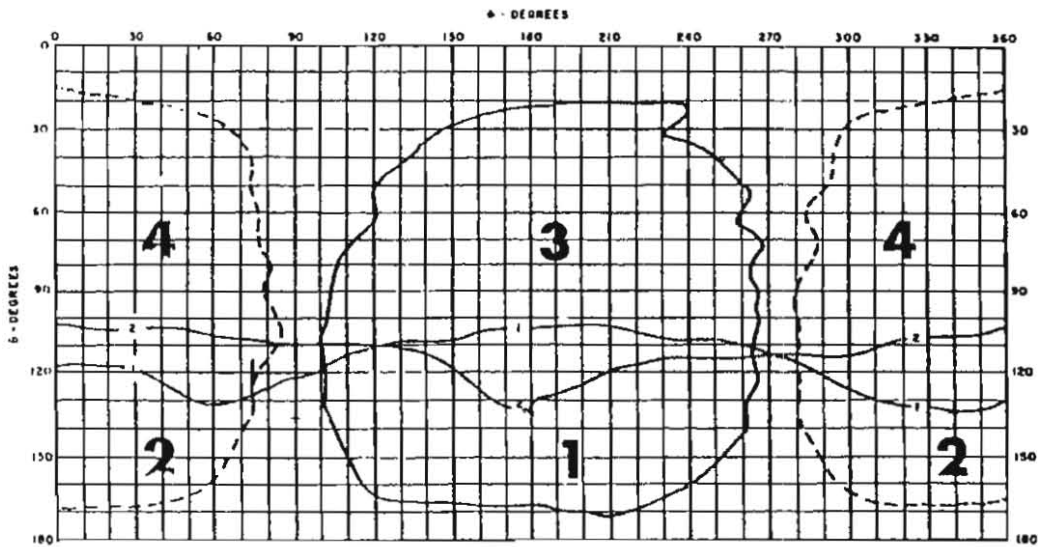


Figure 5-19. IUE S-Band antenna sensitivity plot.

The angles theta (θ) and phi (Φ) are the spacecraft look angles from the tracking stations. The contours plotted on figure are -6 dbi curves found during prelaunch thermal vacuum testing.

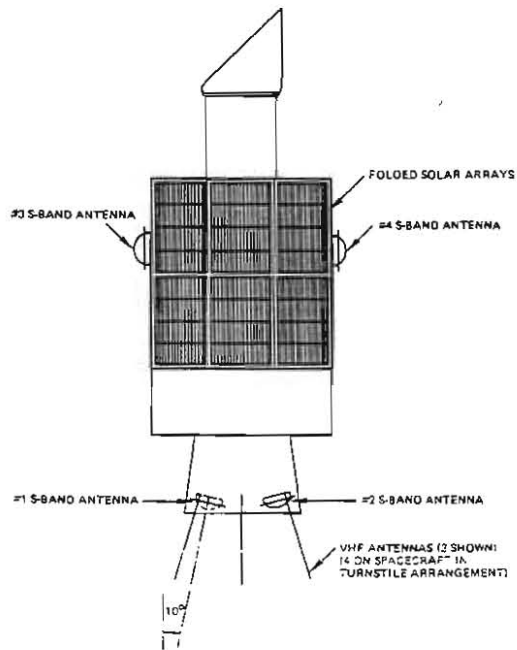


Figure 5-20. Antenna locations on the S/C

Antennas 1 and 2 are located on the bottom of the spacecraft on the anti-Sun and Sun side (figure 5-20), respectively, so they are more useful when the telescope is pointing away from the Earth. Antennas 3 and 4 are located higher up on the body of the spacecraft, above 1 and 2, respectively.

The table below shows approximately the load of each power amplifier.

S-band P.A.	Power load (watts)
P.A.#1	16
P.A.#2	21
P.A.#3	23
P.A.#4	27

The figure 5-21 compares the antenna radiation pattern for each PA at the end of the IUE. The AGC (automatic gain control) is the combiner output voltage in the reception chain.

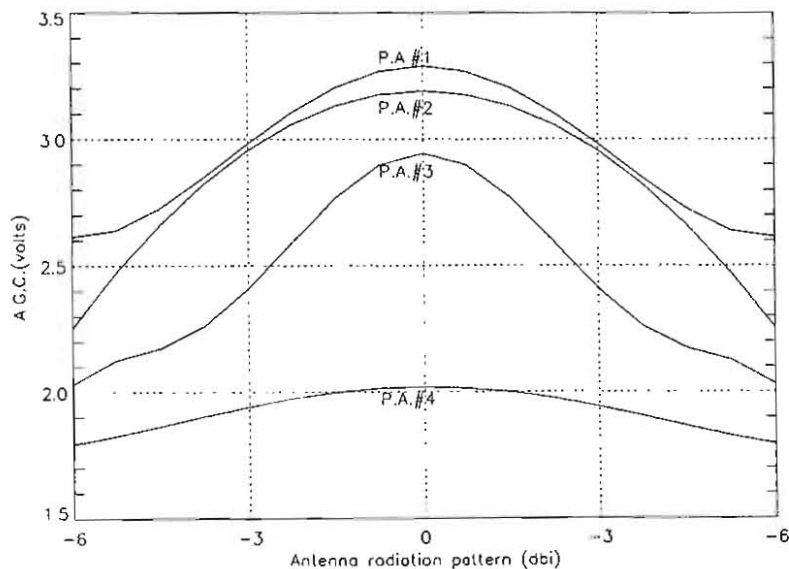


Figure 5-21. Comparison between the output of the four power amplifiers.

5.3.1.1. S-band power amplifier 4 anomaly

A sudden drop in the S-band power amplifier 4 down-link signal strength was observed twice during the spacecraft life, the first time was on the 24th of September of 1984 and, the second time, the 5th of August of 1995. Both times the measured drops were around 10 dBm. The data analysis, in 1995, showed a corresponding drop in the spacecraft bus current of approximately 0.16 A and also, a rapid drop in the S-band power amplifier temperature from 26.2°C to 23.2°C.

PA 4 was expected to become more susceptible to degradation over the years. It was located on the Sun side of the spacecraft, so that solar radiation degraded PA 4 more than the other PAs.

5.3.2. VHF system

Characteristics of the VHF transponder system include the following,

- ▶ Receiver frequency 148.980 MHz
- ▶ Transmitter frequency 136.860 MHz
- ▶ Power output 6 W
- ▶ Output modulation Phase modulation (pm)
- ▶ Receiver sensitivity -106 dBm
- ▶ Antenna polarization Turnstile
- ▶ Antenna pattern Omnidirectional

The VHF transponder system consists of a turnstile antenna system, antenna distribution system and two VHF transponders. The VHF system provides for the transmission of telemetry data, reception of ground generated commands, and the turnaround transmission of R&RR signals. The VHF downlink is essentially an omnidirectional antenna; therefore, it is possible to pick up the VHF signal from any spacecraft attitude. This makes it very useful for use during emergencies where a loss of attitude control condition exists. The VHF system cannot be used effectively at data rates greater than 5 kilobits per second. As the VHF system uses less power than the S-band system, it has been used for data during shadow periods to minimize battery drain.

5.3.2.1. Ranging

The Goddard R&RR system is used to determine the location and rate of motion of the IUE spacecraft throughout its orbit. This ranging information is used by the tracking stations to locate the satellite accurately for the best possible reception of data and to monitor orbit drift. Three tracking stations are capable of performing rangings: Greenbelt (BLT)/Wallops (WPS), Santiago, Chili (AGO) and Ascension Island (ACN).

Ranging was done at 1 hour intervals covering the entire orbit around twice a month. To range with the IUE, the VHF system was turned on and placed in the ranging mode. The station uplinked ranging tones which are fed back to the station by the VHF system. The Doppler shift in these tones was used to calculate the spacecraft radial motion.

5.4. Data Handling Subsystem

At the heart of the data handling subsystem is the DMU (Data Multiplex Unit), which performs the tasks of multiplexing or providing a variety of engineering and scientific values from all onboard systems. By using a time-sharing technique, this data can be made available to the ground station over a RF link and to the OBC, which needs this data to perform calculations and, based on the results, send attitude control commands to the stabilization and control system.

There are two completely redundant data multiplexer units. The DMU 1 was used for the whole spacecraft life.

The basic portion of the DMU, called the dataplexer, contains the main analog and digital multiplexers, the spacecraft clock, and timing and control signal logic all in one box. Also, the DMU uses several submultiplexer units which expand the data handling capacity of this system. There are six subcommutators (subcoms): three analog subcoms, one digital subcom and two experiment subcoms.

The analog data inputs are routed to an eight-bit analog-to-digital (A/D) converter. This is a successive approximation type, running at the rate of 160,000 comparisons per second. The conversion time for an 8 bit word is 50 microseconds. So, the maximum conversion word rate is identical to the maximum word transmission rate through the dataplexer for telemetry and computer (80 Kbps). The range of analog signal voltage input is from 0 volts to 5.1 volts.

Formats.

The dataplexer selects digital or analog data samples from various spacecraft equipment in a time sequence controlled by a format memory. Each data sample is transformed into an eight-bit data word and transferred to a serial data bit stream. One complete sequence is called a minor frame and is 128 words in length. Each word is dedicated to a particular spacecraft parameter. Switching the telemetry format changes these parameters. However, certain words in the minor frame are dedicated to certain spacecraft parameters that must be observed regardless of the type of operation is being performed with the spacecraft. These fixed word parameters, which always appear in the same location, include frame sync words and information such as the contents of the frame counter, the spacecraft clock, variable format memory contents, and the spacecraft status bits. As there is a need to look at more than 128 telemetry channels, some words in the minor frame are set to represent a different group of fixed telemetry points or channels. This process is called subcommutating. A major frame is defined as 256 minor frames. All submultiplexer data samples are included in each major frame.

The IUE ground station has the option of specifying what type of data will be received at any time depending on what type of operations are being performed. On the one hand, there are four fixed-format and one variable-format to supply telemetry to the ground system and, on the other hand, two fixed, one variable and a computer controlled input (Direct Read Table, DRT) formats are available for the OBC. The fixed formats use ROM memories which cannot be altered after fabrication, while the variable format can be loaded with any desired sequence of dataplexer addresses to compose a format. In the DRT case, the OBC has the dataplexer addresses in its own memory.

The OBC receives not only the data specified specifically intended for the OBC but also a copy of the specified data selected for transmission to the ground. The data input to the OBC's memory is done by way of the Direct Memory Access (DMA) on a prioritized time sharing basis. The DMA also provides the means by which the DRT addresses are output to the DMU.

The ROMs available for ground telemetry and their uses are as follow:

- ▶ Format 1A. It was only used during the transfer orbit.
- ▶ Format 1B or Camera format. Three-fourths of each frame is devoted to camera video data. This format was used when reading or preparing the cameras.
- ▶ Format 2A or Operational format. This format contained a balance of housekeeping and science data and was used routinely.
- ▶ Format 2B. It was only used for dumping the OBC memory.

There are also two ROMs used to format data to the OBC. The two ROMs are identical except that ROM 3A provides FES 1 data and ROM 3B provides FES 2 data. In 1985, the change to the 2 gyro/FSS control algorithm required the use of the DRT format by the OBC in order for it to receive the necessary data for this control algorithm.

The figures 5-22, 5-23 and 5-24 show the normal formats used in the last mission years.

BIT RATE = 40 KB/SEC														
MINIMUM SAMPLE TIME														
#	ASCI	ASCI	ASCI	ASCI	ASCI	ASCI	ASCI	ASCI	ASCI	ASCI	ASCI	ASCI	ASCI	ASCI
204 B	204 B	204 B	204 B	204 B	204 B	204 B	204 B	204 B	204 B	204 B	204 B	204 B	204 B	204 B
1	ACCEL A	ACCEL B	PAS 1/2 S PULSE	SPSS 1 PULSE	S/C BUSS 1	S/C BUSS 2	CYRO 1A	CYRO 1B	CYRO 2A	CYRO 2B	CYRO 3A	CYRO 3B	CYRO 4A	CYRO 4B
16	CYRO 5A	CYRO 5B	0	0	PILOC ERROR	ROLL ERROR	FSS#1				FSS#2			0
32			FSS#1			FSS#2								
48	CYRO 5B	CYRO 6A	CYRO 6B	0	1	1	CYRO 7A	CYRO 7B	0			FES 1/2		
64	1	ACCEL A	ACCEL B	PAS 1/2 S PULSE	SPSS 1 PULSE	S/C BUSS 1	S/C BUSS 2	CYRO 1A	CYRO 1B	CYRO 2A	CYRO 2B	CYRO 3A	CYRO 3B	CYRO 4A
80	CYRO 5A	CYRO 5B	CYRO 6A	1	0	0	ASC 1	ASC 2		PITCH TACH	ROLL TACH			
96	1	ACCEL A	ACCEL B	PAS 1/2 S PULSE	SPSS 1 PULSE	S/C BUSS 1	S/C BUSS 2	CYRO 1A	CYRO 1B	CYRO 2A	CYRO 2B	CYRO 3A	CYRO 3B	CYRO 4A
112	CYRO 5A	CYRO 5B	CYRO 6A	1	1	ASC 1	ASC 2	0	0	0	0	0	0	0

NOTE: '1's ARE SIMULATED USING S/C BUSS VOLTS 0-30V. #PPRCLK = 275 COUNTS. * 715 IS SELECTED BY OBC CYRO 6.0 - FES #1
 0's ARE SIMULATED USING DTC-30. OBC CYRO 6.1 - FES #2

W WORD DATE REQUIRED
 #F PUNCH FRAME
 v OBC FORMAT - DIRECT READ

NOV-68 12 1605

Figure 5-22. Direct Read Table (DRT).

BIT RATE=4096/SEC															
AVERAGE SAMPLE TIME:															
MF		25.8		IMSEC											
ASC1		1.64		SEC											
ASC2		1.64		SEC											
ASC3		.83		SEC											
OSC		1.64		SEC											
ESC		1.64		SEC											
0	1	2	3	4	5	6	7	8	9	10	11	12	13	14	15
CAMERA ANALOG VIDEO DATA															
**	**	**	**	**	**	**	**	**	**	**	**	**	**	**	**
16	17	18	19	20	21	22	23	24	25	26	27	28	29	30	31
CAMERA ANALOG VIDEO DATA															
**	**	**	**	**	**	**	**	**	**	**	**	**	**	**	**
32	33	34	35	36	37	38	39	40	41	42	43	44	45	46	47
CAMERA ANALOG VIDEO DATA															
**	**	**	**	**	**	**	**	**	**	**	**	**	**	**	**
48	49	50	51	52	53	54	55	56	57	58	59	60	61	62	63
ASC1	ASC2	ASC3	OSC	OSC	OSC	OSC	OSC	OSC	OSC	OSC	OSC	OSC	OSC	OSC	OSC
F	F	F	F	F	F	F	F	F	F	F	F	F	F	F	F
64	65	66	67	68	69	70	71	72	73	74	75	76	77	78	79
CAMERA ANALOG VIDEO DATA															
**	**	**	**	**	**	**	**	**	**	**	**	**	**	**	**
80	81	82	83	84	85	86	87	88	89	90	91	92	93	94	95
CAMERA ANALOG VIDEO DATA															
**	**	**	**	**	**	**	**	**	**	**	**	**	**	**	**
96	97	98	99	100	101	102	103	104	105	106	107	108	109	110	111
CAMERA ANALOG VIDEO DATA															
**	**	**	**	**	**	**	**	**	**	**	**	**	**	**	**
112	113	114	115	116	117	118	119	120	121	122	123	124	125	126	127
OSC	ESC	ESC	ESC	ESC	ESC	ESC	ESC	ESC	ESC	ESC	ESC	ESC	ESC	ESC	ESC
F	F	F	F	F	F	F	F	F	F	F	F	F	F	F	F

* INDIRECT ADDRESS REGISTER
 ** INDIRECT ADDRESS REGISTER 2
 # WORD GATE REQUIRED
 MF MINOR FRAME

TELEMETRY FORMAT - 1676 SCIENTIFIC INSTRUMENTAL VIDEO DATA JUNE 1, 1979

Figure 5-23. Format 1B (Camera format).

BIT RATE=4096/SEC															
AVERAGE SAMPLE TIME:															
MF		25.8		IMSEC											
ASC1		.41		SEC											
ASC2		.41		SEC											
ASC3		.83		SEC											
OSC		.41		SEC											
ESC		.83		SEC											
0	1	2	3	4	5	6	7	8	9	10	11	12	13	14	15
FES DATA															
**	**	**	**	**	**	**	**	**	**	**	**	**	**	**	**
16	17	18	19	20	21	22	23	24	25	26	27	28	29	30	31
FES DATA															
**	**	**	**	**	**	**	**	**	**	**	**	**	**	**	**
32	33	34	35	36	37	38	39	40	41	42	43	44	45	46	47
FES DATA															
**	**	**	**	**	**	**	**	**	**	**	**	**	**	**	**
48	49	50	51	52	53	54	55	56	57	58	59	60	61	62	63
FES DATA															
**	**	**	**	**	**	**	**	**	**	**	**	**	**	**	**
64	65	66	67	68	69	70	71	72	73	74	75	76	77	78	79
FES DATA															
**	**	**	**	**	**	**	**	**	**	**	**	**	**	**	**
80	81	82	83	84	85	86	87	88	89	90	91	92	93	94	95
FES DATA															
**	**	**	**	**	**	**	**	**	**	**	**	**	**	**	**
96	97	98	99	100	101	102	103	104	105	106	107	108	109	110	111
FES DATA															
**	**	**	**	**	**	**	**	**	**	**	**	**	**	**	**
112	113	114	115	116	117	118	119	120	121	122	123	124	125	126	127
FES/PAS DATA															
**	**	**	**	**	**	**	**	**	**	**	**	**	**	**	**

* INDIRECT ADDRESS REGISTER
 ** INDIRECT ADDRESS REGISTER 2
 # WORD GATE REQUIRED
 MF MINOR FRAME

TELEMETRY FORMAT - 2476 OPERATIONAL FORMAT JUNE 1, 1979

Figure 5-24. Format 2A (Engineering format).

Indirect addressing (IA) is used as a method to conserve hardware and software space. As it was noted earlier, more than one unit device has been designed to perform the same function, for example there are two FES units, two PAS units, two OBC units, four camera units, etc. The data words allocated to record one of these units may also be used with the redundant unit. The method by which this is possible utilizes the indirect address method which specifies indirectly the address of the unit to be sampled. In other words, this approach minimizes the need for changing an entire format for an experiment having several channels of outputs.

Telemetry and computer sample rates.

The maximum data sample rate (SRATE) through the multiplexer is 80 Kbps with 40 Kbps maximum telemetry data rate and 40 Kbps maximum data rate to the OBC. The DMU is used for both telemetry and computer data-collecting functions, so the input data are split into 2 serial data bit channels, one for each use. The computer and telemetry channels would receive alternate words from the multiplexer if the telemetry bit rate were maximum. In this case, the ratio of computer-to-telemetry words, called the multiplex ratio (MXR) is 1:1, for low telemetry bit rates, the MXR is greater than this and can be selected by ground command as the rest of the DMU parameters (bit rate, indirect addressing, encoding, ground telemetry format, computer format, etc).

The figure 5-25 shows the possible combinations of MXR and SRATE.

TLM BITRATE(KBPS)	OBC BITRATE(KBPS)	MXR	SRATE
80	0	0=ALL TLM	0
40	0		1
20	0		2
10	0		3
5	0		4
2.5	0	5	
40	40	1	0
20	20		1
10	10		2
5	5		3
2.5	2.5		4
1.25	1.25	5	
20	40	2	0
10	20		1
5	10		2
2.5	5		3
1.25	2.5		4
---	---	5	
10	40	3	0
5	20		1
2.5	10		2
1.25	5		3
---	---		4
---	---	5	
5	40	4	0
2.5	20		1
1.25	10		2
---	---		3
---	---		4
---	---	5	
2.5	40	5	0
1.25	20		1
---	---		2
---	---		3
---	---		4
---	---	5	
1.25	40	8	0
---	---		1
---	---		2
---	---		3
---	---		4
---	---	5	

Figure 5-25. Telemetry bitrate possibilities.

Although there were many possible combinations of MXR and SRATE, some of them proved to be the source of many problems during operations, so some restrictions were implemented.

- ▶ The 40 Kbps telemetry data rate resulted in faulty data decommutation and was suspected of causing OBC crashes; for this reason, operations were limited to 20 Kbps on November 15, 1978.
- ▶ The OBC data rates of less than 20 Kbps were not normally allowed because they resulted in less accurate attitude control.
- ▶ The MXR parameter was not permitted to be equal 4 because this caused problems with the DMU.

Operations were usually conducted using 20 Kbps for computer telemetry and 20 Kbps or 5 Kbps (when the signal strength was very low) for ground telemetry.

In addition to the normal mode of transmitting data, another method, known as convolutional encoding exists on the IUE. It is commonly referred to as the convolved data mode. Using a complex algorithm where two bits are telemetered for each data bit, this mode can produce an effective 3 dB gain in signal strength. Since convolved data effectively reduces the amount of data dropouts, it was the nominal mode used during the IUE mission.

5.4.1. The DMU anomaly

The DMU anomaly was a problem related with erroneous fluctuations in telemetry data. Some telemetry words with values between 160 and 191 were reported as 159. Also, some values around 127 were changed to 63. The 159 wrong values affected both engineering and science data, while the second one only occurred in a few channels and was never observed in science images. As all corrupted values were always analog ones, it was assumed to be a malfunction of the A/D converter of the DMU.

The corruption of specific data points, in particular the reaction wheel tach values, in telemetry was first noted on October 24, 1994 and continued to be observed on a frequent but sporadic basis. At this time, the values of the tachs as received by the OBC DRT format were placed in telemetry, which showed that the OBC was also receiving corrupt values (159s). The corruption only appeared sporadically when the telemetry format was 1B.

On January 1, 1995 the SWP y-alignment value was observed to be corrupted. This parameter had a normal value of 127, its value when corrupted was 63.

On January 6, 1995 the corruption of data was observed with the DMU set to format 2A. When it happened, the DMU and OBC had reached very high temperatures, around 25.6° C and 55.8°C, respectively, for several hours.

A few days later, the 159 corrupted value also appeared in science images. New operation restrictions were applied to avoid high OBC and DMU temperatures. As the OBC was also

receiving bad data, a main concern was that the spacecraft attitude control could be affected (some analog values were used by the OBC to determine if its direct read was in synchronization. If the data was determined to not be in synchronization, no attitude programs would be permitted to run).

During the rest of the IUE life, the corrupted data continued appearing in some spectral images, but this problem never affected the spacecraft attitude control. The conclusions reached about this problem are as follow,

- ▶ The corruption is directly associated with the DMU and OBC temperatures, as is shown in the figures 5-26 and 5-27.
- ▶ The corruption seemed not to be dependent of the radiation environment, as could be seen in the figure 5-28.
- ▶ The frequency of corrupted data increased with the time spent in format 1B. The format 1B exercises the A/D converter more frequently than the format 2A. The table below shows the results of a test conducted to check this dependency on November 22, 1995.
- ▶ The images did not seem to begin to be corrupted until the level of corruption in the engineering parameters reached values up to 60 %. The engineering data corruption is computed as the number of points corrupted over the total during the time considered. The image corruption is measured as,

$$(n^{\circ} (159s) - n^{\circ} (168:170))/\text{standard deviation}$$

The figure 5-29 shows this effect.

Image n°	Time spent in 1B	Time spent in 2A since the last time the s/c was in 1B	Average around 159 (148-158 and 160-170)	159s
LWP 31732	26 m	-	79	85
LWP 31733	26 m	7 m	82	119
LWP 31734	26 m	14 m	78	121
LWP 31735	26 m	22 m	77	212
LWP 31736	30 m	5 m	71	522
LWP 31737	29 m	2 m	69	633
LWP 31738	29 m	130 m	77	254

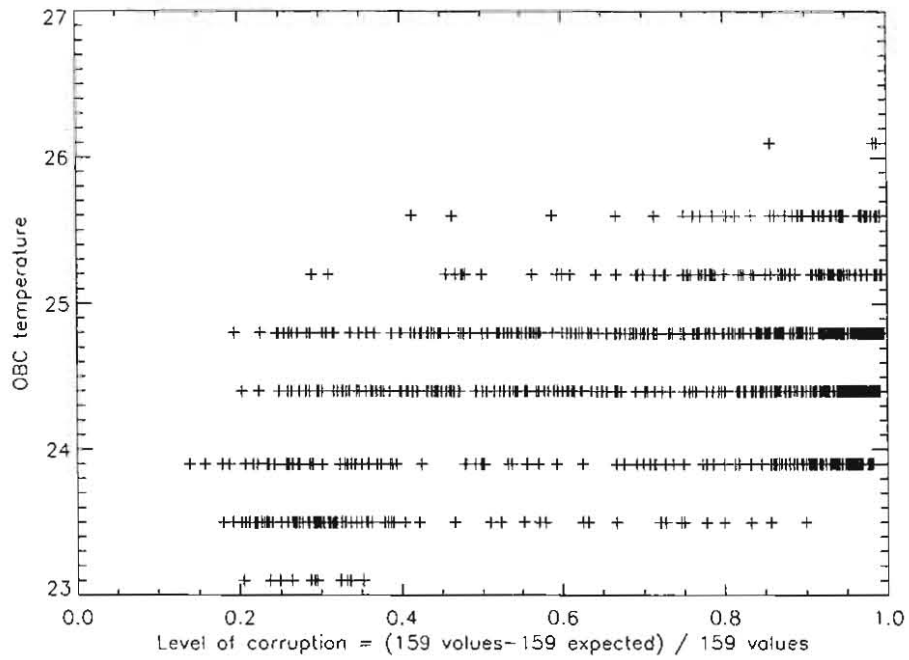


Figure 5-26. Corruption vs DMU temperature.

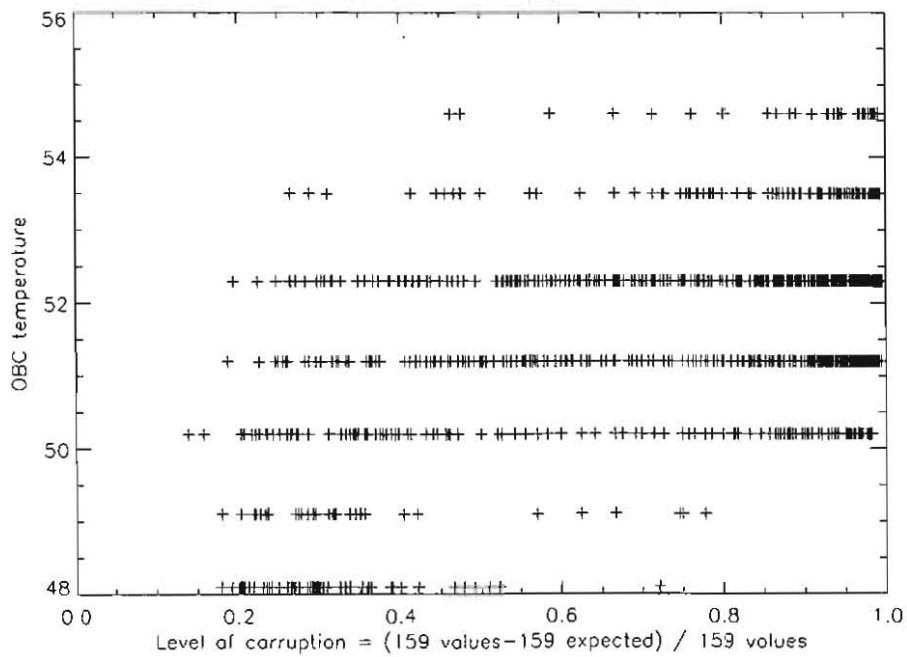


Figure 5-27. Corruption vs OBC temperature.

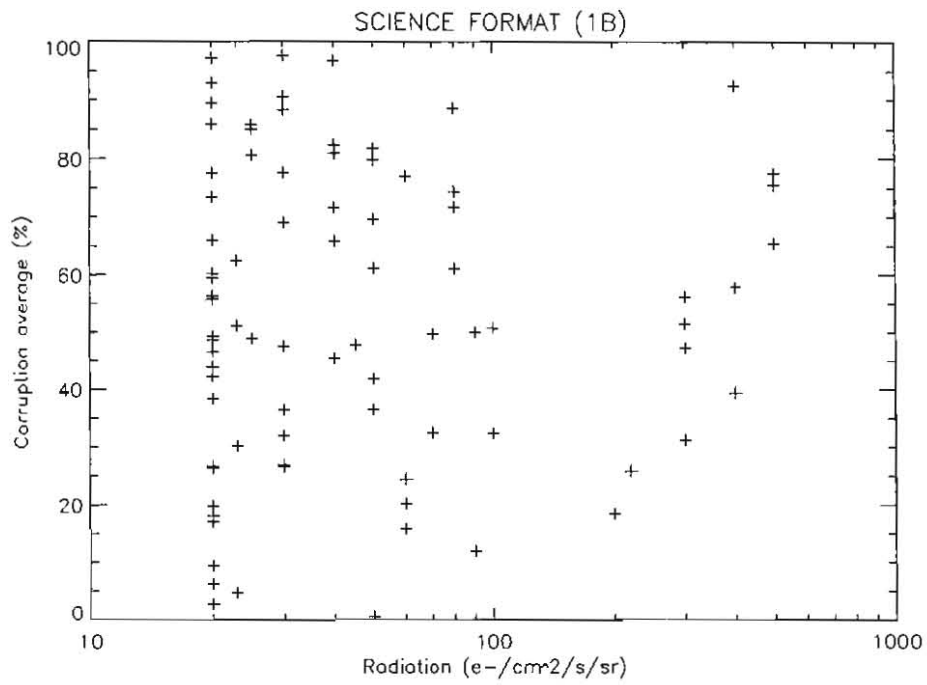


Figure 5-28. Corruption vs radiation.

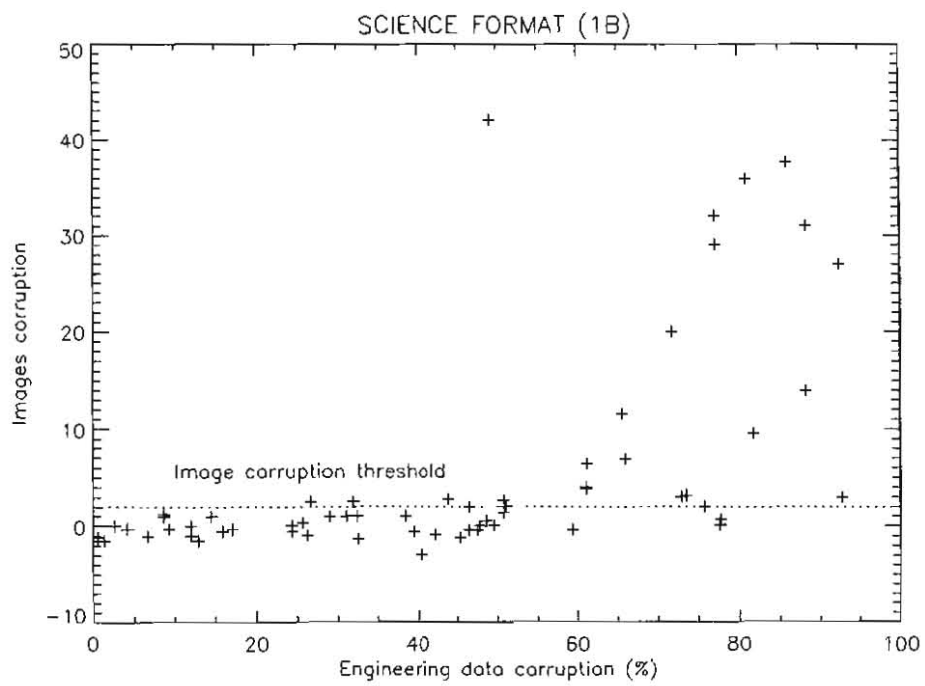


Figure 5-29. Image corruption vs engineering data corruption.

Operational restrictions

The appearance of corrupted telemetry values had made it necessary to restrict the operating temperatures of the OBC and DMU. A Flight Operations Directive (FOD) limited the OBC and DMU temperatures to 54.6° and 26.1° respectively since January 17, 1995.

The limits imposed on the OBC were intended to prevent the DMU from reaching the temperature where the rate of data corruption becomes excessive. The DMU temperature follows the OBC temperature trend closely but with a lag time; therefore restricting the OBC temperature should prevent the DMU temperature from reaching its critical point.

5.4.2. DMU radiation monitor

The DMU Radiation Monitor is a type of “free running” experiment on board the spacecraft. The purpose of the package is to examine the damaging effect of radiation in space on certain COS/MOS types of chips. These chips are similar to those used in the data and command systems on board the satellite.

Each of the eight chips was monitored for about five minutes, during a monitor sequence, with data collected every 0.512 sec on all chips. A complete period of all eight cycles appears on the figure 5-30.

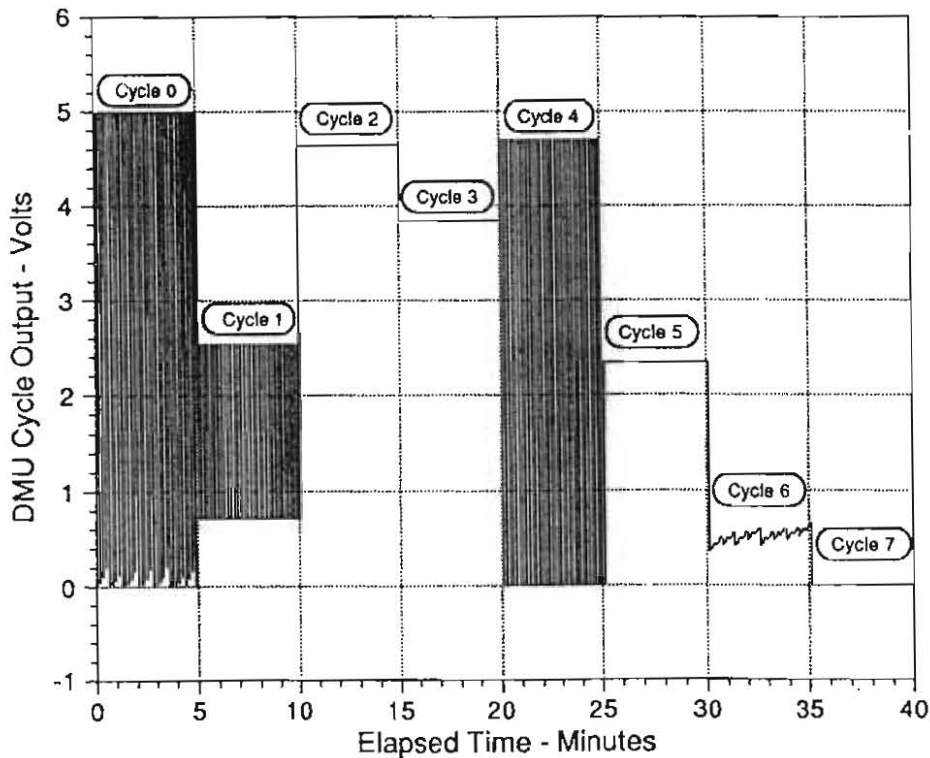


Figure 5-30. DMU Radiation monitor sequence output.

Cycles 0, 1, 4 and 6 produce fluctuating voltages which are graphed along with historical data. Cycles 2, 3, 5 and 7 are constant values and are displayed in historical graph form. A brief explanation of the cycles accompanies each graph.

- **Cycle 0.** (Figures 5-31 and 5-32)
32 cycles of an exponential rise and fall between an approximate 5.20 v and ground.

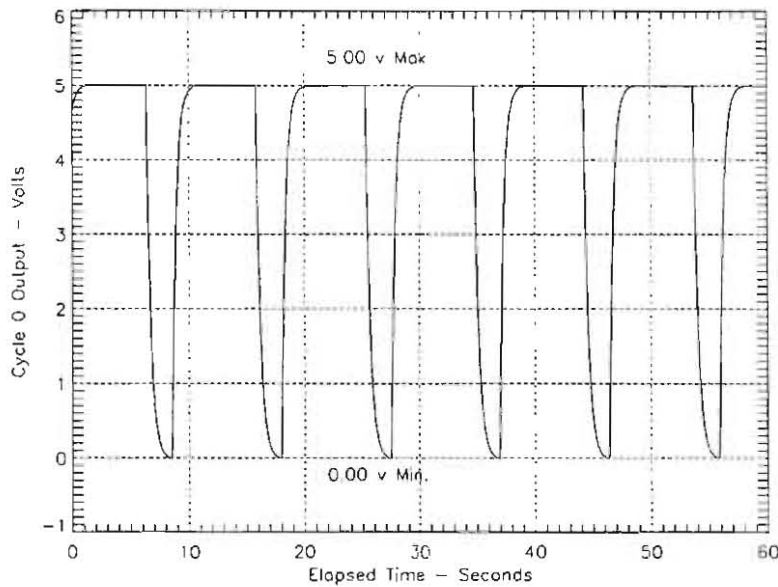


Figure 5-31. Cycle 0 output.

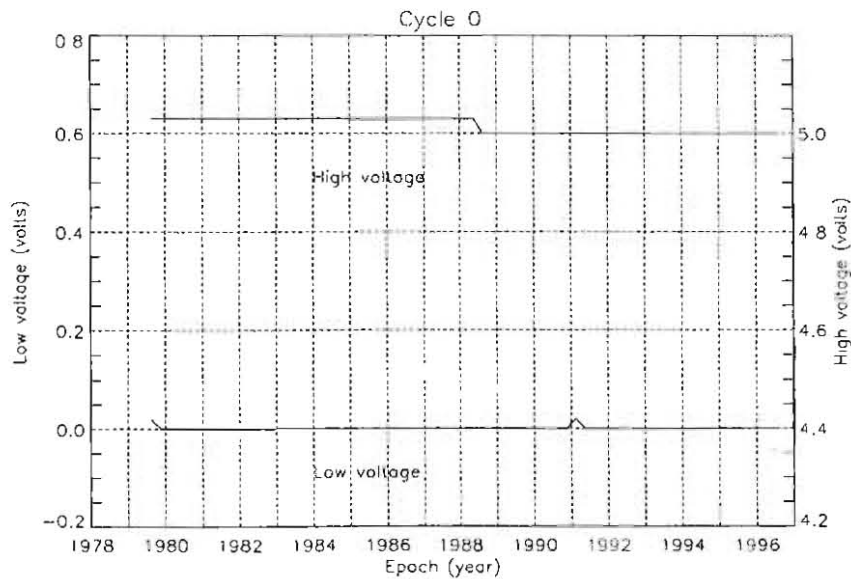


Figure 5-32. History of the Cycle 0 output.

- **Cycle 1.** (Figures 5-33 and 5-34)
32 switchings between off and device threshold of a PMOS unit.

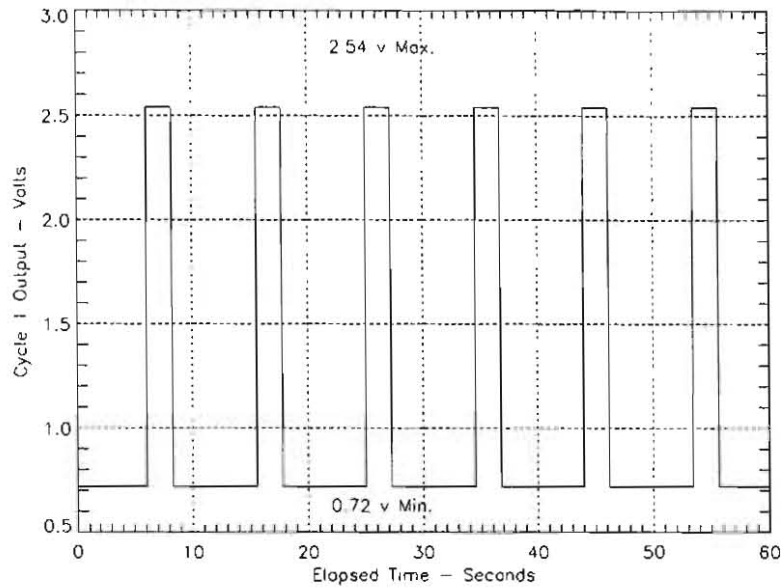


Figure 5-33. Cycle 1 output.

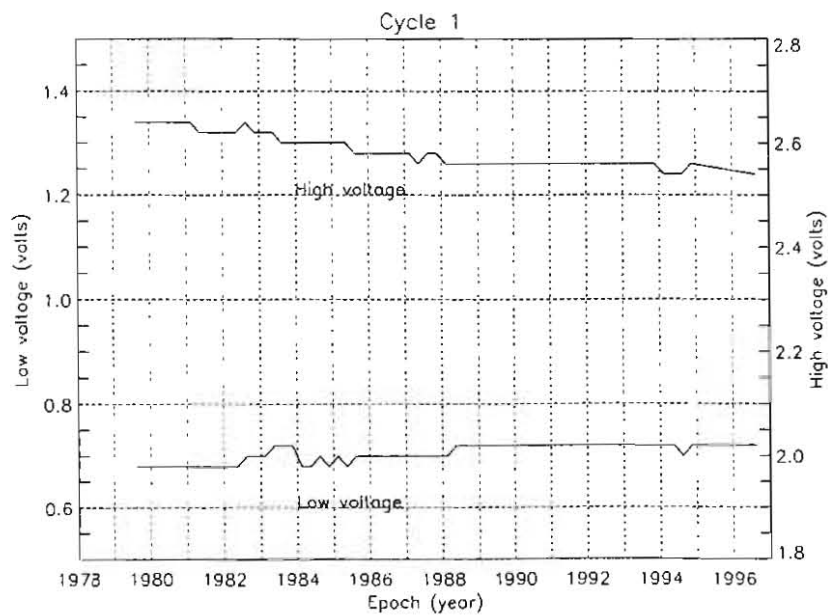


Figure 5-34. History of the Cycle 1 output.

- **Cycle 2.** (Figure 5-35)
The reading of a low threshold device at a continuous threshold.

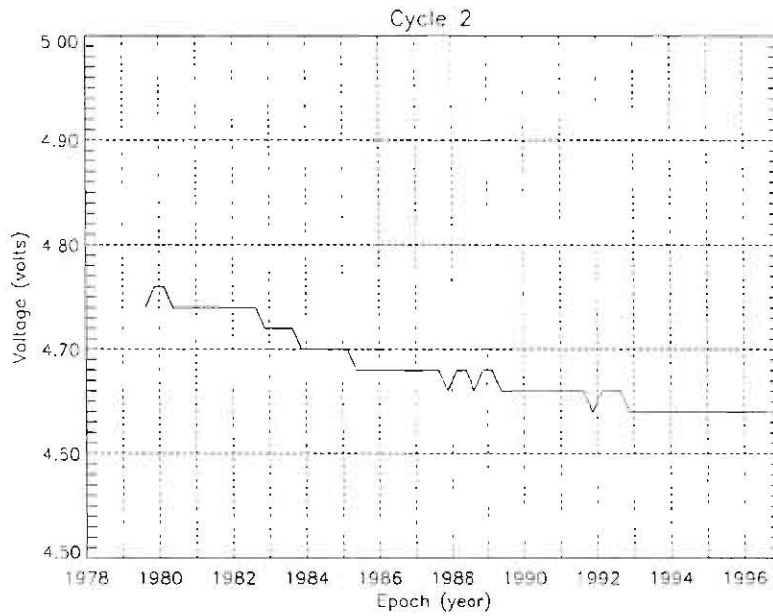


Figure 5-35. History of Cycle 2 output.

- **Cycle 3.** (Figure 5-36)
The operating threshold of a COS/MOS device.

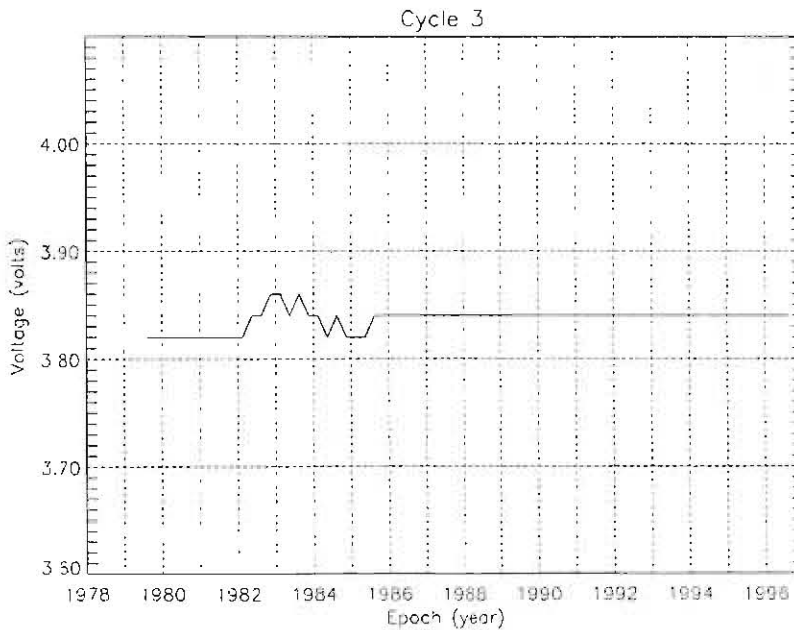


Figure 5-36. History of Cycle 3 output.

- **Cycle 4.** (Figures 5-37 and 5-38)
32 switchings between off and device threshold of a low threshold device.

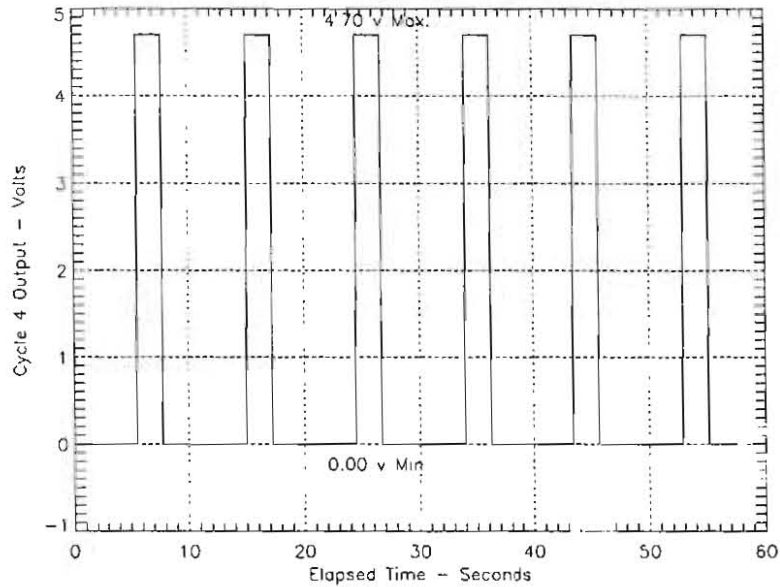


Figure 5-37. Cycle 4 output.

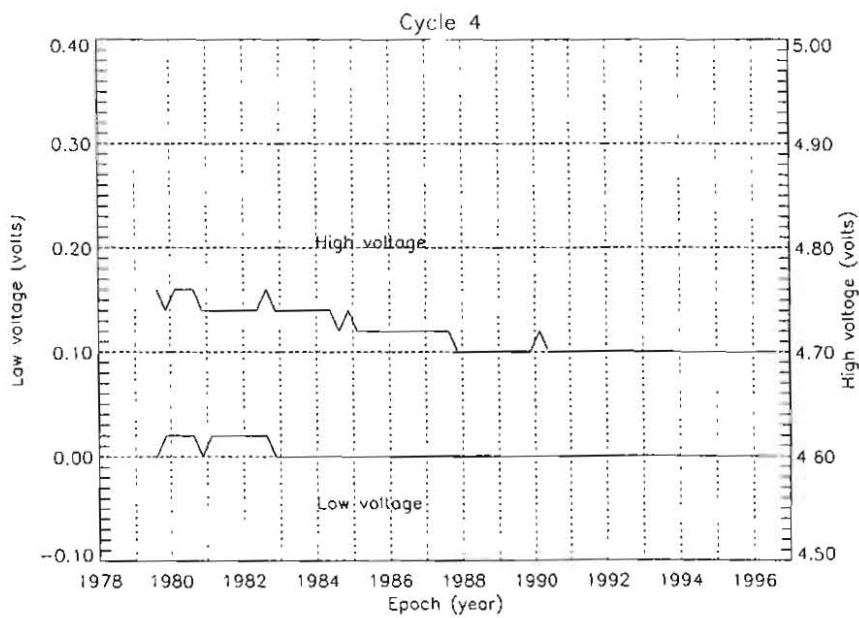


Figure 5-38. History of the Cycle 4 output.

- **Cycle 5.** (Figure 5-39)
The reading of a high threshold device at a continuous threshold.

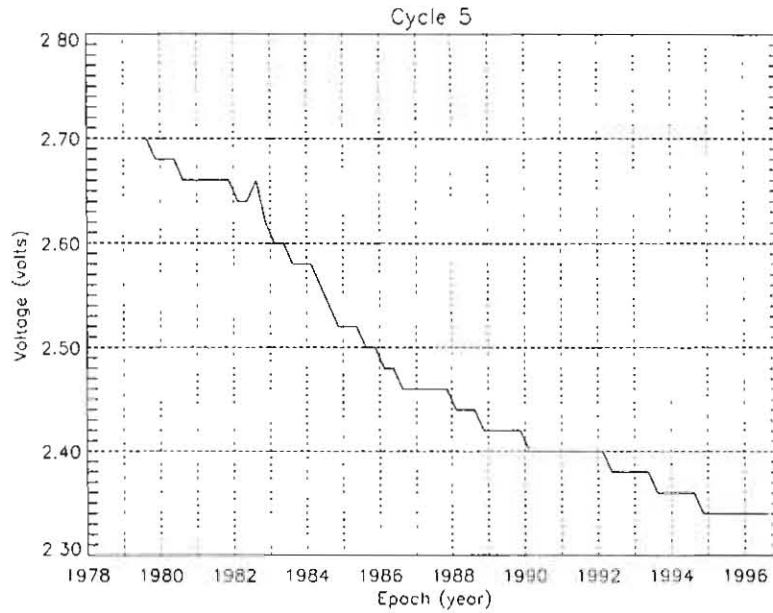


Figure 5-39. History of Cycle 5 output.

- **Cycle 6.** (Figure 5-40)
The voltage of a PMOS chip going through small changes, as it advances through 32 states.

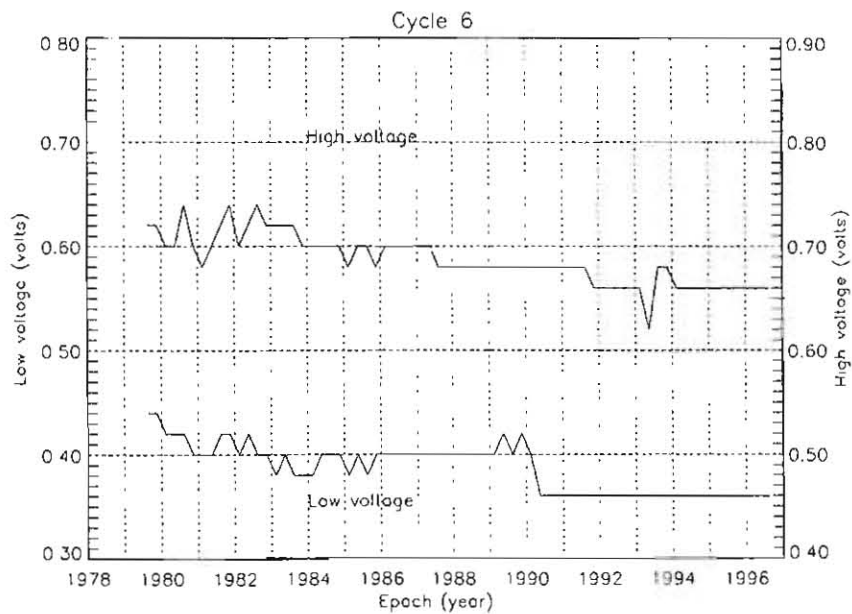


Figure 5-40. History of Cycle 6 output.

- **Cycle 7.** (Figures 5-41 and 5-42)
Measures degree of COS/MOS saturation of an N-channel device.

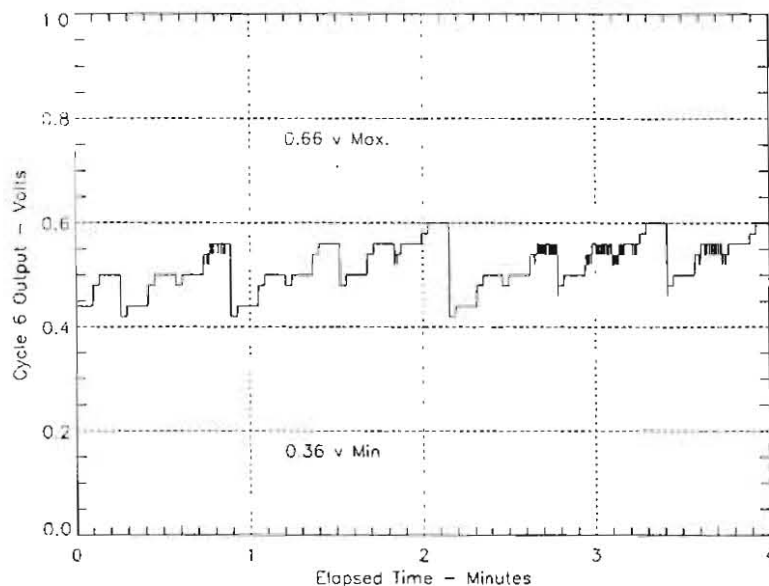


Figure 5-41. Cycle 7 output.

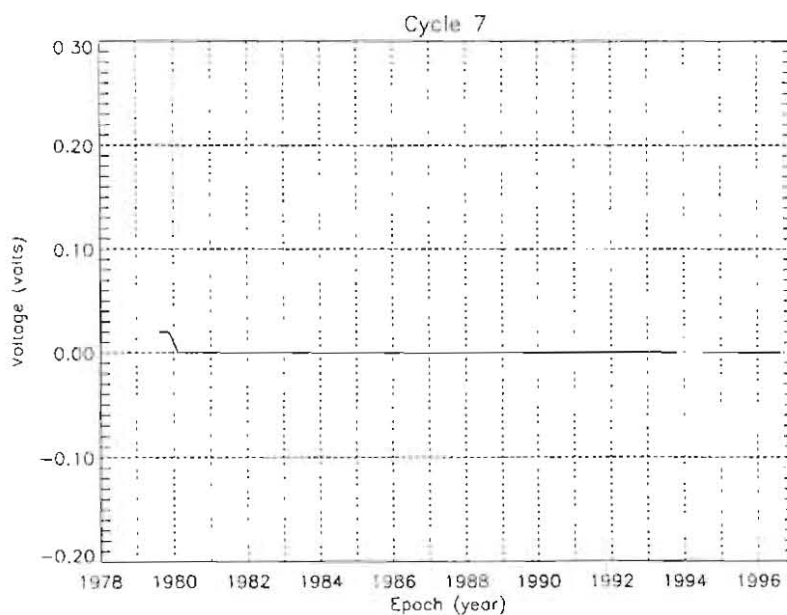


Figure 5-42. History of the Cycle 7 output.

In summary, all of the chips have deteriorated 3 % or less except for the chip utilized during cycle five. This chip has deteriorated approximately 13 % since launch at a slow rate of approximately 0.02 to 0.04 volts per year.

5.5. Attitude Control Subsystem

The IUE stabilization and attitude control subsystem consists of all equipment used to maintain or change the direction at which the spacecraft is pointing. In order for spacecraft attitude to be controlled, there must be some sort of attitude sensors, some equipment capable of producing a change in the orientation of the spacecraft (actuators) and an interface between the two. The IUE is capable of controlling attitude using a number of combinations of sensors, actuators, and interface.

This subsystem is without question the most complex subsystem aboard the IUE spacecraft. It was designed to be simple, light weight, low powered and reliable on one hand, and on the other hand, it was required that the control subsystem satisfy precise pointing and slew accuracy specifications. The principal requirements that have largely influenced the control subsystem design philosophy are the following:

- ▶ Three-axis stabilization in inertial space with a ± 1 arc second pointing accuracy requirement in pitch and yaw, for periods typically of $\frac{1}{2}$ hour and more.
- ▶ Following a slew or a sequence of slew maneuvers, a new source target must be acquired to within the 8 arc-minute half-cone angle field of the telescope.
- ▶ The pointing accuracy requirement must be satisfied for extended periods of time even when stellar attitude measurements of sufficient accuracy and frequency are not available.
- ▶ The expected useful operating life was to be 3 or 5 years.
- ▶ The stabilization and control subsystem was to be autonomous from a safety standpoint even though the spacecraft would be in synchronous orbit and in nearly continuous contact with the ground.

The attitude sensors include Earth and Sun sensors for use in ground computer aided attitude determination, accelerometers for on-board nutation control as well as rate gyro sets, analog Sun sensors for initial spacecraft acquisition, and an Inertial Reference Assembly, fine Sun sensors, and fine error sensors (or star trackers) for use in inertial star acquisition and subsequent hold and slew operations.

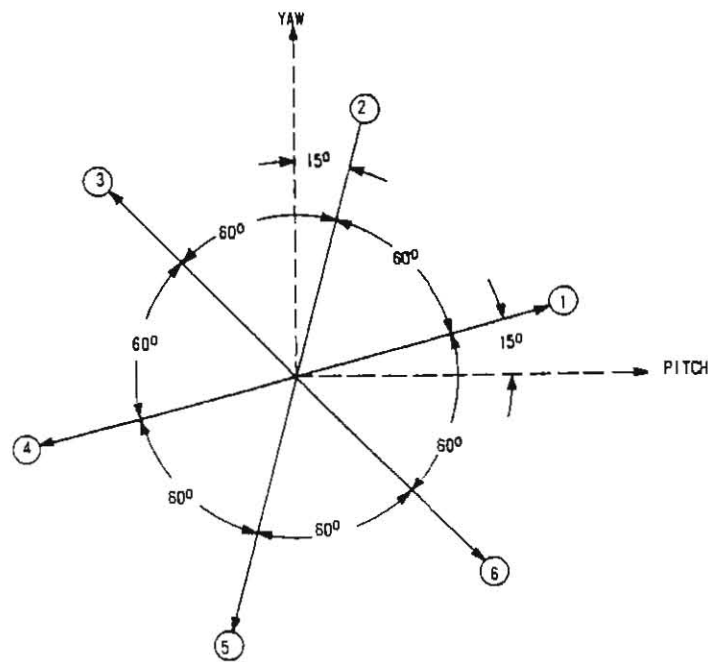
Hardwired analog control algorithms were incorporated to perform nutation control and all spacecraft initial acquisition functions as well as to provide an emergency rate hold function. The on-board computer was programmed to duplicate all the hardwired algorithms in addition to its primary attitude control functions of star acquisition, hold and slew.

For actuators, the IUE uses any three of the four reaction wheels in the hold and slew operations, and the hydrazine propulsion system in emergency attitude control and station keeping maneuvers.

5.5.1. Inertial Reference Assembly

The Inertial Reference Assembly is the prime attitude sensor of the IUE spacecraft. The IRA consists of six single-degree-of-freedom, hydrodynamic gas bearing, rate-integrating gyroscopes with pulse-rebalance electronics.

A gyroscope can be described as an instrument that uses a rapidly spinning mass to sense and respond to changes in the inertial orientation of its spin axis. The gas bearing effectively eliminates the gyro bearing failure mechanism and significantly reduces its output noise, while pulse rebalancing provides a much improved readout accuracy as compared to analog rebalancing techniques. The assembly provides redundant analog rate information proportioned to body axis rates and digital attitude change information referenced to each gyro input axis. Each gyro senses inputs in all three spacecraft axes, by virtue of being skewed to all axes, as shown by the projections of the input axes of the six gyros on the spacecraft pitch-yaw plane.



PROJECTIONS OF THE INPUT AXES OF THE SIX GYROS ON SPACECRAFT PITCH-YAW PLANE

INPUT AXES LIE ON A CONE ABOUT ROLL AXIS WITH 85° HALF CONE ANGLE

Figure 5-43. Projections of the input axes of the six gyros.

The OBC transforms and combines the gyro signals to create the composite control signals. Each gyro also generates analog signals to the control electronics assembly which drives the low-thrust engines and reaction wheels for analog Sun acquisition and Sun hold modes.

Each gyro has two operational modes and the resolution of each gyro is different in the two

modes. In hold/slew mode, the gyro generates digital signals with a resolution of 0.01 arcseconds. While in rate mode, the gyro generates analog signals with a resolution of 0.3 arcseconds.

The IRA was not used in the transfer orbit. Only the low-power heaters were on during this mission mode to maintain each gyro at or above 70° Fahrenheit. The following list summarizes the IRA modes used during the mission orbit:

- ▶ Despin. The IRA provided a redundant set of analog voltages proportional to sensed pitch, yaw and roll body rates. This information was used to automatically despin the vehicle from 5 rpm to near zero rates in all three axes.
- ▶ Respin. The IRA acted as a rate reference during the respin maneuver necessary for solar array deployment.
- ▶ Sun acquisition. Analog rate information from the IRA is mixed with position information from the course sun sensor to rotate the spacecraft. So that the sunline is normal to the solar array central panel and limit the rate of rotation about the sunline.
- ▶ Sun hold. Analog rate information from the IRA is mixed with position information from the course sun sensors to drive the pitch, yaw and roll reaction wheels and hold the solar array normal parallel to the sunline.
- ▶ Hold during velocity burn. Digital position information is provided by the IRA during this mission mode to permit the hydrazine system to operate without changing the spacecraft thrust axis inertial attitude.
- ▶ Backup sun acquisition and rate damping. Digital position information is provided by the IRA during those backup mission modes to permit an OBC algorithm to despin and stabilize the spacecraft in three axes.
- ▶ Hold/slew mode. Digital information is provided by the IRA during the mission to permit an OBC algorithm to hold the spacecraft inertial attitude in three axes and to slew the spacecraft from target star-to-target star.

5.5.1.1. Gyro failures

At the end of the IUE spacecraft life, only the Gyro 4 remained operational. The other five gyros were lost as is summarized below.

- **Gyro 6**

During the first two shadow seasons, the 80% depth of discharge limit had been nearly reached on one battery, so it was decided to reduce the power load during the third shadow season by transferring operations to 3 gyros and turning off Gyros 2, 4 and 6. On April 18, 1979, Gyro 6 failed to restart.

The test carried out in an attempt to identify the Gyro 6 problem indicated that the proper

amount of current was being drawn by the gyro. The gyro rotor was apparently stuck. All engineering procedures executed in attempting to restart Gyro 6 were unsuccessful.

- **Gyro 1**

Since June 28, 1981, the Gyro 1 temperature had been slowly dropping. The drift rate was also changing slightly, which indicated that the change in temperature was real and not the result of a faulty telemetry thermistor.

On March 2, 1982 Gyro 1 was considered lost when its analog and digital telemetry was very quickly saturated, making it useless for either digital or analog control. The problem was diagnosed as a failure in the Pulsed Rebalance Loop of Gyro 1's electronics.

In that gyro 1 had previously been judged unsuitable for use in the OBC's hold/slew algorithm, and was not in the gyro matrix used for attitude control at the time, the failure did not immediately impact operations.

- **Gyro 2**

On July 27, 1982 Gyro 2 failed. Its motor current rose from a nominal 60 mA to 220 mA in 9 seconds. A similar problem had been observed in this gyro on August 18, 1981; the gyro current increased from 64 mA to 118 mA and then it returned to normal when the gyro was turned off and back on immediately.

In this failure, several attempts were made to start up the gyro by commanding it off then on again very quickly. This method did not work and so the gyro was turned off due to high temperature, the Gyro 2 temperature increased to 69.3° C.

It appeared that the failure could be the result of a small particle jamming the rotor. During the turn-on attempts, maximum current was used to try to spin-up the gyro however no change in spacecraft momentum was observed.

- **Gyro 3**

On August 17, 1985 Gyro 3 failed. Its motor current dropped from a nominal 60 mA to 2 mA and the spacecraft momentum changed quickly.

The spacecraft was put in sun-hold mode and the 2 Gyros/FSS backup control mode was loaded and enabled in the on-board computer. The commissioning of this system was successfully carried and on September 30, 1985 the observing program was restarted.

- **Gyro 5**

On February 5, 1991, the Gyro 5 motor current dropped from a nominal 60 mA to 0 mA and remained there. However, Gyro 5 continued to work properly and no change in spacecraft angular momentum was observed (the rotor continued to spin). The manufacturer's final conclusion was that Gyro 5's prime winding was open, so its performance should be nominal unless it became necessary to restart Gyro 5.

On March 6, 1996 Gyro 5 was switched off by conflicting commands being sent to the

spacecraft and it could not be restarted. The IUE was placed in sun-hold mode and the previously prepared and tested 1-Gyro control mode was loaded into the on-board computer. On April 4, 1996 the observing program was restarted.

5.5.1.2. Gyro Drift Rates

Changes in the drift rates of the individual gyros caused some degradation of the spacecraft maneuvers and had to be corrected by updating the gyro scale factors in the OBC. New scale factors were calculated using data from maneuvers. The scale factors only changed rarely, and only once after 2 Gyro/FSS system implemented.

During the last years of the mission, the Gyro 5 drift rate increased very quickly, which was associated with the degradation of the gyro's condition. At the same time, Gyro 5's drift rate was subjected to short term fluctuations, which were thermally induced. In order to correct all these variations, the Gyro 5 drift rate offset was updated very frequently during normal operations.

The gyro counts were converted to differential angles following the equation below.

$$\text{ABD (differential body angle)} = \text{WG (scale factor)} * \text{Gyro counts} - \text{BGDT (drift rate offset)}$$

The figure 5-44 shows the gyro drift rates along the whole spacecraft life.

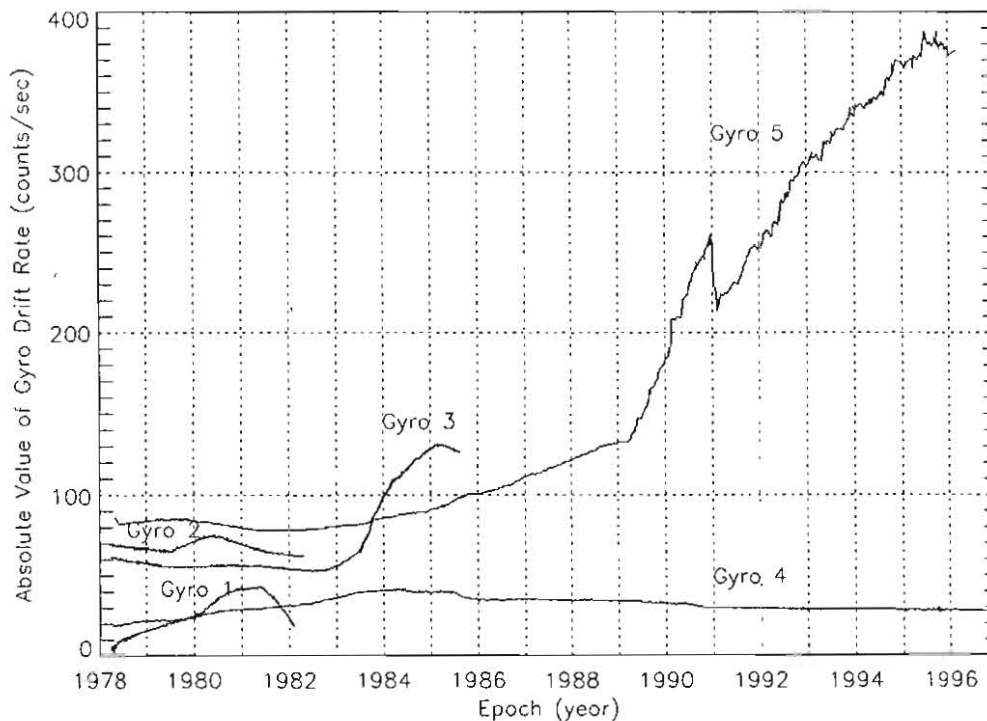


Figure 5-44. Gyro drift rates.

5.5.2. Fine Sun Sensor

The Fine Sun Sensor (FSS) is a Digital Sun Sensor, which measures the spacecraft's position relative to the sun. In the pitch direction (rotation about the Y axis) the FSS measures the angle between the XZ component of the sun vector to the spacecraft -X axis, which is known as the beta angle (β). In the roll direction (rotation about the X axis), the FSS measures the angle between the YZ component of the sun vector and the +Z axis.

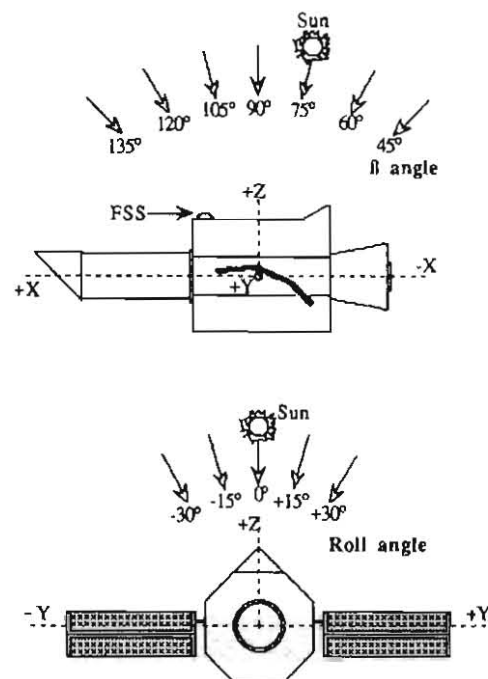


Figure 5-45. Definition of the beta and roll angles.

Two independent FSS systems are used to provide functional redundancy. Each system consists of two sensor heads and a separate electronics unit. The orientation of the two systems is identical. The heads are set up in such a way that Head 1 can view the sun from beta angles ranging from 137° to 73° and Head 2 can view the sun from beta 77° to 13° . Both heads are designed to sense the sun up to $\pm 32^\circ$ in Roll. In this way, sun presence could originally be maintained from beta 13° to 137° and at any Roll angle from $\pm 32^\circ$. During the IUE life, both systems were powered on and the following combinations were used during normal spacecraft operations; System 1/Head 2 for operations below beta 75° and System 2/Head 1 for operations above beta 75° .

Each sensor has two reticles, a fine reticle and a coarse reticle, for each axis. The coarse reticle encodes the Sun angle in six-bit Gray code format over the field of view to an average resolution of 1° . The fine reticle produces a quadrature sinusoidal output with an average period of 2° . The quadrature outputs are combined with four quadrature square waves to give a position signal whose phase angle is proportional to the Sun position within the 2° reticle period. This phase angle is measured by counting the number of high frequency reference pulses that occur between

zero crossings of the position signal and a reference ac signal.

The overlap between the 2° period of the fine reticles and the 1° resolution of the coarse reticles gives two digital values, NA and NB, which are transferred to the OBC and ground. These values are put through nine-term equations with the end result being a beta and roll measurement.

The FSS resolution is dependent of the actual sun to spacecraft angle. Both the beta and Roll angles affect the sensitivity of the FSS. The figure 5-46 and 5-47 show how the resolution varies with beta. Betadel is defined as the difference between the calculated beta angles corresponding to a FSS output measurement differing by a single count in the least significant bit weight position.

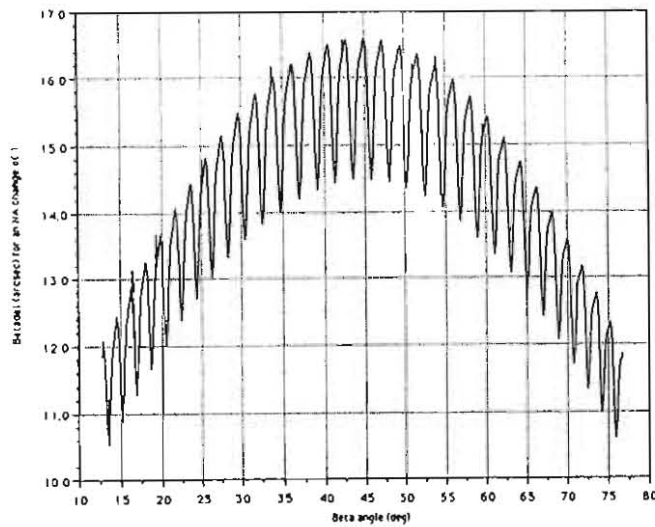


Figure 5-46. FSS beta and roll resolution vs beta angle.

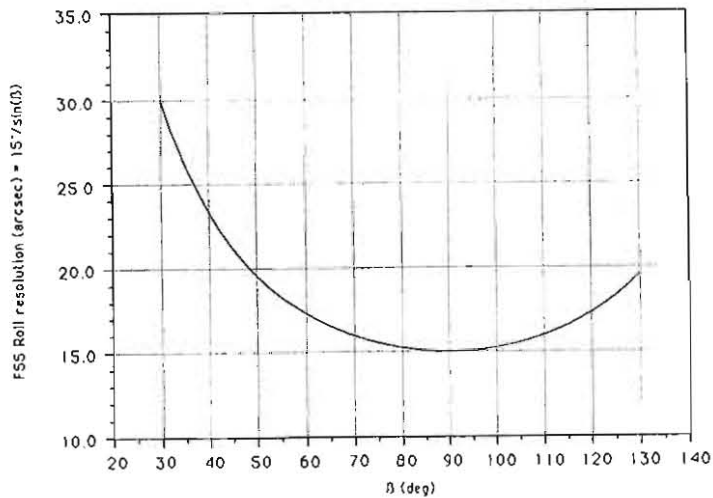


Figure 5-47. FSS beta and roll resolution vs beta angle.

While the FSS was always used as an attitude reference tool, its importance to the IUE mission was not fully realized until the middle of 1985, when the fourth of six gyros failed. This left IUE with 2 remaining gyros, FES, and the FSS to build an useable attitude control system. The 2-Gyros/FSS system used the FSS to control the Roll axis and, also, for position control on the Pitch axis during slews. After the fifth gyro failed, the 1 Gyro control system had to be implemented. In the default mode, when there was not any available star to guide on, the FSS data was used to control both the pitch and roll axis with position and rate information. The yaw axis was computed using Gyro 4 information corrected with FSS data to remove Pitch and Roll components.

5.5.2.1. FSS anomalies

Until April 1986, no reported spacecraft anomalies involved the FSS. It was noticed that in 1986, the ability of the FSS to correctly sense the sun position at beta angles less than 20° had degraded.

On March 9, 1988, it appeared that the degraded region slowly grew towards higher beta angles causing a loss of attitude control while the spacecraft was slewing at beta 22° . At the end of the maneuver the FSS gave corrupted data to the OBC in such a way that the maneuver continued towards lower beta angles and the sun presence was lost. The spacecraft had to be stabilized by commanding the sun hold mode. Shortly thereafter it was decided to limit spacecraft operations to beta angles above 28° .

On July 29, 1988 a spacecraft test was performed to determine the feasibility of switching to the redundant FSS heads. A switch would have been desirable if the redundant heads offered an improvement to the existing FSS operating limits. This proved to be useless. The back head (System 1/Head 1) provided worse data than the prime one (System 2/Head 1).

In 1990, a new corruption to the FSS data was observed. Because the sensor is not perfectly aligned with the spacecraft axes, the FSS roll angle not only has a component in the spacecraft roll axis, but also contributes a small amount to the spacecraft pitch angle, beta. In 1990 it was discovered that the information coming from the FSS roll axis had become corrupted and was adversely affecting control in both the pitch and roll axes. An investigation into this event showed that one of the 6 Coarse Gray code bits that come from the FSS roll axis was intermittently dropping out (from 1 to 0), and that it was happening consistently in the beta region between 35° and 38° . A software workaround was uplinked to the OBC to detect this situation and correct it.

While the spacecraft was controlled by the 2 Gyro/FSS system, the regions in which the FSS produces corrupted data had been increasing in number for several years, but had been compensated by restricting operational beta ranges or by implementing software patches. While an increase in anomalous functioning would be expected as the spacecraft aged, the lack of reported FSS anomalies prior to the implementation of the 2 Gyro/FSS system probably resulted from the use of this sensor in only a secondary manner. Anomalous FSS readings would not have been as noticeable since they would not impact the attitude control function.

On the 1 Gyro system, the effects of the FSS corrupted data have a more significant impact than they had on the 2 Gyro/FSS system. The yaw was now affected by corrupt FSS data as well as

the pitch and roll axes. The affect of corrupt FSS data on the yaw axes as well as an inconsistent handling of overflows by the onboard computer would typically cause a loss of spacecraft attitude under the 1 Gyro system.

5.5.3. Coarse Analog Sun Sensor

The coarse analog sun sensor is used to provide two-axis attitude information with respect to the spacecraft pitch and roll solar array paddle axes. Six sensors (2 for roll, 4 for pitch) are utilized and are arranged to provide 4π steradian coverage. The output of the CSS is in the form of an error from roll equals 0° and beta equals 67.5° .

The CSS resolution is approximately 1° . So, the pitch and roll sets would both yield a sensor null when the Sun is at some point within 1° half-cone of the CSS null axis (roll equals 0° and beta equals 67.5°). The information from the CSS was used to drive the reaction wheels in the sun hold mode (Sunbath mode). Because the CSS did not have a yaw component, this axis was not controlled in the Sunbath mode, the spacecraft would spin about the yaw axes while the pitch and roll axes were maintained.

5.5.4. Spin Mode Sun Sensor

This system consists of a single sensor head and its associated electronics package. The sensor field-of-view is $180^\circ \times 0.5^\circ$. Spacecraft alignment is such that its field-of-view is centred on $-Z$ axis along the spacecraft X axis. This sensor also provides a sun centred pulse as the field-of-view sweeps past the sun.

The SMSS was used in the transfer ellipse to measure sun angle with respect to the spacecraft X axis.

5.5.5. Panoramic Attitude Sensor

This system consists of two redundant sensor heads each having a dedicated electronics package. Each head provides a redundant 4π steradian coverage from a spinning spacecraft for earth/moon "look" angles and a sun-centred pulse so that "spin-sectoring" can be accomplished during the transfer ellipse.

The PAS was used during the transfer orbit and, in addition, was used to help establish spacecraft attitude prior to stellar acquisition.

5.5.5.1 PAS anomalies

The PAS 1 failed shortly after launch. On January 29, 1978 the PAS counters continued displaying data present for 30 minutes after expected loss of signal had occurred. The failure

seemed to be a chip failure in the data register.

On April 30, 1985 both PAS's were turned off. The purpose of this action was to reduce the IUE power consumption and thereby increase the range of power positive beta angles. The PAS 2 had not been used for the last four years and, in case the spacecraft attitude was lost, there were other available recovery modes.

On August 28, 1985 a test was performed to see if the PAS 2 was still operational. It was turned on and a camera image taken. The stepping motor of the optical scanner would cause noise in the image if it was operating, but this test showed none. The PAS 2 was no longer working.

On July 29, 1988 an attempt to discharge the batteries was made. For this reason, both PAS's were commanded on, but only PAS 1 drew current. Analysis of the data suggested a relay failure for PAS 2.

5.5.6. Accelerometer.

This system consists of redundant, linear force-rebalanced accelerometers. The redundant accelerometers are aligned such that their input axes are parallel to the vehicle thrust (or spin) axes. Information from these units was used to implement active nutation control during the spin portion of the mission.

5.5.7. Fine Error Sensor.

The Fine Error Sensor (FES) is a photometer which performs the star tracker function on the IUE spacecraft. Because the FES is not internally redundant and because of its importance to the mission, two FES's are installed in the IUE. Near on-axis energy passes through one aperture of either two sets of aperture holes in the fold mirror at the telescope focal plane. One set of holes, the small apertures, are 3 arcseconds in diameter and the other set of holes, the large apertures, are ovals 10 arcseconds by 20 arcseconds. This plate also contains the fiducial lamps, which are used as references to determine star positions relative to the apertures, and a low reflectivity patch near the center that attenuates star images by five orders of magnitude. The FES's receive all of the off-axis energy, which is divided by a beam splitter in a 70/30 percent ratio. As a result, the FES receiving the 30 %, FES 1, is about 0.93 magnitude less sensitive, and the FES that receives the 70 % share is designated the prime unit, FES 2.

The FES operates in various modes, which are based on counting the number of photons of sufficient energy impinging on a 12.62 arcsecond square or pixel of photo-cathode surface and then electromagnetically shifting this square in discrete steps in various fashions. The total number of photon-events counted will be a function of stellar radiation within the square and the length of time that the count is continued. This digital count can be compared with commandable preset values to establish magnitude thresholds. If the stellar flux is excessive and/or the counting period is excessive, the counter will become inhibited at a count of 28,672 photon-events.

Basically, the FES uses this pixel in either of the two following deflection modes:

- The search deflection mode is a square raster formed by a repeated step and dwell sequence. The start coordinates and size of the square are commandable functions which make it possible to position the raster square anywhere in the tracker field and trade off raster scan time against raster field size.
- The track deflection mode consists of a four position, symmetrical pattern, centred about the sensor's latest determination of star position. Photo event data collected from opposite sides are compared and used to determine the relative position of the star image to the dwell points of the scan. In order to accommodate the wide dynamic range of star intensities, the dwell times at the four points of the track pattern can be selected between 0.048 seconds, fast track, and 0.192 second, slow track. The distance of the opposite points can also be selected between 10.8 arcseconds, overlap, or 31.3 arcseconds, underlap.

The FES combines these modes with logic operations and dwell periods to function in one or another of three system modes called primary, search and track, and field camera mode.

- Primary mode. In this mode track deflection is used to track a guide star in the FOV of the FES. The ground command specifies the approximate location of the star to be tracked, the track pattern size (overlap/underlap) and the track scan rate (slow/fast) to use. These combinations are capable of tracking guide stars from +14 magnitude to +2 magnitude. The accuracy achieved is approximately 0.27 arcseconds, which is considered as a fine unit (32 fine units are called a coarse unit).
- Search and track mode. This mode is used to automatically search out a particular magnitude star by forming a commanded square raster and proceeding to track the first star encountered which exceeds the commanded threshold. First, the search deflection mode is used and then, once the star magnitude threshold is exceeded, the FES switches to the track deflection mode and tracks the star.
- Field camera mode. This mode is used to map the star field within a commanded FOV. Search deflection, synchronized with the telemetry system, is used to accomplish this search. A signal from the DMU initiates readout of the sensor data and directly controls the stepping through the raster. So, the time needed to take the star field is directly proportional to the telemetry bit rate. The maximum field diameter is approximately 18 arcminutes, which corresponds to 4,063 fine units. The photon count data and position of each pixel is collected by the ground system and reconstructed into an image.

During the IUE life the FES has performed the following functions,

- ▶ The information from which initial IUE orientation in the celestial sphere was established was provided by the FES operating in the field camera mode. The ground computer used this information to recreate the telescope view. From this display, the astronomer performed comparison between the scientific instrument view and a star map until a pattern is recognized.
- ▶ After performing a slew, the FES operated in the field camera mode to recreate an image

on the ground. The astronomer identified the star field and designated one star in the pattern as the desired target star and a second one, when there was a second star available, as the guide star.

- ▶ After the slew is ended and the star field identified, the FES permitted manual or automatic acquisition of guidance stars. The search and track mode was commanded for automatic acquisition or the primary mode was used for manual acquisition. In any case, the FES was finally placed in the primary mode tracking on a star. In this mode, the FES generated a digital error signal showing the offset from star center to the commanded coordinates which was used to both center the track pattern on the star and provide an indication of off-null pointing.
- ▶ After the guide star was acquired, the FES provided two-axes error data from an offset star for either open-or-closed-loop positioning of the target star in the experiment aperture. The FES was also used to detect, quantize and correct the drift in the gyros. This was done by allowing the FES to track a guide star and then using the resultant errors either directly in the OBC algorithm or indirectly as ground computer generated gyro bias compensating for the drift.
- ▶ In the 1 Gyro control system, the FES was particularly important. The spacecraft used the FSS and the remaining Gyro to provide coarse control. So, the FES was necessary to accomplish fine pointing control. With the FES commanded to primary mode tracking on a guide star, the spacecraft could perform the small, very accurate slews needed to place the target in the desired aperture and start the exposure.

The figure 5-48 shows a null FES 2 image, which is represented in FES coordinates (X,Y). The relation between the FES axes (X,Y) and the spacecraft axes (P,Y) are also displayed. The fiducial lamps are named by letters.

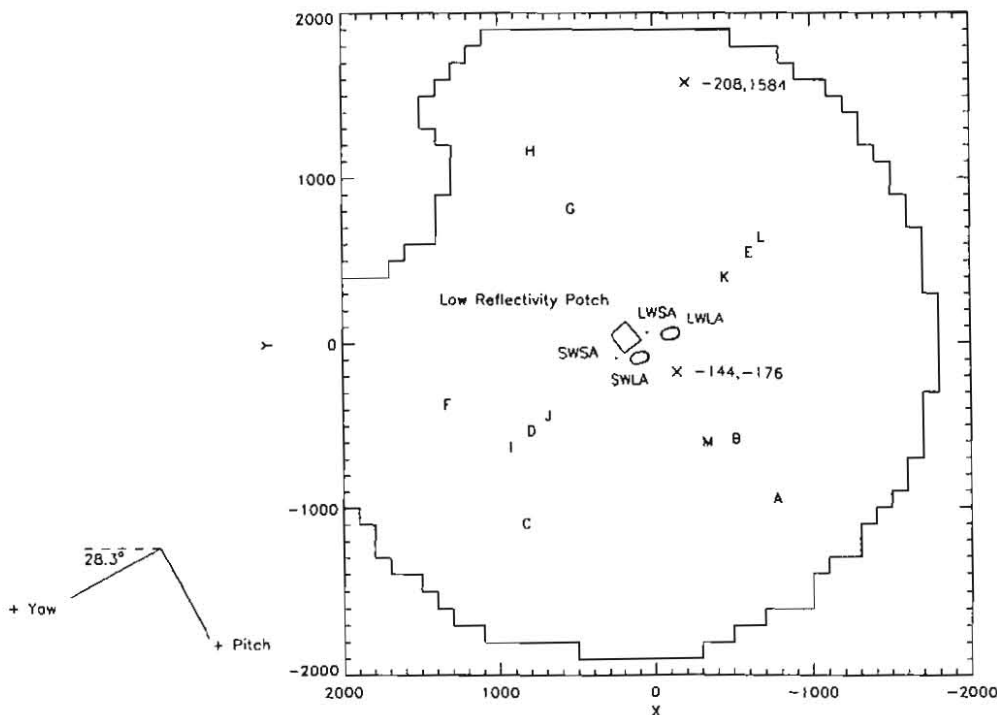


Figure 5-48. FES field-of-view.

The two points marked with an x were known as the reference point (-144,-176) and the offset reference point (-208,-1584). During normal operations, the target was usually placed at one of them before it was moved into the aperture. In April, 1989 the first one (-144,-176) was chosen to replace the old one (-16, -208), which had lost sensitivity due to fatigue effects from repeated saturation. On March, 1993 the offset reference point had to be chosen in the less contaminated part of the FES field due to the FES streak light anomaly.

5.5.7.1. FES geometric calibration

The FES suffers from geometrical distortion across its field of view. The overall pattern is that of a distorted S-shape. For instance, if a star is moved from one point to another in the FES field of view, the star will not be precisely at the expected point, but displaced by an amount roughly equal to the relative FES geometrical distortion between the star's original and final positions in the field. This effect had a great importance under the 1 Gyro control system, which had to rely on accurate positioning of a guide star in the FES field to place the target in the aperture.

Most of the distortion appears to come from the nature of the FES itself which is a magnetically focused device. In addition there appears to be an "edge effect". As one approaches the edge of the aperture plate, there is a general tendency for the level of distortion to rapidly increase, for the reflectivity of the aperture plate to drop, and the distortion to be radially directed away from the center of the FES. Data taking for the FES geometric distortion measurement indicated that the distortion was stable over the years.

The figure 5-49 shows the FES 2 distortion values.

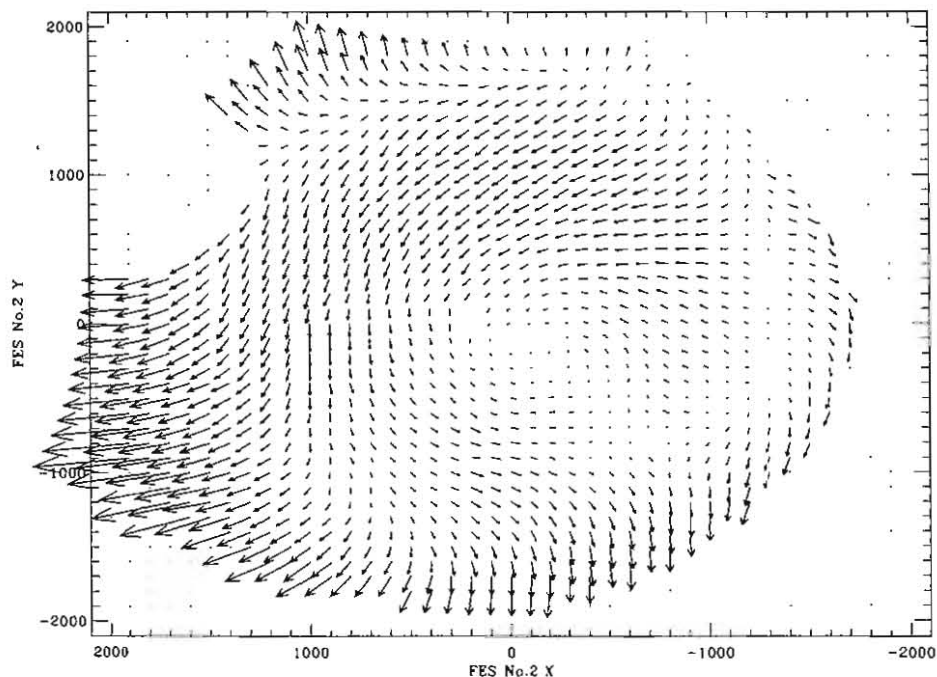


Figure 5-49. FES distortion values.

5.5.7.2. FES 2 reference point shift anomaly

On October 25, 1979 an intermittent change of aperture locations in the FES 2 was noted. The usual drop of light did not take place when targets were moved into the small apertures.

A few months later, the same behaviour was seen again. The problem was thought to be related with the FES electronics.

On January 9, 1981 a test was conducted to analyze this FES problem. The result suggested that the apertures, the aperture plate, and the cameras are remaining fixed relative to each other.

5.5.7.3. FES 2 star count variations anomaly

On April 15, 1985 an anomalous behaviour of the FES 2 was noted. During an observation of a star with known magnitude, count variations of up to 100 times of its known counts were seen.

Along the spacecraft life, several cases had shown similar behaviour. All cases occurred while having the FES configured in fast track/underlap mode and in a period when the spacecraft passed the radiation belts of the Earth.

5.5.7.4. Scattered light anomaly

On January 27, 1991 an increase of background light in the FES was first noticed, which was called the scattered light anomaly. The following ideas were proposed as the cause of this problem.

- A FES temperature dependent problem.
- A hydrazine cloud reflecting sunlight. The hydrazine cloud could have been formed by the unloads performed on a routine basis.
- A Barium cloud with forward scattering of the 4554.03 resonance line of Ba II. On January 20, 1991 a barium canister was exploded at 30,000 km near the longitude of the IUE orbit.
- The sunlight could be coming in the telescope tube due to a pinhole caused by a micrometeoroid. Another idea was that insulation had been torn loose and was drifting on the opposite side of the tube-end from the sunshade.

Several test were done in order to determine the cause of the light and its dependance on certain parameters (telescope tube temperature, beta angle, roll angle, etc). The following characteristics of the scattered light were determined:

- ▶ The scattered light was independent of the electronic configuration of the spacecraft. For instance, it was independent of the telemetry bit rate.

- ▶ The scattered light was present in both FES's.
- ▶ The scattered light was distributed in a uniform pattern over the FES FOV.
- ▶ The light could be made to disappear by closing the sun shutter.
- ▶ The spectrograph images were not affected by the scattered light.
- ▶ The light usually increased in intensity with increasing beta angle, as is shown in the figure 5-50.
- ▶ The light intensity decreased with positive roll angle.
- ▶ The FES scattered light is strongly affected by shadow season periods. The figure 5-51 shows the evolution with time of the FES background of two stars at beta 90°. Since the anomaly first appeared, the background became enhanced during each of the shadow seasons, but returned to pre-shadow levels after the shadow season was over. The exception to this is shadow season 30; the lack of an increase in the counts during the shadow season was thought to be the result of the deliberate attempts to pass shadow each day at beta angles less than or equals to 65°, thus minimizing the thermal shock experienced by the end of the telescope tube.

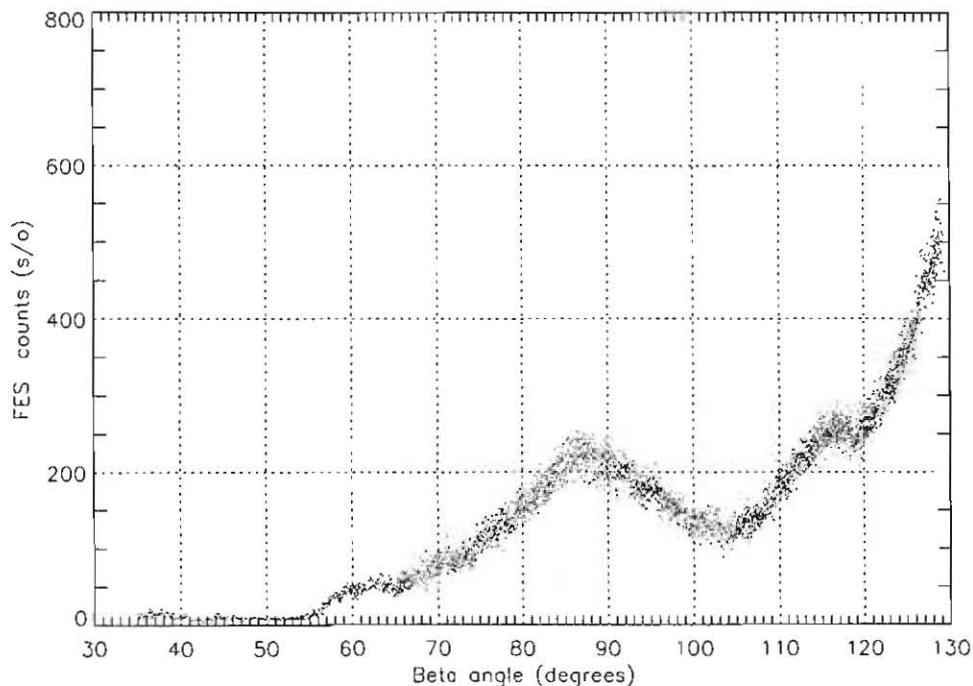


Figure 5-50. FES background counts (s/o) vs Beta angle on June 29, 1992

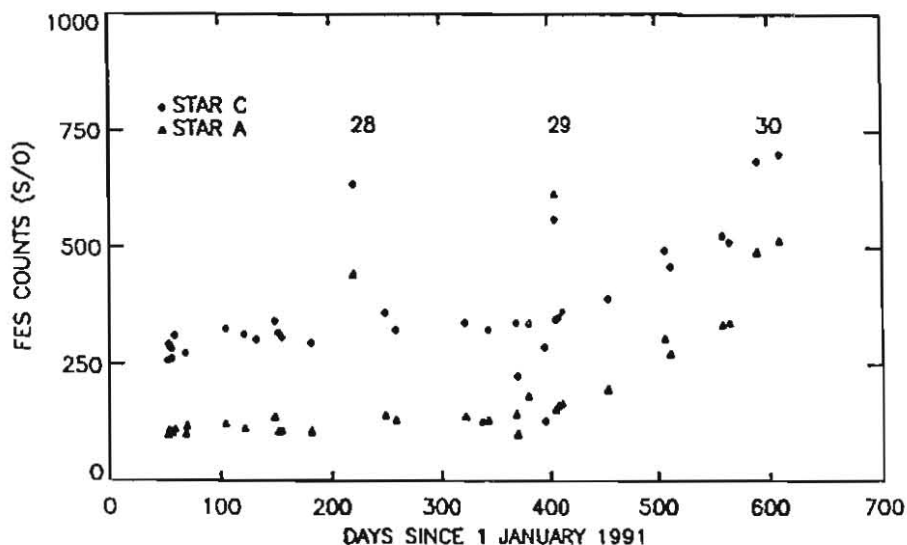


Figure 5-51. FES counts (s/o) from January 1991 until September 1992

A 12.0 magnitude star is approximately equivalent to 225 FES counts slow track/overlap, and 11.0 magnitude, to 560 counts slow track/overlap. Fast track mode measures approximately four times less counts than slow track mode since its dwell time is one fourth the duration of slow track.

5.5.7.5. Streak light anomaly

A significant enhancement of the scattered light was detected on September 14, 1992. This was known as the FES streak light anomaly and was mainly associated with Sun and Earth irradiation.

The behaviour of this anomaly was different than the previous light in several aspects.

- ▶ The light decreases with negative roll angles.
- ▶ The long duration long wavelength spectra could be contaminated.
- ▶ The light was always seen in the same area of the FES fields. A typical FES contaminated image is shown in the figure 5-52.
- ▶ The streak was highly variable. The figures 5-53 and 5-54 show the background measured during two similar maneuvers, from low beta to high beta and from a high beta to low beta respectively. So, one could attempt to reduce the extent of the streak in the FES by performing a straight pitch maneuver to beta 105°, then maneuver back at beta 90°. During the first year of this anomaly, this procedure dramatically reduced the level of the streak at beta 90°. The figure 5-55 shows the streak evolution during the last four years of IUE's mission.

The streak presented some difficulties for operations in the identification of the target field. It also precluded tracking on any guide stars which fall in the affected portion of the FES, unless they were high enough in magnitude to sit well above the level of the streak.

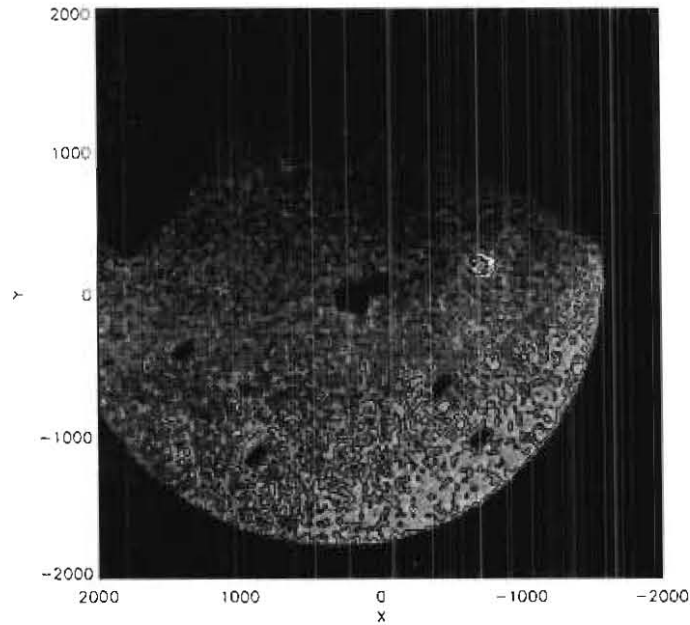


Figure 5-52. FES contaminated image.

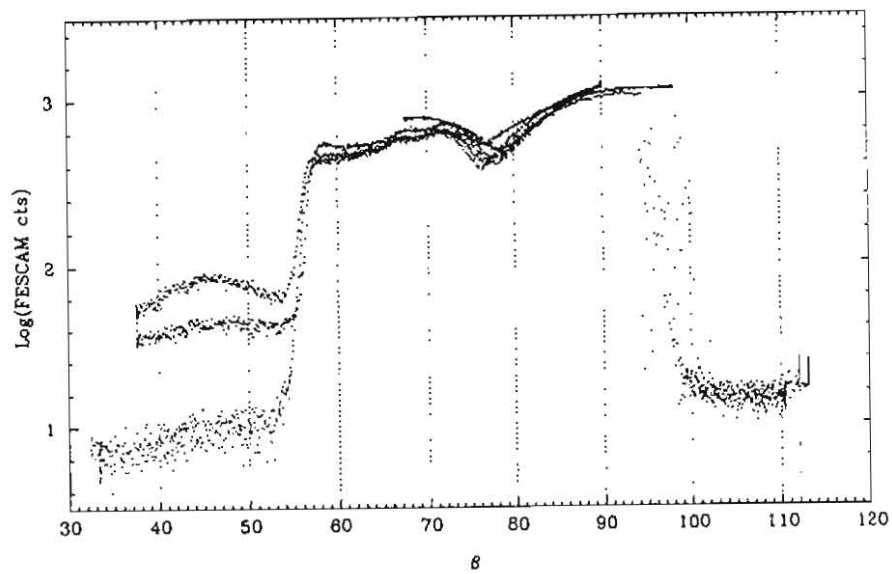


Figure 5-53. FESCAM counts vs β summarized maneuvering from beta 35° to 115° .

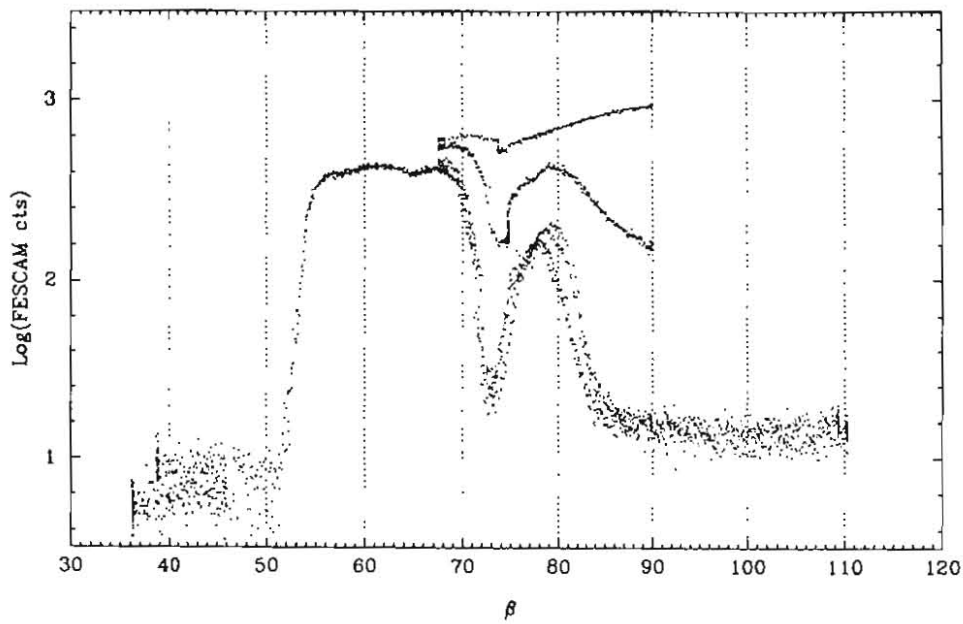


Figure 5-54. FESCAM counts vs β summarized maneuvering from beta 115° to 35°

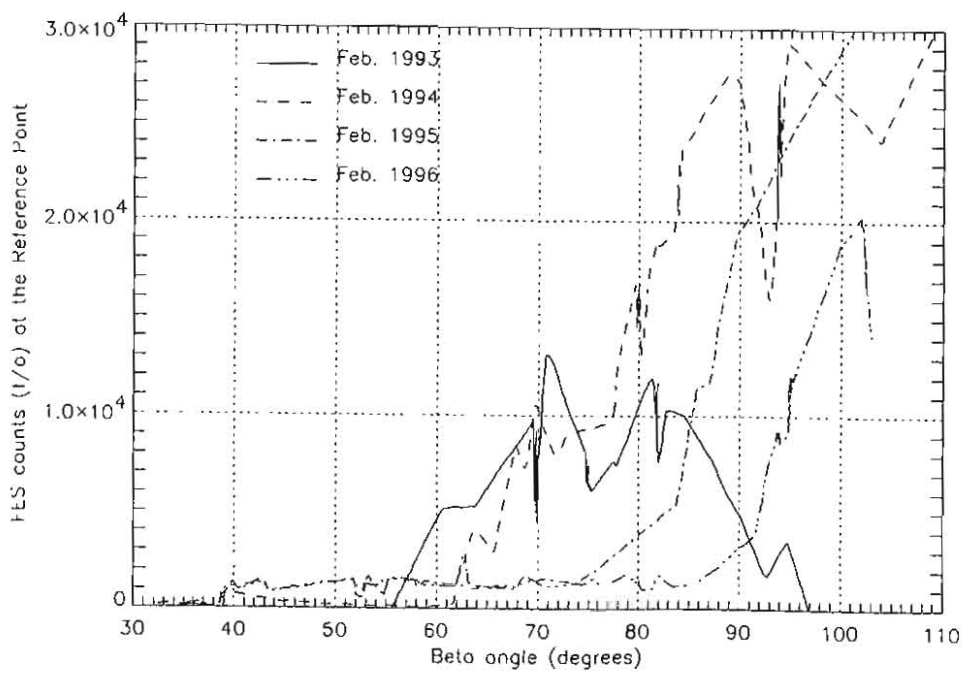


Figure 5-55. FES counts (f/o) at the Reference Point.

5.5.8. Reaction wheel

The reaction wheel assembly consists of four wheels, four wheel driver modules and a redundant power converter. Three reaction wheels are aligned to the spacecraft pitch, yaw and roll control axes. The fourth wheel is skewed symmetrically with respect to the orthogonal control axes. This unique configuration provides redundancy in the event the pitch, yaw or roll wheel fails. During the whole IUE mission, the three prime wheels worked properly, so the redundant wheel was not used.

A reaction wheel is a rotating disk used to store momentum or transfer momentum to the spacecraft body for the purpose of executing slews. When the wheel is accelerated or decelerated, the reaction torque can be used as the actuating torque for an attitude control system. Thus, a transfer of angular momentum between the vehicle and the wheels is possible. The reaction wheels provide the following advantages for a three axis stabilized platform.

- ▶ The capability of continuous high accuracy pointing control.
- ▶ Large angle slewing maneuvers without fuel consumption.
- ▶ Sun hold acquisition.

The angular momentum that can be stored in the wheels is limited, so a secondary control system is used to prevent the stored momentum from becoming too high or too low. The secondary dumping system is a jet thruster system (HAPS). The reaction wheels must be kept within certain rpm limits to assure optimum control and to prevent bearing wear. The limits are as follows: Pitch ($|200|$ - $|1000|$ rpm), Yaw ($|200|$ - $|500|$ rpm) and Roll ($|200|$ - $|500|$ rpm). The momentum dumping operations are carried out during specified limited periods of spacecraft activities, so that unacceptable attitude errors are not introduced into the scientific instrument experiments.

Each wheel driver module generates a two phase square wave signal to drive its associated reaction wheel. Either half of the redundant digital to analog converter (DAC) and command decoder module provides wheel command information to the wheel driver module. The pitch, yaw and roll reaction wheel driver modules are also able to receive information from the compensation and mixing card (C&M) of the control electronics assembly (CEA). This card provides processed analog sun sensor information and rate information for the reaction wheels for use in the sun hold emergency mode.

5.5.9. Hydrazine Auxiliary Propulsion System

The IUE hydrazine auxiliary propulsion system (HAPS) is a monopropellant catalytic hydrazine blow down propulsion system. It consists of six propellant tanks, fill/vent valves for each tank, fill/drain valves for each pair of tanks, pressure sensors, filters, seven latching valves, heaters, temperature sensors, twelve monopropellant engines (eight 0.2 pound low-thrust engines, LTE's, and four 5 pound high-thrust engines, HTE's) and an electrical junction box which contains all necessary connections, circuits and current shunts for the heaters and valves.

The HAPS unit comprises two physically distinct sections. The first section is located in the body of the spacecraft between the main equipment platform and the apogee boost motor, and contains the hydrazine fuel tanks, four LTE's and the associated lines and valves. The second section consists of two remote engine modules (REM's), which extend about 2 feet below the propulsion bay. Each REM contains two LTE's, two HTE's and the associated lines and valves.

The figure 5-56 shows a diagram of the HAPS assembly.

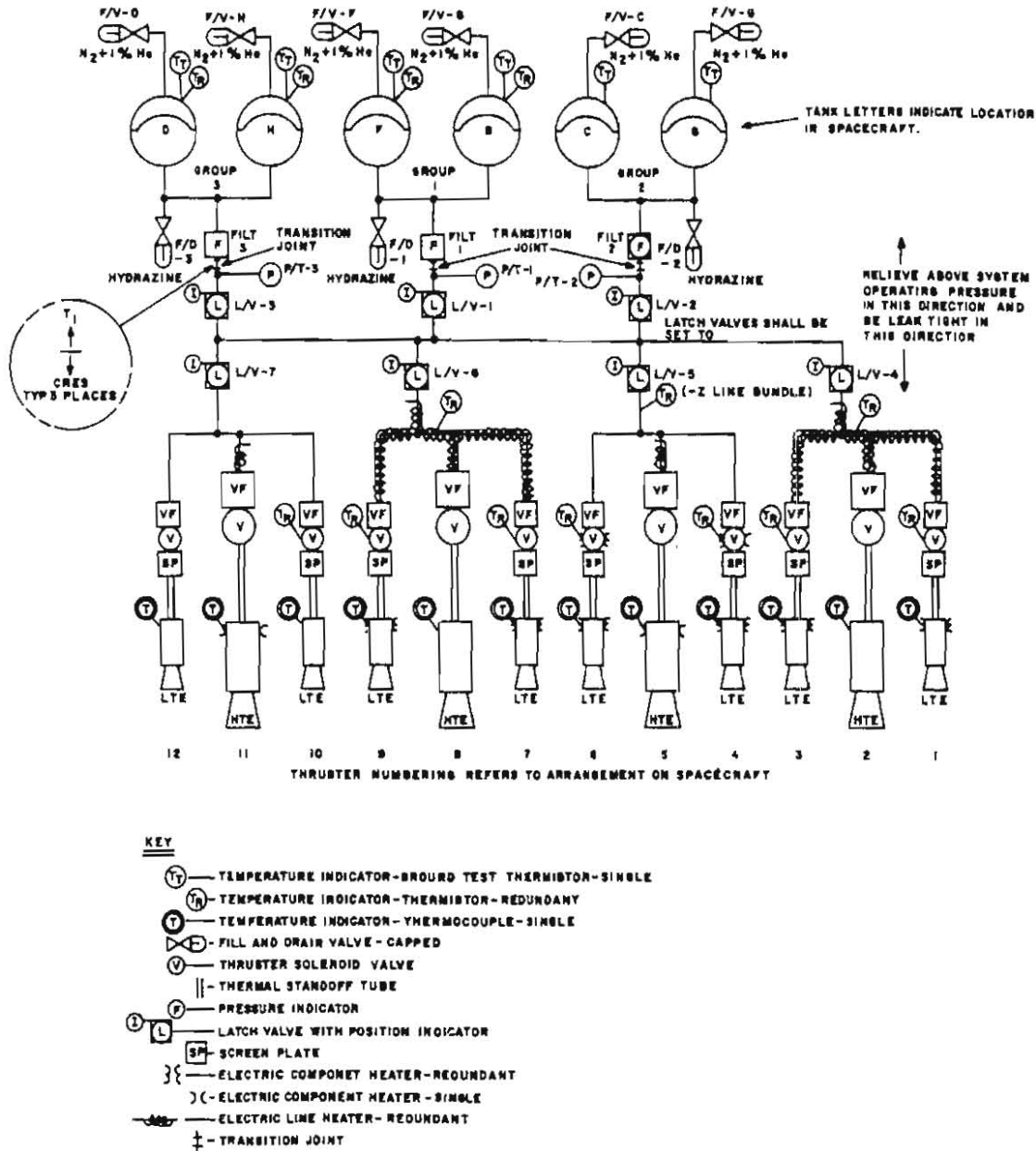


Figure 5-56. HAPS, schematic.

The tanks are connected in pairs and are located at equal distances from the spacecraft x axis. This arrangement permits fuel to be depleted from two, four or six tanks at once and permits system balance to be maintained. Each tank contains a flexible diaphragm to separate the hydrazine from the pressurizing gas, nitrogen. The hydrazine flows from the tank pairs through a common filter past a pressure monitor. A latching valve separates each tank pair from a common manifold which feeds four engine groups. Each group is separated from the rest of the system by a latching valve, which allows operations to continue if there is a component failure. The problem area is isolated from the system by closing the specific latching valve, and the secondary jet or tanks would be used.

The propellant, hydrazine (N_2H_4), was chosen for the IUE because it is fairly inexpensive, is flight proven, can handle both long and short jet firings, and will not contaminate the scientific instruments.

The system was originally loaded with 27.3 kg of hydrazine divided equally among the six tanks. Before launch, the system was filled with hydrazine down to the engine valves. All latch valves were closed and two tanks were pressurized to 200 psi, and the other four were pressurized to 350 psi. Once in orbit, latch valves 2, 4, 5, 6 and 7 were opened. Then, latch valve 2 was closed, and latch valves 1 and 3 were opened. This loading procedure was followed to prevent possible latch valve problems because of sudden pressure changes when the latch valves were initially opened. During the whole mission, the IUE had all latch valves open except latch valve 2. This valve separates the two tanks C & G, which were only used to pressurize the system initially following launch. The tanks could have been opened if needed but the other four tanks supplied sufficient N_2H_4 through out the mission.

The figures 5-57 and 5-58 show the temperature and pressure evolution in the tanks.

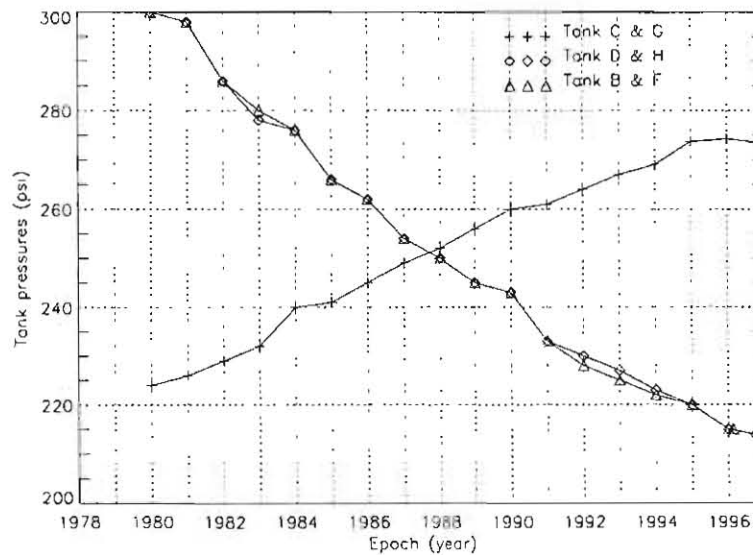


Figure 5-57. Tank group pressures.

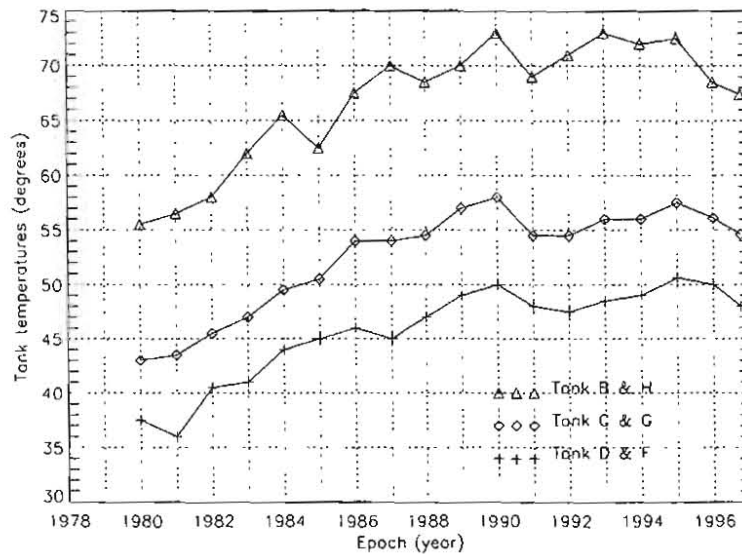


Figure 5-58. Tank group temperatures.

On February 18, 1996 the B&F tank pressure indication dropped to 14.2 psi, which corresponds to a raw telemetry value of zero for the tank pressure signal, and remained there. As, there was not any spacecraft momentum change, the failure was assigned to the pressure sensor for Tanks B&F, either directly or in the wire connections to the telemetry system.

Prior to the N_2H_4 venting on September 30, 1996 there was approximately 17.7 kg of hydrazine remaining in the tanks. The figure 5-59 shows the hydrazine consumption during the mission.

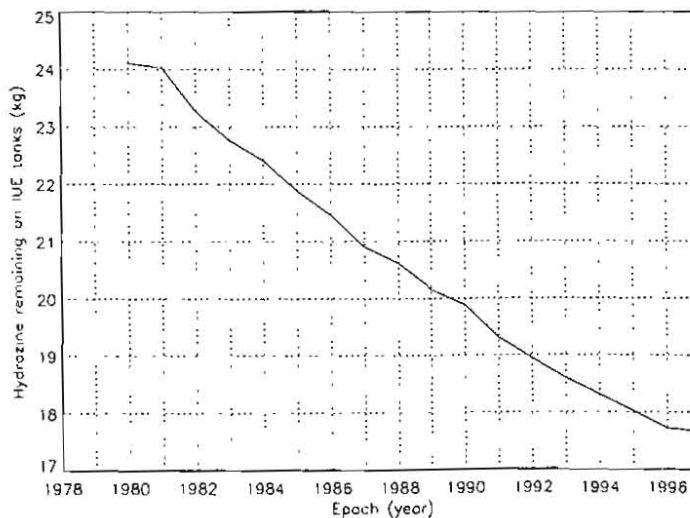
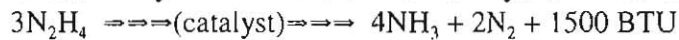


Figure 5-59. Hydrazine remaining on IUE tanks.

A jet can be fired in a continuous mode or a pulsed mode. In the continuous mode, the engine valve is activated and remains open until commanded to stop firing. The continuous mode was never used, except accidentally. In the pulsed mode, the engine valve is open only for 30 milliseconds, the hydrazine flows over the catalyst beds and this chemical reaction occurs:



These gases expand and are forced out of the nozzle producing the thrust.

The HAPS provides the spacecraft with the attitude torquing capability needed to perform the following functions:

- ▶ Nutation control. The spacecraft spun at a rate of approximately 60 rpm around its X axis after it was separated from the Delta third stage. Because it was an unfavourable moment of inertia axis, the spacecraft would develop an increasingly conical wobble, which, if unchecked, would cause it to enter into a flat spin around the transverse axis with a maximum moment of inertia. This conical wobble was monitored by the nutation sensor assembly (NSA). The NSA contains two redundant accelerometers which provide information for computing the nutation cone buildup. The spin axis nutation is controlled using either of the angled 5 pound thrust jets (jets 5 and 11). The firing of these jets was controlled by an onboard nutation control algorithm.
- ▶ Precession control. During the transfer orbit, the spacecraft was released from the Delta third stage with its ABM facing aft. After the separation, the spacecraft was precessed, or flipped, 180 degrees to facilitate the ABM burn. This precession maneuver maintained a constant solar array exposure. The maneuver was performed using the angled 5 pound thrusters (jet 5 and 11). During the precession maneuver, the NSA was disabled. After completion of the precession maneuver, the NSA was enabled to remove any nutation prior to the ABM burn and despin operations.
- ▶ Velocity correction to initially acquire the orbit station. After the ABM was commanded to ignite by ground command, the hydrazine provided the velocity change required to get on station. It was actually achieved with very little hydrazine consumption.
- ▶ Despin of the spacecraft. When the desired station was obtained, the spacecraft was despun in two phases to calibrate the HAPS thrusters and gain three-axis gyro rate control. The IUE was spun up to 2 to 5 degrees per second, and the solar arrays were deployed. After deployment, the IUE was rate damped to 0.25 degree per second. The solar acquisition phase was then initiated and the spacecraft was aligned with the sunline normal to the primary plane of the solar arrays.
- ▶ Spacecraft torquing to acquire proper Sun angle in the event of attitude loss. Rate + Position Hold mode was a backup attitude control configuration that is available in an emergency. An OBC program, Worker 19, used the information coming from the attitude sensors (initially gyros, in rate mode, only; under the 2 Gyro/FSS control mode, gyros, in rate mode, and FSS) to compute the jet torques.
- ▶ Velocity correction for east-west station keeping (Delta-V). The HTE's 2 & 8 were used to control the yaw axis and give the thrust to induce translational spacecraft motion while

LTE continued to provide pointing control in the pitch and roll axes. The three axes were controlled in a similar way to the Rate + Position Hold mode.

- ▶ Spacecraft torquing to unload reaction wheels. Firing a jet produces an external force upon the spacecraft. The gyros sense this force in the form of spacecraft rotations and send the information to the OBC. The jet firings produce both rotational and translational motion. The rotational motion, through hold/slew program's (Worker 0) intervention, results in wheel velocities being changed. Worker 0 changes the wheel speeds in order to counteract the external force and keep IUE from moving. The translational motion was an ignored side-effect until a program was developed on October 2, 1989 to select the most favourable momentum wheel unload jet firing to counteract the westward drift of the spacecraft. This was done to reduce the frequency of the Delta-Vs.

The effectiveness of the HAPS in performing reaction wheel unloads depended largely on EV temperature, propellant tank pressure and catalyst bed temperature.

- ▶ High EV temperature were believed to cause the disassociation of the hydrazine within the fuel lines. Small pockets of disassociated or partially disassociated fuel produced low thrust when they move through the engine catalyst chambers.
- ▶ The system pressure affected how much fuel could be delivered to the engine per unit time. The continuing decrease in tank pressure due to fuel usage resulted in a decreased flow of hydrazine through a jet during a firing, decreasing the thrust of the jet.
- ▶ Catalyst beds are generally more efficient at higher temperatures. This was demonstrated in the low performance of the LTE which did not have chamber heaters, and in the locally high output of engines which had recently been fired and had higher than normal catbed temperatures.

Unload performance is measured by comparing the change in reaction wheel speed in each axis to the number of 30 millisecond engine firing pulses performed. The Δ RPM per pulse measurements for the single jet unloads are compared to the benchmark 1980 data and a composite percentage decrease is calculated. The figures 5-60, 5-61, 5-62, 5-63 and 5-64 demonstrate the trends in unload performance.

HAPS thermal design

The mission requirements for thermal control throughout the HAPS unit were dictated by the freezing and vaporization points of the hydrazine fuel. The region was maintained above 5°C to prevent freezing, which would have both disrupted the fuel supply and damaged the control valve assemblies. The upper temperature limit on all HAPS component was initially set at 65°C but had to be raised to 85°C for all components except for two sensors, +ZLN and -ZLN, which had an upper limit of 90°C. This was done in a effort to reduce cycling of the catalyst bed heaters, after the HAPS heater group 1 failed due to excessive cycling.

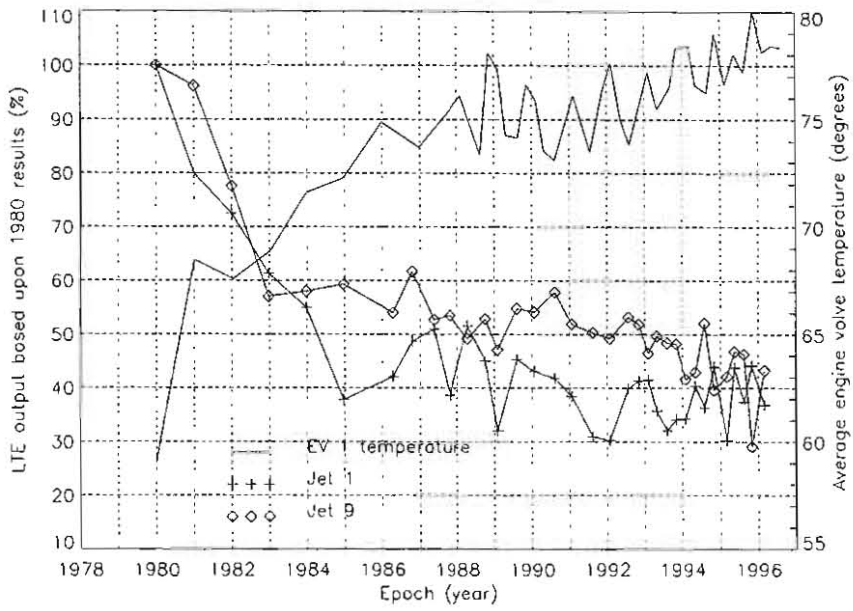


Figure 5-60. Comparison of LTE 1 & 9 output and associated EV 1 temperature.

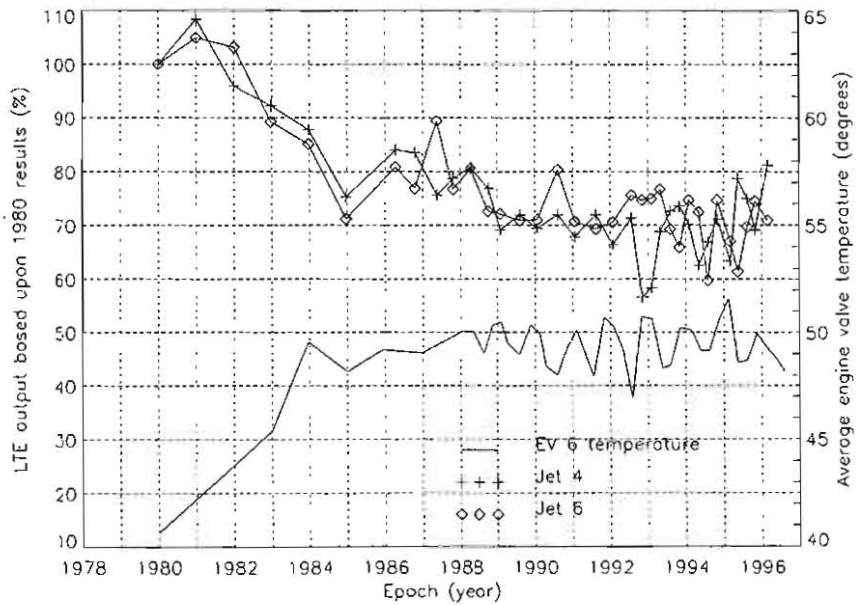


Figure 5-61. Comparison of LTE 4 & 6 output and associated EV 6 temperature.

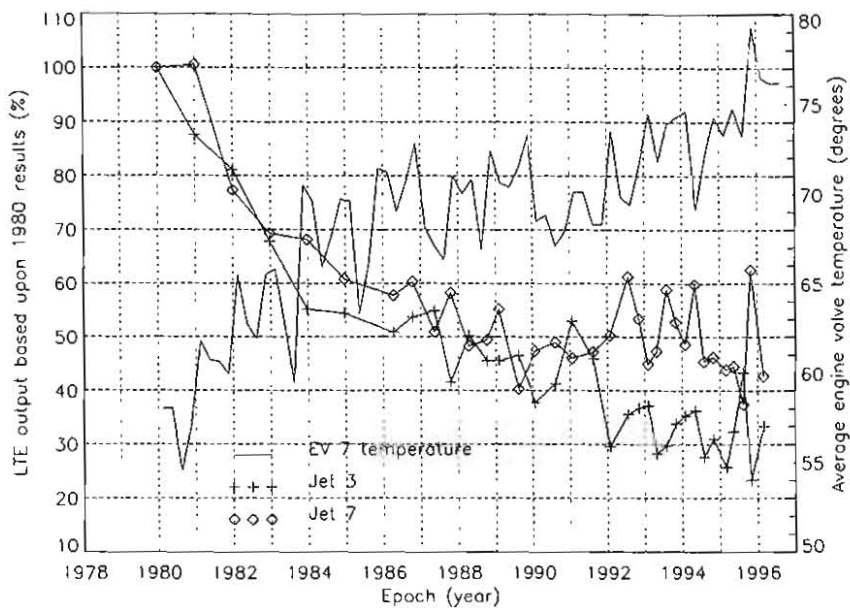


Figure 5-62. Comparison of LTE 3 & 7 output and associated EV 7 temperature.

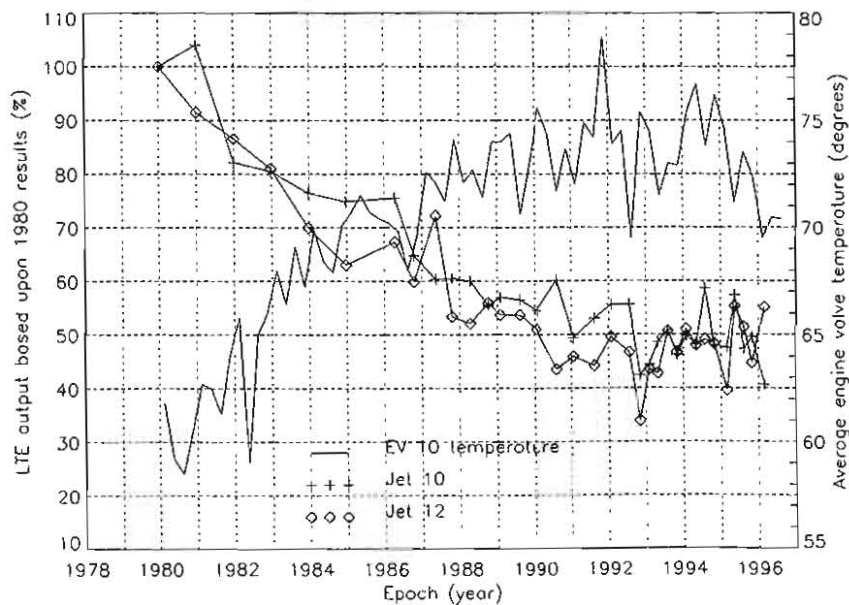


Figure 5-63. Comparison of LTE 10 & 12 output and associated EV 10 temperature.

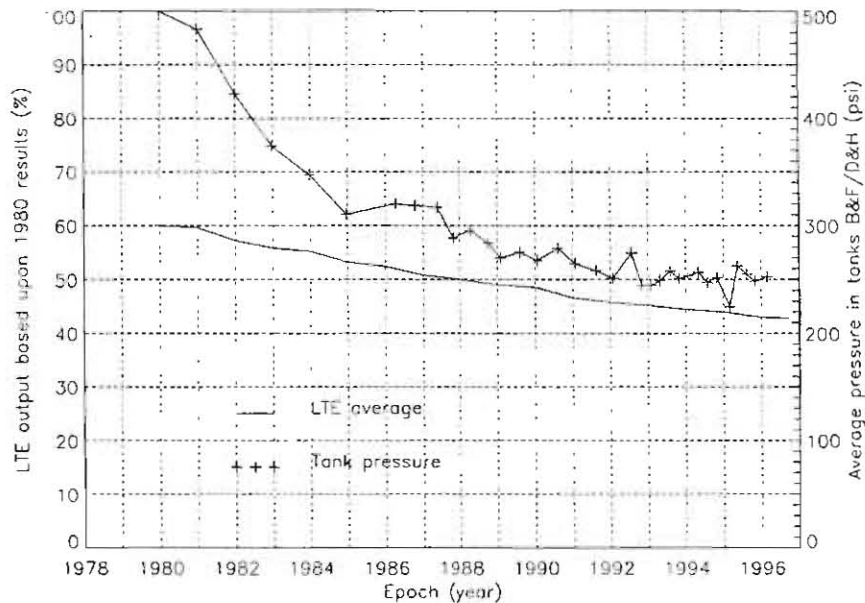


Figure 5-64. Comparison of LTE average output and hydrazine tank pressure.

Although there was a need for additional heater units, the primary thermal control was provided by solar energy. The following HAPS heater groups are present.

- Group 1. Primary chamber heaters LTE 1, 3, 4, 6, 7 and 9.
- Group 2. Backup heaters for group 1.
- Group 3. Backup heaters for group 7, plus primary heater on +Z hydrazine lines, hydrazine tanks B and H, and LTE 10 and 12 valves.
- Group 4. Primary heaters on +Y and -Y REM struts, +Y and -Y REM mount, and LTE 4 and 6 valves.
- Group 5. Backup heaters for group 4.
- Group 6. Primary heaters on HTE 5 and 11.
- Group 7. Primary heaters on -Z hydrazine line, hydrazine tanks C, D, F and G.

The IUE used only the low-thrust engine chamber heaters (HAPS heater group 1 and its backup, group 2). The other heaters were not needed during the mission because temperatures in the HAPS area remained higher than predicted.

5.5.9.1. HAPS heater group 1 failure

On December 15, 1980 the heaters on jets 4 and 6 failed. They are wired in series with each other and in parallel with the other two pairs. The other heaters continued to function properly. A switch was made to heater group 2, backup for the low-thrust engines.

The cause of the failure was believed to be excessive cycling. To guard against this type of failure again, the decision was made to raise the red-line limits of the HAPS to 85°, and only turn off the heater group when that limit was reached. This option was chosen at the recommendation of the HAPS designers, who preferred a hot HAPS rather than firing cold jets. The problem with an 85° limit on the HAPS was a possibility of hydrazine decomposing and gas bubbles forming near the engine valves. These gas bubbles would not cause any harm but would show up as weak firings or give the appearance of a missing pulse in a unload. Operationally, it was a simple matter to just uplink commands for more pulses, so this reduced thrust was a minimum problem.

5.5.9.2. N₂H₄ venting

On September 30, 1996 the N₂H₄ venting procedure was performed and was the start of the final shut down operations. The need to vent the remaining N₂H₄ was based on the assumption that eventually after being left unattended, the HAPS system components would freeze and thaw. This action would lead to a structural failure of the system venting N₂H₄, which could be catastrophic to any ill-fated satellite in the vicinity of IUE. The venting process decomposed the N₂H₄, eliminating this possible event.

The venting procedure was named the roll spin venting method. In this method of N₂H₄ venting, the spacecraft was maneuvered to a specified attitude, which was selected to give a planned change to the orbit based on the expected Delta-V that resulted from the venting process. Once at the desired target, all the non-essential pieces of equipment were powered off. The pitch and yaw reaction wheels were dumped as close to zero as possible, while the roll wheel was dumped close to the saturation limit (around 1460 rpm) to cause +Roll rotation of spacecraft. Then, the reaction wheels were disabled. There was no control on the spacecraft pointing attitude at this time, so IUE began to spin.

The valve 2 was open at approximately 15:10 UT. The N₂H₄ venting was achieved in approximately two hours while several jets were firing in continuous mode. The figures 5-65 and 5-66 show the tank temperatures and pressures during the venting (the B&F tank pressure is not present due to its sensor pressure failure).

The LTE's used to spin up the spacecraft were selected so that most of the non-Roll axis momentum was cancelled, although the spin was not purely about the Roll axis since all of the LTE's have a Roll component as well as a component in either the Pitch and Yaw axis. While the jets were fired, high temperatures were reached (around 170°C). The figure 5-67 shows the LTE's and HTE's used. In the last minutes, the HTEs were fired due to the slow venting achieved with the LTE's.

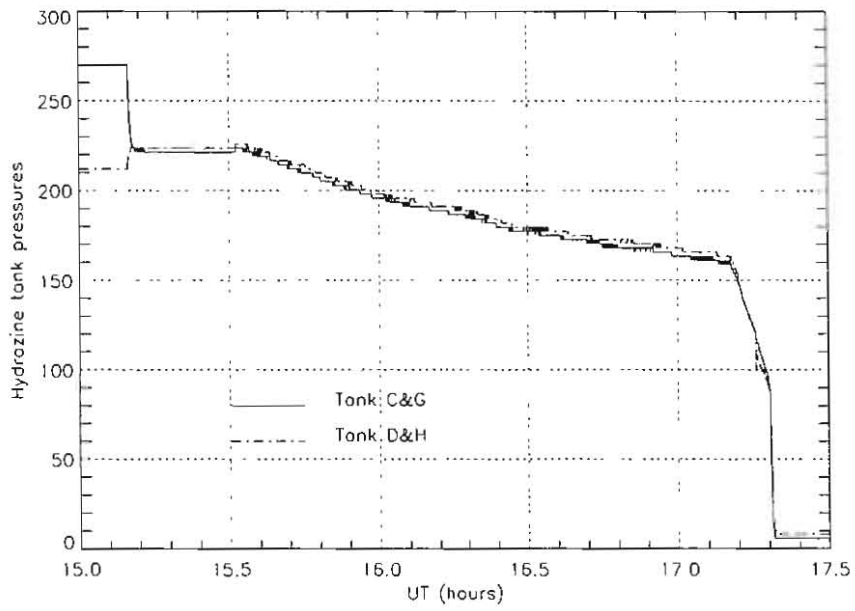


Figure 5-65. Tank pressures during the N_2H_4 venting.

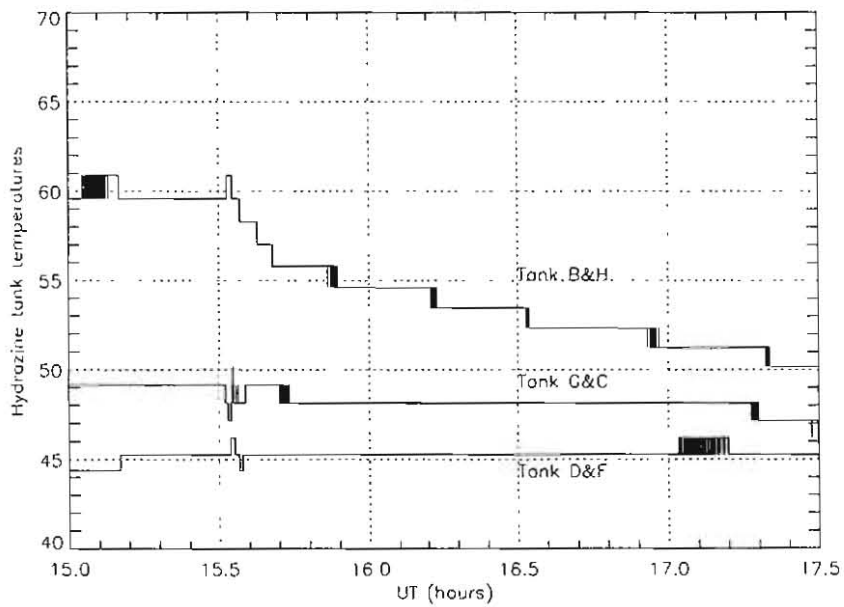


Figure 5-66. Tank temperatures during the N_2H_4 venting.

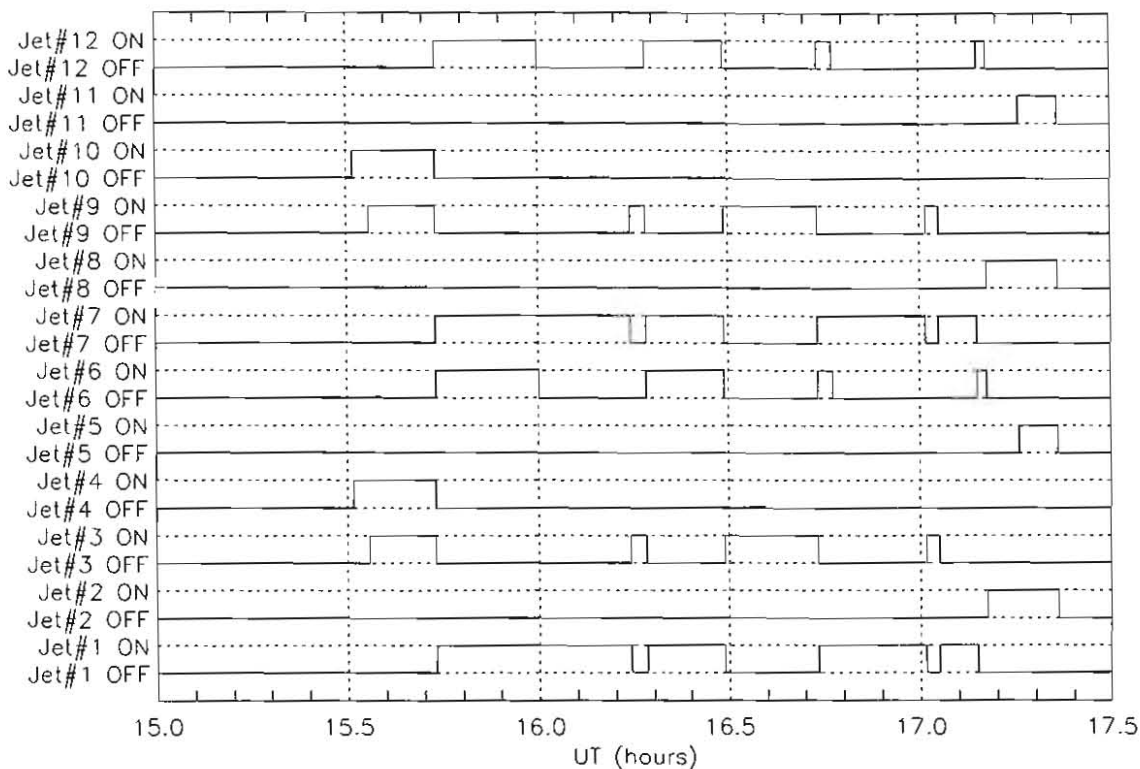


Figure 5-67. Jets fired during the N_2H_4 venting.

5.5.10. Control Electronics Assembly

The Control Electronics Assembly (CEA) which provides the interface between the sensors and the actuators performs the following functions: provides certain hardwired logic functions (primarily through the launch phase commencing at Delta separation and ending after Sun acquisition in elliptical synchronous orbit), provides power switching internal and external to the unit, decodes digital command words from the OBC, generates analog signals for inertial wheel driving, provides high-level signals for energizing hydrazine thrusters and provides telemetry conditioning for the various telemetry sensors in the HAPS.

The unit consists of eight cards with functions as defined below.

► Card 1. Precession/Nutation Card

This card provides the digital logic for spin sectoring, precession commands, active nutation control and engine mode selection. The spin sectoring portion receives a sur-centered pulse from the PAS and an input from the spacecraft clock. With this information available, the spin period is divided into 128 parts. The current sector status (position) is maintained and updated throughout each spin cycle. This logic information

on the spin status is interfaced with both the precession command logic and active nutation control logic. In the precession logic the current sector status is compared with a ground command consisting of three parts: sector ID to start firing a precession thruster, sector ID to stop firing a precession thruster and the number of consecutive spin cycles during which the precession jet will be fired.

▶ **Card 2. Relay Card**

This module contains a bank of latch relays and relay drivers to enable power switching to all cards within the control electronics assembly and wheel driver assembly. The effect of switching between the buses is not only to ensure power by being able to select between redundant buses, but to remove power from unneeded functions by switching them to the standby bus.

▶ **Card 3. Digital-to-Analog Converter and Wheel Commands**

These are redundant cards that develop the analog signals used by the wheel drivers. Reaction wheel commands are serially gated into this card from either Command Decoder and converted to analog voltages for the pitch, yaw, roll and redundant wheel drivers.

▶ **Card 4. Engine Valve Command Logic**

These are redundant cards that provide low-level signals used by the engine valve drivers to activate the hydrazine system. Inputs to the cards are through the spacecraft command system, DMU, compensation/mixing card and the precession/nutation card.

▶ **Card 5. Compensation/Mixing Card**

This card receives analog sun sensor information and rate information and combines them to form logic levels to drive the low level thrusters during despin and sun acquisition. In addition, this card drives the reaction wheels during the sun hold mode of operation (SUNBATH mode) which serves as a backup in the event of an OBC hangup preventing the normal digital control algorithm from being processed. In this mode, the card receives position from the set of six coarse sun sensors distributed about the IUE spacecraft. These signals are combined and the analog error signals are used to drive the reaction wheels.

▶ **Card 6. HAPS Telemetry Conditioning Card**

The functions of this card are to condition the signals to and/or from the various temperature and pressure sensors in the HAPS and monitor and indicate the positions of various latch valves between tanks and manifolds and jet valves. This card is powered by the redundant power supplies in the wheel driver assembly.

▶ **Card 7. Engine/Valve Driver Cards 1 and 2**

These redundant cards serve as the power stage to drive the hydrazine system's engine solenoids and transfer valve solenoids. The output from each of the redundant cards are logically OR'ed together via isolation diodes to drive the common solenoids.

5.6. The Onboard Computer

The onboard computer (OBC) maintains attitude control and controls the scientific experiment operation. Because it is so vital to spacecraft operation, the OBC must be highly reliable. The general characteristics of the Advanced Onboard Processor (AOP) are presented below.

- Power consumption. 15 watts maximum while computing (including power converter and full memory complement). 9 watts when halted.
- Speed. Add time, 5 microseconds. Multiply time, 38 microseconds. Divide time, 75 microseconds.
- Memory. 3 modules of 4K by 18 bit word (each 4K module incorporates cycle by cycle power switching).
- 55 Instructions.
- Simple to Program: one double length accumulator (36 bits), one index register, smooth handling of interrupts by hardware, powerful bit manipulating instructions and direct addressing of all 4096 words in any page.
- Multilevel Interrupts. 16 priority interrupt levels with program control over lock-out status and interrupt disable.
- Direct Memory Access (DMA). Up to 16 independent cycle-steal operations time share one DMA channel. Maximum I/O rate of 100 k words per second.
- Memory Write Protection. In orbit reprogramming dictates that storage limits must be modifiable. Storage areas can be assigned in increments of 128 word blocks.
- System utilizes a bus concept so that unpowered spare memory modules or processors may be flown. An automatic switch-over control for real-time repair can be readily implemented.
- Any spare memory bank may be used to functionally replace any other bank. The memory bank used for fixed (Interrupt and I/O) locations can be reassigned by command.

The OBC consists of several modular components, a central processing module (CPM, which contains a central processing unit, CPU, and a special input/output, SIO, unit integrated into a single package), memory modules and a power converter. Redundant modules are used to ensure that there is no individual component failure. There are two CPM's, two power converters and three 4K 18-bit word memory units. These units are interconnected so that any remaining component can be connected to the functioning counterparts to create a whole system. Two data buses are used to ensure data flow between any combination of memory units and CPM's. Operating software systems requiring 8K and 4K are used.

- **Central Processing Unit (CPU).** The CPU uses large-scale integration and transistor-transistor logic. The processor employs a fully parallel adder and parallel data transfers between registers and at the Processor/Memory interface. 16 individually armed priority interrupts are used, which allow asynchronous spacecraft events to gain access to computer operation at event dependent intervals. The interrupt handling logic is designed so that when an interrupt is honoured, three critical registers are automatically saved and initialized to new values from fixed memory locations. These are the instruction counter, the interrupt lockout registers and the storage limit register. The hardware handling of these registers is important in providing security of program execution in a long term unattended environment.
- **Special Input/Output Unit (SIO).** The SIO handles all communication between the CPU and the spacecraft (e.g., command, attitude control and scientific instrument). These events are asynchronous, relative to regular computer operation, and must be introduced so they will not disturb normal CPU operations. Program independent data transfers are accomplished by the AOP through the use of buffered I/O channels, operated in a cycle steal mode similar to the priority interrupt technique. These channels time-share a single set of Direct Memory Access (DMA) hardware.

The SIO receives data from the DMU and converts it from serial to parallel format for the CPU. It also receives digital data from the CPU and converts them to the proper multiplexer format. The SIO converts signals from the DMU level to transistor-transistor logic and vice versa.

The command system accepts commands from both the computer and the command receiver on a time-shared basis. Therefore, the OBC can control any commandable system if it is programmed to do so. This includes the capability of issuing stored commands on a time delayed or event dependent basis. Commands related to the computer's basis task of attitude control are computed, formatted, and sent to the reaction wheels or jets via the command system.

- **Memory Units.** The OBC has three 4096 by 18-bit word plated wire memory units. These memories feature cycle-by-cycle power switching which reduces the power dissipation in the nonaddressed memory units from 4 watts to 150 milliwatts. They are nonvolatile and readout is nondestructive. The access time is 500 nanoseconds and cycle time is 1 microsecond.
- **Power converter.** All components of the OBC operate on a power supply of 5 volts direct current. Since the spacecraft main power bus is 28 volts direct current, a direct current-direct current power converter is provided for the OBC. Two 28 volt to 5 volt converters are used; the second unit being redundant. The power converters have an efficiency of 70% and have power clear circuitry, which anticipates power shutdown and causes a graceful shutdown of the processor when power is interrupted. The power converter units also contain the control circuits for selecting the redundant CPU and SIO and memory unit combinations.

Flight Software.

The OBC 8K flight software provided for attitude control, camera exposure control, station keeping maneuvers and other vital functions. It was contained in banks 0 and 2 memories. The flight software was divided into two categories: the Flight Executive and the Workers.

The Flight Executive program performed specific tasks mainly dealing with I/O functions, controlled time-critical operations, scheduled and initiated the application programs (Workers), and performed the following tasks:

- ▶ Initialized the flight software.
- ▶ Real-time interrupt services and processor schedules.
- ▶ Saved and restored critical registers.
- ▶ Accepted and stored OBC and ground telemetry data.
- ▶ Accepted commands and data blocks to the OBC.
- ▶ Generated OBC status words which indicate current errors, operational modes and software selected options.
- ▶ Issued OBC telemetry to the DMU.
- ▶ Issued commands to any subsystem including itself in response to software or hardware generated interrupts.
- ▶ Controlled the start of hold/slew algorithm.
- ▶ Issued stored or uplinked command groups (delayed commands).
- ▶ Controlled any automatic mode sequencing.

There were 16 interrupts available. The Flight Executive code used 8 spacecraft initiated (int. 4, 5, 9, 11, 12, 14, 15 and 16) and 4 ground initiated interrupts (int. 0, 1, 8 and 10), the other ones were not defined. An interrupt was a software service routine called by external devices handled on a time dependant basis. A priority decoder ensured that only one interrupt was selected at a time, and interrupts were serviced in order of priority. If an interrupt occurred during the execution of an instruction, it was not honoured until that instruction was completed. If several allowable interrupts occurred at one time, there was one CPU instruction executed before each interrupt was serviced. The following list is a summary of the OBC interrupts along with their functional description.

- **Int 0.** Initiate the OBC program.
- **Int 1.** Command input for OBC software load.

- **Int 4.** Ground Telemetry Data in.
- **Int 5.** Computer Data in.
- **Int 8.** OBC software dump.
- **Int 9.** Command out to command decoder.
- **Int 10.** Ground command to OBC (executive request handler).
- **Int 11.** Frame synchronization check for Ground and Computer Data in.
- **Int 12.** Direct Address to DMU.
- **Int 14.** OBC Data out.
- **Int 15.** Scheduler for Workers and Out-of-Limits handler.
- **Int 16.** Exit. Executive services (sets up Int 9).

A Worker was an OBC application program that performed a specific task. Workers were called by the flight executive. The following list explains the task performed by each Worker.

- **Worker 0 - Hold/Slew Algorithm**
This attitude control algorithm was the single most important routine on board the IUE. The purpose of this program was to provide a method by which the spacecraft might be slewed to a command region and/or hold an existing orientation for an extended period of time. The program integrated rate and position sensor data and calculated the reaction wheel commands necessary to hold or slew the spacecraft. Worker 0 used a set of variables, called Mode Bits, to select appropriate inputs to the operational mode (e.g. the sensor which were to be used on that iteration to calculate the three control variables). Worker 0 also checked for violations on axis/sensor configurations and changed the configuration as necessary. Worker 0 underwent periodic code changes to improve spacecraft pointing accuracy and slew control as well as to account for sensor failures. It was the most affected Worker when a new attitude control system was implemented.
- **Worker 1 - Maneuver Processor**
Worker 1 was a service routine. It processed the minimum time slew information (axes and angles) contained in a Datablock 11 and set telemetry flags to indicate the status of the maneuver. The processing of the information basically consisted of feeding the slew information to worker 0 one leg at a time.
- **Worker 2 - Exposure Control**
This service routine accurately timed to within 409.6 milliseconds, camera exposures for collection of scientific data. It used the information contained in a Datablock 14 to perform the exposures. The Datablock 14 indicated which camera was to be exposed and for how long. Worker 2 commanded the camera to "expose" mode, counts up from zero

to the indicated time in 409.6 millisecond ticks, and then issued a “standby” command to the camera.

- **Worker 3 - Cyclic Delayed Command Worker**

In 1988, Worker 3 was designed to use the DMU clock in conjunction with Interrupt 5's scheduled execution time to provide accurate cyclical executions of an uplinked block of commands (Datablock 18). It was intended to be used to “strobe” the spectroscopic cameras to obtain phase coverage of pulsar-like variables with very short periods. Worker 3 was never used because the rapid cycling on the cameras could damage them.

- **Worker 4 - Bright Light Protection**

This diagnostic algorithm checked star intensity. If it was too great, a command to shut down the FES, close the sunshutter and put the cameras in standby mode was given to protect the equipment from permanent damage. This worker was only used early in the mission.

- **Worker 5 - Pointing Constraint**

Worker 5 was a diagnostic algorithm. If Worker 5 was active, it would command the FES to shut down and close the sunshutter, put the cameras in standby mode and the spacecraft in Sun acquisition hold-on-wheels mode whenever it sensed the absence of sunlight from the digital sun sensor. This worker was only used early in the mission.

- **Worker 6 - Memory Checksum**

This self-check algorithm performed an exclusive OR operation on the contents of the OBC memory banks, excluding variable data points. The result of the XOR was compared to a constant stored in memory. If the checksum failed, an error flag was set to indicate possible corruption of the OBC contents.

- **Worker 7 - Central Processing Unit Functional Test**

Worker 7 was a self-check algorithm. It checked the OBC logic and arithmetic instructions for correctness. A series of manipulations were done and compared to a set of constants in memory. If an unfavourable compare was found, an error flag was set.

- **Worker 8 - Attitude Control System Worker Timeout**

Worker 8 had top priority of the self-check algorithms. It performed a time limit check to verify that Worker 0 completed running within a prescribed time. If this condition failed, an error flag was set and Worker 0 was rescheduled.

- **Worker 9 - Rate Arrest**

This diagnostic algorithm monitored the wheel speeds when there were no slews in progress. An error flag was set when the absolute value of the wheel speed change was greater than a given threshold and a change was in the same direction on three consecutive iterations. This worker had a commandable option to allow the program to switch to the inertial (Worker 10) hold on wheels control mode when an error was detected.

- **Worker 10 - Wheel Speed Hold.**

Worker 10 was an attitude control algorithm. It maintained the reaction wheel speeds at

a designated rate. The reference wheel speeds could be uplinked in a Datablock 16 or the current values could be captured as references at the time Worker 10 was turned on. Wheel hold was used for control in case of ACS sensor malfunctions and, sometimes, during shadow periods (Shadtrack mode).

- **Worker 11 - Safe Attitude Slew.**
Worker 11 was a diagnostic algorithm. When enable, it allowed the OBC or user to have the spacecraft automatically slew from a constrained (violation of spacecraft orientation limits) to an unconstrained region. The safe attitude coordinates were stored in a Datablock 11.
- **Worker 12 - Shuts Down Fine Error Sensor, Camera and Shutter.**
This diagnostic algorithm gave the user a quick way of protecting the spectrograph hardware and could be activated by ground command or by Worker 4 or 5. Worker 12 shut down the FES, closed the sunshutter and put the cameras in a standby mode.
- **Worker 13 - Delayed Commands.**
This service routine retrieved and processed stored commands contained in Datablock 17 and directed them out to the command decoder. Any type of command could be transmitted to the OBC via a Datablock 17 and then executed at a later time by commanding Worker 13 on. Camera preparation and wheel unloads were the most common uses for delayed commanding. When all the commands had been retrieved and sent to the command decoder, Worker 13 turned itself off.
- **Worker 18 - Software Loads.**
Worker 18 was a service routine which handled all Datablocks and OBC patches. The first command in the load triggered Interrupt 10 and identified the number of commands to follow. The commands were then stored in one of two temporary storage buffers by the DMA. Worker 18 would then copy the commands to the final buffer or address in the OBC. After loading was complete Worker 18 would shut itself off. If Worker 18 remained on, software loads could not be processed until the Worker was turned off by a ground command.
- **Worker 19 - Rate+Position Hold / Delta-V.**
This attitude control algorithm used much of the same sensor data used by Worker 0 to calculate and send commands to the HAPS jets. It was designed to provide control of the IUE during Delta-V burns. In the Rate+Position Hold mode, the three spacecraft axes were controlled by the low-thrust jets. Delta-V mode was similar to Rate+Position except that the yaw axis was controlled by high-thrust jets, which were being commanded to fire for the velocity correction burn. Datablock 19 contains the control information for Worker 19.
- **Worker 22 - Zero Out Gyro Bias Angles.**
This service routine reset the pitch and yaw gyro measured body angles to zero.

In the course of operations many Workers were left inactive. The limited memory of the OBC became critical in the transition from the 3-Gyro to the 2-Gyro system and Workers 4, 5, 7, 9, 11,

12 and 22 were removed.

Commands and Datablocks

The command structure was set up to achieve maximum flexibility and allowed the OBC to detect the various requests and process them properly.

Single commands were used for different utilities, for example to start the OBC code, stop the OBC, select the memory banks, dump the memory contents to ground, load instructions from the ground to the OBC code, switch on/off the workers, select FES 1/FES 2 data and so on.

Datablocks were the most common type of software load sent to the OBC. They contained either commands that were issued to the spacecraft or operating parameters for a particular worker. Each Datablock had a specific function and carried specific types of commands or information within it. These five Datablocks were used in everyday operations:

- Datablock 11 - Minimum Time Maneuvers. It contained the slew leg angles and the axes to be slewed for minimum time slews (long maneuvers were performed one axis at a time).
- Datablock 14 - Camera Exposure. It contained the identification of the camera to be exposed and the length of the exposure.
- Datablock 15 - Attitude Readout. It placed the ground generated Right Ascension, Declination and Roll angles into the OBC telemetry stream.
- Datablock 17 - Delayed Commanding. It could store any set of commands in the OBC to be sent at a later time. This Datablock was most often used for wheel unloads and camera preps.
- Datablock 21 - Worker 0 Configurations. It was a versatile Datablock that handled Mode Bit configurations, gyro trims and fixed rate slews (usually short slews in both pitch and yaw axis). This Datablock was labelled Datablock 10 under the 3 Gyro system.

There were also other Datablocks used in special circumstances like Datablock 12 (used to sequentially define the desired order of the OBC telemetry frames for ground inspection), Datablock 13 (used to define the content of 6 OBC programable addresses contained in OBC telemetry), Datablock 16 (used to provide reference wheel speeds for OBC Worker 10) or Datablock 19 (used to uplink information needed by Worker 19).

Datablocks were uplinked to the spacecraft and handled by Worker 18 which was controlled by Interrupt 1, the software load Interrupt. Worker 18 verified that each Datablock was built correctly and then stored the data in a buffer set aside for particular datablock, each datablock had its own storage area. The data contained in the datablock were then available for the associated worker to use.

Error Flags

An error flag was a status bit set by OBC Workers or Interrupts to indicate some parameter violation or the identification of a specific condition. Error flags came down in OBC telemetry to be displayed at the control consoles and to alert the analyst of a potential problem.

Memory Dumps

The contents of the OBC memory banks could be examined by dumping the contents into the telemetry stream and reconstructing them on the ground. This was often done after an anomaly involving the OBC to pin-point the cause and to ensure that no part of the memory has been corrupted. Dumps were also done whenever software changes were made to improve or correct the OBC workers to verify the patch were properly stored in memory.

Temperature Limits

The OBC required that certain temperature limits be maintained to ensure proper and reliable operation. The prelaunch maximum predicted value was 35°C, but soon after launch it was apparent that this early prediction could not be met. The operational temperature limit for the OBC was raised over the spacecraft lifetime and reached 58.3°C. At elevated temperatures the OBC might begin taking “hits” and cease to operate, resulting in an OBC crash and a loss of attitude control.

On January 10, 1995 the OBC temperature upper limit was reduced from 58.3°C to 56.4°C due to the DMU anomaly (see section 4.4.1.).

4K Operational System

OBC memory bank 1 contained a complete operating system that only occupied 4K of space. This system was developed as a backup in case of an anomaly with the 8K system. The 4K system was also used during spacecraft tests for attitude control while the other two memory banks were being loaded with test software. In order to make the system small enough to fit in 4K, many workers had to be eliminated.

For the first 3 years of the IUE mission, the OBC 4K operational system was used strictly as an emergency backup to the 8K operational system. It could not support science operations, but was used to recover attitude and monitor spacecraft telemetry until the 8K operational system was operational again.

During 1981, a new 4K operational system was developed which could be used to support science operations.

After the third gyro failed, science operations could not be supported by the new two-Gyro-FSS 4K operational system, it had no Worker 13, so delayed commanding via Datablock 17 could not be performed and no Worker 14, so no exposures could be taken. Also, it had only Worker 0 for attitude control.

5.6.1. OBC Patches

OBC patches were used to introduce new values or instructions to the existing OBC code. These modifications were realized in an attempt to improve the OBC control or to solve a new problem. The list below explains the main patches introduced to the OBC code and, also, the different system versions used in the 4K and 8K code.

- On November 4, 1979 two changes were introduced in the 4K system. The first one was to introduce a new gyro matrix with Gyros 2, 4 and 5. So, it would be used in the event of Gyro 1 or 3 failure or a failure of the 8K system. The second one consisted of a "hit" protection to automatically restart the OBC.
- On November 8, 1979 some patches were applied to the 8K system to prevent a missing interrupt from halting the OBC, eliminate the static OBC telemetry problem and store the contents of certain registers to aid in later analysis in the event of an OBC crash.
- On January 29, 1980 the "NO-OP" instruction in the idle loop was replaced by the "HALT" instruction to permit the memory power to cycle. The "HALT" instruction was expected to save power and reduce the OBC temperature by a couple of degrees.
- On March 31, 1980 the "NO-OP" instruction was again inserted in place of "HALT" instruction. The "NO-OP" instruction greatly reduced bus noise and the change did not reduce the power or temperature.
- On May 20, 1980 a new sequence was introduced to automatically restart the OBC in the event of a crash.
- On June 16, 1980 the Interrupt 9 was modified to improve its command capability.
- On August 31, 1981 a new 4K system was uplinked and successfully tested, which was capable of supporting science operations. In order to squeeze this much into 4K, many programs were deleted or changed. The following workers were deleted: Worker 4, 5, 7, 9, 10, 12 and 19. Worker 8 and 18 no longer existed as separate workers, their functions still existed, however, and were included in Interrupts 15 and 1. The Worker 0 was slightly changed from the 8K version.
- On August 18, 1985 the 2 Gyro/FSS system was uplinked to the spacecraft. It required many changes with respect to the previous system. Datablock 10 was replaced by Datablock 21. The Workers 4, 5, 7, 11 and 12 were deleted to gain memory. The Workers that had to do with slewing and attitude control were substantially changed and, also, the Mode Bits were redefined.
- On April 25, 1986 the roll control law was completely changed from the original 2 Gyro/FSS code to do a much better job of controlling large oscillations at low beta angles. Some attempts to improve the roll control were made during the previous with minimal improvement. The new law improved the roll control by holding the sun centred on the edge between two FSS buckets.

- On October 17, 1990 a new 4K system was developed. Only basic hold/slew capabilities were provided by the available Workers 0 and 1. Worker 1 was essentially identical to the current version used in the 8K system. Worker 0 was greatly reduced in size and capabilities (no FES processing, no filtered modes, no low gain option). Worker 18's function was still included in the flight executive code but it was not distinguished as a separate Worker.
- On December 21, 1990 a patch was implemented to effectively correct the roll FSS data used by the OBC when coarse bit 5 had dropped out. Because of the current control algorithm and the symmetry of the FSS, the patch simply reset the bit when it dropped out. An error flag was set by the patch simply reset the bit when it dropped out. An error flag was set by the patch when the bit was reset by the code to enable the ground controllers to keep track of this anomaly.
- On May 6, 1991 a patch was introduced to the OBC code to correct another FSS anomaly. When an erroneous beta value greater than 136° was measured, the value was ignored and the patch set an error flag. Worker 9 had to be deleted to implement this correction due to a lack of available memory.
- On July 8, 1991 a patch was uplinked to enhance Worker 0 control during minimum time slews. It also improved Worker 19 control. The new law produced a better roll angle control. The roll angle was corrected on each worker iteration to be always as close to zero as possible during slews. This resulted in smaller maneuver errors.
- On July 19, 1991 a patch was uplinked to prevent a complete loss of attitude control in the event that track was accidentally broken during an eclipse. If a loss of star occurred, the spacecraft attitude control was automatically switched to Worker 10, which provide control independent of the FES and FSS. The patch was made to allow Worker 0 to perform its calculations even if a no sun presence condition existed. So, control was returned to Worker 0 at the end of the eclipse and it could zero out the net errors accumulated while under Worker 10.
- On September 9, 1992 a patch was introduced to the OBC to correct all code inconsistencies that produced a discrepancy between the decoder used by the OBC and the telemetry point indication of the decoder being used.
- On July 1, 1993 a patch was developed to detect most incidents of the FES tracking on scattered light and automatically placed the spacecraft in a stable hold mode.
- On March 11, 1996 the 1 Gyro system was loaded into the OBC. The primary change in this system was the attitude control Workers. The Mode Bits also had to be redefined.
- On March 26, 1996 the yaw axis control was improved after several attempts. Also, the FES scattered light check had to be changed and the error threshold adjusted to compensate for the relatively larger errors experienced during fixed rate slews when using the FES.

5.6.2. Three-Gyro System

The three-Gyro system was the original control mode. It was used until the fourth gyro failed. In this system, there were two basic ways of controlling the pointing of the spacecraft:

- ▶ Gyro mode. The gyros sensed motion in three axes (pitch, yaw and roll) and this information was used to control the spacecraft.
- ▶ FES mode. "Put track on" meant that the FES and filtered gyro data were used to control the pitch and yaw, while roll was controlled using filtered gyro data. The attitude sensor data coming to the OBC could also be filtered.

The normal sequence of events from preparing for a maneuver to starting an exposure proceeded as follows:

- ▶ The maneuver was computed by the ground system.
- ▶ Before and during the slew, the spacecraft remained in Gyro mode. The minimum time maneuver was done slewing one axis at a time, pitch, yaw and roll.
- ▶ After the maneuver, the star field was identified and a wheel unload performed (if needed). Some fixed rate slews were performed in Gyro mode to acquire the target and put it into the aperture.
- ▶ Once the star was in the aperture, a guide mode (FES mode) was chosen and the exposure started.

Special techniques were used for certain types of observations:

- ▶ Blind offsets were slews from a visible target or guide star to non-visible target (those targets which could not be seen by the FES). Accurate coordinates for both the target and the visible reference star in the FES field of view were needed. Then, the guide star was placed at computed FES (X,Y) coordinates so that the target fell in the aperture. This required an accurate FES geometric calibration.
- ▶ Moving targets were performed under Gyro control. The spacecraft was made to follow the star motion by changing the gyro drifts.
- ▶ Trails were exposures taken of a star while the spacecraft moved such that the aperture crossed the target. Trails were performed under Gyro control.

The failures of the gyros and the reconfiguration of the gyro heaters resulted in a degradation in maneuver accuracy. New gyro scale factors corrections were calculated monthly based on the month's observed maneuver errors. Plots were created showing the actual observed maneuver errors and what they would have been had new gyro scale factors been uplinked. The figure 5-68 shows this comparison (maneuver length and error the square root of the squares, only pitch and yaw errors included) with data from 1981. When large variations began appearing, the new gyro

scale factor corrections were uplinked to the spacecraft (see section 5.5.1.2.).

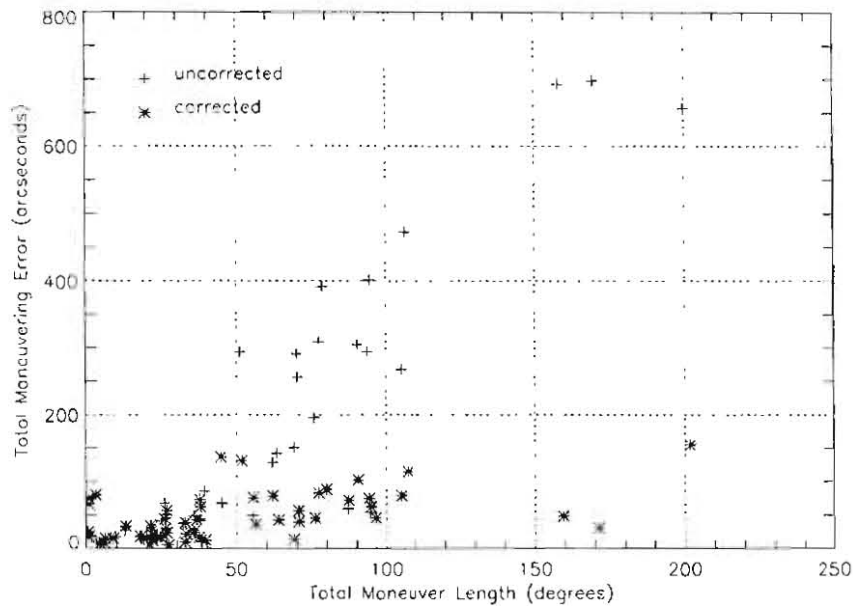


Figure 5-68. Comparison of errors with derived correction, 3-Gyro system.

5.6.3. Two-Gyro/FSS System

The basic idea of this system was to use the FSS data to provide attitude information in place of a gyro. The FSS can sense both pitch and roll motions, but not yaw motion directly. Also the FSS control was cruder than gyro control, around 15 arcsecond instead of 1 arcsecond accuracy. The motion in pitch and yaw axes could be measured from the gyros, while the roll angle was maintained as close to zero as possible based on the FSS measurements.

In the 2-Gyro system, the OBC could use several different combinations of the two gyros, the FSS and the FES to monitor spacecraft motion in the three axes. The following modes were the more used ones:

- ▶ Default mode (pitch on FSS + gyro, yaw on gyro, roll on FSS). This was the mode normally used for minimum time slews.
- ▶ Acquisition mode (pitch and yaw on gyros, roll on FSS). This was the mode normally used to set up on the star or target and to perform all fixed-rate slews.
- ▶ Tracking mode 1 (pitch and yaw on FES + gyro, roll on FSS). This mode was normally used during the exposures.

- ▶ Tracking mode 2 (pitch and yaw on FES, roll on gyro). This is the only sun independent mode. So, this mode was normally used during the shadow periods.

During daily operations, the normal sequence of events was carried out as follows:

- ▶ The maneuvers were computed as usual, but there were no longer any allowed constrained maneuvers (e.g. it was not possible to slew to beta angles of less than 13° , because the FSS would lose sun presence).
- ▶ The spacecraft had to be prepared for the maneuver, which was performed in default mode. There were two types of slews: pitch and sunline. The sunline was actually a combination of a yaw slew and a roll slew, balanced so that a constant beta was maintained.
- ▶ After the minimum time slew was completed, the control mode was changed from default mode to acquisition mode. It was important to get out of the default mode, in which pitch was controlled through the FSS, quickly. As the sun moves slowly through the sky, the beta angle of a given star changes slightly. If the spacecraft was maintained at a fixed beta angle, then the star would appear to move across the FES field.
- ▶ The star field was identified and a wheel unload performed (if needed). Some fixed rate slews were performed to acquire the target and put it into the aperture.
- ▶ Once the star was in the aperture, a guide mode (Tracking mode 1) was enabled and the exposure started.

The special types of observations were achieved in a similar way to the three-gyro system. Blind offsets, moving targets and trails were performed while the spacecraft was under acquisition mode.

After the FES streak light anomaly appeared, the blind offset started to be used very frequently. Many stars were hidden by the streak light. So, a lot of times, fixed rate slews were to be performed from far (not included in the same FES field) bright stars. Sometimes, it also implied that there was not any available star to guide, so, the exposure had to be taken while the spacecraft was controlled in acquisition mode. As this mode was strongly dependent of the gyro drift (pitch and yaw were controlled on gyros), the exposure time could not be very long (up to 40 minutes). Long exposures were performed divided in segments. At the end of each segment, the target (or another bright star close to the target) position was checked and the gyro drift measured from the position errors. From these drift measurements corrections to the gyro drift bias were calculated and uplinked to the spacecraft (see section 5.5.1.2).

The spacecraft appeared to maneuver better under the 2-Gyro/FSS control mode than under the 3 Gyros control mode. In the 2-Gyro/FSS system, pitch slew errors were not usually greater than ± 2 arcseconds. Sunline slew trends are shown in the figure 5-69. The FSS resolution was rather poor at low betas, so this fact very much increased the final errors.

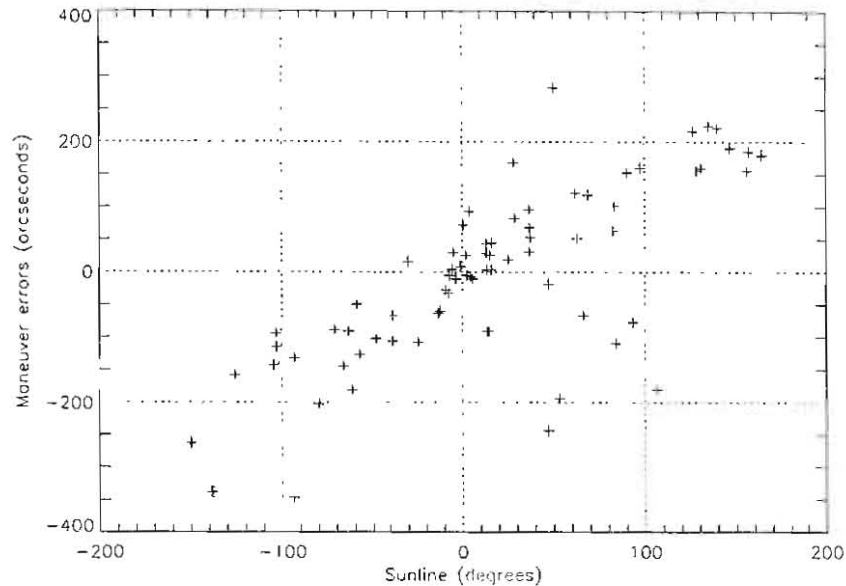


Figure 5-69. Sunline slew errors, 2-Gyro/FSS system.

5.6.4. 1-Gyro System

The 1-Gyro flight code processed information for 2 axes from the FSS or the FES and the one remaining gyro to provide 3 axes control. Having one operational gyro required that this gyro be used as a sensor for only one axis at a time. This was necessary because the gyro's input axis was equivalent to having one equation with three unknown variables, which could not be solved. In order to derive useful single axis information from the gyro, the motion sensed from the other 2 axes was removed from the gyro data. Information from the FSS and/or the FES provided the necessary information to solve the equation.

The following modes were the most used ones:

- ▶ FSS default mode (pitch and roll on FSS, yaw on gyro). This control mode provided the most robust control and was used for minimum time maneuvers and wheel momentum unloads. It was the only FES independent mode and provided a coarse control. The accuracy in the pitch axis was around 15 arcseconds (the FSS resolution changes with beta) and in yaw axis around 1 arcminute (it was strongly dependent on beta angle).
- ▶ Tracking mode 1 (pitch and yaw on FES, roll on FSS). This mode provided the fine pointing control to perform fixed rate slews and exposures. FES 1, FES 2 or both FES's data could be used, but, due to thermal and power constraints, the FES 2 data was actually the only one used.

- ▶ Tracking mode 2 (pitch and yaw on FES, roll on gyro). It was the only sun independent mode and was used during the shadow periods.

The normal sequence of events from preparing for a maneuver to starting an exposure was carried out as follows:

- ▶ The maneuver was computed as usual.
- ▶ The spacecraft had to be prepared for the maneuver, which was performed in FSS default mode. As in the 2-Gyro/FSS system, there were two types of slews: pitch and sunline.
- ▶ After the minimum time slew was completed, an FES image was taken and the star field identified.
- ▶ The tracking mode 1 was put on the guide star. It was important to get off the FSS default mode as quickly as possible. As the sun moves slowly through the sky, the beta angle of a given star changes slightly. This apparent sun motion produced spacecraft motion in both pitch and yaw axes.
- ▶ Some fixed rate slews were performed to acquire the target and put it into the aperture. As the fixed rate slews were done in tracking mode, they had to be performed inside the FES field.
- ▶ Once the star was in the aperture, an exposure was started. The only mode to have fine pointing control was to use a guide star, so, each target needed a bright enough star to be used as a guide star.

Blind offsets could be performed in FSS default mode or in tracking mode. The first mode had to be used when the initial star and the target were not in the same FES field, but the accuracy was very poor.

Moving targets and trails could be performed using a guide star in tracking mode 1. An exception was the observation of Comet Hyakutake from March 23 to 27, 1996. At this time, no moving target procedure had been developed for the 1-Gyro control system (Gyro 5 had been lost on March 6, 1996). The operational mode chosen was to follow the comet in FSS default mode by direct commanding of drift rates to the OBC. On the one hand, these rates compensated for the spacecraft drift following the solar motion and, on the other hand, brought the comet into the aperture by introducing the same comet motion in the spacecraft reference system.

The figures 5-70 and 5-71 show pitch and sunline errors at different beta angles.

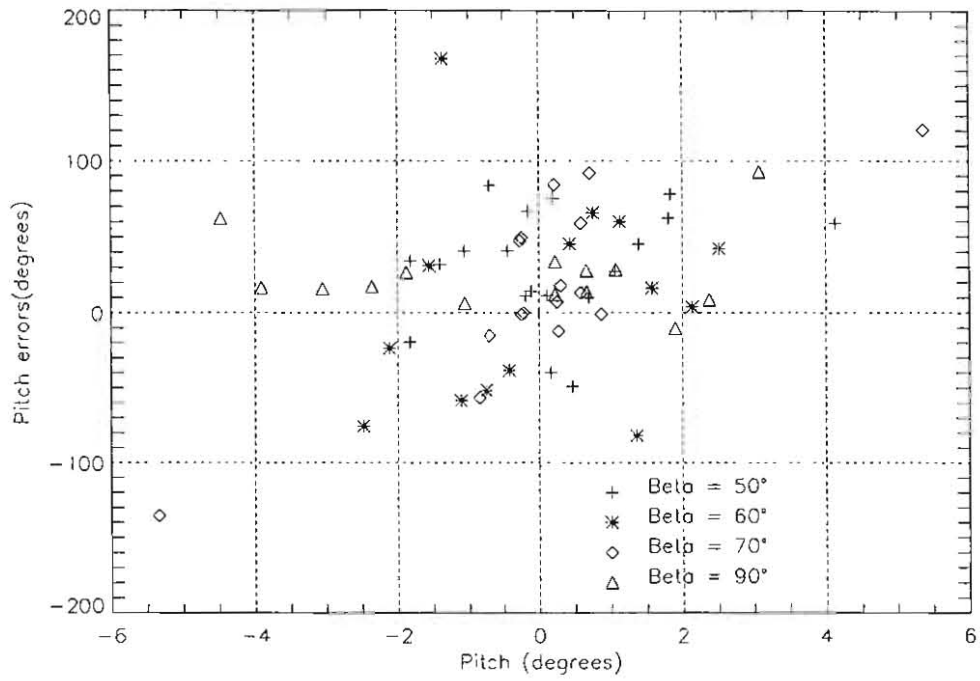


Figure 5-70. Pitch slew errors, 1-Gyro system.

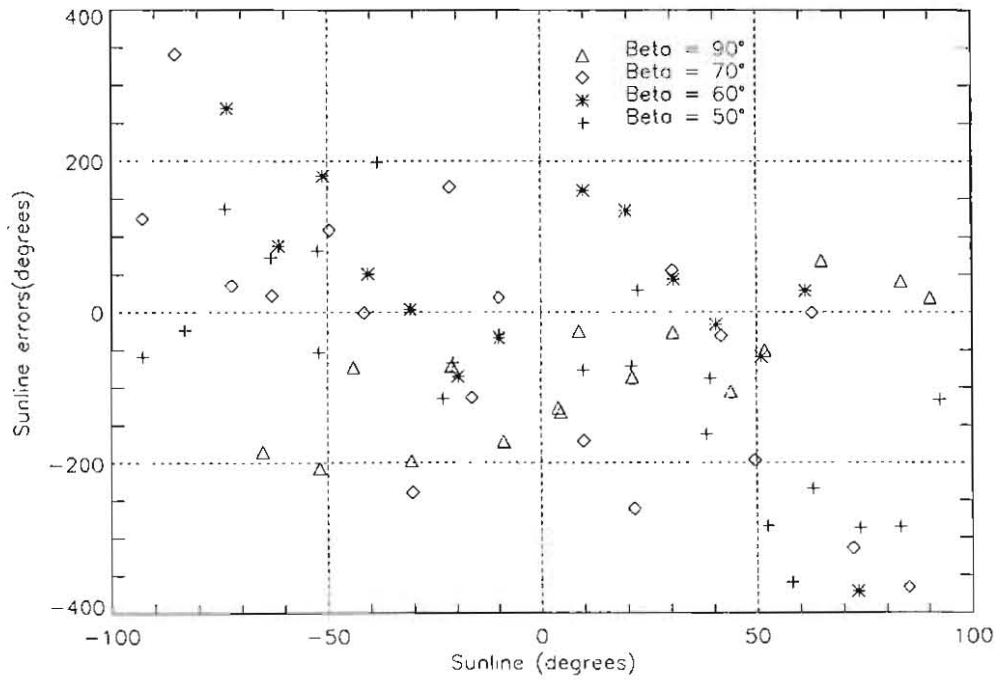


Figure 5-71. Sunline slew errors, 1-Gyro system.

5.6.5. Attitude recovery procedures

During the IUE's mission, the spacecraft experienced several losses of attitude due to an OBC crash or other spacecraft problem. The primary symptom of loss of attitude was the inability of identify the star pattern in the current FES field-of-view. Following these events, an attitude recovery was necessary. The following attitude recovery procedures were available.

▶ **Attitude recovery at beta = 0°**

At beta = 0°, the spacecraft pointing was towards the anti-sun position at a given time, which right ascension and declination could be interpolated from the solar ephemeris (to the nearest minute of time). The spacecraft maneuvered to this position, where the north direction on the finding chart and the north arrow on the identified FES field-of-view were compared. From the difference, a correction to the roll attitude currently in the system was estimated.

The attitude should be verified to eliminate small pointing errors, and to improve the accuracy of the spacecraft roll determination. Before going to beta equal 0°, a maneuver to beta equal 20° was usually performed to optimize the FSS before the sun was lost. This maneuver also introduced errors from optimum roll of no more than a few arcminutes.

▶ **Coarse attitude recovery**

This procedure provided a deterministic 3-axes attitude using FSS and PAS data. The course attitude recovery had to be performed at beta equals 90°. A ground program provided a list of the time intervals during which the Earth may be target by the PAS (it viewed the Earth twice a day at a time span of 12 hours between the viewing slots). If the Earth path was due within the next hour or two, one should take into consideration to recover attitude using this method.

Experience showed an error of ± 0.5 degrees in spacecraft attitude using this procedure.

▶ **Attitude recovery using wheel speeds.**

This procedure was valid only if no external sources of momentum had been introduced onto the spacecraft, such as haps jet firing. The wheel speed data was used to calculate how much movement the spacecraft had experienced about a selected axis combining this with the relative sun spacecraft angles. A pitch-yaw-pitch maneuver was calculated from the wheel speeds, and the yaw leg is calculated at beta equals 90°. The pitch legs of the maneuver were determined solely by the initial and final betas, while the yaw leg depended on the wheel speed change.

The new attitude could be derived to an accuracy of about two degrees in each axis. The primary source of errors was in the inaccurate wheel speed telemetry and the resolution of the speeds (average resolution was 9 rpm / telemetry count).

▶ **Beta-dot.**

The beta-dot (β -dot) procedure was based on the effect of the daily solar motion as seen by the FSS. It was measured by the movement of a star in the FES field-of-view. For beta equals 90°, the next equation shows the relation between beta-dot and the ecliptic latitude.

$$\dot{\beta} = \dot{\lambda} * \cos(\epsilon)$$

Where $\dot{\lambda}$ was the sun's movement at the time of the recovery. There was also a sign ambiguity which was resolved by measuring the roll-dot (the sign of the ecliptic latitude is the same as the sign of the roll variation).

The accuracy of this procedure did not seem to be much better than 3 degrees. Beta 90° was the best beta to apply it not only because it simplified the original equation, but also because the beta variation was maximum at this beta angle.

5.6.6. OBC anomalies

The OBC experienced different malfunctions which had repercussion on IUE operations. These anomalies could affect the scientific experiment operations or the spacecraft control, which had to be rapidly identified and corrected. A list of the OBC anomalies experienced by the IUE during the mission are detailed in Appendix C.

OBC crashes

When the OBC halted, it ceased issuing wheel control voltages and a loss of attitude control resulted. Because of this, quick recognition and recovery were essential.

Switching to the 4K backup system was the normal mode to recover the attitude control. If this failed to stabilize the spacecraft, Sunbath mode could be entered. Sometimes, the Sunbath mode was extremely important since it was the only mode available to stabilize the spacecraft when the 8K system halted. There was not a 4K backup system available at the beginning of the two-gyro/FSS control mode (from August, 1985, to October, 1990) and under the one-gyro control mode.

Following stabilization of the spacecraft after an OBC crash, the 8K memory was dumped and compared to its expected contents. If 8K corruption was found, the memory banks were reloaded with the proper OBC load tape.

Most of the times, the OBC crashed without a known reason although it could be associated with high OBC temperatures, unusual bit rates, etc. In other cases, some telemetry parameters helped in understanding the cause of the crash, as was the case with the hit counter (HITCTR) and the synchronization counter (SYNCTR).

- ▶ An OBC hit was a specific type of corruption to the data stored in the registers called the "Interrupt Return Vector". This corruption had detrimental effects to the proper functioning of the OBC programs (usually resulting in an OBC crash). The OBC included a hit analysis code to detect this problem and avoid the usage of the corrupted values.
- ▶ The SYNCTR value was incremented each time the Direct Read Table was out of sync (the OBC and the DMU were out of sync). During normal operations, the only time the SYNCTR was expected to increase was during a bitrate change. When a large increase in the SYNCTR occurred, there was the potential risk of an OBC crash.

Worker failures

A brief explanation of the worker failures experienced is given below.

- ▶ Worker 22 was cycled on and off to zero out the ABG's were not zeroed.
- ▶ Worker 18 was turned on to load a Datablock but, for some reason, it was not scheduled to run. This resulted in the Datablock being lost and Worker 18 being unable to turn itself off. It had to be switched off manually to avoid all subsequent Datablocks being rejected. The majority of these cases were identified as resulting from two programs (Interrupt 15 and Interrupt 1) messing with Worker 18's downcounter at the same time. Also the Worker 22 and 13 failures can be explained in a similar way.
- ▶ Worker 13 failed to execute the commands in the Datablock 17 and remained on. It had to be switched off by ground command.
- ▶ Worker 2 did not terminate an exposure properly, ending it early by two Worker 2 counts. This anomaly seems to be data dependent.

Command and Datablock skipped

On several occasions, a single command or a Datablock was uplinked and received by the spacecraft but not executed. The commands were verified by the ground system and the spacecraft command decoder but there was not any action related with them. In general, it did not produce a great impact on operations. The command or Datablock had to be retransmitted and the operations resumed.

Beta 75° anomaly

On November 28, 1988 the spacecraft attitude control degraded into oscillations, as a result of the beta 75° crossover point of the FSS. As the sun's apparent position drifted to a point near the spacecraft referenced beta angle of 75°, the misalignment of the FSS system's head caused the control algorithm to produce oscillations. A switch between the two system heads at beta 75° was accompanied by a roll axis correction due to the sensor misalignments. This roll axis rotation affected the beta angle, giving it a value that indicated that the other FSS system, head combination should be used. Thus, while the sun angle remained within a region close to beta 75°, the control algorithm continually cycled between the two FSS system/head combinations. On every FSS system/head switch the spacecraft rolled to some degree to account for the misalignment of the FSS system/head, resulting in the observed spacecraft oscillations. With sufficient time elapsed the sun angle moved far enough from beta 75° so that the Roll motion resulting from the switch in FSS system, heads did not indicate that the other FSS system, head should be used, and the oscillations ceased.

The OBC changes the FSS system/head at beta 75°, which did not produce any problem until the spacecraft began to be controlled under the 2-gyro/FSS system. It was decided that no normal operations would be conducted around this beta (± 5 arcseconds) due to the misalignment of the FSS systems and heads. The margin around beta 75° had to be increased (around ± 1 arcminute) with the one-gyro control mode.

5.7. Scientific Instrument

The IUE scientific instrument (SI) collects the astronomical data and is designed to obtain ultraviolet spectra of astronomical objects down to a faint limit of approximately fifteenth magnitude. The SI consists of two assemblies. The optical unit includes the sunshade, telescope, spectrographs, four spectrograph cameras and two FES's. The electronic assembly includes the experiment electronics assembly (EEA), two FES electronics modules, camera system interface unit (CSIU), and camera electronics box (CEB). The figure 5-72 shows the distribution of these units.

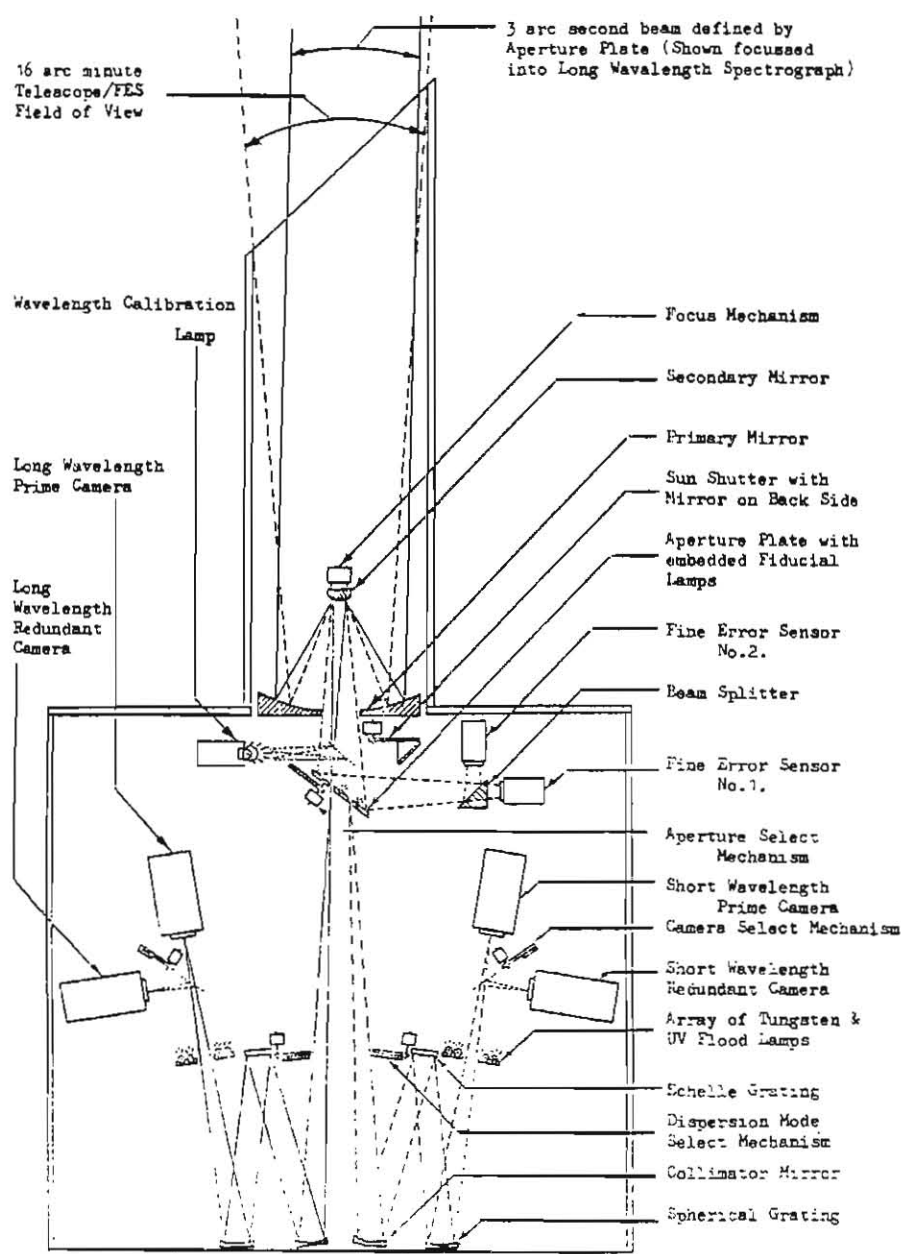


Figure 5-72. Detailed Optical Schematic of the IUE Scientific Instrument.

Sunshade, Baffling and Shutter

The sunshade, a hood with a 43° cutaway angle placed over the front of the telescope tube, and the baffle system, exclude stray light from the FES's which have longer wavelength response and wider effective passbands per image element than the spectrograph cameras. Test and calculations indicated that with the proposed design, scattered sunlight will cause no difficulties in making observations of faint objects down to a magnitude equal to 16.

The sun shutter protects the cameras and FES's from prolonged exposures to high-level sources. The shutter can protect the instrument from direct Earth or moonlight if required, and from direct sunlight for short periods. It automatically closes in the event that excessive telescope illumination is detected by a photodiode. In addition to its automatic mode the Sun Shutter may also be operated by command.

The sun shutter experienced several anomalies during the mission. The most frequent one happened five times, it unexpectedly closed itself without apparent reason. On November 26, 1985 the sun shutter remained in the "slew" mode after the command to close it had been uplinked, it was re-opened and closed successfully. Additionally incidents of the anomaly occurred through the remainder of the mission.

Telescope

The telescope is an f/15 folded reflective optical system used to collect photons from celestial objects and deliver them to the ultraviolet spectrograph for analysis. It consists mainly of the primary and secondary mirrors and the mechanical structure required to support mirrors.

The telescope gathers light from the object under observation and focuses it to provide the proper image at the entrance aperture of the spectrograph. The telescope, a 45 cm diameter f/15 Ritchey-Chretien design, consists of a beryllium concave hyperbolic primary mirror 45 cm in diameter and a convex hyperbolic fused silica secondary mirror 9 cm in diameter, which produce an image size for the 80% collection ring of 1 arcsecond for a point source of light. The telescope is 130 cm long and has an effective focal length of 675 cm. It provides a 16 arcminute useful field of view at the focal plane.

After launch, the telescope's focus was adjusted to compensate for the extraterrestrial environment. This was achieved by movement of the secondary mirror along the longitudinal axis of the telescope. The mirror was driven by an incremental stepper motor in the focus mechanism. After that, only thermal focus adjustments were made.

Spectrographs

The spectrographs disperse the on-axis image formed by the telescope into a spectral display at the face of the selected spectrograph television camera. The spectrograph consists of two similar instruments, each of which operates over a selected portion of the spectral range, from 1150\AA to 3300\AA , and provides a resolution no worse than 0.2\AA at any wavelength. The long wavelength spectrograph covers the range from approximately 1800\AA to 3300\AA and the short wavelength spectrograph from approximately 1150\AA to 2000\AA .

The spectrograph design permits operation of each spectrograph in either of two modes: high dispersion (1Å/mm)/high resolution (0.1Å) and low dispersion (60Å/mm)/low resolution (6Å), which produce velocity resolutions between 10 and 25 km/sec for high resolution and between 600 and 1500 km/sec for low resolution.

Each of the spectrographic instruments consists of an entrance aperture, a collimator mirror, an echelle grating for the high-dispersion mode of operation (replaced by a mirror for the low-dispersion mode), and a spherical diffraction grating, which acts as both a camera mirror and spectral disperser. Its dispersion direction is perpendicular to that of the echelle grating. The echelle grating disperses the spectrum, dividing the entire ultraviolet spectrum into many overlapping orders. The spherical gratings separate these orders.

The aperture plate contains four holes, one pair for each spectrograph. The small apertures are nominal 3 arcseconds in diameter. This aperture size, in conjunction with the shade design, will limit the background light to the equivalent of a 16th magnitude object or less. The large apertures, nominally 10 by 20 arcseconds, were the most frequently used. These two large holes could be closed by use of the aperture select mechanism.

The IUE Three Agency Coordination Meeting adopted recommended values for the dimensions of the apertures, which are presented in the table below. These values do not reflect the true physical size of the apertures but rather the size as projected on the camera faceplate.

Dimension	LWP	SWP
Major Axis Trail Length (arcsec)	21.84 ± 0.39	21.48 ± 0.39
Large-Aperture Length (arcsec)	22.51 ± 0.40	21.65 ± 0.39
Minor Axis Trail Length (arcsec)	10.21 ± 0.18	9.24 ± 0.11
Large-Aperture Width (arcsec)	9.91 ± 0.17	9.07 ± 0.11
Large-Aperture Area (arcsec ²)	203.26 ± 9.28	209.74 ± 6.23
Small-Aperture Area (arcsec ²)	6.32 ± 0.86	6.58 ± 0.86

After passing through the selected aperture, the diverging beam is directed to a collimator mirror. The collimate beam then falls upon an echelle grating which produces a spectrum dispersed in one dimension. This dispersed beam is redispersed and focused by a spherical grating providing a two dimensional spectrum display on the camera faceplate. The low dispersion mode is selected by placing a plane mirror in the optical path in front of the echelle, so that the collimate beam is dispersed only by the spherical cross-disperser. The result is a conventional single-dimension spectral display. This low dispersion image is approximately 60 times as bright as the equivalent high dispersion image, but the spectral resolution is degraded correspondingly to 6Å.

Only one camera (prime or redundant) in the active spectrograph (long wavelength or short wavelength) may be used to observe the target at any one time. The prime or redundant camera is selected by the appropriate camera select mechanism. So, redundant cameras are reached by the interposition of a small plane mirror set at 45° to the optical path.

Spectrograph camera system

The function of the spectrograph camera system is to convert the spectral display from the spectrograph into a suitable video signal. The system uses a Westinghouse WX 32224 SEC television camera tube. The photocathode of this tube, designed for visible light response, requires the use of a wavelength converter to transform the ultraviolet spectral display into visible radiation. The combination of the converter and the WX 32224 SEC vidicon provides a UV wavelength sensitive system in the range of 1150Å to 3300Å. The figure 5-73 shows a diagram of a spectrograph camera.

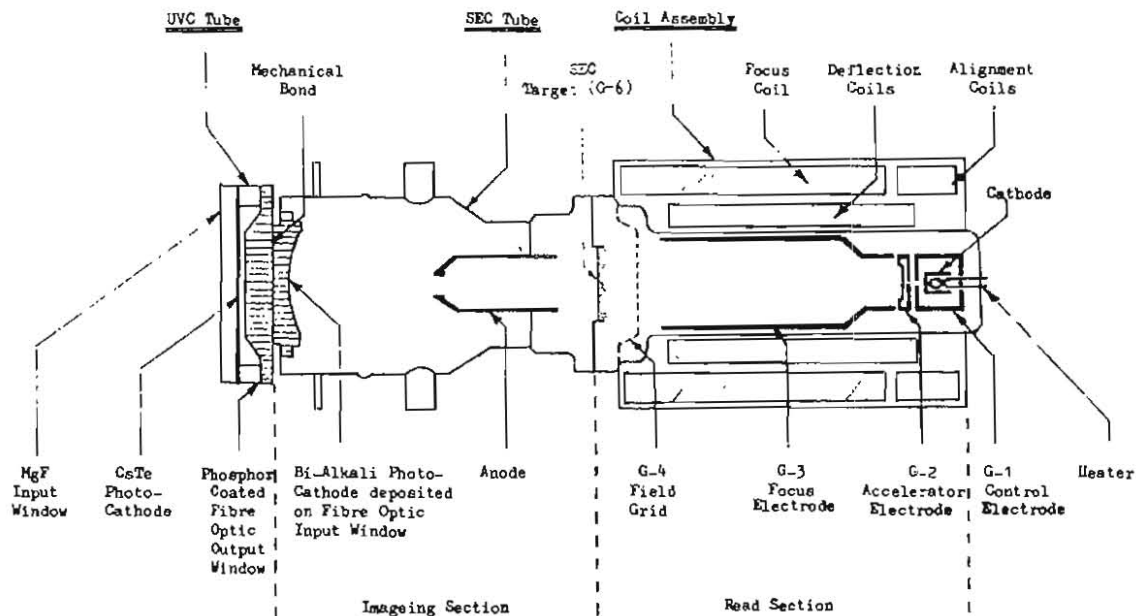


Figure 5-73. SEC/UVC Tube Pair and Coil Assembly.

The converter selected for use in the spectrograph camera is an ITT (type F4122) 40 millimeter proximity-focused UV converter. This tube uses a magnesium fluoride input window with a CsTe photocathode and a fiber optic output window that can be coupled to the secondary electron conduction (SEC) tube. The photocathode converts the incident ultraviolet spectrum into a corresponding photoelectron image. These photoelectrons are accelerated by a high electric field (5 kilovolts across a 1.3 millimeter gap) and proximity-focused onto the output phosphor screen where much of their energy is dissipated in the production of photons of blue light. The yield at the phosphor is typically 60 photons out per photoelectron; with a photocathode efficiency of approximately 15%, the overall gain of the UV is approximately 10 blue photons out per ultraviolet photon in. The efficiency of the screen is maximized by a surface layer of aluminum which reflects backward emitted photons in the direction of the output window and eliminates halation effects because of ultraviolet photons transmitted by the photocathode and reflected back to it.

The converted image from the UVC is transferred by way of a fiber optic coupling to the blue-sensitive bialkali photocathode of the SEC television camera tube. Included in this fiber optic

coupling is a set of fiducial marks, a square array of 13 by 13 opaque areas each 100 micrometers square and $(2.0 + 0.005)$ millimeters apart which provides a geometrical reference for the evaluation of the spectra. The photoelectrons generated at the SEC tube photocathode is accelerated through the electrostatically-focused image section onto the target. The target consists of a low-density porous layer of potassium chloride (approximately 10 micrometers thick) supported by an aluminum oxide membrane (approximately 50 nanometers thick) and backed by a thin aluminum signal plate. Some fraction of the energy of each photoelectron is expended in the production of several secondary electrons in the potassium chloride. This energy is swept towards the signal plate by a 12 volt bias across the target leaving a multiplied positive charge image on the target. The secondary electron gain (positive charges on target per incident photoelectron) is a function of the incident electron energy. The gain should be different (around 50, 15 and 5) in function of the voltage setting (6.1 kilovolts, 4 kilovolts and 3.2 kilovolts respectively). Operationally, the maximum voltage was almost always used. The SEC target can integrate and store the image for many hours.

During the readout mode, an electronic beam effectively scans the SEC target in a rectangular pattern of digital steps. The scan parameter counters are decremented in response to a signal generated by the spacecraft data system, so that the read scan is synchronized with the output of telemetry. The beam is deflected digitally to scan a raster maximum of 768 by 768 picture elements (pixels) in 37 micro steps across the image. At each pixel, the read beam is pulsed on by the GI modulator for 6 microseconds, after allowing time for the deflection amplifiers to settle. The beam recharges the target, giving rise to an output video pulse corresponding to the positive charge on the target at that pixel. The analog video signal is transferred to the DMU.

The LWR and SWP were the normal operational cameras until September 14, 1983. On this date the LWP camera was used as prime until the end of the IUE mission.

Fine Error Sensor

The FES is an image dissector sensor capable of multimode operation accomplishing the dual role of a field camera, target recognition and acquisition, and fine error sensing for pointing error generation. A more detailed description of the FES is contained in section 4.5.7.

Additionally, the FES functions as a photometer (for providing information on objects brightness). In 1990, it was approved that a data archive should be created consisting of the FES guide star tracking data taken during long exposures. In early November, 1992, the FES streak light anomaly appeared and the photometer archive was found not to be useful any more.

Lamps

- ▶ **Flood Lamps.** The camera faceplate may be illuminated by arrays of incandescent (tungsten filament) or ultraviolet (mercury discharge) flood lamps. The tungsten flood lamps are used in the camera target preparation sequences, and the UV flood lamps are used for calibration purposes.
- ▶ **Wavelength Calibration Lamps.** The SI contains a single hollow cathode platinum wavelength calibration lamp which produces a large number of resonance lines over the

entire IUE spectral range and is used to generate reference echellograms for both spectrographs. Radiation from this lamp is directed into both spectrographs simultaneously by means of a plane mirror positioned on the back side of the sunshutter which must be closed for the operation.

- ▶ **Fiducial and Black-hole Lamps.** Embedded in the aperture plate are small lamps that provide fiducial references for the FES and back-hole lamps that are positioned behind the various aperture openings to illuminate these openings for additional references for the FES.

Heaters

In order to maintain a proper thermal environment, three redundant sets of heaters are used. Two of the sets are attached to the back sides of the primary and secondary mirrors. The third heater set is attached to the camera deck. Thermal control is provided by powering either the prime or backup heater of each heater set by ground command.

Electronics

The scientific instrument electronics are required for the following: camera operation, mechanisms control, fine error sensor, power conversion and fiducial and calibration lamp control. The electronics necessary for these tasks are housed within the EEA, the FES electronics box, the CEB and the CSIU. Each camera subsystem consists of a camera head module (CHM) located inside the spectrographs of the optical unit, an associated CEM located in the CEB, and an associated camera supply interface module (CSIM) located in the CSIU.

Flux Particular Monitor

The Flux Particular Monitor (FPM) senses the environment radiation level the spacecraft is experiencing. The IUE satellite passes through the outer Van Allen radiation belts each day. The trapped particle radiation causes increased fogging on the cameras during the time period of this passage. This radiation background often limits the length of the exposures that can be obtained during this passage.

The radiation levels are recorded as a voltage on the FPM and converted to an equivalent exposure on the camera in DN (digitized video data from the video chain) per hour. The approximate relation for the most sensitive portion of the cameras is: $n \text{ DN/hr} = 10^{\text{FPM}}$. Typically, the daily variations of the radiation level produced FPM readings between 0 and 3 volts.

Since May 14, 1991 the voltage readings from the FPM became increasingly erratic and did not represent the true radiation environment. Therefore, it was concluded that the FPM was no longer a useful device. On October 4, 1991, the SMSS and FPM were turned off. The SMSS was turned off for two reasons. First, the FPM was a last minute add on to the spacecraft and was tied into the SMSS. Second, the SMSS was only useful during launch.

5.7.1. Camera Operating Sequences

Camera operations sequences are controlled by commands issued by the ground-station computer in response to keyboard procedure calls. They are conducted in three operational phases: SEC target preparation, camera exposure and image readout.

- **Expose mode.**

An image may be integrated on the SEC target in this mode where UVC and SEC image section high voltages are on (the readout section of the SEC tube is off).

The exposure time, SEC image section gain (the maximum gain was the normal one), spectrograph mode (short/long wavelength, entrance aperture, dispersion) and light source (stellar spectrum or onboard source such as wavelength calibration lamp or UV flood lamp) may be selected by the astronomer according to the needs of the observation. The minimum exposure time is 0.4096 seconds.

- **Read mode.**

The stored charge image is read out from the SEC target to the ground using a pulsed digitally stepped electron beam. The readout section of the SEC tube is active whilst the image section and the UVC are off. This type of readout is destructive.

The telemetered video data is sent to the ground in 5.24 minutes with a telemetry bit rate of 20 kilobit/s.

The astronomer may select HI or LO head-amplifier gain (LO was normally used). In certain exceptional circumstances, the scan format, other than 768 x 768 pixels, may be permitted. Sometimes, these partial read-outs were done to only read the spectra area to save time.

In 1989, non-standard partial reads were useful to check how the high solar radiation was affecting the spectra. A small area of the image being exposed was read to check the background. Of course, the image area had to be selected such that the scientific data were not affected. As the effect of these reads on the images was unknown, this procedure was taken off-line.

- **Prepare sequence**

A prepare operation is carried out before each expose in order to erase all trace of previous images, and to provide a reproducible low-noise pedestal or baseline on which the new image will be superimposed. Several prepare sequences are available; essentially, they all consist of pre-programmed sequences of exposures to the tungsten floodlamps followed by read scans. The options are:

1. Normal Standard Prepare ("SPREP"). Suitable for the majority of observations. It takes around 19 minutes for the LWP camera and around 15 minutes for the other cameras (the tungsten floodlamp exposures must be longer in the LWP) with a telemetry bit rate of 20 kilobit/s.

2. Fast Prepare ("FPREP"). A fast preparation sequence (around 3 minutes) designed for use when speed of operation is important and some degradation in image quality can be tolerated.
3. High-level Extra Prepare ("XPREP"). Designed to be used following severely over-exposed images. It takes around 15 minutes for the LWP camera and around 4 minutes for the other cameras. This mode must be followed by an SPREP or an FPREP.

5.7.2. LWP Scan Control Logic anomaly

The LWP camera occasionally experienced problems in performing read scan; the scan was commanded but it did not start at all or did not start at the proper position. This anomaly was named the Scan Control Logic (SCL) anomaly and was first noted during the Commissioning Phase of IUE in February/March 1978. This problem was the initiator for selecting the LWR camera as the prime one in the long wavelength spectrograph.

A ground software fix was written to deal with the bad scans, so the chance of losing an image to a scan failure was very small. Indeed, once the LWP camera was used as prime, the frequency of these bad scans dropped dramatically. Apparently, the camera functions best when used often.

5.7.3. LWP flux anomaly

A small number of LWP images had lower-than-expected flux levels due to unknown causes. This was detected from spectra of photometrically stable targets during monitoring campaigns, in which an occasional spectrum would have low fluxes compared to other spectra of the same target with similar setup and observing conditions. The LWP flux anomaly was first noted on July 24, 1991.

There were no indications of unusual pointing errors or engineering telemetry changes to account for the flux drop-off, which was about 25% below the expected flux. While the number of affected images is unknown, the number of identified images is believed to be small (on the order of a dozen).

5.7.4. LWR anomaly

The LWR images were affected by a bright extended spot at the lower edge of the SEC target that was visible in long exposures. It appeared the first time between March 30 and April 14, 1983. The intensity of the spot was a linear function of the exposure time. The maximum intensity of the spot (and consequently its extension) linearly increased with time at a rate of $2.17E-3$ DN/minute per day.

It was suggested that the spot was due to a flare in the UV converter. So, the LWR was used with reduced UVC voltage. The LWP camera was used as prime.

5.7.5. Microphonics

A significant proportion of the spectral images obtained by IUE were affected by periodic noise artifacts (often called “microphonics”). This noise was different for each camera.

- ▶ In the LWP camera, the noise was introduced by the roll wheel speed change during maneuvers. However, only the portion of the image which was read down at the time the roll slew was in progress was affected.
- ▶ In the LWR camera, this problem was very obvious but was confined to a relatively small band in the image, the interference had all the characteristics of a damped electronic oscillator and pointed to an instability in the camera head preamplifier as a possible source of the problem.
- ▶ In the SWP, the noise was introduced by the roll wheel speed change during maneuvers and by the roll wheel spinning below ± 100 rpm or above ± 400 rpm. In SWP most, if not all, of the image was affected but normally with a lower amplitude than the LWR.

5.7.6. SWP pings

The SWP pings were characterized by an enhanced noise level of 2-3 DN above normal over a few tens of lines. These had the appearance of an exponentially decaying sinusoid in the raw image and were similar to LWR anomalies, but of much lower amplitude.

They were related to low SWP camera head temperatures (THDA), appearing occasionally when the THDA reached 7.8°C , and becoming common for THDA's of 7.5°C and cooler.

5.7.7. SWR failure

The first malfunction of the SWR camera was detected during the initial inflight check-out phase in the period between February 15 and 18, 1978, when all of the sudden the GRID-1 voltage supply went from the nominal value -130 volts $\pm 2\%$ to 0 volts.

During the continuation of the camera reoptimization on August 23, 1978, the GRID-1 voltage failed again during camera switch on. On this date, several attempts were made to turn on the camera and most of them were unsuccessful. The camera was declared to be not operational.

6. Spacecraft Thermal Design

The purpose of the thermal control design is to maintain all of the elements of the spacecraft system within their temperature limits for all mission phases. From this viewpoint, the IUE spacecraft may be conveniently divided into five separate and distinguishable sections, which are delimited referring to figure 6-1: the HAPS bay from station 0 to station 45.5, the main equipment bay from station 45.5 to station 87.5, the spectrograph which is mounted in its canister within the main equipment bay, the telescope from station 87.5 to station 164.5, and the solar array. The station numbers refer to the position in inches from the separation plane from the Delta launch vehicle.

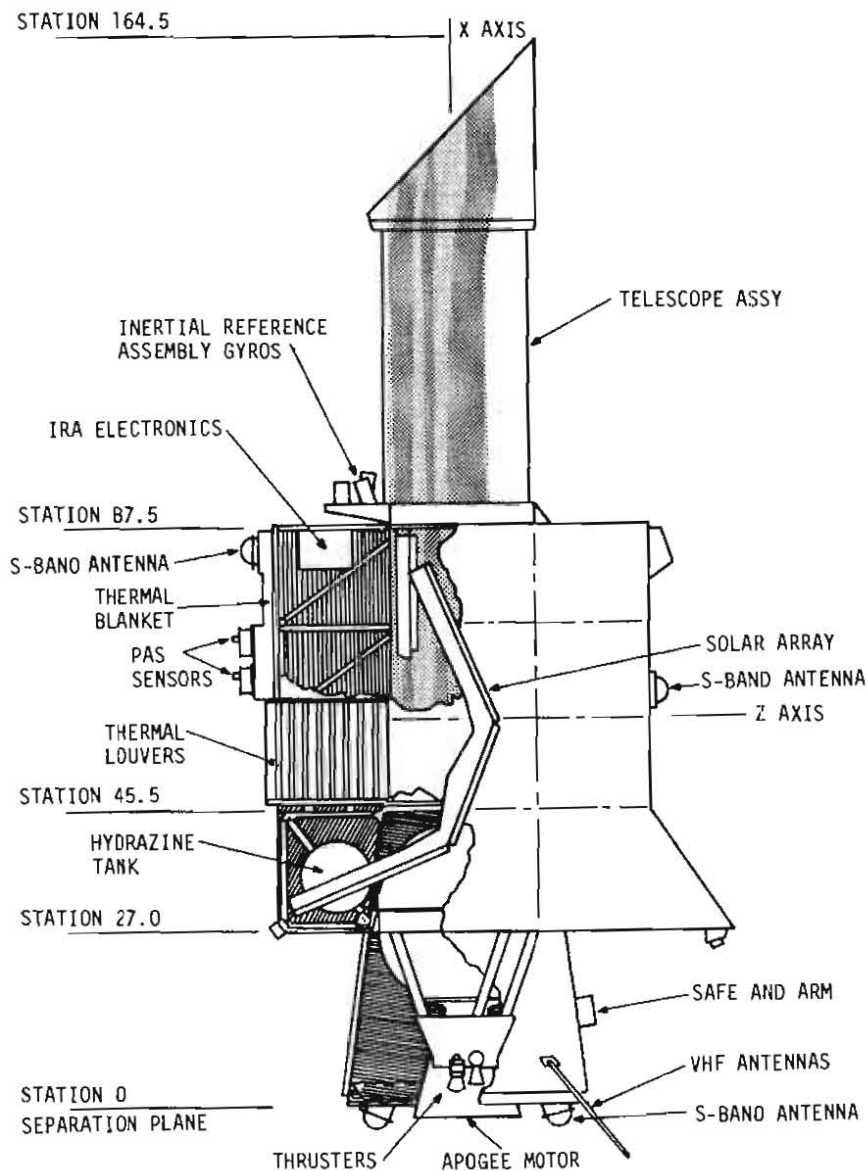


Figure 6-1. IUE Interior and Exterior Features.

The HAPS bay

The HAPS bay consists of the apogee boost motor, the HAPS and the surrounding spacecraft structure.

The only thermal requirement on the ABM was to maintain its temperature between -15°C and $+38^{\circ}\text{C}$ prior to ABM ignition. The HAPS was kept between $+5^{\circ}\text{C}$ and $+65^{\circ}\text{C}$ at the beginning of the mission. Due to the HAPS heater group 1 failure (section 5.5.9.1), the temperature upper limit was raised to $+85^{\circ}\text{C}$ (except +ZLN and -ZLN which had an upper limit of $+90^{\circ}\text{C}$).

Since the hydrazine system could withstand rather wide temperature limits, it was decided to make use of solar energy to reduce the dependence on heaters. The canted side ("sun catcher") of the HAPS bay is a single layer of kapton with a VDA-SiO-SiO_x coating having an absorptance (α) of 0.25 and an emittance (ϵ) of 0.23. This surface provides a solar input of approximately 20 watts at a 135° beta angle solar aspect and aids in maintaining a more uniform energy balance over all solar aspects. The sides of the HAPS bay are covered with multilayer insulation with an external surface of Vapor Deposited Aluminum (VDA). The remainder of the propulsion area is covered with multilayer insulation with a black exterior layer. The propulsion area is radiatively isolated from the main equipment platform by a multilayer blanket.

The apogee motor is covered with multilayer insulation to prevent heat leaks to the main equipment bay during firing and to prevent heat leaks to space during orbital flight. In addition, a heat shield covers the nozzle exit plane during the transitional phase of the flight to keep the ABM warm before firing.

The main equipment bay

The main equipment bay was intended to be maintained between 0°C and $+40^{\circ}\text{C}$. The batteries were an exception as were the gyros in the IRA. The batteries were not to exceed $+25^{\circ}\text{C}$ (see section 5.1.1.) while the gyros contain their own thermal controller to maintain the temperature in the IRA.

The main equipment bay which surrounds the spectrograph is covered with multilayer insulation to reduce the effect of solar input. The spectrograph is further decoupled from the main equipment bay by utilizing low emittance surfaces. As a further reduction of the solar effect, the outer layer of the insulation is silverized teflon.

To achieve the required temperatures at a minimum power dissipation of about 130 watts, approximately 0.55 m^2 of radiating area is required. Since this power dissipation is not constant and the spacecraft must operate over a wide range of solar aspects, this radiating area is provided by thermal louvers. Three sets of louvers consisting of nine blades each are located on the anti-sun side of the spacecraft. Each louver blade is individually controlled by its own bimetallic spring within the honeycomb of the main equipment platform. The louvers provide approximately 0.6 m^2 of radiating area in the fully open position and are calibrated to move from fully closed at 0°C to fully open at $+10^{\circ}\text{C}$. To further reduce thermal gradients, two circular heat pipes are mounted to the underside of the main equipment platform. These pipes are ammonia-filled grooved heat pipes, which are capable of transporting 75 watt-metres. It was calculated that the

heat pipes reduce the gradients on the platform to less than 5°C.

The spectrograph

The objectives of the spectrograph thermal design were to maintain the environment between 0°C and 15°C and the secondary mirror/focus drive mechanism below 30°C and above -20°C with minimum heater power.

The spectrograph is enclosed by a single dust cover. All surfaces (except for optical components) internal to the dust cover are either painted black with Chemglaze Z306 or anodized. These surface finishes minimize temperature gradients by enhancing radiative exchange. The dust cover is made of aluminum and is conductively coupled to the strong ring. Heat dissipated in the spectrograph is radiatively transferred to the primary mirror, the strong ring, and the dust cover. The primary mirror was maintained above a temperature of -15°C at all times using heaters attached to the back surface of the mirror (see section 5.7.). The strong ring is covered with a 20 layer insulation blanket with the external layer 5 mil FEP Teflon/Ag. Some heat transfer takes place between the strong ring and the spacecraft and IRA package, but the principal path for heat dissipation is through conduction to the telescope tube.

The telescope

The objective of the telescope thermal design was to minimize the peripheral and longitudinal temperature gradients in the main structure of the telescope.

The telescope and sunshade have a 20 layer blanket of insulation on the external surface maintaining the circumferential temperature gradients of the telescope within a few degrees Celsius and minimizing temperature variation with sun angle. Again, the external layer of the blanket is 5 mil FEP Teflon/Silver.

The primary mirror is conductively isolated from the telescope's structure to minimize axial and circumferential gradients, and is held above -15°C by turning on one of the two heaters (one heater provides 3 W of power and the other provides about 4.5 W) attached to the back surface. Heaters using about 1.5 W of power each are attached to the back of the secondary mirror to keep it and the focus drive mechanism above -20°C. The focus drive mechanism is covered with a 20 layer insulation blanket and dissipates about 1.0 W continuously to help maintain the temperature above its lower limit. Low conductivity material is utilized between the sunshade and the secondary support ring to limit the conductive interaction with the cold sunshade.

The solar array

A thermal analysis of the IUE solar arrays showed that the array had to be deployed within five minutes of completion of the despin maneuver. When the satellite is spinning and the arrays are in the stowed configuration with a beta angle of 90°, the highest cell junction temperature is 20.5°C. Under the same circumstances as above but with the satellite not spinning and one paddle directly facing the sun, the hot paddle would reach temperatures as high as 93°C in spots. The cold paddle could see temperatures as low as -183°C. This condition could be serious for two reasons. First, the power from the array would be small because the hot paddle's cells would have

a greatly reduced voltage output. Secondly, the cold paddle's deployment mechanism may not function at such cold temperatures. Thus, it was necessary to deploy the array immediately after the despin.

The solar array experienced very large temperature gradients, from -180°C to $+80^{\circ}\text{C}$. The solar array temperature sensors failed soon after launch, so the only available data is from the first three years in orbit (see section 5.1.1.).

Thermal factors

Fluctuations in the spacecraft temperatures result from a number of factors. The thermal effects caused by these factors have a range in duration from hours or days to long term of months or years.

Short Term Factors

- ▶ **The spacecraft's beta angle**

During typical operations, the beta angle varied a large amount (up to 60° in the last IUE year, the operational beta range was decreasing during the IUE life, see section 5.1.1.) within an hour or it could remain constant for up to 24 hours or more. The significance of the beta angle on the warming or cooling of individual pieces of equipment depended on the location, the thermal insulation, and the thermal isolation of each item.

- ▶ **Onboard heater configurations**

There are several heaters onboard IUE that were used to maintain a specific thermal environment for the scientific instruments. Since the DKSP and DKLP thermistors are part of the scientific instrument, they are greatly influenced by the setting of these heaters. With the selective use of the scientific instrument heaters, the thermal environment about these thermistors was controlled so that the heating and cooling effects due to other factors were minimized.

Another heater routinely controlled by ground command was HAPS heater group 2. The status of this heater affected the temperatures of EV#2 and EV#7. During the winter months, this heater was cycled more often than in the summer months; however, it normally remained on unless a low beta angle (less than approximately 50°) was maintained for an extended time.

- ▶ **Lunar and daily earth shadows**

During shadow seasons, the spacecraft's view of the sun was eclipsed by the earth on a daily basis. This resulted in the solar radiation that normally impinges on the spacecraft being completely blocked from the spacecraft. The thermal effect of a shadow season were observed on a daily basis as well as a monthly basis. On a daily basis, the temperature of the spacecraft as a whole was reduced during the eclipse period. Following the eclipse period the spacecraft began to warm and re-establish its pre-shadow thermal balance. This sequence of cooling and warming occurred each day of the shadow season.

During the daily earth shadow periods, all scientific heaters and HAPS heater group 2

were commanded off to save power. Therefore, the thermal stability provided by these heaters was not in effect during the eclipse periods. This might have the effect of lowering the daily average temperatures for these points through the shadow season.

Lunar shadows occurred several times throughout any given year. However, significant lunar shadows only occurred approximately twice a year. During a lunar shadow the solar radiation was partially blocked from the spacecraft; therefore, the cooling effect on the spacecraft was not as drastic as an earth shadow.

Intermediate Term Factors

▶ **Earth Shadows**

Earth shadows not only resulted in a daily cycle of cooling the spacecraft, as mentioned above, but also affected certain spacecraft temperatures for an extended period following the shadow season. This extended period might last from a few days to more than a week. During earth shadow seasons, the overall temperature of the spacecraft was reduced. Those onboard components really influenced by the beta angle or heaters recovered fairly quickly after each daily eclipse period as well as at the completion of the shadow season. However, those components that were isolated from their surroundings by a high thermal resistance required a longer time to re-establish their pre shadow thermal balance.

▶ **Mean distance to the sun**

The solar radiation flux varies with the distance from the sun as $1/r^2$. Therefore, during the summer months when the earth is farthest from the sun, temperatures on the spacecraft generally run slightly lower than during the winter months. This factor was most noticeable in those components that were greatly influenced by the beta angle.

Long Term Factors

▶ **Decreased equipment power dissipation**

When IUE was launched, its nominal power requirement was listed as 186 watts. At the end of the mission, its nominal power was approximately 148 watts. This reduction in the power requirements resulted from the failure of various instruments onboard the spacecraft. This decrease in equipment power dissipation mainly affected those components internal to or on the back side of the spacecraft that received heat from the failed components.

▶ **Red line temperature limits**

Specific maximum and/or minimum temperatures were set for a large portion of the instruments onboard IUE (Red Line Limits). The temperature of these instruments was either influenced by the beta angle or a heater or both. Components that had an associated Red Line Limit for their temperature might show a false maximum or minimum temperature equal to the Red Line Limit value, since ground intervention to change the beta angle or heater configuration occurred when this limit was reached.

The thermal balance of the spacecraft was also effected by occasional changes to the Red Line Limits. Such changes were made to reduce the effect of an imposed temperature

limit on normal operations when other constraining factors were involved or to excessive cycling of a heater when deemed necessary. Such changes to a Red Line Limit were not made in haste but were only permitted after close examination and a trial period was passed. Such changes to a Red Line Limit, when it was a maximum limit, might cause the historical data to give a false indication of an increase in the temperature; when in fact the temperature would have reached this new maximum value in previous years if it had been permitted to do so. A similar effect would apply if a minimum temperature Red Line Limit were decreased.

► **Deterioration of thermal controls**

The IUE thermal control system included several temperature control techniques: reflective covers, coatings, insulation, heat sinks and thermal louvers. Deterioration of the covers, coatings and insulation was expected and was cumulative with time. The extent of deterioration for various components of the thermal control system, as well as different portions of the same component might vary. This general deterioration of the thermal control system might be observed in the long term increase or decrease of specific temperatures, depending on the intended purpose of the thermal control.

Average temperatures on the spacecraft

The figures present the history of average temperatures for several component and general areas.

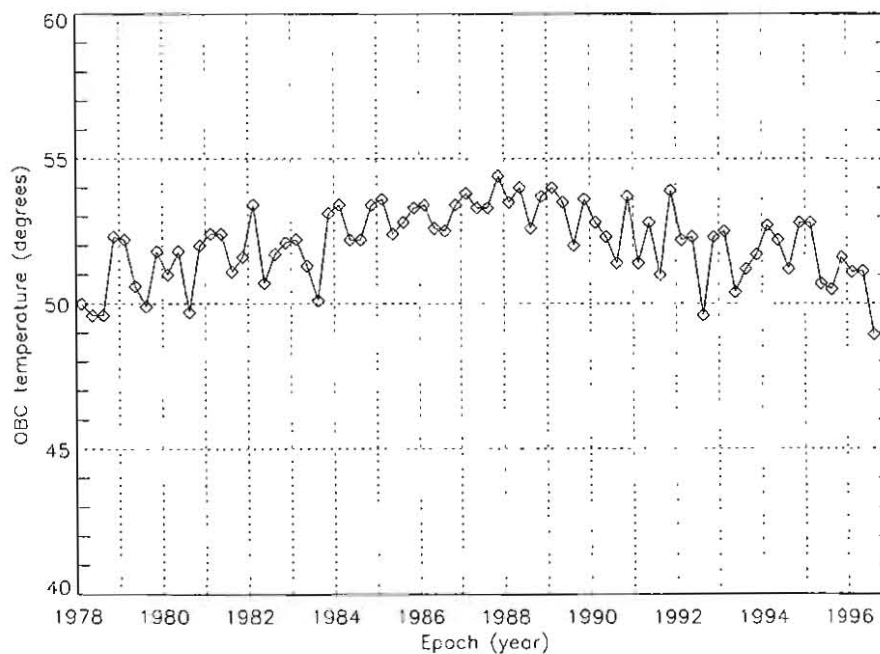


Figure 6-2. History of average Onboard Processor 1 temperatures.

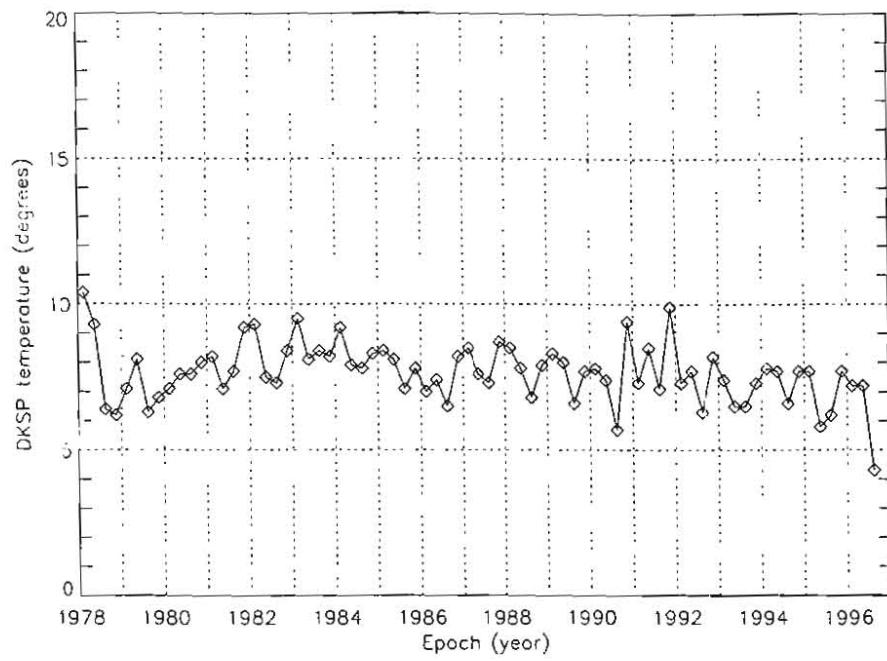


Figure 6-3. History of average camera deck temperatures near SWP.

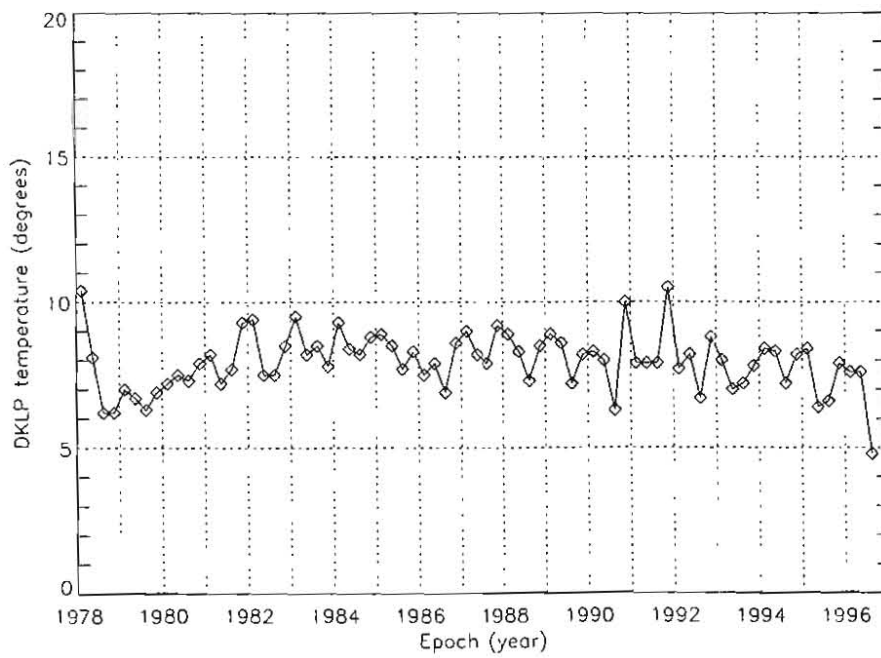


Figure 6-4. History of average camera deck temperatures near LWP.

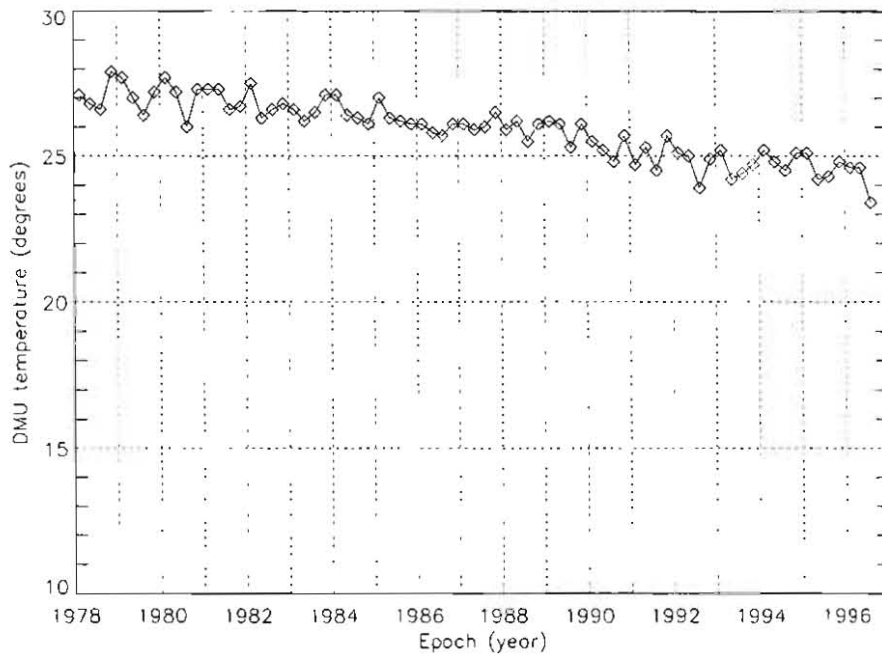


Figure 6-5. History of average Data Multiplexer 1 temperatures.

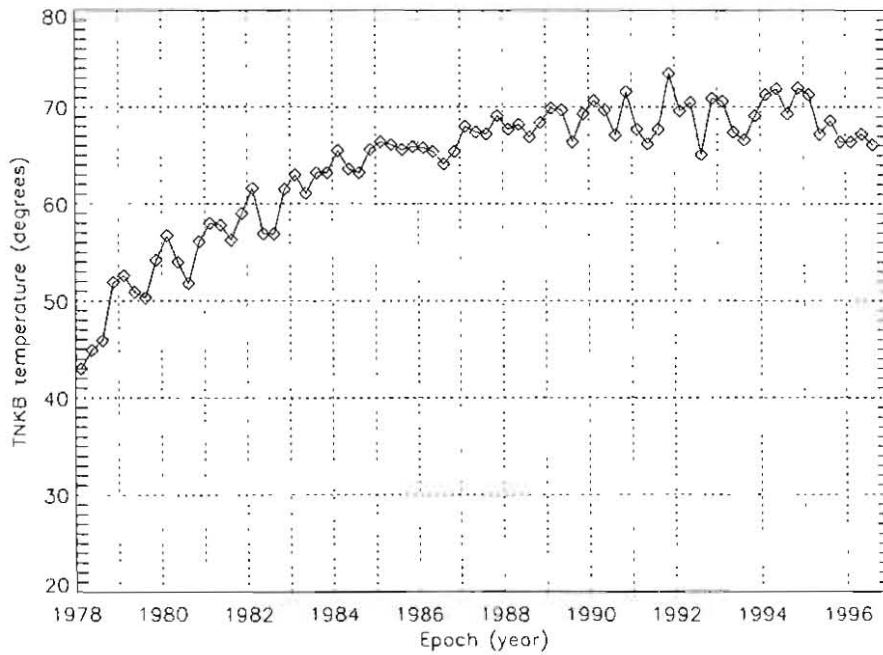


Figure 6-6. History of average Hydrazine Tank B temperatures.

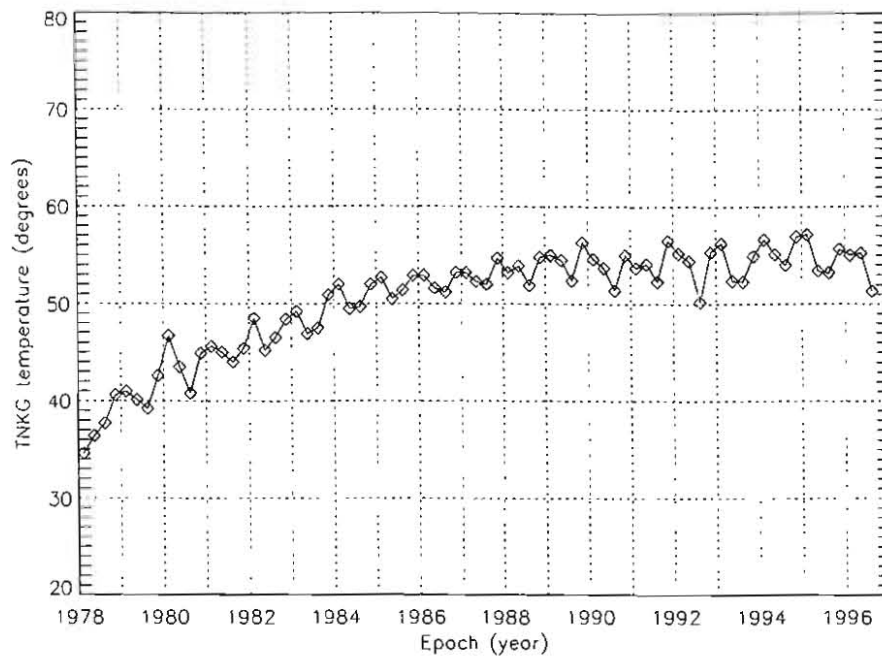


Figure 6-7. History of average Hydrazine Tank G temperatures.

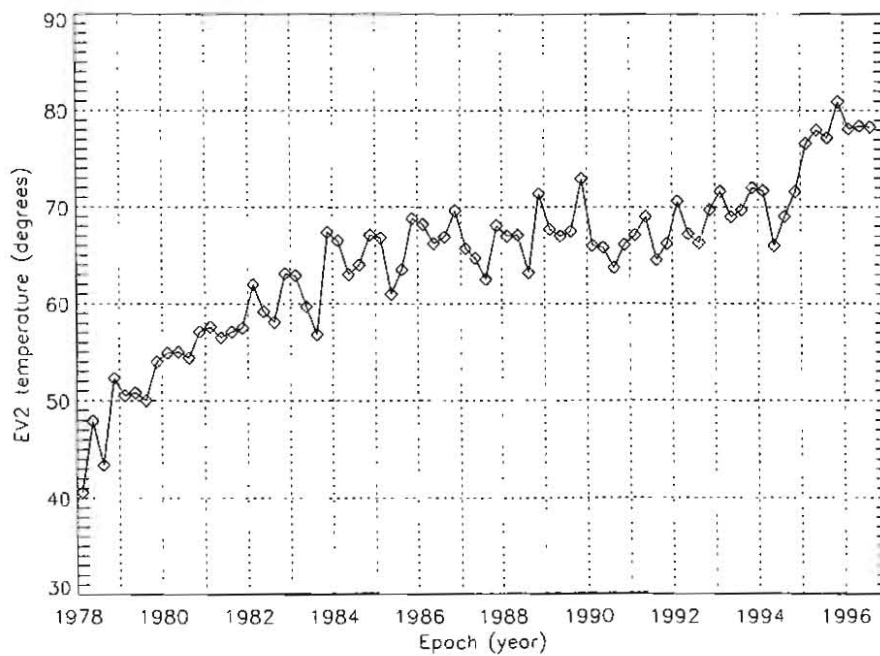


Figure 6-8. History of average Engine Valve 2 temperatures.

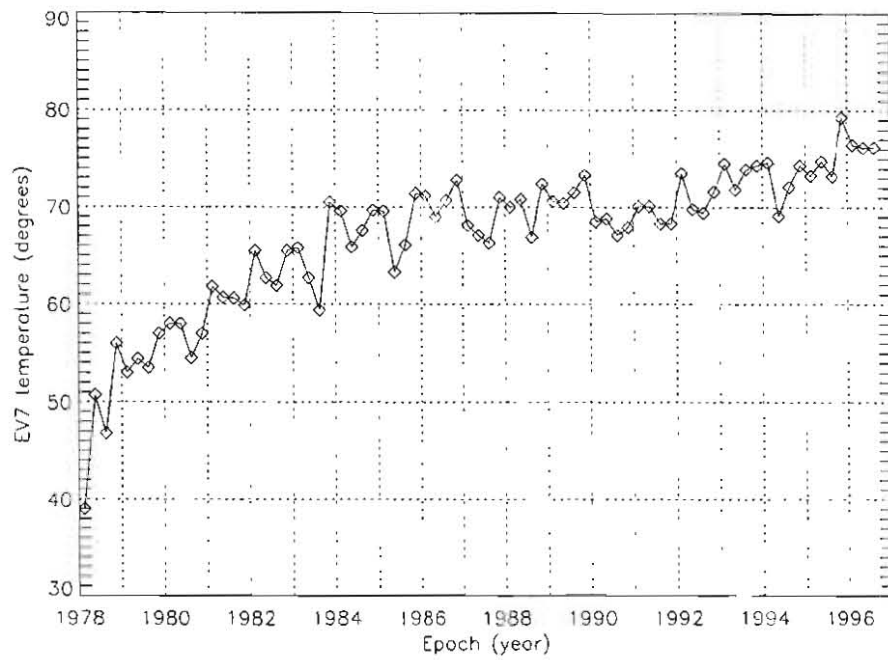


Figure 6-9. History of average Engine Valve 7 temperatures.

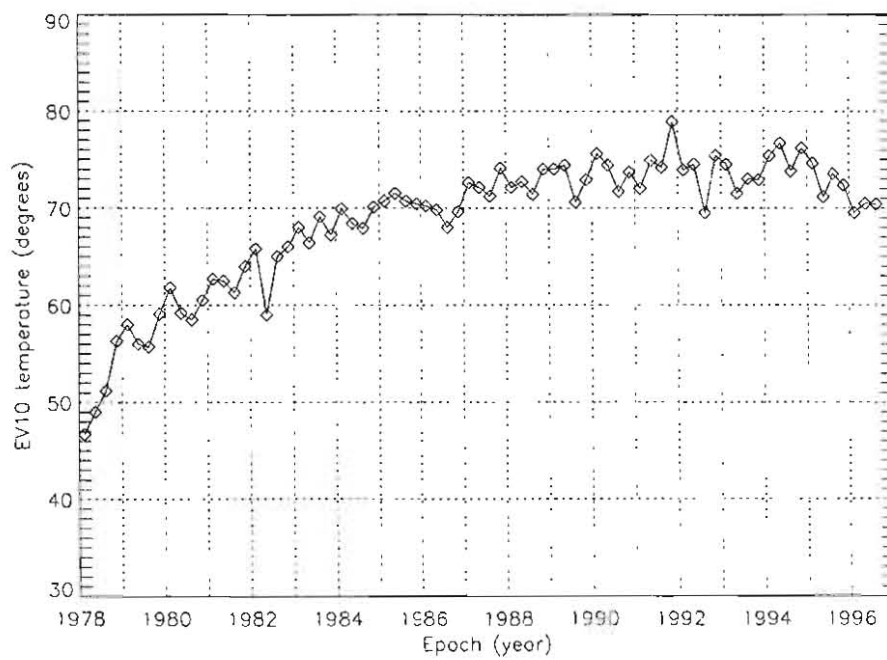


Figure 6-10. History of average Engine Valve 10 temperatures.

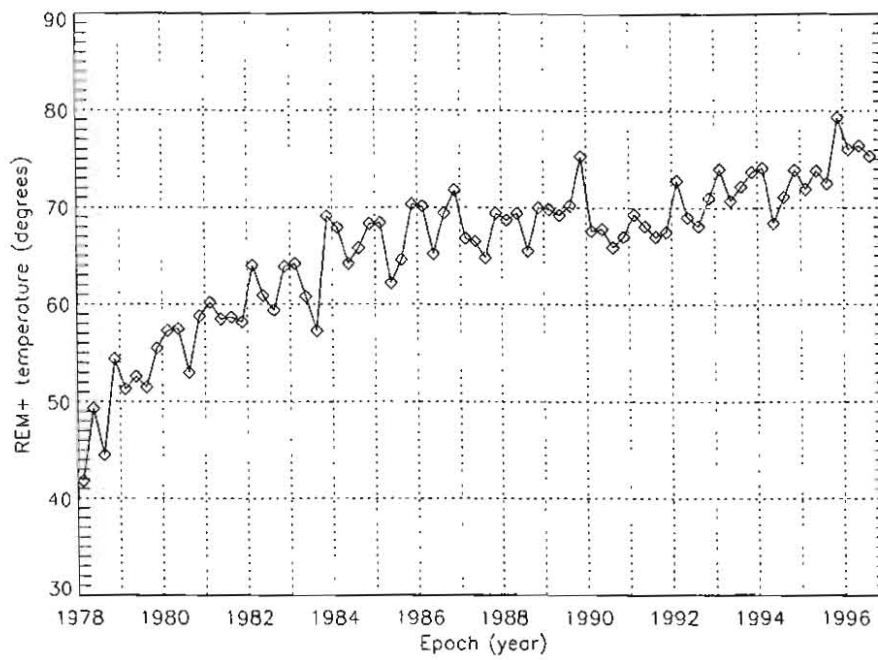


Figure 6-11. History of average remote engine module temperatures.

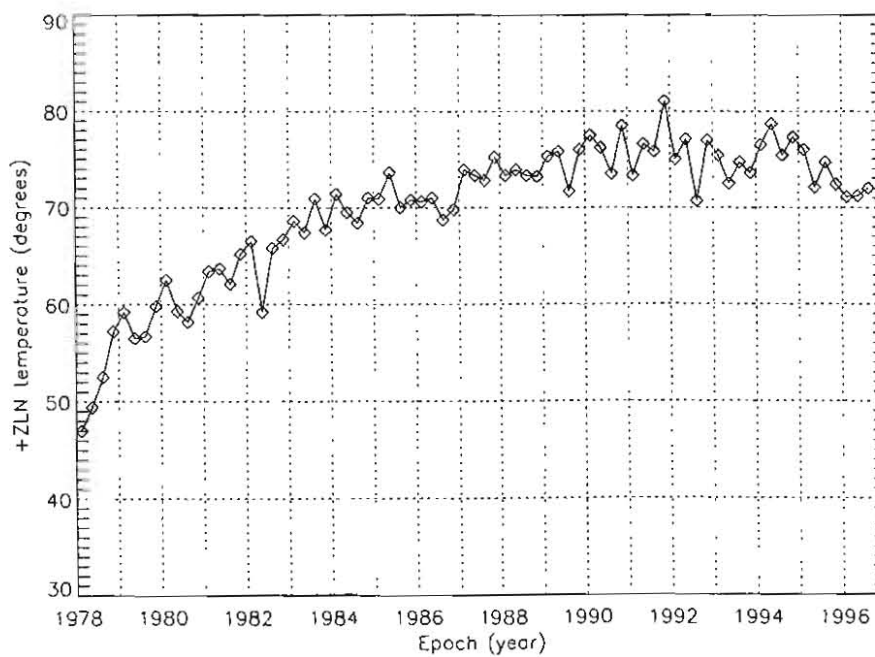


Figure 6-12. History of average +Z line temperatures.

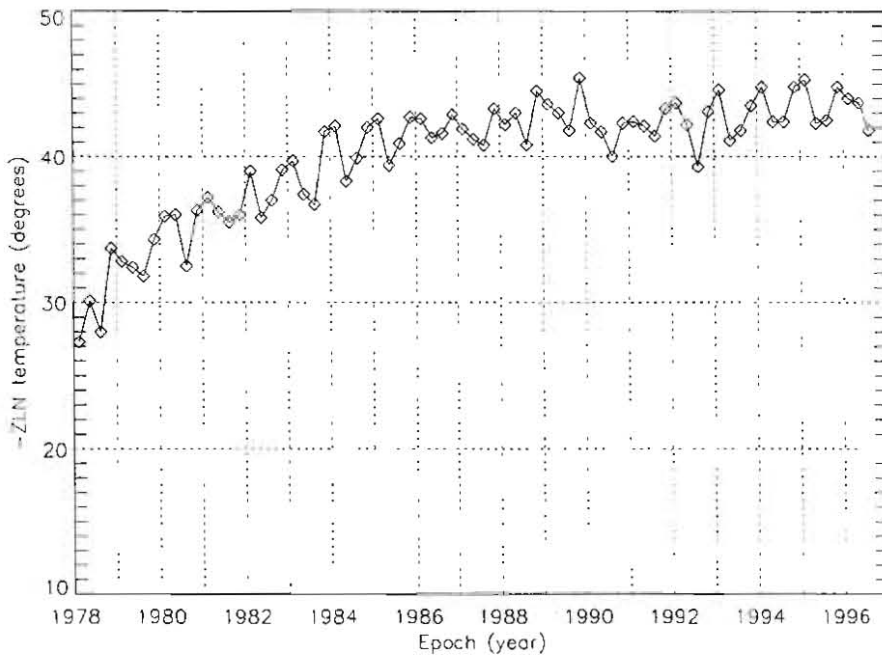


Figure 6-13. History of average -Z line temperatures.

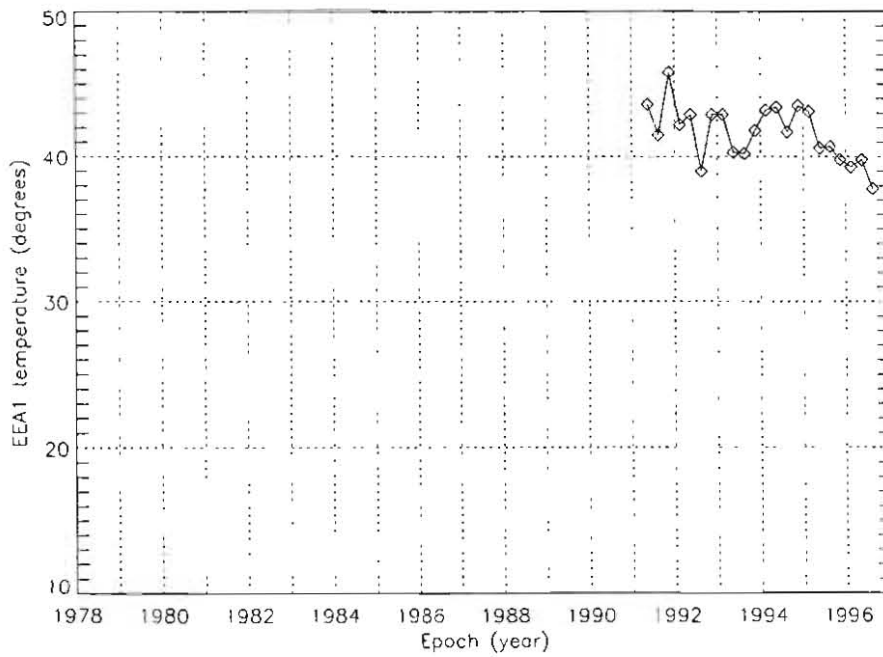


Figure 6-14. History of average EEA1 temperatures.

Appendix A. Earth shadow seasons

Shad. season	Starting date	Deepest day					Ending date
		Date	Duration (minutes)	Starting Time (UT)	DOD#1 (%)	#2 (%)	
1	May 25, 1978	April 5, 1978	69	02:01	71	72	April 18, 1978
2	Sept. 26, 1978	Oct. 7, 1978	71	05:41	77	80	Oct. 18, 1978
3	March 20, 1979	April 2, 1979	68	02:25	68	68	April 13, 1979
4	Sept. 21, 1979	Oct. 2, 1979	72	05:37	69	75	Oct. 14, 1979
5	March 15, 1980	March 27, 1980	67	02:05	54	58	April 8, 1980
6	Sept. 18, 1980	Sept. 26, 1980	72	05:05	60	64	Oct. 8, 1980
7	March 10, 1981	March 23, 1981	66	02:00	57	60	April 4, 1981
8	Sept. 12, 1981	Sept. 23, 1981	74	05:32	67	69	Oct. 4, 1981
9	March 6, 1982	March 19, 1982	66	02:01	61	61	March 30, 1982
10	Sept. 7, 1982	Sept. 17, 1982	71	05:17	61	61	Sept. 29, 1982
11	March 1, 1983	March 14, 1983	62	02:07	56	55	March 26, 1983
12	Sept. 3, 1983	Sept. 14, 1983	77	04:46	64	62	Sept. 25, 1983
13	Feb. 25, 1984	March 10, 1984	65	02:24	52	51	March 21, 1984
14	Aug. 28, 1984	Sept. 10, 1984	73	04:34	63	61	Sept. 21, 1984
15	Feb. 20, 1985	March 5, 1985	64	02:03	52	51	March 17, 1985
16	Aug. 25, 1985	Sept. 6, 1985	76	04:48	62	59	Sept. 15, 1985
17	Feb. 16, 1986	Feb. 28, 1986	64	02:21	53	52	March 13, 1986
18	Aug. 20, 1986	Aug. 30, 1986	79	04:32	62	60	Sept. 11, 1986
19	Feb. 11, 1987	Feb. 24, 1987	64	02:13	50	49	March 9, 1987
20	Aug. 16, 1987	Aug. 28, 1987	80	04:31	51	49	Sept. 6, 1987
21	Feb. 7, 1988	Feb. 20, 1988	64	02:39	50	49	March 4, 1988
22	Aug. 11, 1988	Aug. 21, 1988	80	04:21	64	60	Sept. 1, 1988
23	Feb. 2, 1989	Feb. 15, 1989	64	02:36	49	50	Feb. 28, 1989
24	Aug. 7, 1989	Aug. 17, 1989	81	04:06	62	59	Aug. 28, 1989
25	Jan. 29, 1990	Feb. 11, 1990	64	02:36	48	49	Feb. 24, 1990

26	Aug. 2, 1990	Aug. 12, 1990	81	03:53	55	54	Aug. 24, 1990
27	Jan. 25, 1991	Feb. 7, 1991	63	03:05	37	43	Feb. 20, 1991
28	July 29, 1991	Aug. 9, 1991	82	03:29	52	52	Aug. 20, 1991
29	Jan. 21, 1992	Feb. 3, 1992	63	02:57	45	49	Feb. 17, 1992
30	July 23, 1992	Aug. 3, 1992	82	04:19	49	53	Aug. 15, 1992
31	Jan. 15, 1993	Jan. 29, 1993	63	03:16	44	48	Feb. 2, 1993
32	July 19, 1993	July 30, 1993	82	03:20	49	53	Aug. 11, 1993
33	Jan. 11, 1994	Jan. 25, 1994	63	03:28	40	46	Feb. 8, 1994
34	July 14, 1994	July 26, 1994	82	03:06	49	53	Aug. 7, 1994
35	Jan. 16, 1995	Jan. 22, 1995	63	03:20	49	53	Feb. 5, 1995
36	July 9, 1995	July 23, 1995	82	02:38	47	53	Aug. 2, 1995
37	Jan. 2, 1996	Jan. 17, 1996	63	02:21	39	45	Feb. 1, 1996
38	July 3, 1996	July 15, 1996	82	02:23	45	52	July 28, 1996

Appendix B. Delta-Vs

Delta-V	Date
1	February 14, 1978
2	July 24, 1978
3	June 20, 1979
4	February 13, 1980
5	June 24, 1980
6	December 16, 1980
7	October 29, 1981
8	August 17, 1982
9	May 27, 1983
10	February 14, 1984 (a previous Delta-V had been tried on January 12, 1984, but the OBC failed during the burn and the spacecraft had to be stabilized using the Sunbath mode)
11	November 16, 1984
12	August 9, 1985 (a previous Delta-V had been tried on July 18, 1985, which resulted in a loss of attitude control due to OBC Worker 19 overflow)
13	March 19, 1986
14	July 29, 1986
15	December 18, 1986
16	September 9, 1987
17	March 18, 1988
18	September 8, 1988
19	March 13, 1989
20	September 8, 1989
21	June 6, 1990
22	January 12, 1991
23	October 18, 1991
24	August 19, 1992
25	November 20, 1992

26	August 19, 1993
27	February 15, 1994
28	September 20, 1994
29	May 3, 1995
30	June 6, 1995

Appendix C. OBC malfunctions

OBC crashes	Date	Remarks
	March 11, 1978	It appeared to be related to the high OBC temperature.
	November 15, 1978	The OBC halted during a test whilst running on 40 kbps. Operations were limited to 20 kbps.
	December 3, 1978	It seemed to be related to the high OBC temperature.
	February 1, 1979	It seemed to be related to the high OBC temperature.
	July 18, 1979	The OBC crashed during a maneuver due to a data block 10 incorrect scaling.
	August 18, 1979	The OBC crashed and s/c began to drift in pitch and roll direction. The stabilization was achieved when it was commanded into sun acquisition mode.
	October 9, 1979	The OBC crashed at 20:52 UT, but the spacecraft was stabilized in 3-axis again with the 4K back-up computer at 20:57 UT.
	October 23, 1979	It was thought to be caused by a high OBC temperature.
	May 7, 1980	The OBC halted at 04:09 UT which caused the spacecraft lost attitude.
	January 21, 1981	The spacecraft attitude was lost when the OBC halted at 04:25 UT.
	February 1, 1981	The OBC halted due to an interrupt 14 anomaly.
	March 1, 1981	The OBC halted due to an interrupt 14 anomaly.
	May 2, 1981	The OBC halted due to an interrupt 14 anomaly.
	May 11, 1981	The OBC halted due to an interrupt 14 anomaly.
	June 20, 1981	The OBC halted due to an interrupt 14 anomaly.
	February 20, 1982	The OBC halted due to an interrupt 14 anomaly.
	February 21, 1982	The OBC halted due to an interrupt 14 anomaly.
	November 25, 1982	At 15:20 UT the OBC crashed during a maneuver. The spacecraft was stabilized using the 4K back-up system.

OBC crashes	December 24, 1982	An OBC crash occurred. The spacecraft had to be commanded to sunbath.
	February 14, 1985	The 4K backup OBC halted at 16:10 UT while the annual refresh of the 8K system was performed.
	March 28, 1988	The OBC crashed while unloading wheels.
	December 27, 1990	The OBC halted. The control was regained by switching to the 4K system.
	November 6, 1991	The OBC crashed during a maneuver. The control was regained by switching to the 4K system.
Worker failures	Worker 22 failed to zero the ABGs on the following dates: 7-Nov-1979, 3-May-1982, 27-Nov-1982, 15-Dec-1984 and 6-Jun-1985.	
	Worker 18 failed to turn off after a data block was loaded. This resulted in all subsequent data blocks being rejected until worker 18 was turned off by ground command. This anomaly was seen on the following dates: 14-Feb-1980, 5-Mar-1983, 6-Jun-1984, 1-May-1985, 5-Oct-1986, 16-Nov-1986, 9-Sep-1987, 14-Nov-1988, 8-Feb-1990 and 25-Jul-1992.	
	Worker 13 did not run properly, so it had to be manually turned off, on two occasions: 9-Oct-1983 and 28-Oct-1983.	
	Worker 2 did not work properly and finished the running exposure until the end of it. It happened six times: 22-Jun-1989, 6-Nov-1991, 19-May-1992, 23-Jan-1993, 2-Mar-1993 and 14-Mar-1994.	
Commands skipped	<p>On several occasions a single command uplinked to the spacecraft was received but not executed. It happened on the following dates:</p> <ul style="list-style-type: none"> • 16-Mar-1983, to turn worker 22 off. • 17-Mar-1985, to turn off power amplifier 4. • 9-Mar-1986, to start an exposure. • 27-Jul-1986, to start an exposure. • 19-Feb-1988, to start an exposure. • 15-Oct-1989, to switch telemetry formats. • 17-Apr-1990, to command the FES in save position. • 1-Aug-1990, to start an exposure. • 21-Aug-1992, to start an exposure. • 1-Feb-1994, to switch telemetry formats. • 26-Mar-1994, to switch power amplifiers. • 7-Apr-1994, to take a FES image. 	
Data blocks skipped	<p>On several occasions a data block uplinked to the spacecraft was received but not executed. It happened on the following dates:</p> <ul style="list-style-type: none"> ▪ 24-Jul-1980, DB#10 to perform an slew. ▪ 6-Aug-1980, DB#17 to prepare a camera. ▪ 13-Jan-1981, DB#17 to prepare a camera. 	

<p>Data blocks skipped</p>	<ul style="list-style-type: none"> • 28-May-1982, DB#17 to prepare a camera. • 8-Aug-1983, DB#10 to perform an slew. • 18-Aug-1983, DB#17 to prepare a camera. • 2-Oct-1983, DB#10 to perform an slew. • 30-Oct-1983, DB#10 to perform an slew. • 25-Jul-1984, DB#10 to perform an slew. • 28-Aug-1984, DB#10 to perform an slew. • 10-Dec-1984, DB#17 to unload the wheels. • 12-Jun-1985, DB#14 to perform an exposure. • 1-May-1986, DB#17 to unload the wheels. • 4-Sep-1986, DB#17 to prepare a camera. • 7-Mar-1987, DB#21 to perform an slew. • 19-Apr-1988, DB#21 to perform an slew. • 3-Aug-1988, DB#21 to perform an slew. • 11-Mar-1989, DB#17 to prepare a camera. • 10-Jul-1989, DB#17 to prepare a camera. • 24-Apr-1990, DB#21 to perform an slew. • 6-Jun-1990, DB#17 to unload the wheels. • 15-Aug-1990, DB#21 to perform an slew. • 24-Aug-1990, DB#21 to perform an slew. • 20-Oct-1990, DB#15 to uplink the spacecraft attitude . • 28-Oct-1990, DB#17 to prepare a camera. • 30-Oct-1990, DB#17 to unload the wheels. • 23-Feb-1991, DB#21 to perform an slew. • 11-Mar-1991, DB#21 to perform an slew. • 16-Aug-1991, DB#14 to perform an exposure. • 17-Aug-1991, DB#21 to perform an slew. • 26-Nov-1991, DB#21 to perform an slew. • 2-Apr-1992, DB#17 to unload the wheels. • 18-Apr-1992, DB#21 to perform an slew. • 7-Jul-1992, DB#17 to prepare a camera. • 12-Aug-1992, DB#17 to prepare a camera. • 11-Dec-1992, DB#11 to perform a maneuver. • 14-Dec-1992, DB#17 to prepare a camera. • 7-Feb-1992, DB#21 to perform an slew. • 13-Apr-1993, DB#17 to prepare a camera. • 14-Jul-1993, DB#21 to perform an slew. • 25-Jul-1991, DB#14 to perform an exposure. • 24-Aug-1993, DB#17 to prepare a camera. • 30-Sep-1993, DB#21 to perform an slew. • 23-Oct-1993, DB#17 to prepare a camera. • 19-Nov-1993, DB#17 to prepare a camera. • 27-Jan-1994, DB#17 to unload the wheels. • 9-Jul-1994, DB#17 to unload the wheels • 24-Jul-1994, DB#21 to perform a slew. • 25-Jul-1994, DB#14 to perform an exposure.
-----------------------------------	---

Data blocks skipped	<ul style="list-style-type: none">• 26-Jul-1994, DB#17 to prepare a camera.• 31-Jul-1994, DB#17 to prepare a camera.• 7-Jul-1995, DB#17 to prepare a camera.• 8-Jan-1996, DB#17 to perform a slew.
--------------------------------	---

Source Documents

- ▶ “System Design Report for the International Ultraviolet Explorer. Volume I (Scientific Instrument)”, August 1976, Goddard Space Flight Center.
- ▶ “System Design Report for the International Ultraviolet Explorer. Volume II (Spacecraft design)”, June 1976, Goddard Space Flight Center.
- ▶ “IUE T&C Subsystems”, May 1977, Goddard Space Flight Center.
- ▶ “IUE Camera Operations Manual”, October 1977, Appleton Laboratory, University College London.
- ▶ “IUE Camera Users’s Guide”, October 1977, Appleton Laboratory, University College London.
- ▶ “IUE Fine Error Sensor Operations Manual”, November 1977, Astronomy Systems Branch.
- ▶ “IUE OBC Handbook”, January 1978, Goddard Space Flight Center.
- ▶ “The IUE spacecraft and instrumentation”, October 1978, Goddard Space Flight Center.
- ▶ “Case Study in Spacecraft Design”, August 1979, Goddard Space Flight Center.
- ▶ “Spacecraft Analyst Training Manual”, August 1984, Goddard Space Flight Center.
- ▶ Spacecraft Anomaly Reports (IUESCAR), Goddard & Vilspa.
- ▶ Shadow Season 1-38 Battery Performance for the IUE. Goddard Space Flight Center.
- ▶ IUE Solar Array Report. From 1978 to 1990. Goddard Space Flight Center.
- ▶ IUE Temperature Report. From 1978 to 1990. Goddard Space Flight Center.
- ▶ HAPS Performance Report. From 1978 to 1990. Goddard Space Flight Center.
- ▶ DMU Radiation Report. From 1978 to 1990. Goddard Space Flight Center.
- ▶ Spacecraft Performance Report. From 1990 to 1994. Goddard Space Flight Center.
- ▶ IUE Observing Beta Restrictions for the 7th to 18th Episode. Vilspa.
- ▶ IUE Weekly Spacecraft Status and Operations Summary. From 1978 to 1996. Vilspa.
- ▶ IUE Monthly Spacecraft Activity Report. From 1978 to 1996. Vilspa.

- ▶ IUE Quarterly Spacecraft Activity Report to Council. From 1978 to 1996. Vilspa.
- ▶ IUE Annual Report. From 1978 to 1996. Vilspa.
- ▶ Memo from Vilspa dated 03/14/1979. Subject: "GRID-1 Voltage Supply Anomaly on SWR-Camera".
- ▶ Memo from Vilspa dated 03/28/1979. Subject: "Microphonics Noise".
- ▶ Memo from Goddard dated 06/05/1979. Subject: "IUE Gyro 6 Failure. Summary of Related Events".
- ▶ Memo from Goddard dated 11/08/1979. Subject: "Operational Impact of OBC Patching of 11/08/1979".
- ▶ Memo from Vilspa dated 05/21/1980. Subject: "Attitude recovery using wheel speeds".
- ▶ Memo from Vilspa dated 08/18/1980. Subject: "Beta = 0° recovery during shift Sep. 08/1980 at Vilspa".
- ▶ Memo from Goddard dated 08/27/1981. Subject: "Gyros".
- ▶ Memo from Goddard dated 09/03/1981. Subject: "Maneuvering Errors".
- ▶ Memo from Goddard dated 09/18/1981. Subject: "OBC 4K Operational System".
- ▶ Memo from Goddard dated 11/25/1981. Subject: "LWP scan anomaly".
- ▶ Memo from Goddard dated 02/23/1982. Subject: "Calculation of the IUE spacecraft attitude using reaction wheel speeds and sun angles".
- ▶ Memo from Goddard dated 05/21/1982. Subject: "IUE Gyro Performance for First Quarter 1982".
- ▶ Memo from Goddard dated 05/21/1982. Subject: "OBC Hit Analysis - Preliminary Findings".
- ▶ Memo from Vilspa dated 06/30/1982. Subject: "Periodic Noise (Microphonics) on the LWP Camera".
- ▶ Memo from Goddard dated 07/27/1982. Subject: "IUE Gyro 2 Failure and Alternate IUE s/c Control Technique".
- ▶ Memo from Goddard dated 12/16/1982. Subject: "Daily IUE peak radiation levels".
- ▶ Memo from Goddard dated 01/11/1983. Subject: "LWR Exposure Tag Two Counts Short".

- ▶ Memo from Goddard dated 01/20/1983. Subject: "Gyro Status Report".
- ▶ Memo from Vilspa dated 09/12/1983. Subject: "Anomaly in the LWR Camera".
- ▶ Memo from Vilspa dated 10/20/1983. Subject: "LWP Camera Anomalies".
- ▶ Memo from Vilspa dated 12/01/1983. Subject: "IUE course attitude recovery procedure".
- ▶ Memo from Goddard dated 12/21/1983. Subject: "Gyro 1 Failure of December 10/11".
- ▶ Memo from Goddard dated 01/27/1984. Subject: "Summary of IUE maneuver error analysis for 1983".
- ▶ Memo from Goddard dated 02/04/1985. Subject: "IRA Status".
- ▶ Memo from Vilspa dated 04/07/1985. Subject: "FES 2 star count variations anomaly".
- ▶ Memo from Goddard dated 05/06/1985. Subject: "Reduced Spacecraft Power Loads".
- ▶ Memo from Goddard dated 08/22/1985. Subject: "Everything you want to know about the Two-Gyro Mode and were afraid to ask?".
- ▶ Memo from Goddard dated 09/19/1985. Subject: "Beta-dot recovery".
- ▶ Memo from Goddard dated 10/04/1985. Subject: "The beta-dot attitude recovery".
- ▶ Memo from Goddard dated 04/25/1986. Subject: "New Roll Control Law".
- ▶ Memo from Goddard dated 10/20/1986. Subject: "FES Geometrical Calibration".
- ▶ Memo from Goddard dated 01/30/1987. Subject: "Battery 1 Summary".
- ▶ Memo from Vilspa dated 04/20/1987. Subject: "IUE maneuvering performance".
- ▶ Memo from Goddard dated 04/28/1987. Subject: "Battery 1 Summary".
- ▶ Memo from Goddard dated 03/04/1988. Subject: "IUE One-Gyro Attitude Control".
- ▶ "Selection and Calibration of a Proposed New Reference Point". September 1988. Goddard Space Flight Center.
- ▶ Memo from Goddard dated 09/02/1988. Subject: "The feasibility of switching to the redundant FSS heads".
- ▶ Memo from Goddard dated 01/05/1989. Subject: "Beta 75° Oscillations".

- ▶ Memo from Goddard dated 01/18/1989. Subject: "Worker 3 Test".
- ▶ "Progress on Implementation of New FES Reference Point". April 1989. Goddard Space Flight Center.
- ▶ Memo from Vilspa dated 10/24/1989. Subject: "How to monitor the effects of high particle background during an ongoing exposure".
- ▶ Memo from Goddard dated 10/18/1990. Subject: "Test Summary of the Modified IUE16A 4K system".
- ▶ Memo from Goddard dated 12/12/1990. Subject: "Anomalous FSS readings".
- ▶ Memo from Goddard dated 12/21/1990. Subject: "FSS roll law".
- ▶ Memo from Goddard dated 02/07/1991. Subject: "FES Anomaly Update".
- ▶ Memo from Goddard dated 05/06/1991. Subject: "Patch to automatically correct the anomalous switch to SYS2/HD1 FSS data while at beta 72°".
- ▶ Memo from Goddard dated 07/01/1991. Subject: "Automatic Worker 10 mode for shadows".
- ▶ Memo from Goddard dated 07/08/1991. Subject: "Changes to the 2-gyro code".
- ▶ Memo from Goddard dated 08/05/1991. Subject: "Flux Particle Monitor readings and interpretations".
- ▶ FAX from Goddard dated 10/04/1991. Subject: "FPM and SMSS turned off".
- ▶ "Status of archive of high speed photometry data with FES". November 1991. Vilspa.
- ▶ Memo from Goddard dated 11/11/1991. Subject: "OBC hits".
- ▶ Memo from Goddard dated 09/14/1992. Subject: "Incorrect OBC decoder selection".
- ▶ Memo from Vilspa dated 09/15/1992. Subject: "Scattered Light Update".
- ▶ "The FES Scattered Light Anomaly: A Summary". November 1992. Goddard Space Flight Center.
- ▶ Memo from Vilspa dated 12/04/1992. Subject: "Baffle anomaly IUE".
- ▶ Memo from Vilspa dated 03/17/1993. Subject: "FES distortion and the use of a non-standard reference point".
- ▶ Memo from Goddard dated 07/08/1993. Subject: "2-Gyro Scattered light check".

- ▶ “The IUE FES Photometric Archive: Status and Plans”. November 1993. Vilspa.
- ▶ “IUE New Spectral Image Processing System Information Manual: Low Dispersion Data”. December 1993. Goddard Space Flight Center.
- ▶ “The IUE orbit”. October 1994. Goddard Space Flight Center.
- ▶ Memo from Goddard dated 10/17/1994. Subject: “1-gyro update”.
- ▶ “16 Years with the IUE Fine Sun Sensor”. December 1994. Goddard Space Flight Center.
- ▶ Memo from Vilspa dated 07/07/1995. Subject: “IUE Orbit Change”.
- ▶ Memo from Vilspa dated 07/14/1995. Subject: “Test of Beta-dot attitude recovery procedure”.
- ▶ Memo from Goddard dated 01/10/1995. Subject: “New restrictions on the OBC and DMU temperatures”.
- ▶ Memo from Vilspa dated 11/21/1995. Subject: “Corrupted Images”.
- ▶ Memo from Vilspa dated 01/05/1996. Subject: “DMU anomaly study”.
- ▶ Memo from Goddard dated 03/06/1996. Subject: “IRA failure & OBC/DMU anomaly”.
- ▶ Memo from Vilspa dated 04/03/1996. Subject: “Course & Fine slews recommendations”.
- ▶ Memo from Goddard dated 08/23/1996. Subject: “End of operations option analysis for the IUE”.

List of figures

- Figure 2-1.** IUE Spacecraft in Mission Orbit Configuration.
Figure 2-2. IUE Exploded View.
Figure 2-3. IUE System Block Diagram.
Figure 2-4. Hyakutake FES image (March 26, 1996).
Figure 2-5. SWP 58388 raw image.
Figure 2-6. SWP 58388 extracted spectrum.
Figure 2-7. LWP 32696 raw image.
Figure 2-8. LWP 32696 extracted spectrum.
Figure 4-1. History of semi-major axis.
Figure 4-2. History of eccentricity.
Figure 4-3. History of inclination.
Figure 4-4. History of right ascension of the ascending node.
Figure 4-5. History of argument of perigee.
Figure 4-6. History of mean anomaly.
Figure 4-7. Predicted Long-Term Changes in IUE Orbital Eccentricity.
Figure 4-8. Predicted Long-Term Changes in IUE Orbital Inclination.
Figure 4-9. Periodical changes in eccentricity.
Figure 4-10. Periodical changes in inclination.
Figure 4-11. Ground trace at 01/30/1978.
Figure 4-12. Ground trace at 01/01/1980.
Figure 4-13. Ground trace at 01/01/1982.
Figure 4-14. Ground trace at 01/01/1984.
Figure 4-15. Ground trace at 01/01/1986.
Figure 4-16. Ground trace at 01/01/1988.
Figure 4-17. Ground trace at 01/08/1989.
Figure 4-18. Ground trace at 01/09/1990.
Figure 4-19. Ground trace at 01/08/1992.
Figure 4-20. Ground trace at 01/08/1994.
Figure 4-21. Ground trace at 01/10/1995.
Figure 4-22. Ground trace at 07/09/1995.
Figure 4-23. History of east longitude.
Figure 5-1. Solar Intensity vs. Time of Year.
Figure 5-2. Solar Panel Temperatures.
Figure 5-3. History of average solar array output.
Figure 5-4. History of solar array degradation.
Figure 5-5. Solar array 1 and 2 output on September 29, 1996.
Figure 5-6. Comparison between solar array 1 and 2 vs. Beta.
Figure 5-7. Solar array EOL characterization.
Figure 5-8. History of average temperature of the batteries.
Figure 5-9. Average Battery Power Sharing vs. Shadow Season.
Figure 5-10. Average Booster Efficiency vs. Shadow Season.
Figure 5-11. Maximum Umbra Length vs. Shadow Season.
Figure 5-12. Winter Shadow Season Temporal Occurrence.
Figure 5-13. Summer Shadow Season Temporal Occurrence.

- Figure 5-14.** S/C Bus Power During Minimum Load vs. Shadow Season.
- Figure 5-15.** Maximum DOD vs. Shadow Season.
- Figure 5-16.** Battery 1 Voltage vs. DOD during Season 1-38.
- Figure 5-17.** Battery 2 Voltage vs. DOD during Season 1-38.
- Figure 5-18.** IUE Command Subsystem Block Diagram.
- Figure 5-19.** IUE S-Band antenna sensitivity plot.
- Figure 5-20.** Antenna locations on the S/C.
- Figure 5-21.** Comparison between the output of the four power amplifiers.
- Figure 5-22.** Direct Read Table (DRT).
- Figure 5-23.** Format 1B (Camera format).
- Figure 5-24.** Format 2A (Engineering format).
- Figure 5-25.** Telemetry bitrate possibilities.
- Figure 5-26.** Corruption vs DMU temperature.
- Figure 5-27.** Corruption vs OBC temperature.
- Figure 5-28.** Corruption vs radiation.
- Figure 5-29.** Image corruption vs engineering data corruption.
- Figure 5-30.** Image corruption vs engineering data corruption.
- Figure 5-31.** Cycle 0 output.
- Figure 5-32.** History of the Cycle 0 output.
- Figure 5-33.** Cycle 1 output.
- Figure 5-34.** History of the Cycle 1 output.
- Figure 5-35.** History of Cycle 2 output.
- Figure 5-36.** History of Cycle 3 output.
- Figure 5-37.** Cycle 4 output.
- Figure 5-38.** History of the Cycle 4 output.
- Figure 5-39.** History of Cycle 5 output.
- Figure 5-40.** History of Cycle 6 output.
- Figure 5-41.** Cycle 7 output.
- Figure 5-42.** History of the Cycle 7 output.
- Figure 5-43.** Projections of the input axes of the six gyros.
- Figure 5-44.** Gyro drift rates.
- Figure 5-45.** Definition of the beta and roll angles.
- Figure 5-46.** FSS beta and roll resolution vs beta angle.
- Figure 5-47.** FSS beta and roll resolution vs beta angle.
- Figure 5-48.** FES field-of-view.
- Figure 5-49.** FES distortion values.
- Figure 5-50.** FES background counts (s/o) vs Beta angle on June 29, 1992.
- Figure 5-51.** FES counts (s/o) vs since January 1991 until September 1992.
- Figure 5-52.** FES contaminated image.
- Figure 5-53.** FESCAM counts vs β angle summarized maneuvering from beta 35° to 115°.
- Figure 5-54.** FESCAM counts vs β angle summarized maneuvering from beta 115° to 35°.
- Figure 5-55.** FES counts (f/o) at the Reference Point.
- Figure 5-56.** HAPS, schematic.
- Figure 5-57.** Tank group pressures.
- Figure 5-58.** Tank group temperatures.
- Figure 5-59.** Hydrazine remaining on IUE tanks.

- Figure 5-60.** Comparison of LTE 1 & 9 output and associated EV 1 temperature.
- Figure 5-61.** Comparison of LTE 4 & 6 output and associated EV 6 temperature.
- Figure 5-62.** Comparison of LTE 3 & 7 output and associated EV 7 temperature.
- Figure 5-63.** Comparison of LTE 10 & 12 output and associated EV 10 temperature.
- Figure 5-64.** Comparison of LTE average output and hydrazine tank pressure.
- Figure 5-65.** Tank pressures during the N_2H_4 venting.
- Figure 5-66.** Tank temperatures during the N_2H_4 venting.
- Figure 5-67.** Jets fired during the N_2H_4 venting.
- Figure 5-68.** Comparison of errors with derived correction, 3-Gyro system
- Figure 5-69.** Sunline slew errors, 2-Gyro/FSS system.
- Figure 5-70.** Pitch slew errors, 1-Gyro system
- Figure 5-71.** Sunline slew errors, 1-Gyro system.
- Figure 5-72.** Detailed Optical Schematic of the IUE Scientific Instrument.
- Figure 5-73.** SEC/UVC Tube Pair and Coil Assembly.
- Figure 6-1.** IUE Interior and Exterior Features.
- Figure 6-2.** History of average Onboard Processor 1 temperatures.
- Figure 6-3.** History of average camera deck temperatures near SWP.
- Figure 6-4.** History of average camera deck temperatures near LWP.
- Figure 6-5.** History of average Data Multiplexer 1 temperatures.
- Figure 6-6.** History of average Hydrazine Tank B temperatures.
- Figure 6-7.** History of average Hydrazine Tank G temperatures.
- Figure 6-8.** History of average Engine Valve 2 temperatures.
- Figure 6-9.** History of average Engine Valve 7 temperatures.
- Figure 6-10.** History of average Engine Valve 10 temperatures.
- Figure 6-11.** History of average remote engine module temperatures.
- Figure 6-12.** History of average +Z line temperatures.
- Figure 6-13.** History of average -Z line temperatures.
- Figure 6-14.** History of average EEA1 temperatures.